INVESTIGATIONS ON THE RADIATION CHARACTERISTICS OF COMPACT MULTIPLE ANTENNA SYSTEMS FOR MIMO APPLICATIONS

Thesis submitted by

ANITHA R

in partial fulfillment of the requirements for the degree of

DOCTOR OF PHILOSOPHY

Under the guidance of

Prof. K. VASUDEVAN

Department of Electronics
Faculty of Technology
Cochin University of Science and Technology
Cochin - 682 022, Kerala, India

June 2017

Investigations on the Radiation Characteristics of Compact Multiple Antenna Systems for MIMO Applications

Ph.D. Thesis under the Faculty of Technology

Author:

ANITHA R

Centre for Research in Electromagnetics and Antennas (CREMA)

Department of Electronics

Cochin University of Science and Technology

Cochin - 682 022, Kerala, India.

Email: anithar2@gmail.com

Supervisor:

Dr. K. Vasudevan

Emeritus Professor

Centre for Research in Electromagnetics and Antennas (CREMA)

Department of Electronics

Cochin University of Science and Technology

Cochin - 682 022, Kerala, India.

Email:vasudevankdr@gmail.com

Department of Electronics

Cochin University of Science and Technology

Cochin - 682 022, Kerala, India.

www.doe.cusat.edu

June 2017

Dedicated to the Almighty, Family, Teachers and Dear ones...

DEAPARTMENT OF ELECTRONICS
COCHIN UNIVERSITY OF SCIENCE AND TECHNOLOGY
COCHIN-682 022

Prof. K. Vasudevan
(Supervising Guide)
Emeritus Professor
Department of Electronics
Cochin University of Science and Technology

Certificate

This is to certify that this thesis entitled "**Investigations on the Radiation Characteristics of Compact Multiple Antenna Systems for MIMO Applications**"is a bonafide record of the research work carried out by ANITHA R under my supervision in the Centre for Research in Electromagnetics and Antennas, Department of Electronics, Cochin University of Science and Technology. The results embodied in this thesis or parts of it have not been presented for the award of any other degree.

I further certify that the corrections and modifications suggested by the audience during the pre-synopsis seminar and recommended by the Doctoral committee of Ms. Anitha R are incorporated in the thesis.

Cochin - 22
June 2017   **Prof. K. Vasudevan**

Declaration

I hereby declare that the work presented in this thesis entitled "**Investigations on the radiation characteristics of compact multiple antenna systems for MIMO applications**"is based on the original research work carried out by me under the supervision and guidance of Prof. K. Vasudevan, Emeritus Professor, Department of Electronics, Cochin University of Science and Technology, Cochin-682 022 and has not been included in any other thesis submitted previously for the award of any degree.

Anitha R
Research scholar,
Department of Electronics,
Cochin - 22   CUSAT,
June 2017   Cochin-22.

Acknowledgments

I owe my sincere gratitude to the many people, without their generous support, this thesis would not have been possible. First and foremost, I would like to express my deepest gratitude to Dr. K. Vasudevan, Emeritus Professor, Department of Electronics, Cochin University of Science and Technology, for providing a great research platform, for profuse support and guidance. I am grateful for his insightful suggestions, constant encouragement and timely care extended to me throughout the research period.

I also thank Prof. P. Mohanan and Prof. C. K. Aanandan, Department of Electronics, Cochin University of Science and Technology for the support and valuable suggestions during these years. Their constant encouragement has been an important source of inspiration for me to overcome challenges along the way.

I thank Prof. M. H. Supriya, Head, Dept. of Electronics, CUSAT, for her support during the process of writing this dissertation.

I take this opportunity to thank Prof. K. G. Nair for his vision in setting up Center for Research in Electromagnetics and Antennas (CREMA) at CUSAT. My sincere thanks to Prof. Tessamma Thomas, Prof. James Kurian, Prof. K. T. Mathew, Prof. P. R. S Pillai, Mr. Arun Balakrishnan, Mr. Mithun Haridas, Dr. Bijoy Jose and all other faculty members of the Department of Electronics for their support and encouragement. I extend my gratitude to all the non-teaching staff at the Department of Electronics for the help and cooperation extended to me.

Mere words are not enough to express my special thanks to Dr. Sarin V.P., Assistant Professor, Department of Electronics, Govt. College, Chittur, Palakkad, India, who had been a helping hand throughout my research period. The discussions with him and the helpful suggestions have always been of vital importance during my research work.

I take this opportunity to thank my colleagues Manoj Melpadam, Sumitha Mathew, Vinesh P. V., Prakash K. C., Vivek Rajan, Mohammed Ameen, Remsha Moolat, Sajitha V. R., Deepak U., Roshna T. K, Anila P.V, Lindo

Abstract

Future antenna solutions are based on innovative technologies like multiple-input-multiple-output (MIMO), which can substantially increase data rate and improve the reliability of wireless communication, without extra spectrum and power resources. The multiple-antenna systems play a key role in providing high spectrum efficiency and improved quality of service for next generation wireless systems. Motivated by this, this thesis provides valuable insights in the design of compact, decoupled multiple antennas for efficient MIMO communications.

In the course of the thesis work, five novel compact quad element MIMO antennas have been proposed, utilizing the various forms of diversity mechanisms to exploit the degrees of freedom between the multiple elements. The thesis examines the potential of combining different decoupled microstrip patch antennas utilizing their multiple resonant modes to adapt in a compact co-located multi-element antenna. The thesis also demonstrates efficient design of compact multiband and wideband MIMO antenna systems for use in small wireless terminals. These antennas supports multiple bands, compatible with different wireless standards like LTE, UMTS, WLAN, WiMAX, Bluetooth and sZigBEE.

To design, efficient multiple antenna systems in compact terminals, several decoupling methods are proposed to reduce mutual coupling between antenna elements. These include radiating slots on the ground, stop band structures and reversing the polarity of coupling waves. The working mechanism and design procedure of each method are investigated, and their effectiveness is compared. These methods can be applied to the terminal antennas, for reducing the mutual coupling by 6 - 13 dB.

Critical factors influencing the performance of multiple antenna systems are also analyzed in detail. MIMO diversity and system performances are evaluated using the figure of merit parameters like mutual coupling, envelope correlation coefficient, channel capacity and throughput. The ultimate aim of this thesis is to investigate and enhance the MIMO/diversity performance of multiple antenna systems for future wireless communication.

List of Figures

List of Tables

Glossary

2G .... Second Generation

3G .... Third Generation

4G .... Fourth Generation

5G .... Fifth Generation

3GPP .... 3rd Generation Partnership Project

AOA .... Angle of Arrival

AOD .... Angle of Departure

AWGN .... Additive White Gaussian Noise

AUT .... Antenna Under Test

BLER .... Block Error Rate

CAGR .... Compound Annual Growth Rate

CDMA .... Code Division Multiple Access

COST .... European Cooperation in Science and Technology

CPW .... Coplanar Waveguide

CSI .... Channel State Information

CSRR .... Complementary Split Ring Resonator

CTIA .... Cellular Telecommunications Industry Association

DGS .... Defected Ground Structure

DG .... Diversity Gain

DOF .... Degrees Of Freedom

EBG .... Electromagnetic Band Gap

ECC .... Envelope Correlation Coefficient

EDG .... Effective Diversity Gain

EDGE .... Enhanced Data for GSM Evolution

EGC .... Equal Gain Combining

EM .... ElectroMagnetic

FDMA .... Frequency Division Multiple Access

GPRS .... General Packet Radio Service

GSM .... Global System for Mobiles

GUI .... Graphical User Interface

IEEE .... Institute of Electrical and Electronics Engineers

IID .... Independent and Identically Distributed

ISM .... Industrial Scientific and Medical

LOS .... Line Of Sight

LTE .... Long Term Evolution

MEG .... Mean Effective Gain

MIMO .... Multiple Input Multiple Output

MISO .... Multiple Input Single Output

ML .... Maximum Likelihood

MRC .... Maximal Ratio Combining

MWS .... Microwave Studio

NLOS .... Non Line of Sight

OFDM .... Orthogonal Frequency Division Multiplexing

OTA .... Over The Air

PCB .... Printed Circuit Board

PAS .... Power Azimuth Spectrum

PDF .... Probability density function

PDP .... Power Delay Profile

PIFA .... Planar Inverted-F Antenna

QoS .... Quality of Service

RAN .... Radio Access Network

RF .... Radio Frequency

SC .... Selection Combining

SCPI .... Standard Commands for Programmable Instruments

SIMO .... Single Input Multiple Output

SISO .... Single Input Single Output

SM .... Spatial Multiplexing

SER .... Symbol Error Rate

SNR .... Signal to Noise Ratio

SRR .... Split Ring Resonator

STBC .... Space Time Block Code

STC .... Space Time Code

SWC .... Switched Combining

TDD .... Time Division Duplex

TDMA .... Time Division Multiple Access

TM .... Transverse Magnetic

UMTS .... Universal Mobile Telecommunications Service

UWB .... Ultra Wide Band

VNA .... Vector Network Analyzer

VSWR .... Voltage Standing Wave Ratio

WCDMA .... Wideband Code Division Multiple Access

WiMAX ..... Worldwide Interoperability for Microwave Access

WLAN .... Wireless Local Area Network

Contents

Chapter 1

Introduction

Contents

Advances in wireless communication over the past two decades have shaped our society and way of life to a point where access to wireless transmitted information is ubiquitous in both our personal and professional lives. A number of outstanding researchers, scientists, engineers and visionaries have contributed to this core technology, whose outcome, our generations have been so fortunate to enjoy. This chapter aims to guide the reader through the evolution of wireless technology from the past with a vision of modern wireless communications. The scope of introduction is mainly focused on a core technology, multiple-input-multiple-output (MIMO) which has emerged as an integral part in modern wireless communication systems. A description of the motivation behind the research investigations is presented and the chapter concludes with the details of the organization of the thesis.

1.1 Wireless Communication Systems

Experiments in the transmission and reception of electromagnetic waves in the late 19th century by Heinrich Hertz, was the first of its kind in communication history. Later in the 20th century, wireless communication was successfully accomplished by Marconi, which marked the beginning of a new era for wireless communication. Following decades saw a proliferation of wireless communication standards, devices and systems. Wireless technology advanced rapidly to enable transmission over larger distances with low cost devices having compact size and less power requirements, thereby enabling public and private radio communications, mobile communications and wireless networking.

The demand for faster transmission and reception of information seems to be endless and has been the thriving force behind the development of modern wireless communication systems. Since 1985, wireless communication has been emerging from the very basic first generation analog systems (1G) to second-generation (2G) digital systems (TDMA, CDMA), and later to 2.5G systems (GPRS and EDGE). In order to further increase wireless capability and data rate, third generation (3G) systems like WCDMA and fourth generation (4G) systems like LTE was introduced, which became widely popular.

Existing wireless standards like LTE advanced and IEEE 802.11ac are able to provide reliable wireless services at high data rates. The more stringent requirement on data rate, latency and spectrum efficiency defines the scope of 5G networks or next generation wireless systems. Figure 1.1 summarizes the evolution of wireless communication standards. It can be observed that a large portion of the available RF spectrum is reserved for these systems.

Numerous highly efficient wireless networking technologies have been developed and widely deployed. The demand for wireless internet data is expected to increase by more than 50 times over the next decade [1] as shown in Figure 1.2. As 'wireless internet' is progressing to evolve its forms, today's commercial wireless communications landscape is powering a transformation in the way people access and share information. Users are embracing these new potential and are demanding additional competencies to satisfy their needs. This interdependent relationship is creating an astonishing evolution

Generation Features	1G	2G	3G	4G	5G
Years	1970 - 1984	1980-1999	1990-2002	2010s	2020s
Data Bandwidth	2 Kbps	14.4 to 64 Kbps	2 Mbps	200 Mbps to 1Gbps	≥ 1Gbps
Standards	AMPS	TDMA, CDMA< GSM, GPRS, EDGE	WCDMA, CDMA-2000	Single unified standards	Single unified standards
Technology	Analog cellular	Digital cellular	Broad bandwidth CDMA, IP technology	Unified IP and seamless combination of broadband, LAN, WAN & WLAN	Unified IP and seamless combination of broadband, LAN, WAN WLAN, WWWW
Multiplexing	FDMA	TDMA, CDMA	CDMA	CDMA	CDMA
Services	Mobile telephony (voice)	Digital voice, SMS, Higher capacity packetized	Integrated high quality audio, video and data	Dynamic information access, wearable devices	Dynamic information access, wearable devices with AI capabilities
Switching	Circuit	Circuit & packet	Packet	All packet	All packet

Figure 1.1: Evolution of wireless communication standards

in wireless networking capabilities in the commercial domain. A recent analysis performed by Cisco shows the global internet traffic by means of local access technology in Figure 1.3. It can be observed that there is a 29 % growth in compound annual growth rate (CAGR) in the period from 2011 - 2016 and by 2016, the wifi or the wireless traffic surpasses the traffic through a fixed wired connection.

It is still astounding how wireless technologies have become so integrated in our daily lives, even in the remotest parts of the world. Cell phones, laptops, smart TVs, tablets, and other devices provide a medium of connectivity to the world and media content that we could not have thought up in the recent past. This trend continues to accelerate, making it tough to visualize the type of wireless society we might find in another 20 years. The vast increase of data in the various forms needs to go through the available spectrum in a fast and reliable manner. Therefore designing and building future wireless devices and networks becomes more and more challenging.
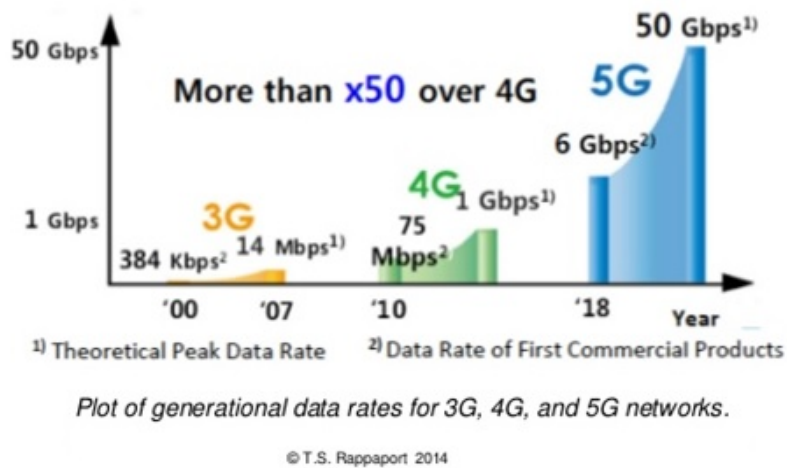
Figure 1.2: Plot of generational data rates for 3G, 4G and 5G networks
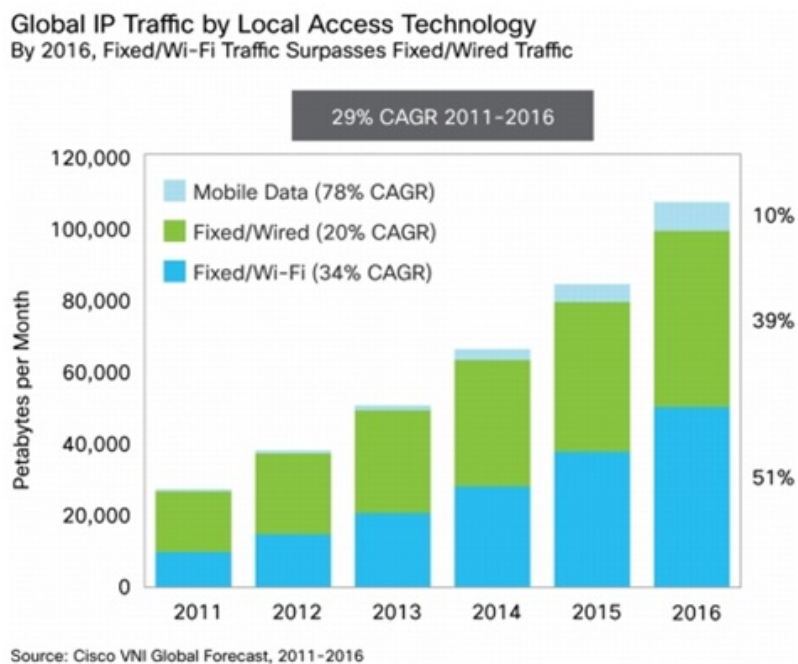
Figure 1.3: Global internet traffic by local access technology

1.1.1   Need for Multiple Antennas

The wireless revolution has progressed with the developments in technology
and wireless standards and algorithms. The initial thrust was for having re-
liable portable wireless devices, then miniaturization came into the picture,
later multi-standard support and multiband operation were concentrated on,
and finally the thrive is for achieving higher data rates, that exceed the the-
oretical limits set for single channel communication systems. Generally, in
urban and indoor environments, there is no clear line-of-sight (LOS) between
transmitter and receiver. Instead the signal is reflected along multiple paths,
before finally being received at the receiver. Each of these rebounds can pro-
duce phase shifts, time delays, and distortions that can destructively interfere
with one another at the aperture of the receiving antenna.

Generally, the wireless data that is transferred from transmitter (TX) to
receiver (RX) through a communication channel takes different paths on its
travel to the receiving end. Strength of signal at the receiving end will vary
depending on the distance traveled by the signal as shown in Figure 1.4(a) [2].
The loss of signal power can be attributed mainly to the path loss and to the
fading across the channel as shown in Figure 1.4(b). According to Friss free
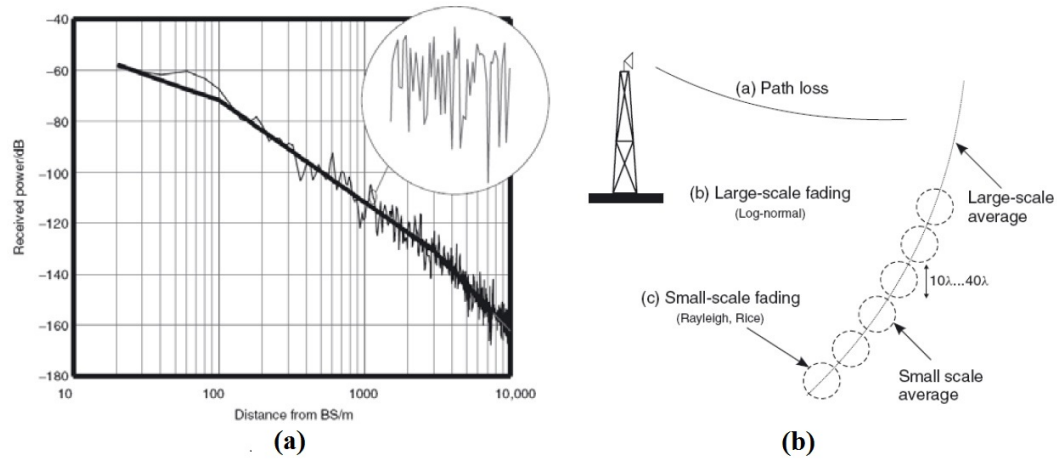
*Figure 1.4: (a) Received Power v/s distance between TX and RX (b) Losses in the
received power*

space equation [3], the signal strength at receiver, in case of a clear line of

sight (LOS) path between TX and RX is

$$P_{R(d)} = \frac{P_T \ G_T \ G_R \ \lambda^2}{(4\pi^2)d^2 L} \qquad (1.1)$$

where d is $TX - RX$ separation distance (in meters), P_T and P_R represents the powers of transmitted and received signal, G_T and G_R are the power gains of transmitting and receiving antennas respectively, λ is the wavelength, L is the system loss factor or propagation loss in channel given by

$$L = L_P L_S L_F \qquad (1.2)$$

where L_P is the path loss, L_S is the slow fading and L_F is the fast fading. For Friss equation (1.1) to hold true, distance d should be in the farfield of the transmitting antenna. Path loss or free space loss depends on the distance between transmitter and receiver. It represents the signal attenuation in dB or the difference between effective TX power and RX power.

$$PL(dB) = -10 \ log \ \frac{P_R}{P_T} = -10 \ log \frac{G_T \ G_R \ \lambda^2}{(4\pi^2)d^2 L} \qquad (1.3)$$

Various channel models depicting the path loss are developed and reported [4–6]. The fading effect is usually divided into two types, namely large-scale fading and small-scale fading. Large scale fading is mainly due to path loss as a function of distance and shadowing by large objects, such as mountains and tall buildings. As the receiver moves away from the transmitter over large distances, the local average of the received signal will gradually decrease or in other words, slow fading.

On the other hand, small-scale fading is due to the constructive and destructive combination of randomly scattered, reflected, diffracted and delayed multiple path signals. Multiple copies of the transmitted signals arriving at different time delays add at the receiver and this results in fading. Here rapid and severe signal fluctuation happens around a slowly varying mean, or in other words, fast fading occurs because it occurs over a relatively short distance.

As the complexity of propagation channel increases, the number of propagation paths between transmitter and receiver increases. Each path is unique

on it own with distinct amplitude, phase, delay, direction of departure and arrival. At the receiver these multipath components are combined to reconstruct the original transmitted signal. The multipath components interfere either constructively or destructively in reconstructing the signal, which results in the good or bad quality of the recovered data. The disturbances on channel combined with the destructive interference of multipath components can produce a weak signal at the receiver.

Apart from this fading disturbances, the demand for the high rate to be communicated over the existing wireless channel, also needs to be addressed. Whether it be WLAN, home A/V networks or mobile networks, all of them require more and more data to be transferred. The wireless link is expected to meet or surpass the performance of a wired link which promises up to 10 Gb/s. In other words, spectral efficiency or throughput of the wireless link needs to be enhanced.

Hence, to overcome the adverse effect of multipath communication and increasing the reliability of wireless communication, multiple antennas can be employed at TX and RX. It is designed in such a manner that multipath effects are taken full advantage of, and has evolved as a new dimension to increase data rate and spectrum efficiency without any increase in the spectrum.

1.2   MIMO Wireless Communications

MIMO is a modern wireless communications technology that uses multiple antennas on both TX and RX ends of a wireless communication link. With multiple antennas, spatial characteristics of the radio transmission can be controlled and manipulated to improve the performance of the wireless link. Although the concept and theories of MIMO were developed in the 1990s, commercial products using MIMO technologies first began appearing on the market around 2003. The first reference to the term MIMO in the newer communications scenario was deliberated in [7], showing a performance analysis on the theoretical capacity of a communication system, with multiple transmit and multiple receive antennas.

In a broad sense, a communication system can have multiple antennas at either the transmitter, the receiver, or both. The term MIMO is used particularly when referring to systems that have multiple antennas at both ends of the link. The conventional radio system has one transmitting and one receiving antenna, which is commonly called as single-input-single-output (SISO). When there are multiple antennas at the transmitter and only one receiver, as may occur, for example, on a cellular forward link between the base station and a single mobile user, we call that type of system a Multiple Input Single Output (MISO) system.

Conversely, if there are multiple receive antennas but only one transmit antenna, that system is called a Single Input Multiple Output (SIMO) system. When using the term in the broad sense, we often refer to MISO and SIMO systems as particular types of MIMO configurations. Figure 1.5 illustrates the four types of antenna configurations. Comparison in channel capacity between SIMO/ MISO and MIMO antenna systems has been shown Figure 1.6.
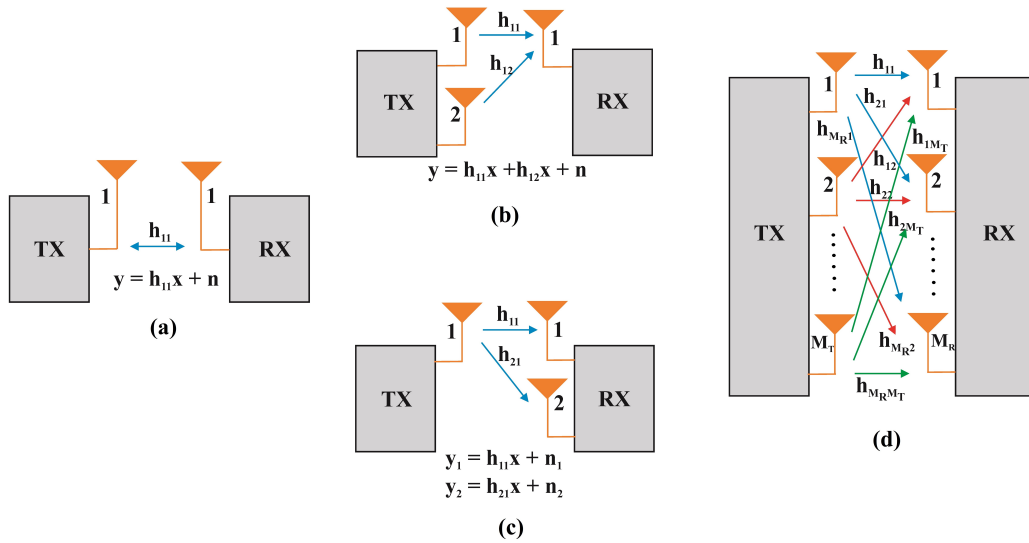
Figure 1.5: Block diagram of (a) SISO (b) MISO (c) SIMO (d) MIMO system

The maximum possible data rate of a conventional communication system having one transmit (TX) antenna and one receiving (RX) antenna, is fundamentally limited by [8] capacity of the communication channel. For a narrow band system operating in a static environment, which is time and frequency

MIMO vs. SIMO/MISO
(Linear vs. Logarithmic Improvement)

Channel
Capacity

MIMO

linear

C = log₂ (det [I + SNR/M HHᵀ])

SIMO/MISO

logarithmic

C = log₂ (1 + SNR)

No. of Antenna
Elements
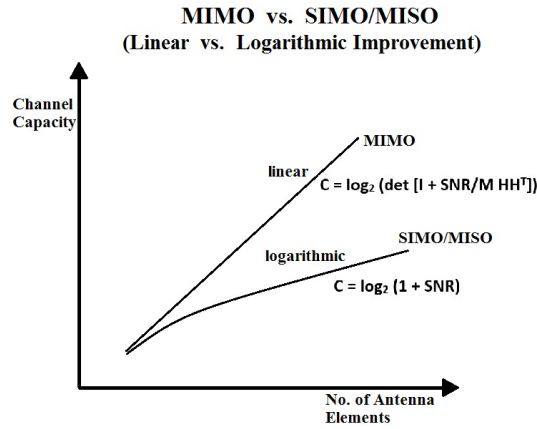
Figure 1.6: Comparison in channel capacity between SIMO/ MISO and MIMO configurations

invariant, channel can be simply represented by a scalar h. A signal through such a channel can be modeled as

$$y = hx + n \tag{1.4}$$

where y is the received signal, x is the transmitted signal, n is the additive white Gaussian noise with zero mean and variance and h is the channel response. According to [8], the channel capacity of a SISO with additive white Gaussian noise (AWGN) channel is

$$C = W \ log_2 \ (1 + \frac{P}{N_0 \ W}) \tag{1.5}$$

where C is the channel capacity in bits/sec, W is the bandwidth in Hz, P is the total transmitted power and N_0 is the noise power spectral density. Note that signal to noise ratio $SNR = P/N_0 W$, hence $AWGN$ capacity for a bandwidth of 1 Hz can be rewritten as

$$C = log_2 \ (1 + SNR) \tag{1.6}$$

This formula measures the maximum realizable spectral efficiency through an $AWGN$ channel in terms of SNR. When multipath effects of the communication channel is taken in to consideration, the channel capacity expressed in

bits per second per hertz (bps/Hz) is given by [9]

$$C = log_2 \left(1 + \frac{P}{N_0}|h|^2\right) \tag{1.7}$$

where $|h|^2$ is the power gain of a scalar channel. From equation(1.7), the channel capacity of a SISO channel increases logarithmically with the transmitted power. For high SNR levels, an increase in channel capacity by 1 bps/ Hz requires a 3 dB increase in transmitted power P. From this it can be inferred that, the performance of wireless communication system is limited by transmitted power and available bandwidth.

For a given bandwidth, to improve the spectral efficiency of wireless communication system, multiple antennas can be employed at either the TX and RX ends or both. For a MISO channel with M_T transmit antennas and a single receiving antenna,

$$y = h^* x + n \tag{1.8}$$

where $h^* = [h_1, h_2, ..., h_{M_T}]^T$ and h_{M_T} is the channel gain from transmit antenna M_T to the receiving antenna. There is a total power constraint of P across the transmit antennas. Therefore the rate achieved by a MISO channel is at most the capacity of scalar AWGN channel with same received SNR. However, by introducing some intelligence in the transmission scheme, the received SNR can be increased.

By having the received signals from the various transmit antennas to add up in-phase (coherently) and by allocating more power to the transmit antenna with the better gain, SNR can be improved. This technique of, aligning the transmit signal in the direction of the transmit antenna array pattern, is called transmit beamforming. Through beamforming, the MISO channel is converted into a scalar AWGN channel and thus any code which is optimal for the AWGN channel can be used directly. For a SIMO channel with one transmit antenna and M_R receiving antennas,

$$y_m = h_m^* x + n_m \qquad m = 1, 2, ..., M_R \tag{1.9}$$

where h_m is the channel gain from transmit antenna to m^{th} receiving antenna and n_m is the additive Gaussian noise independent across the antennas. Multiple receive antennas increase the effective SNR and provide a power gain.

The linear combining maximizes the output SNR and is sometimes called receive beamforming. In both the MISO and the SIMO, the system benefit from power gain by having multiple antennas. To get a gain in degrees of freedom, one has to use multiple antennas at both the transmitter and the receiver (MIMO) [10, 11].

The study of MIMO systems have been given significant importance and investigated for its capability to enhance data rate and channel capacity in several pioneering works [12–14]. In MIMO system, the multiple signals from transmit antennas to receive antennas will experience a cross coupling between themselves, which introduces a path dependency through the radio channel. This will create an impact on the overall capacity of the system [15].

The channel response of a MIMO system with M number of transmit and receiver antennas, is given by channel matrix H whose element $h_{M_T M_R}$ denotes the scalar SISO channel between the $M^{th} RX$ antenna and $M^{th} TX$ antenna [14]. The sampled vector signal model for the scenario is given by

$$y = Hx + n \tag{1.10}$$

where y is the received signal vector at M_R received antennas, x is the transmitted signal vector for M_T transmitting antennas and n is the AWGN vector at M_R receive antennas.

$$y = [y_1, y_2, ..., y_{M_R}]^T \tag{1.11}$$

$$x = [x_1, x_2, ..., x_{M_T}]^T \tag{1.12}$$

The channel matrix H is given by

$$H = \begin{bmatrix} h_{11} & h_{12} & . & . & . & h_{1M_R} \\ h_{21} & h_{22} & . & . & . & h_{2M_R} \\ . & . & . & . & . & . \\ . & . & . & . & . & . \\ h_{M_T 1} & h_{M_T 2} & . & . & . & h_{M_T M_R} \end{bmatrix} \tag{1.13}$$

The transmission matrix, channel state information (CSI) refers to known channel properties of a communication link. This information describes how a signal propagates from the transmitter to the receiver and represents the

combined effect of, for example, scattering, fading and power decay with distance. Channel capacity of an instantaneous MIMO channel, when its channel state information is unknown to the transmitter is given by [12]

$$C = log_2 |I_{M_R} + \frac{P}{M_T N_0} H H^H|$$
(1.14)

where I_{M_R} is an $M_R \times M_R$ identity matrix, and $(\bullet)^H$ denotes the hermitian transpose. In the expression equation (1.14), the transmit power P is equally allocated over the M_T transmitted antennas. Thus multiple spatial data pipes are created between TX and RX, by making use of multiple transmitter and receiver antennas in the wireless link.

For a given bandwidth, the use of multiple antennas increases the spectrum efficiency linearly, with the number of antennas. The channel capacity of a MIMO system primarily depends on the available channel information at either transmitter or receiver, the channel SNR and the correlation between channel gains on each antenna element. Mutually uncorrelated, independent and identically distributed (IID) channel with a channel matrix H is characterized by [14]. The expected values of the channel matrix H has the following properties

$$E\{[H]_{i,j}\} = 0$$
(1.15)

$$E\{|[H]_{i,j}|^2\} = 1$$
(1.16)

$$E\{[H]_{i,j}.[H]^*_{m,n}\} = 0, \quad if \ i \neq m \ or \ j \neq n$$
(1.17)

With IID channels, the capacity of MIMO systems is $min(M_T, M_R)$ times the capacity of a SISO channel. On the other hand, if M_R is fixed and M_T increases, then the capacity saturates at some fixed value; whereas if M_T is fixed and M_R increases, the capacity increases logarithmically with M_R. When the channel information is known to receiver, the channel capacity from equation (1.14) can be represented as

$$C = \sum_{i=1}^{R} log_2 (1 + \frac{P}{M_T N_0} \lambda_i^2)$$
(1.18)

where R is the rank of channel matrix H and $\lambda_1, \lambda_2, ..., \lambda_R$ are the singular values of H, which are non negative square roots of the eigen values of the matrix HH^*. In a richly scattered environment, the transfer functions of MIMO sub-channels are not correlated, R is maximum and is equal to $min(M_T, M_R)$. Here the capacity of MIMO channel increases proportionally to R.

In the case of fading, the channel capacities described by the above notation is not appropriate. In such cases capacity can be expressed in two different terms outage capacity and ergodic capacity. Outage capacity is defined for channels characteristics that are changing slowly, and deep fade can be very long [16]. In such cases, time can be divided in to short periods and channel capacity can be computed for each of these short intervals. Then cumulative distribution function is calculated over these values of capacity [17].

Till now we have assumed that the CSI is known to the receiver but not to the transmitter. Another scenario is that the channel is known at both the transmitter and receiver ends. Take for example, when the system employs time-division duplex (TDD), so that the uplink and downlink channels are reciprocal to each other. In this case, the instantaneous capacity is given by the following "water-filling" equation [18]. On the other hand, when fading is rapid, the channel can be in deep fade in short periods [19]. The loss of data here can be compensated by joint coding and interleaving, this expectation value is called ergodic capacity [20]. It is seen that by knowing the channel at the transmitter, some capacity gain can be obtained at low signal-to-noise ratios.

1.2.1   MIMO Techniques

The block diagram of a MIMO wireless communication system employing multiple antennas is shown in Figure 1.7. Here, data streams are passed to different antennas for transmission. Each stream will have a unique signature for the channel path it takes, the receiving antennas can distinguish between the multiple data streams and decode the data. Multiple antennas at transmitter and receiver ends improve the performance of wireless link by either, combating the multipath by forming a diversity, or exploiting the multipath effects using spatial multiplexing (SM).
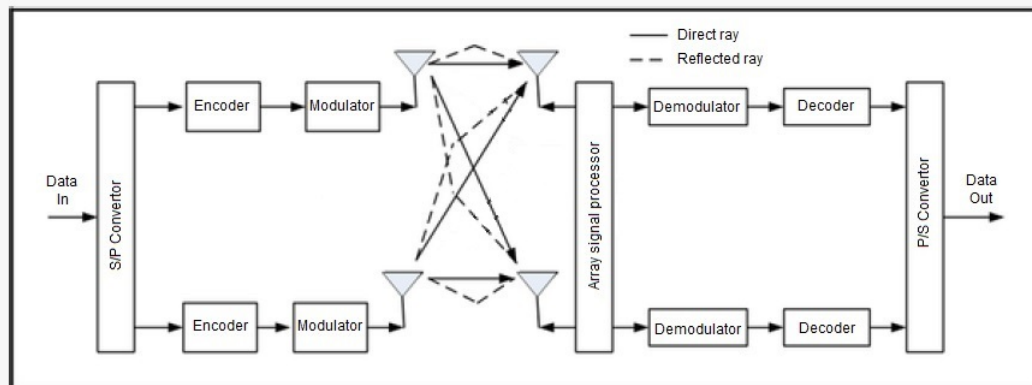
Figure 1.7: MIMO communication system

Diversity combats fading, improving the reliability of the system. This technique provides diversity against channel fading, yielding higher transmission reliability in wireless communications scenarios. The goal of diversity is to make the transmission more robust by using redundant data on different paths. A special coding technique, referred to as space-time block coding (STBC), can be used to transmit multiple copies of a data stream across a number of transmitter antennas and to make full use of the various received versions of the data, for improving the reliability of data transfer [21].

The other major MIMO technique is Spatial multiplexing (SM). SM is not intended to make the transmission more robust, however, it increases the data rate. In-order to achieve this, the data to be transmitted is divided into separate streams, and these streams are then transmitted independently via separate antennas. Spatial multiplexing takes advantage of independent non-correlated channel paths, whose information is known at either the RX or both at the TX and RX. Once the channel matrix H is known, the cross components can be calculated at the receiver. An open-loop method performs a channel estimation at the receiver end, while in a closed-loop method, the receiver sends the channel information to the transmitter using a feedback channel, thereby responding to the changing circumstances.

Beamforming is the another technique used generally to create the radiation pattern of an antenna array. It can be applied to all antenna array systems as well as in MIMO systems. In beamforming, the phases and ampli-

tude of each transmitter are adjusted. The goal is to combine the energy from each transmitter and direct it towards the receiver to improve the received SNR but not the data rate. The following discusses each of these MIMO techniques in detail.

1.2.1.1 Diversity

Diversity generally takes advantage of the multiple spatial channels, by transmitting the same data over these channels. The diversity technique can be commonly applied to various dimensions, namely antenna diversity, temporal diversity [22] and frequency diversity [23].

In temporal diversity, with space-time block coding, different versions of the same data are transmitted using multiple antennas and multiple time slots. In many practical systems, instead of using multiple time slots, multiple orthogonal frequency-division multiplexing sub carriers are used. Such a scheme is thus called space-frequency block coding employing frequency diversity. Antennas diversity makes use of multiple antennas at the TX and or RX to combat the fading through three different approaches, i.e. spatial diversity, polarization diversity and angle diversity. This thesis mainly focuses on antenna diversity techniques and factors influencing the performance of such systems.

Generally, diversity transmits the same data through many independent branches. With an increase in the number of independent branches, the probability that all the branches are experiencing the same fading deep is reduced [24, 25]. Thus the symbol error rate (SER) is reduced as well. Block diagram of MIMO system employing diversity is shown in Figure 1.8. Here, information bits are initially encoded and then modulated using conventional error correction coding and modulation techniques prior to undergoing some form of space-time coding (STC). At the receiver, space-time decoding is performed on the received signal, followed by demodulation and error decoding. Considering an IID channel and maximum likelihood (ML) detection at the receiver end, the average probability of symbol error is upper bound by [11,26]

$$P_e \leq N \prod_{i=1}^{M} \frac{1}{1 + \rho d^2/4M} \tag{1.19}$$
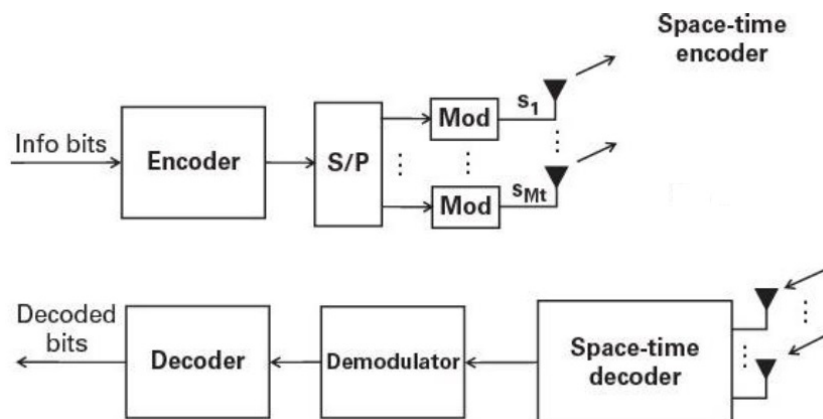
Figure 1.8: MIMO system for diversity

where N is the number of nearest neighbors, d is the minimum distance of separation of underlying scalar constellation, M is the number of independent diversity branches and ρ is the SNR at the receiver. For an IID MIMO channel having M_T transmit antennas and M_R receiver antennas, $M = M_T M_R$. For $\rho > 1$, i.e. in high SNR scenarios, equation (1.19) can be rewritten as

$$P_e \leq N(\frac{\rho d^2}{4M})^{-M} \tag{1.20}$$

It is observed that with the same SNR, the SER is greatly reduced when multiple antenna branches are used in the channel link.

Similar to transmit diversity, receiver diversity can be used in channels with N multiple antennas at the receiver side. The receive signals are assumed to fade independently and are combined at the receiver so that the resulting signal shows significantly reduced fading [27]. Receive diversity is characterized by the number of independent fading branches and it is at most equal to the number of receive antennas.

The key feature of all diversity methods is a low probability of simultaneous deep fades in the various diversity channels. In general, the system performance with diversity techniques depends on how many signal replicas are combined at the receiver to increase the overall SNR. We assume that CSI is known to the receiver in most cases, in reality, CSI is obtained by channel estimation involving training sequences [28] or by other methods [29].

At the receiver end, the data streams are combined using any of the combining techniques. There are mainly four generally employed diversity combining methods like switched combining (SWC), selection combining (SC), equal gain combining (EGC) and maximal ratio combining (MRC). In SWC, when the SNR of the currently selected signal drops below the threshold, the receiver switches to another antenna branch that satisfies the threshold criterion. In SWC all the diverse branches can share the same RF chain which makes it cost effective. However, since it does not checks all the branches, there is a possibility of a higher SNR branch unchecked. This possibility makes SWC less efficient method.

The selection combining is an improved method compared to the switched combining method. It monitors all the signal branches simultaneously, and chooses the one with highest SNR [22]. In equal gain combining, all the signals are added coherently [30]. The sum of the signal can be constructive or destructive, since there are phase difference between the branches, or in other words, the phase of the signals at each antenna element is not the same. To guarantee that all the branches are in phase, so as to have an output signal as the constructive sum of signals in all the branches, a phase compensation is added to each branch before combining [31]. The phase information of the channel is required at the receiver.

The most widely adopted combining scheme, is the maximal ratio combining (MRC). Here, replicas are first scaled in proportion to the signal-to-noise ratio of each replica, then are added together in the same way as they are added in equal gain combining [32]. Each diversity branch is weighted with its own complex conjugate, so that the phase difference is removed as in the equal gain combining method. At the same time, the branches with higher SNRs are provided with more weight. Thus we make maximum use of the efficient branches, and the optimal output signal is achieved.

However, MRC method has certain disadvantages too. When compared with the SC method, it is expensive to implement multiple RF chains in MRC. Also, a perfect channel knowledge including both the magnitude and the phase is required at the receiver, which is difficult to estimate in practice [33]. At low SNR scenarios, where the channel cannot be accurately estimated, the SC method can give a better performance than the MRC method.

1.2.1.2 Spatial Multiplexing

In addition to diversity techniques, MIMO technology includes spatial multiplexing technique, which makes uses of multiple antennas at both TX and RX for transmission of parallel data streams, to maximize the throughput of the system [2]. Using multiple antennas at both transmit and receive sides and with a scattering-rich channel, multiple spatial channels are generated to support the parallel transmission of multiple data streams [13]. This technique results in a higher data rate under comparable signal-to-noise ratio conditions.

SM can be performed with and without knowledge of the channel state information at the transmitter (i.e., closed loop and open loop). Block diagrams of MIMO system employing spatial multiplexing is shown in Figure 1.9. In the case of spatial multiplexing, the information error encoded bits are passed through a serial-to-parallel converter and the individual output streams are modulated before being transmitted over separate antennas. In other words, original data stream is multiplexed into several parallel streams, and sent through M_T transmit antennas.

At the receiver, each antenna receives a signal that contains the sum of the signals from all of the transmit antennas; therefore, it is necessary to separate each of the transmitted streams before demodulating them. An SM decoder or demultiplexer strips off each transmitted data stream from the combined received signal of all TX antennas. Zero-forcing and minimum mean square error based techniques are few of the commonly used spatial demultiplexing schemes.

In this case, the channel capacity or maximum achievable data rate for a system having M_T transmit antennas and M_R receive antennas, is expressed as in [14]:

$$C = MAX_{(tr(X_{ss})=M_T)} \; log_2 \; |(I_{M_R} + \frac{P}{M_T N_0} H X_{SS} H^*)| \qquad (1.21)$$

where X_{ss} denotes the co-variance matrix of x in equation (1.12) and must satisfy $tr(X_{ss}) = M_T$ to constrain the total transmitted power. P is the total transmitted power, N_0 is the noise power spectral density and I_{M_R} is an $M_R \times M_R$ identity matrix.
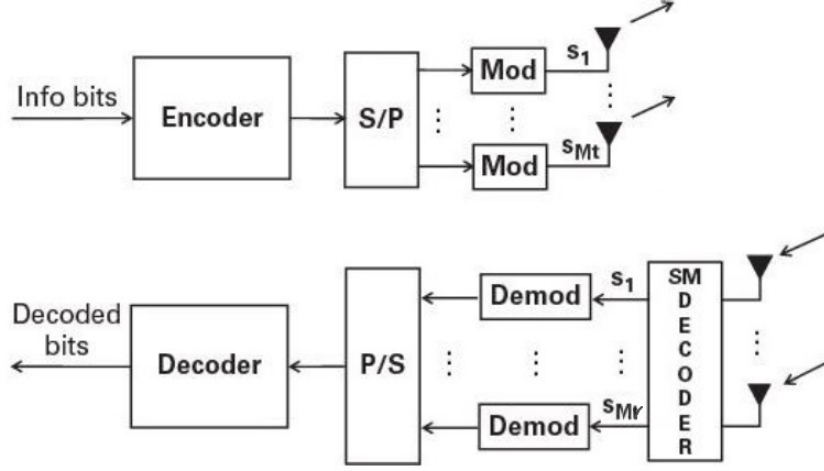
Figure 1.9: MIMO system for spatial multiplexing

When the channel information is not known to transmitter, the powers of M_T transmit antennas are equally distributed. The channel capacity of such a system is given by equation (1.14) i.e.

$$C = log_2(I_{M_R} + \frac{P}{M_T N_0} H H^*) \tag{1.22}$$

By applying the eigen value decomposition, the capacity given in equation (1.22) becomes,

$$C = \Sigma_{i=1}^{Mmin} log_2(1 + \frac{P}{M_T N_0} \lambda_i) bits/sec/Hz \tag{1.23}$$

where M_{min} is the rank of the channel and λ_i denotes the positive eigenvalues of HH^H.

From equation (1.23), it can be inferred that the channel capacity of a MIMO channel is the sum of the capacity of M_{min} SISO channels. When the TX and RX channels are placed very closely, and the direction of transmitted and received waveforms can not be distinguished from each other, the transfer function $h_{i,j}$ seen by all the antennas are identical. Thus the rank of the matrix HH^H is unity. In this case, $\lambda_i = M_T M_R$ and $\lambda_i(i \neq 1) = 0$. The channel capacity from equation (1.23) is computed as

$$C = log_2(1 + \frac{P}{N_0} M_R) \tag{1.24}$$

Compared with the capacity of the SISO system in equation (1.7), it is observed that the SNR is increased by a factor of M_R, i.e. a logarithmic increase occurs with an increase in the number of antenna elements. If both the antennas at TX and RX are separated far apart, so that the antenna elements can see different transfer functions, the channel matrix H is full rank. Under this condition assuming that $M_R = M_T = M$ and H is an orthogonal matrix satisfying $HH^* = H^*H$, the resulting channel capacity is given by

$$C = Mlog_2(1 + \frac{P}{N_0})$$

(1.25)

Here, in this case, channel capacity increases linearly with the number of antenna elements. On the other hand, when the channel information is known to the transmitter, the channel capacity can be further increased by assigning unequal power to the transmit antennas. A well known power allocation method is water filling. With this method, the best eigen modes of the propagation channel are selected, whereas the weaker channels are discarded, i.e. advantages are taken over the sub channels with higher gains [34–36].

1.2.1.3   Beamforming

In addition to diversity and spatial multiplexing techniques, beam forming technique is used to increase the coverage of the transmitter. Similar to antenna array techniques, beam forming focuses the radiation energy onto the receiver, improving signal quality. It also reduces interference to other users, enabling more simultaneous radio links at the same frequency. The receiver can operate in the conventional single-antenna mode in receiving operations.

However, the protocol design requires the channel state information to be obtained at the transmitter. If the position of the transmitter antenna is known, the receiver antenna array can form a pattern in the direction of the transmitter, resulting in a higher signal level at the receiver. The improvement in SNR thus increases the area that can be covered by the transmitter. Beam forming addresses the signal processing, rather than antenna design, as the beamforming antenna is also called a smart antenna. It increases coverage, by increasing the received SNR and reducing the interference.

In a receiver, the direction of arrival (DOA) of the signal is computed, based on the time delay of the received signal on the antenna elements. Then it adjusts the magnitude and the phase of the excitation signals of the antenna elements to produce a radiation pattern, which focuses its peak gain towards the signal of interest and turns the pattern nulls to the interferers. In the transmitter, the transmit signal is weighted, to make sure that the receiver obtains a constructive sum of different signal paths [37]. Channel knowledge is essential in beamforming. Generally speaking, the beamforming antenna is classified as fixed beam antenna and adaptive antenna. Their working principles are briefly introduced below.

A fixed beam antenna utilizes multiple antennas to form a limited discrete set of patterns. The beam giving the strongest SNR or SINR (signal to interference and noise ratio) can be selected through the switches after the signal detection. There are many different ways to realize the process of beam switching. For example, multiple directional antennas can be simply put together and oriented towards different directions. Then selections can be made between them.

A more popular and efficient method is the phased array. By changing the phase differences between the antenna elements, the main beam, which is very narrow, can be driven towards different directions as shown in Figure 1.10. One well-known beam switching network is the Butler matrix [38], [39], which works as a spatial Fourier transformation. The outputs of such a Fourier transformation are orthogonal beams pointing to different directions.

Different beams are chosen according to the position estimation of the users, hence better SNR at the user side is achieved. The switched beam antenna approach is simple and cost-effective; however, its flexibility is rather limited. Only a limited number of fixed directions can be selected, and thus there is a risk that the exact direction with the maximum achievable SNR could be missed. Another important drawback is that it only aims to enhance the received power at the user, but does not take into account the direction of interference. In other words, it is possible that the interference is also enhanced due to the lack of control of the beams.

The adaptive antenna system is introduced to solve the problem of beam accuracy and interference. With sophisticated signal processing in the base-
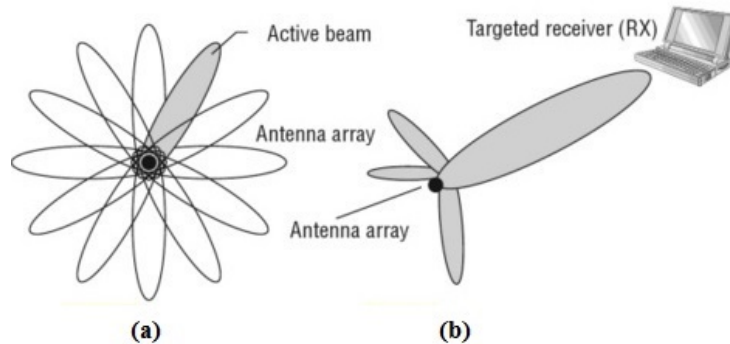
Figure 1.10: (a) Fixed (Switched) beamforming (b) Adaptive beamforming

band, the adaptive antennas distinguish between the desired signals and the interference, calculate the DOA and change the patterns to optimize the system performance [40]. The beam patterns can be varied dynamically and continuously in the adaptive antenna array with a very narrow beam width. Each user adjusts its beam pattern to ensure that there are nulls in the direction of other users while the directivity is maximum in the direction of the desired user.

The adaptive antenna system not only greatly enhances the received SNR at the user, but also turns its pattern nulls to the interference to suppress it (Figure 1.10). Hence, the coverage area is increased. Due to the accurate tracking and the interference rejection capabilities of the adaptive antenna system, multiple users can share the same conventional channel within the same cell. The adaptive array can simultaneously support two mobile users. This way, the system capacity is also increased.

To compare the two beam forming techniques, their coverage capabilities in scenarios with different interference levels are shown in Figure 1.11. The performance of the conventional sectorized antenna system is also described in the figure. The figure reveals that the adaptive antenna system always gives the best performance, followed by the switched beam antennas. The performances of both beam forming methods greatly exceed the conventional antenna system. In the scenarios with significant interference, the performance improvement of the adaptive arrays over the switched beam antennas

is more obvious due to its narrower beam width and the ability to reject the interference [41].
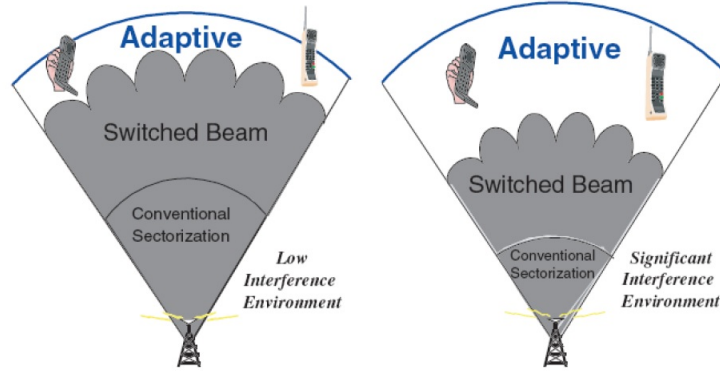
Figure 1.11: Coverage patterns for low interference and high interference region for conventional, fixed beamforming and adaptive beamforming systems

MIMO systems can be either point-to-point, i.e., single- user scenario or a multi-user scenario like in cellular systems as shown in Figure 1.12. Single-user MIMO refers to the basic MIMO technologies where there is no interaction between multiple wireless links. Table 1.1 summarizes some of the commercial wireless technologies that support single-user MIMO operations along with the number of data streams supported. Although there are some differences in details and supporting protocols across these technologies, the basic capabilities are similar. Multi-user MIMO (MU-MIMO) refers to the technology with which multiple users share the same time and frequency in transmission using MIMO technologies.

Some simple forms of MU-MIMO are already in use. Multi-user MIMO studies are more rigorous, as we need to consider multiple RX antennas, each of which represents one user. For example, LTE allows a base station to generate two beams optimized for two receivers. A radio receiver can decode its own beam with a low level of interference from the other beam. Such interference can be further reduced by smart scheduling in choosing the user pairs that are well separated in space channels.

LTE-advanced (LTE-A) increases the capacity to support up to four users. 802.11ac provides a similar capacity, where up to four data streams can be
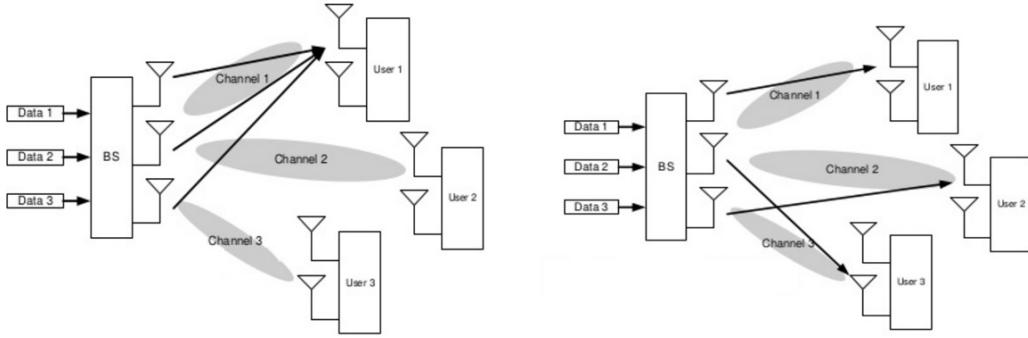
Figure 1.12: Single user and Multi-user MIMO systems

Standard	Max. No. of data streams supported	SD (SFBC/STBC)	BF
3G Cellular	2 DL	-	3
LTE	4 DL	DL	24
LTE-A	8 DL, 4 UL	DL	81
WiMAX	8 Dl, 4 UL	DL	192
802.11n	4	Yes	375
802.11ac	8	Yes	648

BF- beamforming; DL- downlink; SD- spatial diversity; SFBC-
space-frequency block coding; STBC- space-time block coding; UL- uplink.

Table 1.1: MIMO Technology used in various wireless standards

sent to up to four receivers (up to eight total streams) while each receiver can
receive single or multiple data streams. This type of MU-MIMO is actually
a special case of SM, with channel state information at the transmit side.
The transmitter can manipulate the signals to minimize mutual interference.
MU-MIMO can be used for receiving, as well. In this case, a base station can
simultaneously receive from multiple users while removing mutual interference
through receiver beamforming and multi-user detection (MUD).

1.3   Multiple-Antenna Systems

Investigations on multi-antenna architecture for multiple-input-multiple-output systems and its performance is the core research area outlined in this thesis. MIMO antenna systems are used in modern wireless standards, including IEEE 802.11n, IEEE 802.11ac, IEEE 802.11ad, 3GPP LTE, and WiMAX systems. The technique supports enhanced data throughput and high reliability even under conditions of interference, multipath and fading.

In multi-antenna systems, we can individually control the signals transmitted from each antenna and extract the individual signal information received at each antenna. The properties and features of multi-antenna systems are discussed in this section. Multiple antennas can be utilized at the TX and or RX to combat the fading through three different approaches, i.e. spatial diversity, polarization diversity and angle diversity as shown in Figure 1.13. Specifically we consider polarization and pattern diversity based antenna systems in this thesis contrary to generic spatial diversity based systems.

In spatial diversity, in order to achieve uncorrelated signals, a minimum mutual distance between antennas is required according to the fading environments [42, 43]. Polarization diversity is based on the different propagation characteristics of different polarization's, i.e. vertical polarization and horizontal polarization [44]. Pattern/angle diversity is achieved by shaping different radiation patterns for different antenna elements [45, 46]. The antenna diversity is studied in detail in the following section.

In spatial diversity, multiple antennas are separated by a distance. The magnitude of the antenna patterns is almost the same for each antenna, however the phase of the patterns relative to a common coordinate system are different. Multiple antennas on a terminal can be located in different positions around the handset so as to experience a different fading pattern in the radio environment. Thus the signals received by different antenna elements are different.

In order to achieve uncorrelated signals, a minimum mutual distance between antennas are required according to the fading environments. For example the minimum distance is several wavelengths at the base station in urban area [42] while it is half wavelength for a mobile terminal [43]. A frequently
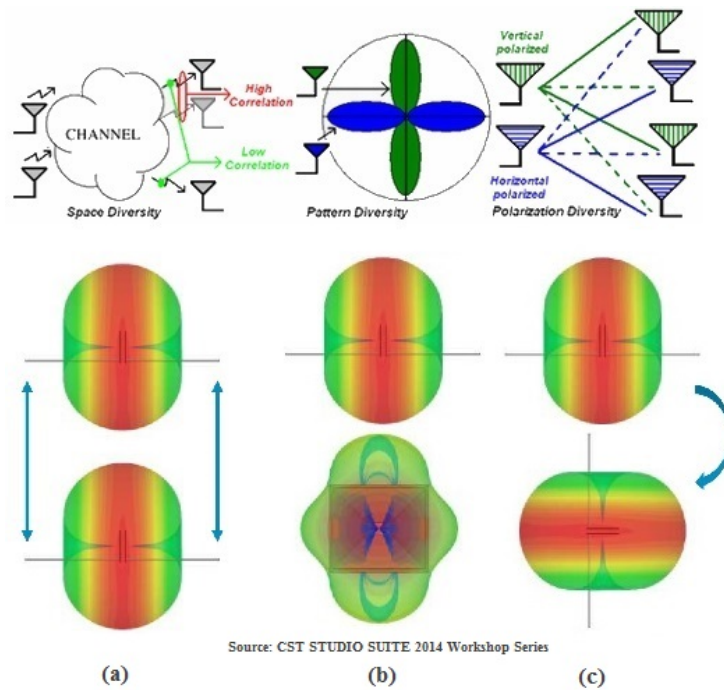
Figure 1.13: Types of Multi-Antenna systems (a) Space diversity (b) Pattern (angle) diversity (c) Polarization diversity

used criterion in antenna design is that in a uniform rich scattering environment, the spatial separation is at least half a wavelength. In electrically small antennas, the antenna elements would need to be as far apart as possible, i.e. in the corners. The theoretical optimum performance is obtained for a distance between the antennas of approximately 38% of a wavelength.

Early measurements on long-distance transmission revealed that propagation characteristics of a wireless medium are not the same for differently polarized waves. Additionally, multiple reflections between the TX and RX cause depolarization of the radio waves, thus dispersing some energy of the transmitted signal into other polarization directions. Due to that attribute, linearly polarized transmitted waves can come out at the RX end with an additional non-trivial orthogonal component. These observations motivated many researchers to investigate the fading statistics associated with radio signals received by antennas of various polarization modes.

Among the first, Glaser demonstrated that the vertical and horizontal

polarized components of the same received signal undergo almost statistically independent fading while propagating through certain wireless environments [47]. This fact has been utilized to improve radio system performance through the use of polarization diversity, where two or more spatially separated uni-polarized antennas are replaced by a single antenna structure (of almost co-located elements) employing multiple polarization's. Polarization diversity is based on the different propagation characteristics of different polarization, i.e. vertical polarization and horizontal polarization [44].

The simplest diversity systems of this kind utilize dual-polarized antennas with two orthogonal (i.e., co-polarized and cross-polarized) components, rendering them very handy for use in cellular radio networks, since antenna installation space is minimized and mobile terminals can experience reliable communication whatever the handset angle of tilt. Generally speaking, in a rich scattering environment, the signal from TX has varying polarization when it arrives at the RX due to reflection or diffraction paths. Thus, the SER performance can be improved by implementing two or more different polarized antennas at the RX and/or TX. It has been reported that polarization diversity performs better than spatial diversity when high multipath components are present [48].

Antenna pattern diversity comprises another form of exploiting the inherent degrees of freedom (DoF) of multipath propagation environment. The concept behind this approach lies in the relationship that holds between the received signal fluctuation and the direction of the main lobe of the RX antenna pattern. The first experimental results validating this statement were reported by [49] and [50], who found a remarkable reduction in fading by using a horizontal rhombic antenna with an extremely sharp directional pattern. The success of their attempt was based on the existence of stable angular separation among signal components following different paths, thus enabling a steerable antenna with sufficiently sharp directivity to accept only one of them (maybe the best after some calibration) at any time.

The qualitative relation between angles of arrival and propagation delays of the received signal components was clearly demonstrated by Friss in [51]. It explains that the greater the delay the greater the angle above the horizontal

(azimuth plane). He exploited this phenomenon with the aid of a special arrangement whereby individual wave groups arriving at different vertical angles were received separately and, after delay equalization, combined coherently to offer directional diversity or directivity diversity [52].

Later, Vogelman extended the concept of a single beam steerable to a multi-beam antenna, where signal components associated with individual beams were particularly combined to offer angle diversity or angle-of-arrival diversity [53]. However, the effectiveness of this system depends upon the antenna characteristics, which have to be properly chosen so that the angle between adjacent beams are always smaller than the angular spread of the channel and that low correlation among different beams is ensured.

Obviously, pattern diversity can also be provided via several antennas with diverse patterns spaced apart from each other. Additionally, field component diversity, first proposed by Edgar Gilbert (1965), utilizes sophisticated energy density antenna arrangements to receive uncorrelated electric and magnetic field components of the transmitted signal so as to reduce fading in mobile radio. Angle diversity is achieved by shaping different radiation patterns for different antenna elements. In this case, several directional antennas face totally different directions, enabling the collection of multiple independent replica of the same signal.

The pattern diversity at the base station is compared with spatial diversity [45], and it is shown that the performance of angular diversity is similar to that of spatial diversity, especially in dense urban areas [46]. For mobile terminals, due to the mutual coupling effect, one antenna acts as the parasitic element to the other, and the radiation patterns of the two closely packed antennas are automatically altered and directed to different angles. It is worth noticing that this kind of angle diversity comes at the expense of antenna efficiency, which is attributed to mutual coupling. The three diversity techniques mentioned above can be used together in antenna design to achieve an optimal performance.

1.4   Motivation of Research

In the light of the description of the current wireless networks, one can conclude that in spite of significant improvement on the establishment of wireless services, there is an underlying strong demand for higher date rate wireless services, mainly driven by wireless data applications, as well as users expectation of wire-equivalent quality wireless service. Wireless communications have supported a plethora of novel applications in recent years thanks to the continuous research efforts to increase the spectral efficiency and energy efficiency of wireless networks.

Multi-antenna technology plays a crucial part towards achieving these accomplishments. In fact, MIMO has been adopted in current and future standards, including WiMAX (Worldwide Interoperability for Microwave Access) IEEE 802.16m [54], WLAN IEEE 802.11n [55], and 3GPP LTE/LTE-Advanced [56], [57]. MIMO has grown much beyond the original point-to-point channel and can nowadays refer to a diverse range of centralized and distributed deployments like multi-cell MIMO, distributed MIMO, massive MIMO and network MIMO.

Providing a high-rate high-quality wireless services is extremely challenging, due to the inherent harsh wireless propagation environment. For a better and more efficient spectrum utilization in future wireless communication, novel antenna designs are to be integrated with MIMO systems to provide efficient wireless communication. The design of multi-antenna systems is very challenging especially at the user terminal side, where the size is a big constraint. Integration and coupling of elements, as well as good gain and efficiency are among the current challenges for designing multi-element antenna.

Consequently, a MIMO antenna designed for future wireless systems is expected to be much reliable, with highly efficient individual elements, a good coverage of required frequency bands, and very low coupling between the individual elements which ensures a low correlation between the waveforms. Isolation between the ports is very important in multi-port and multi antenna systems. If the isolation is poor, some of the energy fed or received by one port will couple to the other thus degrading the antenna and system efficiency, as

the coupled power is effectively lost from the receiving path. So, port isolation is very important in MIMO antenna systems.

Antennas are responsible for emitting electromagnetic (EM) waves in the propagation environment and are therefore crucial for successful wireless transmissions. Key factors in designing antennas are efficiency, directivity, polarization, bandwidth and size, whereas optimum designs are often tradeoffs between these crucial parameters depending on the requirements of the system. In the context of handsets, the size and bandwidth requirements are so stringent that often efficiency is sacrificed to fulfill specifications. Moreover, due to their application, terminal antennas are required to operate in challenging conditions for efficient EM wave propagation such as close proximity to biological tissues (users body) and random propagation environments. When designing a multiple antenna system the following should be considered:

- Antennas should be oriented so that the individual element pattern should face in a direction where other elements have a low gain pattern, i.e. correlation between elements must be very low.

- Coupling via common sharing currents like surface waves and space waves should be minimized either by antenna design or by the introduction of additional features to inhibit current flow.

- For practical integration to a wireless device the antennas need to perform with a compact size, having a planar structure, and need to resonate over the operating range of the system, a few times supporting multiple wireless standards.

Among a variety of MIMO antennas, antenna diversity selection has proved to be a promising approach for efficient and compact systems. For orientation of multiple elements of antenna, polarization and pattern diversities is given more focus compared to conventional spatial diversity approach. This technique requires only very less implementation space and has inherently high isolation, compared to spatially separated antenna elements. Also, antenna system must be robust to coupling errors because this may cause loss of information and cannot take full advantage of multiple antenna elements.

Some research works have considered antenna arrays [58, 59] for multi-element systems in the literature. However, these studies only investigated the systems from either capacity or isolation perspective. Consequently, it is unknown if the existing antenna design approaches are optimal in terms of compactness. In addition, some recent works on efficient high performance MIMO systems [60, 61], focused only on spatial multiplexing of antenna elements, which again did not address concerns on compactness.

Consequently, efficient antenna design for MIMO systems remains as challenge in view of compactness, wide bandwidth or multiband resonances required and high isolation between elements. Motivated by this, the thesis focuses on investigating highly performing multi-antenna systems. It aims to propose and analyze novel antenna designs for improved performance. The methodology for evaluating the performances of MIMO antenna, along with simulation and measurement techniques adopted for validating the MIMO performances, will be discussed in Chapter 2.

1.5   Thesis Organization

The thesis presents the simulation and experimental studies of advanced multi-antenna design and measurements techniques for MIMO antenna systems. The Introduction chapter discusses the basic trends in wireless communication and its evolution. The technological advances in the wireless communication and the need for integrating multiple antennas on transmitter and receiver is discussed next. Considering the significance of MIMO communication in modern wireless communication, a study of channel capacities of different configuration of SISO and MIMO are explained. MIMO technology demonstrating the major techniques like diversity, spatial multiplexing and beamforming are discussed. Multiple antenna systems based on various forms of diversity, which are of great relevance to this research work is briefed in the next section. Towards the end of this chapter motivation for the present research work is also provided.

The next chapter details the methodology used for design, simulation, fabrication, measurements and validating the performances of the developed

MIMO antennas. The factors effecting the design and performance of MIMO is discussed in detail. Performance characteristics of the MIMO antennas are investigated using various figure of merit parameters. The methodology for developing the antennas discussed involves electromagnetic modelling and simulation studies performed using CST Microwave Studio. Fabrication method adopted for the manufacturing of antennas is discussed in the following section. The experimental techniques used to measure the fabricated antennas for its impedance, radiation and MIMO performance are explained.

In Chapter 3, the experimental and theoretical investigations are carried out for the analysis of multimode quad element MIMO antenna designs based on polarization and pattern diversity techniques. A brief discussion of the literature available for multimode MIMO antennas is portrayed. Three configurations of multimodal collocated MIMO antenna designs based on microstrip patches are studied in detail. The coupling in the multi-antennas systems are analyzed. Accordingly, three novel decoupling structures are analyzed, discussed and compared for use in multi-antenna systems. Specific examples of proposed multimode MIMO antennas are taken to better illustrate the isolation enhancement mechanisms. Isolation and impedance characteristics of the MIMO antennas are analyzed and compared. The effectiveness of the isolation enhancement techniques in reducing surface wave coupling is analyzed in detail. The structures can be used interchangeably in the proposed MIMO antennas which demonstrates its generic applicability and can be compared for the best isolation performance. Diversity performances of the proposed configurations are studied in detail for validating the effectiveness of the antenna for use in multi-antenna systems for MIMO communication.

The advantages of polarization diversity based antennas for its equal and efficient performance of all the antenna branches is very clear. The major limitation in practical MIMO antenna design is to obtain highly efficient decorrelated antennas to support multiple wireless standards, which can be incorporated in a compact package. Keeping this in mind, the state-of-the-art of antenna designs for a tri-band and a wideband quad element MIMO antenna system is designed and analyzed in chapter 4. Isolation is improved between elements exhibiting higher coupling, by incorporating stop band structure. The antennas are very beneficial for its high performance in terms of impedance,

isolation, far field radiation and MIMO diversity performance. The antennas are very compact and find application in multiple wireless standards which are of great importance.

In chapter 5, MIMO channel performances of the above quad element antennas are demonstrated using two different channel models. Various MIMO channel performance parameters like channel capacity, channel throughput and block error rate is obtained at varying SNR conditions for all the quad element antenna designs. A comparison with SISO and other 2×2, 3×3 antenna combinations are made, to validate the advantage of using multiple antennas in terms of achieving higher channel performances. Polarization diversity based designs with highly efficient antenna elements have slightly higher performance compared to multimode MIMO antennas using a combination of polarization and pattern diversity.

Chapter 7 presents the conclusion of the thesis work and some thoughts for the future research.

Chapter 2

Methodology

Contents

This chapter presents a detailed account of design techniques, simulations, fabrication and measurement performed for characterizing MIMO antennas. The design guidelines with the major design challenges for multiple antenna systems are addressed. An in-depth study of the various methods or techniques for analyzing the MIMO performance of the multiple antenna elements is discussed. This includes methods to determine and enhance both the isolation performance as well as the diversity performance between the multiple elements. The over the air (OTA) performance of the multiple antenna systems in a wireless communication channel determines whether the performance of the MIMO antenna meets applicable standards in a wireless system.

The antenna simulation studies are carried out using CST Microwave Studio Software. The design of multiple antenna elements is parametrically analyzed for its reflection characteristics. This, along with the radiation pattern and current distribution studies, enables a better understanding of their behavior and the formulation of design guidelines. The MIMO performances are analyzed from transmission characteristics as well as from the correlation between the various antenna elements. The MIMO antennas are then fabricated on microwave laminates using photolithography. The characteristics of the fabricated prototype are measured using Vector Network Analyzer in an anechoic chamber available in the in-house test facility.

2.1 Guidelines for MIMO Antenna Design

This section explains the design procedure of MIMO antennas for various applications. It is desirable to have a defined, systematic procedure according to the specific requirements. This can be accomplished by adopting a few methods. The foremost approach is to have a precise information on the required antenna specifications and performance criteria. This will include information on the number of antennas required, its size, the standard or frequency band in which it needs to operate, as well as how the antenna is placed on the MIMO terminal. The number of antenna elements required as well as the location of the elements in the multiple antenna systems is evaluated by means of various MIMO system metrics. The spacing between the antenna elements has a major role in determining the isolation or the mutual coupling between the elements.

In the design phase, it is better to start with a known antenna type. Choosing a known antenna type, suitable for the particular application is a good practice, as the designer will have a better understanding of the basic working principle of the antenna. The simulation software tool is also a major step as this needs to include all the modeling techniques and studies required for the particular antenna. A good understanding of the software eases the design process. Parametric studies in the simulation tool help to get a clear picture of the antenna behavior for various dimensions. An advanced testing software

provides an optimizing method to simulate the antenna properties for any testing conditions and applications. It also helps to use and apply techniques to improve antenna performances like say for example miniaturization of the antenna or reduction of mutual coupling between closely spaced elements etc.

The coupling between neighboring elements in the design of a MIMO antenna, if not kept within acceptable limits, will reduce the efficiency of the antenna elements. The coupling can also increase the correlation between neighboring antenna elements, which again affect the MIMO diversity performance of the antenna. Generally, if the coupling is higher, isolation enhancement structures need to be designed, considering the geometry and the radiation properties of the main antenna. The structure is designed after investigating the cause for coupling and planning techniques, which alleviate the cause of coupling.

Another significant parameter in the MIMO antenna design is the correlation coefficient. The antenna elements should have high efficiency and maintain a low correlation between its waveforms, to ensure good MIMO diversity performance. Generally, correlation can be reduced by adopting some forms of diversity or by designing decorrelation structures. At lower frequencies, the geometry allows sufficient spacing between antenna elements, which reduces mutual coupling and can provide low correlation too. However, at higher frequencies, the compact antenna has closely spaced elements which have a high correlation between its patterns. Achieving low correlation in such cases is a challenge and needs smart designing of the antenna or the decorrelation structure to keep correlation within acceptable limits.

Once the antenna design is optimized using the simulation software, the fabrication process is initiated. The prototype antenna fabrication is the major step involved. The measurements obtained from the prototype helps to identify if there are any discrepancies between the simulated and measured antenna properties. The major parameters measured for a MIMO antenna include reflection characteristics, transmission characteristics, far-field radiation patterns, envelope correlation coefficient, gain, efficiency etc. If there are significant differences between the measured and simulated results, further investigations are required in the design and tuning of the antennas, to obtain optimized results.

2.2   MIMO Antenna Performance Measures

MIMO technology has been widely used in several existing wireless standards like IEEE 802.11n [62], IEEE 802.11ac [63], WiMAX [64] and LTE [65]. For efficient functioning of diversity based MIMO systems as well as other identical multiple antenna techniques, the signals transmitted or received at the multiple antenna elements have to be different. This implies that the signals should be uncorrelated and is independent of each other. In other words, the following properties are required for the MIMO antenna

1. The signals transmitted by various diverse transmitter antenna elements should take multiple paths on their travel.

2. The multiple antenna receivers should be capable of receiving the diverse signals without significantly reducing their uniqueness.

In practical design of MIMO antennas, three forms of diversity like spatial, polarization and pattern diversity can be incorporated between the elements. Generally, a combination of the diversity techniques assures a perfect multi-element diversity system, although polarization diversity has a weightage among the three techniques.

The finest choice of diversity system is a function of the behavior of the propagation path between the transmitter and receiver, mainly the extent of polarization scattering and the angular power spread of the received signal components. In the MIMO communication system, propagation is distinct with a wide angular separation between the elements of the received signal, hence, pattern diversity is essentially present. Some polarization scattering is also common, so polarization diversity can also add to the channel performance. In any case, when two antenna elements are present, a choice has to be made between the types of diversity techniques. When the number of antennas employed in a MIMO system increases to four or more, there is little choice but to optimize all three types of diversity. Effective diversity performance between multiple antenna elements depends on numerous design factors. A few of their characteristics are listed below.

- Coupling between the antenna elements must be minimized.

- The multiple antenna systems must be as efficient as a single antenna, else the diversity gain of the system will be unused.

- The antennas must be electrically small to decrease the interaction between them.

- The antennas must have correctly matched terminations.

- The directivity of the antennas should be controllable to some extent.

- The antennas must have an appreciable level of cross-polar discrimination.

- The elements of multi antenna system ought to exhibit spatially diverse radiation patterns.

2.2.1   Isolation Performance

Isolation performances of the antenna system or mutual coupling between antenna elements is a very significant factor for achieving antenna diversity, which needs to be maintained at permissible levels in the design stage of a multiple antenna system. In a diversity antenna solution, mutual coupling increases the correlation between the elements and reduces the radiation efficiency of the system [66]. An increase in correlation between ports in the multiple antenna systems, adversely affects the diversity gain of the elements.

The complex cross correlation between the two waveforms for a two element system can be attained from the transmission coefficient or the mutual coupling between the two antenna ports [67], $\rho_c = r_{12}$, where r_{12} is the mutual resistance between port 1 and port 2 normalized by the input resistance of port 1. There are several factors effecting the mutual coupling between elements like polarization, size of the antennas, antenna separation, power pattern, surface wave propagation and ground plane currents etc. A brief analysis of these factors effecting the isolation performances of a multiple antenna system is provided.

Designing and building antennas with single polarization are challenging, as there are only a few types of antennas that generate circular or elliptical polarized waves. Moreover, most of these designs are large in size, and hence find

very less application in compact wireless terminals. Linearly polarized wave are much easier to generate and are obtained from most common antennas. Symmetrical structures can produce polarization pure antennas, however, this is not practically feasible sometimes, because of the complication of printed circuit board (PCB) and other internal circuitry.

The polarization of most of the antennas will be of a mixed type or not fully pure, i.e. polarization will be strong or more biased in some parts of the antenna pattern. This can be taken advantage of in multi-antenna systems, by integrating the antennas in such a way that the directions of maximum polarization biasing are positioned orthogonally, thereby enhancing the isolation performance between elements. Orthogonally polarized waves can be formed by two linearly polarized waves, rotated 90 degrees with respect to each other. These waves do not interact with each other and therefore will be highly isolated from one another. The left hand and right hand circularly polarized waves are also orthogonal to each other. Likewise, there is a continuum of orthogonally polarized waves, few of which are mentioned in Poincare sphere diagram of polarization [68].

The spacing between the antennas and the power pattern are other significant factors which effect the isolation characteristics of antennas. Minimum size of an antenna for a given frequency, bandwidth and efficiency is set by Chu - Harrington limit [69], [70]. This theory also talks about antenna polarization and states that orthogonal polarization being independent to each other, restricting to a single polarization will result in an increase in the size of the antenna.

The coupling between two widely separated antennas is obtained from the path loss equation in (1.3). When the spacing between the antennas is less, reactive near field of the antenna also contributes to coupling. The direction of the maximum reactive field can be different from the direction of maximum far field gain. Furthermore, the strength of reactive near field which contributes to coupling, drops much faster with distance when compared to far-field coupling. If a large portion of the ground plane is used for radiation, this is likely to increase the size of the reactive near field.

2.2.1.1   Isolation Enhancement Techniques

A brief review of the literature on mutual coupling reduction discussed here, analyzes various reported isolation enhancement techniques implemented in MIMO antenna systems. It is difficult to evaluate and compare the mutual coupling reduction techniques used in a MIMO antenna, due to the conflicting individual characteristics (such as operating frequency, antenna area, and the achieved isolation value). Different structures which have the capability to provide low coupling is discussed along with the study of proposed structures which can guarantee low mutual coupling. Few techniques which by default can ensure good isolation between elements include

- Orthogonal polarization

- CPW feeding technique

- Directly connecting antenna elements

Structures which are included additionally to enhance isolation can be generally classified in to

- Defected ground structure (DGS)

- Metamaterial

- Electromagnetic Band Gap (EBG) Structures

- Localization of ground currents

- Decoupling networks

- Neutralization line

- Parasitic elements

Each of these techniques employed in reducing mutual coupling is analyzed in detail.

Orthogonal Polarization:
The mutual coupling between two antenna elements was reduced by 20 - 30

dB [71], by arranging them orthogonally so that the two antenna elements have orthogonal polarization's. The antenna can have good bandwidth and very high isolation using this technique. Though polarization is unpredictable for mobile like wireless communication due to multipath signals and the changes in the positioning of hand held device, it is beneficial that the method does not require any extra bandwidth or physical separations between the antennas. In collocated multi-antenna systems, where it is difficult to add any decoupling structures between the antenna elements, orthogonal polarization becomes the most efficient decoupling method [72,73]. This guarantees diverse antenna elements with low cross polarization levels and diverse patterns.

CPW-Feeding Technique:
Printed antennas with CPW feeds when compared with other printed resonating elements, have a better bandwidth and an improved isolation between adjacent lines. An additional benefit is the easiness of integration with solid state active devices [74–76]. Hence, these antenna elements are well suited for MIMO applications [77]. CPW-fed MIMO antenna in [78] have elements with isolation greater than 25 dB over all the quad bands. An 8 element MIMO antenna array using this technique has achieved a mutual coupling reduction of 22 dB to 51 dB [77]. A dual band quad element MIMO antenna configuration using this feeding technique has reported an isolation greater than 20 dB [79].

Directly connecting antenna elements:
This technique includes a direction connection between the two antenna elements. Thus the current induced from an antenna element passes through the direct connection to the other element rather than through the load [80]. By adjusting the length and position of the direct connection, isolation can be improved. This allows multiple antenna elements to be placed within small and compact terminals, while retaining the adequate isolation between antenna elements [80,81].

Defected Ground Structure (DGS):
The name defected ground plane explains itself, and it is easy to understand

its working principles. It introduces changes in the ground plane to vary the current distribution and surface waves on it. In the conventional antenna design, it has been utilized to suppress harmonics and cross polarization of a patch antenna [82]. It was also used to improve the isolation of a dual-polarized patch antenna [83]. In a multi-element MIMO antenna, it acts as a band-stop filter to reduce the mutual coupling between antenna elements [84]. A common realization is to introduce multiple slits on the ground plane [85–91].

A variety of isolation improvement techniques has been investigated in [92], by designing the ground plane structure. It has been proved that both return loss and isolation can be simultaneously enhanced by appropriate designing of the ground plane structure. The DGS can generally provide both slow wave and stop band characteristics [93, 94]. Defected ground structures designed as a slow wave structure increases the electrical length, thereby increasing the separation between antenna elements [93]. Slots can also be designed as a stop band filter to reduce coupling [94] or to function as a resonator which suppresses surface waves by radiating them to space [95].

Metamaterials:
Metamaterials are engineered materials that are capable of achieving properties such as negative values of permittivity or permeability, which are not normally found in nature. These materials are typically configured by periodically arranging a basic unit element structure. Metamaterials can act as a stop band filter, and this property is exploited to reduce mutual coupling between closely packed antenna elements. The stop band frequency is tuned to the desired resonant frequency of the antennas, to inhibit the flow of coupling currents [96, 97]. An isolation greater than 15 dB is achieved using metamaterial in the 3.5 GHz band [97].

EBG Structure:
Electromagnetic band-gap (EBG) structure [98–101] behaves as the bandstop filter in the antenna decoupling. It is constructed by arranging the cells periodically. A typical EBG cell is a mushroom structure, consisting of a patch

and a via connecting to the ground. The EBG structure can operate as a magnetic wall by which the reflection phase becomes zero for an incident wave, and thus the surface wave propagation is suppressed. The EBG structure can provide a wide stopband with high attenuation. An isolation improvement of over 10 dB can be achieved at the resonant frequency [101]. However, for lower frequencies, a higher circuit area is necessary for an EBG structure due to the Bragg reflection condition constraints [89]. This limits its application due to complexity in practical compact terminals.

Current localization technique:
Current distribution on the shared ground plane is a critical coupling source in the multi-element antenna system. Unlike the DGS method which forms a bandstop filter to trap the current, and prevents it from flowing to the other antennas, the current localization structure aims to reduce the current distributed on the ground plane from the perspective of the antenna itself, i.e., designing antennas with the capability of current localization [102–104].

An efficient method to localize the current induced by the antenna to the confined local ground is by using a small local ground plane that is separated from the main ground. The antenna configuration [104] has a PIFA element, which is modified by introducing a small local ground plane between the PIFA and the main ground plane. An isolation greater than 20 dB is achieved by localizing the current beneath the antenna itself, rather than dispensing it along the whole ground plane [105].

Decoupling Network:
The motivation of the decoupling network is to reduce the mutual impedance or transmission coefficients between antennas to zero and at the same time keep good impedance matching for each antenna element. Some design approaches for the decoupling matching networks are described in [28, 106–108]. Decoupling networks can be made by arranging lumped elements like inductors and capacitors [109, 110], or by using distributed elements [106]. Few other realizations of decoupling networks include decoupler line [87, 106] and using 180^0 hybrid coupler [111–114].

Neutralization Line:

The neutralization line technique is a simple and compact structure mostly used to decouple two PIFA antennas [115–117]. It is an electrical connection between the feeds or the shorting strips of PIFA. It helps in decoupling two elements by trapping the coupling currents flowing from one antenna element to another. The distributed transmission line acts as a new current path, creating more choice for decoupling. In one such design, the neutralization line alters the current distribution making the two ports to excite orthogonal modes with an improved isolation between the elements [118].

The line length and dimensions can be adjusted to cancel the coupling currents at the other port. A 2 dB improvement in diversity gain is achieved by using a neutralization line which enhances isolation by 8 dB [115]. The folded monopole designed for WLAN band shows a diversity gain of 9.95 dB with neutralization line [119]. This also helps in reducing the distance between PIFA elements [117].

Parasitic Scatterer:

A parasitic scatterer like a neutralization creates an additional coupling path between the elements with which it is added to reduce mutual coupling between them [120–124]. In single element antennas, these structures find applications in either improving bandwidth by creating multiple resonances [125] or for designing pattern reconfigurable antennas [126]. In multiple antenna systems, the structure reduces mutual coupling and can be tuned by adjusting the structure dimensions.

Its working mechanism can be explained by using the parameter named mutual impedance, one such investigation is performed for dipole antennas [121]. The mutual distance between radiating antennas was reduced up to 0.0294λ [123]. The port isolation can be enhanced from 3.5 dB to 25 dB with a parasitic element [124]. The structure of the parasitic elements needs to be specifically designed for different multiple antenna systems. Even though only the distance between the antennas is changed, it is necessary to alter the structure of the scatterer, in order to get efficient decoupling. This characteristic limits the application of the parasitic element in the mass production.

Mutual coupling between antennas is considered as a critical parameter, as it has been identified that channel capacity too can be influenced by antenna coupling. On the other hand, low coupling does not always mean low correlation. For example, a combination of collinear dipoles has low mutual coupling between them as they do not radiate into each other. However, they have a high correlation between them, as both of them have same beam and polarization characteristics.

In conclusion, the realization of multiple antenna systems should ensure that the degree of coupling between them can be controlled to suit the application. Usually, designers introduce an isolation enhancement method to increase port isolation. These methods can be chosen from any of the above discussed techniques ranging from adopting orthogonally polarized elements, to use of DGS, use of parasitic or lumped elements, distributed elements, neutralization lines metamaterials or EBGs. The designer should decide, which method is more suitable to his/her design, based on the antenna type and radiation mechanism. For novel antennas designs, innovative isolation enhancement structures can be developed based on any of these existing techniques which still offers a plethora of research opportunities.

2.2.2   Diversity Performance

A multiple antenna system can operate in diversity or multiplexing schemes according to the signal to noise ratio level in a rich scattering environment. Antenna diversity can be employed to combat fading in low SNR levels. Here multiple antennas (TX) transmit the same information over the channel and all the receivers (RX) receive the same information. By incorporating diversity in the antennas, signals are uncorrelated, and the chances of fading deeps are significantly reduced. Thus the reliability of wireless communication link increases.

If the SNR is high, multiple antennas can be used to create spatial multiplexing which makes advantage of the channel fading by creating several uncorrelated channels. Different data are then transmitted over these channels at the same operating frequency simultaneously to achieve maximum data rate. This section discusses the figure of merits of multiple antenna systems

which can evaluate MIMO and diversity performances. The characteristics of an individual antenna like impedance, gain, bandwidth, efficiency and radiation pattern are not discussed here, but are elaborated in section 2.5.

2.2.2.1   MIMO Diversity Quality Measures

Envelope Correlation Coefficient (ECC)
To achieve good MIMO multiplexing performance, the envelope correlation coefficient has to be kept very low. Apart from this, the total efficiency should be maintained very high. To accomplish these requirements in a compact multiple antenna system is a great challenge, considering the small space available in the terminals, where elements are placed closely to each other. The maximum space between the elements can be obtained by placing the elements at the extreme edges of the wireless terminal.

In low frequency bands, a low correlation coefficient can be achieved by increasing the isolation between the antenna elements, by adopting any of the isolation enhancement techniques and designing antenna elements with maximum diversity, having radiation patterns oriented in different directions. For higher frequencies, antenna elements are too close so that, they will have mostly identical patterns and hence correlation will be high. The design of a compact antenna and its de-correlation structure in such cases is a challenging task, as these structures will be too close to the antenna elements.

A general rule of thumb to design antennas with spatial diversity is to allow at least a half wavelength separation between antenna elements. This guarantees an envelope correlation less than or equal to 0.5, which is good enough to provide high diversity gain. The relationship between envelope correlation $\rho_{i,j}$ and separation between antennas is given by Clarke [127] as

$$\rho_{i,j} \cong J_0^2 \left(\frac{2 * pi * d}{\lambda} \right) \tag{2.1}$$

where J_0 is the Bessel function of the first kind with order zero, d is the antenna spacing, and λ is the wavelength. This expression holds true for a uniform angle of arrival distribution in azimuth plane and identically polarized omnidirectional receiving antennas that are matched to the polarization of

the incoming wave. It is assumed that all the multipath components lie in the horizontal plane. It can be said that, the correlation predicted by this formula is in general higher than in reality, mainly for smaller separations. This is due to the fact that the formula does not take into consideration the mutual coupling between the antenna elements at a given distance.

A practical MIMO antenna should have a low signal correlation between the antenna elements and good matching features for input impedance [128]. The envelope correlation coefficient describes how independent is the signal, from signals of other ports in the multi-element system. If one antenna element is completely horizontally polarized, and the other is completely vertically polarized, then the two antennas will have a correlation of zero.

A simple derivation in [129] shows that the envelope correlation coefficient can be calculated from S parameters for a loss-less single mode antenna by

$$|\rho_{ij}| = |\frac{|S_{ii}^* S_{ij} + S_{ji}^* S_{jj}|}{|(1 - |S_{ii}|^2 - |S_{ji}|^2)(1 - |S_{jj}|^2 - |S_{ij}|^2)\eta_{radi}\eta_{radj}|^{0.5}}|^2 \qquad (2.2)$$

where ρ_{ij} is the correlation coefficient between antenna element i and j, S_{ij} is the transmission coefficient or coupling between antenna element i and j and η_{radi} and η_{radj} are the radiation efficiencies of antenna elements i and j respectively. The effect of efficiency on ECC is given by [130]. This is derived from the fact that if two antennas produce highly correlated radiation patterns they will possibly have high coupling between them. This is due to the reciprocity property of antennas exhibiting same property for transmitter and receiver, so if TX antenna is transmitting a radiation pattern, RX antenna will receive energy proportional to how correlated the antennas radiation patterns are. But these are subjected to certain conditions which include

- Antennas are assumed to be lossless, i.e. antennas are of high radiation efficiency and low mutual losses

- Antennas are placed in a uniform multi path environment, which is an ideal case

Computation of the envelope correlation coefficient for a real world antenna using this S parameter equation may lead to a big uncertainty: the more losses the antennas have, the larger this uncertainty will become. However,

it has also been shown that this uncertainty could be drastically reduced if
the radiators are well matched and well isolated [131]. All these limitations
clearly demonstrate that in real antenna systems, the envelope correlation
coefficient calculated from the S_{ij} parameters give only the lowest value that
can be reached, rather than an exact value. However, it is simple to calculate
and thus can be used as a first approximation of the diversity performances
of a multi-antenna structure.

A more accurate computation of envelope correlation coefficient of a MIMO
antenna takes in to consideration the shape of the radiation patterns of the
antenna elements, the polarization's of the elements as well as the relative
phase of the fields between the elements. ECC is mathematically computed
from the vector distribution of the far field radiation patterns of the antenna
elements under consideration, in a spherical coordinate system [129, 132].

$$\rho_e = \frac{|\int\int_{4\pi} |\overrightarrow{F_1}(\theta,\phi) * \overrightarrow{F_2}(\theta,\phi)]d\Omega|^2}{\int\int_{4\pi} |\overrightarrow{F_1}(\theta,\phi)|^2 d\Omega \ \int\int_{4\pi} |\overrightarrow{F_2}(\theta,\phi)|^2 d\Omega} \tag{2.3}$$

where (θ, ϕ) represents the spherical angles in elevation and azimuth, $F_1(\theta, \phi)$
is the three dimensional far field radiation pattern of the antenna when i^{th}
port is excited and all other ports are terminated with matched load, Ω is
the solid angle and $*$ is the Hermitian product operator. It is a complicated
expression and requires the three dimensional radiation pattern measurements
and numerical integration. This equation is valid for an isotropic environment
where multiple paths are uniform and polarizations are balanced.

ECC computed from radiation fields is a better measure as it is based on
actual fields that affect the channel directly. Equation (2.3) is a measure of
how correlated the radiation patterns of two different antennas are. If they
are the exactly similar i.e. $\overrightarrow{F_1} = \overrightarrow{F_2}$, then the ECC would be unity. If they are
entirely independent, the correlation would be zero. It can be recalled that
an ECC of 0.5 is permissible for MIMO applications [133].

Different solutions to the high correlation problem have been reported
recently. The use of neutralization lines is one of the most promising ways of
getting a low correlation, given that the patterns are also not overlapping [134].
Also decoupling networks located after the ports can be an efficient way of
doing it, but can have problems due to high losses [135]. Another interesting

approach is to optimize the Q factor of the individual antennas as proposed in [136]. In general, ECC can be reduced by adopting any of the following techniques

- Increased distance between the antennas, can enhance the isolation and reduce correlation. This is due to the fact that the relative phase between them is not constant. Hence, even if alike antennas, which are oriented in the same direction, are used, ECC can be ensured to be low for the large spacing between elements. It is generally preferred to have at least half wave length separation between antenna elements.

- Polarizations are preferred to be orthogonal or different, in the sense that if one antenna is vertically polarized, the other element is preferred to be horizontal, thus maintaining low correlation coefficient

- Peak radiation directions are kept separate, so that antennas with minimal spacing and identical orientation too can ensure low ECC.

Diversity Gain (DG)

Diversity is an efficient means of combating channel fading. The overall link reliability can be enhanced by receiving multiple independent copies of the transmitted signal at the receiver. In multiple antenna systems, this is achieved by employing spatial diversity or by maintaining low coupling between the antenna elements (by using polarization or pattern diversity). This includes both the receive diversity as well as transmit diversity described in subsection 1.2.1. The received signal will then be uncorrelated on the two antennas, and it is very unlikely that there will be a fading dip simultaneously on both antennas. Therefore, by an appropriate combination of the two signals using any of the combining techniques, the probability of a fading dip will be considerably reduced and the improvement can be as large as 10-12 dB.

The diversity gain (DG) defines the improvement in the received SNR at multiple antenna systems after the signals are combined using certain combining methods, compared to the SNR for the single reference antenna at a certain symbol error rate (SER) probability. If the best branch with the highest SNR in the multiple antenna system is selected as the reference antenna,
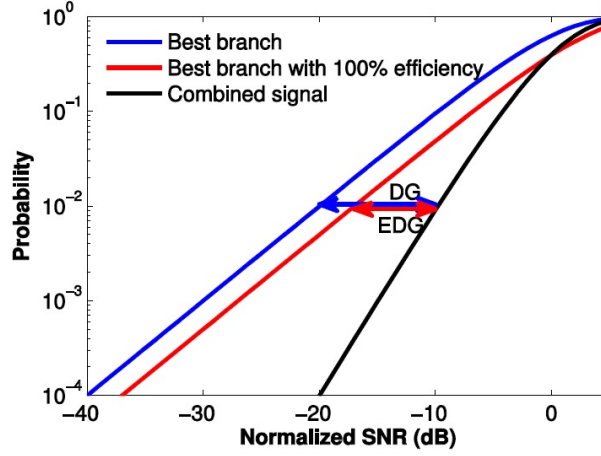
Figure 2.1: Diversity gain and Effective diversity gain

the diversity gain is defined as [137], [138]

$$DG = \frac{(\gamma_c/\Gamma_c)}{(\gamma/\Gamma)_{bestbranch}}|_{P\gamma_c} \qquad (2.4)$$

where γ_c and γ are the instantaneous SNR's, Γ_c and Γ are the SNRs for the combined signal and the signal from the best branch respectively. Equation (2.4) is defined for a probability $P(\gamma_c)$ and the probability is typically set as 1% or 50%. Nevertheless, this comparison is not justifiable due to the presence of the other branches, which induce the mutual coupling and deteriorate the efficiency of the best branch antenna. In this situation, effective diversity gain (EDG) is defined, where the reference antenna is an antenna with 100% efficiency in free space. The EDG is expressed as [139]

$$EDG = \frac{(\gamma_c/\Gamma_c)}{(\gamma/\Gamma)_{bestbranch}}\eta_{bestbranch}|_{P\gamma_c} \qquad (2.5)$$

In EDG, the total antenna efficiency of the best diversity branch is included, which means that the material loss, the mismatch and the mutual coupling are taken into account. Figure 2.1 defines diversity gain and effective diversity gain of a multi-antenna system. In practice, EDG is more frequently used to evaluate the performance of the multiple antenna system.

In general, we will take 1% as probability level. It will indicate that if in our system we allow a fading margin of 20 dB in order to receive with

sufficient quality 99% of the time, the fading margin can be reduced by a value equal to the effective diversity gain using the diversity scheme. For two uncorrelated antennas, the theoretical maximum effective diversity gain is 10 dB at 1% probability level, using selection combining [140]. An imperfect cross-polar discrimination at the receiving antennas can cause the coupling of the polarization components. This will result in an increase in the correlation between the two branches of the diversity system and can reduce the achieved diversity gain.

The diversity gain of a MIMO antenna system can be defined from the correlation based on statistic assumptions. However, if the total radiation efficiency of the two antenna elements is quite different, we cannot apply the equation directly. The apparent diversity gain can be obtained from envelope correlation coefficient by [141]

$$DG = 10 * \sqrt{1 - 0.99 \mid \rho \mid^2} \qquad (2.6)$$

Thus, the effective diversity gain is

$$EDG = \eta * DG \qquad (2.7)$$

where η is the efficiency of the strongest antenna branch and ρ is the correlation between them.

Mean Effective Gain (MEG)

The power imbalance in the diverse branches of a MIMO antenna will cause a diversity loss [139]. This impairment is proportional to the power imbalance, which is affected by the total efficiency of the antenna. In a diversity system, the mismatch between the antenna and the channel becomes significantly important. To evaluate these factors, a widely used method is to calculate the mean effective gain (MEG), which takes into account all the factors like antenna gain, channel characteristics and the total efficiency. The formula is given as follows [142]:

$$MEG = \oint \left(\frac{XPR}{XPR+1} G_\theta(\Omega) P_\theta(\Omega) + \frac{1}{XPR+1} G_\phi(\Omega) P_\phi(\Omega) \right) d\Omega \qquad (2.8)$$

where $d\Omega = \sin\theta d\theta d\phi$, XPR is the cross polarization ratio, $G_\theta(\Omega)$ and $G_\phi(\Omega)$ are the θ and ϕ components of the realized antenna gain pattern. The antenna realized gains in MEG's are normalized to

$$\oint (G_\theta(\Omega) + G_\phi(\Omega))d\Omega = 4\pi \tag{2.9}$$

The statistical power spectrum distributions of both vertically and horizontally polarized incident radio waves can be represented by $P_\theta(\Omega)$ and $P_\phi(\Omega)$, respectively. If $P_\theta(\Omega)$ and $P_\phi(\Omega)$ are separable in elevation and azimuth, they can be described by [143]

$$P_\theta(\Omega) = P_\theta(\theta, \phi) = P_\theta(\theta)P_\theta(\phi) \tag{2.10}$$

$$P_\phi(\Omega) = P_\phi(\theta, \phi) = P_\phi(\theta)P_\phi(\phi) \tag{2.11}$$

$P_\theta(\Omega)$ and $P_\phi(\Omega)$ are normalized to

$$\oint (P_\theta(\Omega))d\Omega = \oint (P_\phi(\Omega))d\Omega = 1 \tag{2.12}$$

The cross polar ratio XPR is the ratio of time averaged vertical $P_\theta(\Omega)$ power to time average horizontal $P_\phi(\Omega)$ power as given in [144]

$$XPR = \frac{P_\theta(\Omega)}{P_\phi(\Omega)} \tag{2.13}$$

In an isotropic environment, it can be characterized by $XPR = 1$, $P_\theta(\Omega) = P_\phi(\Omega) = \frac{1}{4\pi}$ and $MEG = \eta/2$, where η is the total antenna efficiency [137]. In order to obtain optimal diversity performance, the multiple antenna system has to satisfy the balance power requirement

$$MEG_{ant1} \approx MEG_{ant2} \tag{2.14}$$

Multiplexing Efficiency

Another figure of merit of multi-antenna systems is multiplexing efficiency which is used to evaluate the performance of MIMO spatial multiplexing

technique [145]. Multiplexing efficiency is a metric for describing the performance of the MIMO antenna system in spatial multiplexing mode (high SNR mode) that takes into account the efficiency as well as the correlation between the MIMO antenna elements. It is defined as the power penalty of a non-ideal antenna system in achieving a given capacity, compared with an ideal antenna system with 100% total antenna efficiencies and zero correlation between antennas. With the assumption of high SNR and isotropic environment, multiplexing efficiency ME or η_{mux} is given by

$$\eta_{mux} = \sqrt{\eta_1 \eta_2 (1 - |\rho_c|^2)} \qquad (2.15)$$

where η_1 and η_2 are the total efficiencies of two elements in the muti-element system whose product indicates the overall influence of efficiency and efficiency imbalance, while the second term $\sqrt{1 - |\rho_c|^2}$ represents the power loss due to correlation.

In a propagation channel with Gaussian distribution of the angle of arrival (AoA) as given in [146], the MIMO multiplexing efficiency can also be evaluated with the following assumptions: The mean incidence direction is denoted by θ_0 and ϕ_0 (as opposed to the isotropic channel, the likelihood of impinging waves is not the same in all directions but has a maximum at AoA θ_0 and ϕ_0). Following the above conditions, the multiplexing efficiency is a function of the mean incidence direction and is given by

$$\eta_{mux}(\theta_0, \phi_0) = \sqrt{4MEG_1(\theta_0, \phi_0)MEG_2(\theta_0, \phi_0)(1 - |\rho_c(\theta_0, \phi_0)|^2)} \qquad (2.16)$$

where MEG_1 and MEG_2 are the mean effective gains of antenna 1 and antenna 2 respectively and ρ_c is the complex envelope correlation coefficient of the received signal.

2.2.3   Channel Performance

Unlike a single antenna technology, the MIMO technology can take full advantage of the multipath channel. The major challenge for a MIMO antenna is to evaluate the scenario, on how the MIMO antenna radiation characteristics will behave in a wireless propagation environment. Though isolation

and correlation studies provide an understanding of the multiple antenna system performance as a diversity antenna solution, an over the air test (OTA) is required to completely investigate the performance of the MIMO antenna system in a channel.

Various studies are performed for MIMO OTA testing and are proposed by organizations like COST 2100 [147], CTIA [148] and 3GPP RAN WG4 [149]. The major concern is to finalize the way we can produce a repeatable measurement that characterizes a physical MIMO channel for different operating modes of the device (different channel conditions). The three main techniques finalized so far:

- The anechoic chamber multi-probe OTA method [150]

- The reverberation chamber OTA method [151]

- The two-stage OTA method [152]

2.2.3.1   OTA Measurement Techniques

Anechoic Chamber Multi-Probe OTA Method
The anechoic chamber multi-probe method uses a multiple number of probe antennas positioned at arbitrary points at equal distances from the device under test, inside an anechoic chamber. Each antenna is faded by a channel emulator to create a desired temporal component. By intelligently choosing the position and number of probes, we can construct a multipath channel environment identical to the wireless propagation environment. The most common OTA testing using multi-probe method uses probes placed along the azimuthal plane creating a two- dimensional environment. A multi-probe OTA testing configuration is shown in Figure 2.2. A more complex method uses probes placed along an additional plane too to create a three- dimensional environment. The unit under test is placed on a rotating platform which can be tilted to test from all angles.

Reverberation Chamber Method
The reverberation chamber method is a good candidate for MIMO OTA testing for its fast measurement capability. It uses reflective metallic walls and
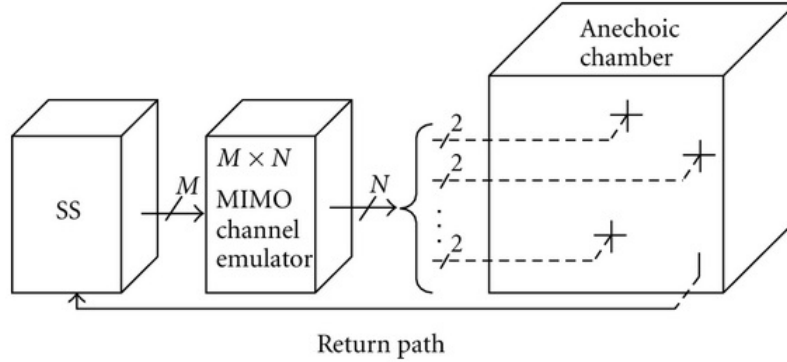
Figure 2.2: Multiprobe configuration (TR 37.976 [150])

these metal stirrers scatter the energy which enters the antenna uniformly in all the directions. The radiation pattern cannot be measured in these chambers, however, the total energy can be measured. This method uses the reflection properties of a mode-stirred reverberation chamber to generate a multipath signal from an input test signal. A reverberation chamber set up is shown in Figure 2.3. The nonuniformity produces diverse signals on each antenna allowing MIMO multiplexing gain. The time domain response of the chamber can be adjusted by large metallic reflective surfaces whose orientations can be adjusted to achieve desired boundary conditions.

Two-Stage OTA Testing Method
The two-Stage method for MIMO OTA testing uses a different approach for testing MIMO over the air performance. Here, in the first stage, the three-dimensional far field radiation patterns of the MIMO antenna are obtained using an anechoic chamber used for standard SISO tests. The magnitude, as well as phase values of the radiation patterns, are required for different phi and theta angles. In the second stage, these patterns are convolved with channel characteristics using channel emulator. The signals obtained after the second stage represents a real channel faded signal which is acted upon by the antenna of the device under test. Therefore the two stages in two-stage OTA testing are shown in Figure 2.4 and can be defined as

- Measuring the radiation pattern in a SISO OTA anechoic chamber
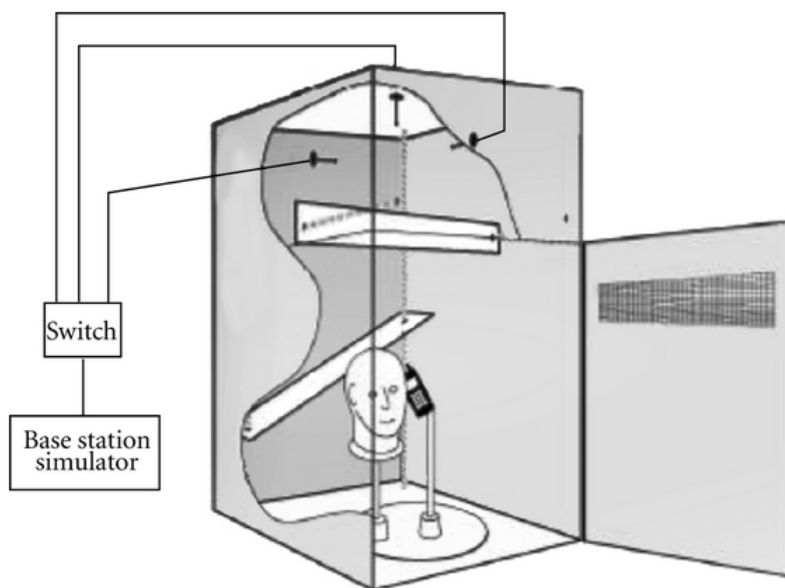
Figure 2.3: Reverberation chamber setup with single cavity (TR 37.976 [150])

- Convolve the radiation pattern with a desired channel model to obtain the fading distribution in a channel

The flexibility of a pattern measurement in a simple anechoic chamber and the emulation of any desired channel distribution makes the two-stage method more cost effective to obtain the fading distribution in a channel. The complexity of the measurement method is very less compared to the multi-probe and other techniques. The emulated channel models are accurate and have the flexibility to choose any desired configuration like indoor, outdoor, for varying Doppler spread and delay spread. We have used the two-stage testing method to evaluate the channel performances of the designed quad element MIMO antennas. The radiation patterns of the proposed antennas are convolved with correlation and WINNER-II channel models in Agilent SystemVUE software to obtain the OTA performances.
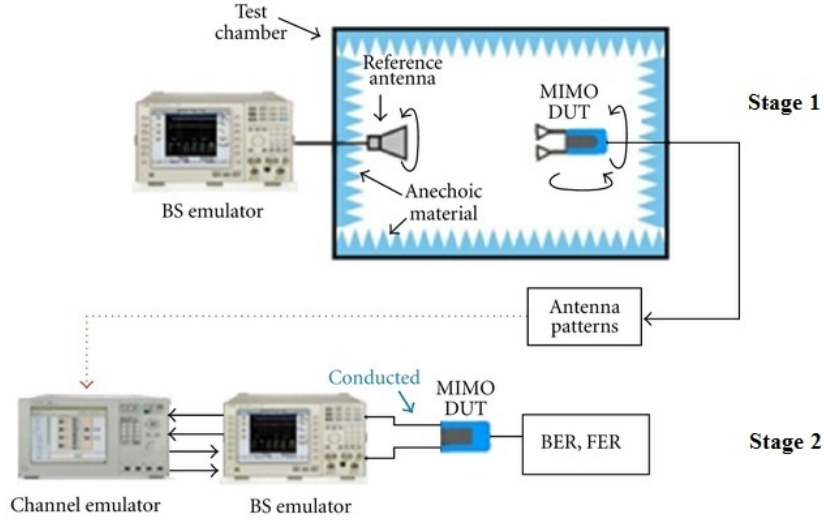
Figure 2.4: Two-Stage testing method for MIMO OTA test (TR 37.976 [150])

2.3 Simulation and Optimization

The simulation prototypes of the proposed antennas are developed in CST Microwave Studio (MWS). It is a specialist tool for the 3D Electromagnetic (EM) simulations of high frequency components [153]. CST MWS comprises of four different solvers and for our studies, a frequency-domain and time-domain solver is used. CST solver is based on the description of electromagnetic problems by differential Maxwell equations that are solved by the finite difference method.

The transient solver could be best for wideband or planar antennas, the frequency domain solver may be more suitable for electrically small and narrowband antennas, while the integral equation solver can efficiently simulate electrically large or wire antennas. Designing compact MIMO antennas on small terminals is a multi-dimension optimization problem. 3D simulation using CST MWS is a powerful tool in designing and understanding performance of MIMO antenna systems. The major challenges in MIMO antenna design include smaller antenna size, the coexistence of multiple elements and the diversity analysis using the desired channel which can be addressed in

CST MWS. This tool provides several weighting functions for modeling the channel.

Channel model can be accurately modeled as a statistical power distribution function (PDF) and choices can be made between predefined PDF or parametrised PDF. An option is provided to specify cross polarization rate (XPR) and solid angle. Few among the models are Isotropic distribution, Rayleigh (Gaussian) distribution for non line of sight communication, Ricean distribution for the line of sight communication which reduces to Gaussian pdf as the line of sight path power decreases, outdoor urban environment typically Gaussian elevation and uniform azimuth, indoor environment Gaussian in both elevation and azimuth etc.

The antenna geometry is modeled in CST MWS by specifying the coordinates for each point of the structure along with appropriate material specifications. The metallization's are specified as copper with a thickness of 0.035 mm and substrates are assigned from either the in-built material data base or user-defined. CST gives the user an option to choose from its pre-defined templates like, in this case, the planar antenna template which automatically assigns the mesh type, mesh size etc. or it can as well be user-defined.

The waveguide ports are assigned to excite the individual antenna elements. It includes multi-signal functionality to simulate various excitations which is a very useful feature for MIMO antenna designers. The boundary conditions are set as open along the three coordinates. The frequency sweep is set over the desired range of frequencies before the simulations are commenced. It allows mesh generation that divided the system to small cells in order to get accurate results.

From the simulated results, the antenna parameters like return losses, VSWR and the input impedances and transmission coefficients are plotted as a function of frequency for each element. The antenna geometry can then be appropriately optimized for the desired impedance response. The radiation patterns, gain, current and field distributions are also determined at the specified frequencies for each antenna in the multi-antenna MIMO system.

The simulation studies using CST MWS helps in design and optimization of the MIMO antenna which is then fabricated and measured using a prototype. The channel performances are investigated for the proposed quad

element MIMO antennas using the Aglient SystemVUE software. SystemVUE
uses two-stage MIMO OTA testing method to analyze the channel capacity
and throughput measurements using two sets of available channels in it, i.e.
a correlation based channel model and WINNER-II channel model.

The three-dimensional radiation pattern data(both magnitude and phase
components) of the antenna elements are obtained from CST microwave stu-
dio. The data is converted into $*.uan$ file format as specified by Agilent
SystemVUE for the various phi and theta angles. Far-field radiation patterns
are obtained for phi angles varying from $0^0 \leq \Phi \leq 360^0$ and theta angles vary-
ing from $0^0 \leq \Phi \leq 180^0$ in steps of 5 degrees. Individual files are created for
each antenna elements in the multi-element MIMO antenna. These files are
then loaded into SystemVUE software where they are convolved with channel
coefficients to obtain channel faded distribution.

The software has in built models for measuring channel capacity, block er-
ror rate (BLER) and throughput measurements. Here codes are implemented
to send a known set of data through multiple transmitter antennas. These
data is received and analyzed at the receiver, for any bits in error as well as
for channel capacity and throughput studies. The simulations are repeated
for varying SNR values to obtain the SNR v/s channel capacity and SNR v/s
throughput curves.

2.4   Fabrication

The various steps involved in the fabrication of the multi-element antenna
are listed below. The first procedure in the antenna fabrication is the se-
lection of suitable substrate with electrical and material properties matching
the required application. The dielectric constant and loss tangent and their
variation with temperature and frequency are important in fabrication. We
selected FR4, a widely used substrate material for microwave applications. It
is low cost, easily available and most suitable for effortless fabrication.

Photolithographic techniques were used to fabricate the multi-element an-
tenna configurations on the selected substrate. In the first step, the double
side copper coated FR4 substrates are chemically cleaned with acetone or

chloroform to remove impurity matter on the surface. A very thin film of photoresist is applied with the help of a spinner. There are two types of photoresists; positive and negative. For positive resists, the resist is exposed with UV light wherever the under lying material is to be removed. In these resists, exposure to the UV light changes the chemical structure of the resist so that it becomes more soluble in the developer solution. The exposed resist is then washed away by the developer solution, leaving windows of the bare underlying metallic region. The photomask, therefore, contains an exact copy of the pattern which is to remain on the substrate. On the other hand, the negative resist which is available in our laboratory, remains on the surface wherever it is exposed and the developer solution removes only the unexposed portions. Masks used for negative photo resist, therefore, contain the inverse of the pattern to be transferred. After developing, the unwanted metallic portions are cleared using Ferric Chloride solution.

2.5   Antenna Measurements

Various antenna parameters like resonant frequency, S-parameters, bandwidth, gain, polarization, radiation pattern, envelope correlation coefficient etc. are measured using different experimental setups as described below. The measurements are carried out at our antenna measurement facility which includes network analyzers (Agilent PNA E8362B, R&S ZVB20, automated antenna positioner, broadband double-ridged horn antennas (2 to 20 GHz) and anechoic chamber.

Measurement of Resonant Frequency, S-parameters and Bandwidth
The two ports of the vector network analyzer (VNA) is calibrated using the suitable standard short, open and thru loads. A proper phase delay is introduced while calibrating, to ensure that the reference plane for all measurements in the desired frequency range is actually at zero, thus taking care of probable cable length variations and losses. The two ports of MIMO antenna is then connected to the two ports of the network analyzer for S-parameter measurement as shown in Figure 2.5 while the other two ports of the four
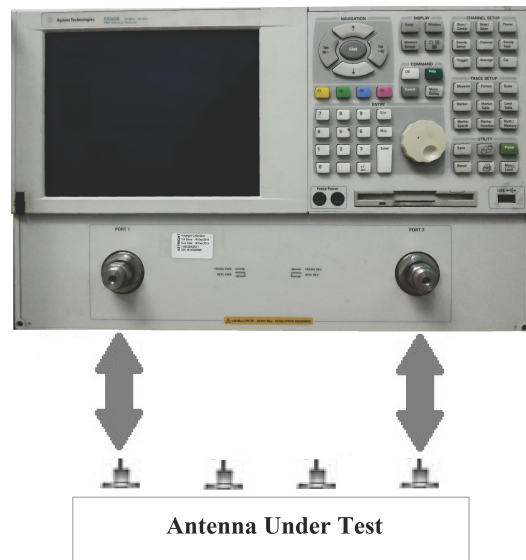
Figure 2.5: S parameter measurement setup using Network Analyzer

port MIMO antennas are terminated with matched loads. The magnitude and phase of the measured S_{11}, S_{22}, S_{12} data can be compared and saved.

The resonant frequencies are determined from the return loss curves, by identifying those frequencies for which the curve shows a maximum dip. The return loss is the number in dB that the reflected signal is below the incident signal. From the S parameter curves, -10 dB impedance bandwidths are determined by observing the range of frequencies (Δfr) about the resonant frequency fr, for which the return loss curves show a -10 dB value.

Measurement of Radiation Pattern

Radiation pattern measurement is carried in an anechoic chamber as shown in Figure 2.6 using the setup consisting of the network analyzer. An automatic turn table assembly kept in the quiet zone is used to mount the test antenna inside the anechoic chamber. A completely automated data acquisition software using the Matlab software developed indigenously at the Center for Research in Electromagnetics and Antennas (CREMA), Department of Electronics, Cochin University of Science and Technology is used. This software communicates with Network Analyzer using Standard Commands for Programmable Instruments (SCPI) and gathers measured data through eth-
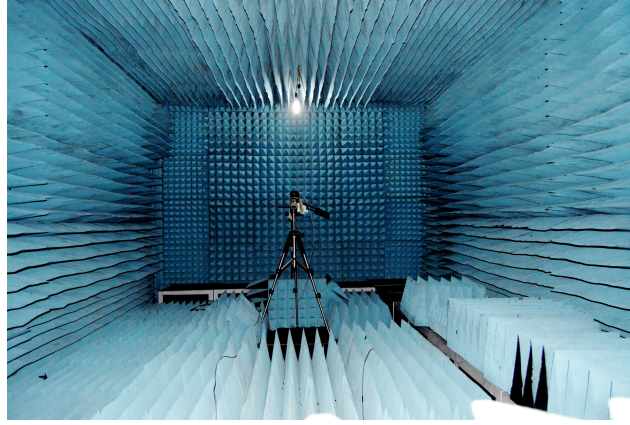
Figure 2.6: Photograph of the anechoic chamber used for the antenna measurements

ernet communication. A serial connection using DB9 connector to the turn table controls the antenna rotation in a user defined angle and direction.

The principal E and H-plane radiation patterns (with both co and cross polar pattern) of the test antenna are measured by keeping the test antenna inside the chamber in the receiving mode. The block diagram of the experimental setup used for this measurement is shown in Figure 2.7. A standard wide band ridge horn antenna is used as the transmitter. The horn is then connected to port-1 and the test antenna in port-2 of the Network Analyzer. The analyzer is configured to make the S_{21} measurements in the step mode with proper averaging.

The radiation patterns of the antenna under test at multiple frequencies can be measured in a single rotation of the positioner using Matlab software. With the test horn antenna aligned in bore sight for maximum reception and polarization matched, the thru response calibration is performed for the frequency of interest and saved in the calibration set. The powerful feature called gating in VNA is enabled that provides the flexibility to selectively remove spurious reflection or unwanted responses.

Once the gate has been applied to the time domain data, the data can be converted back to the frequency domain. The time-gated response can now be evaluated in the frequency domain. This is done by switching it into the time domain and providing a gate span depending on the largest dimension of the test antenna. The turn table is then set to rotate the desired angle
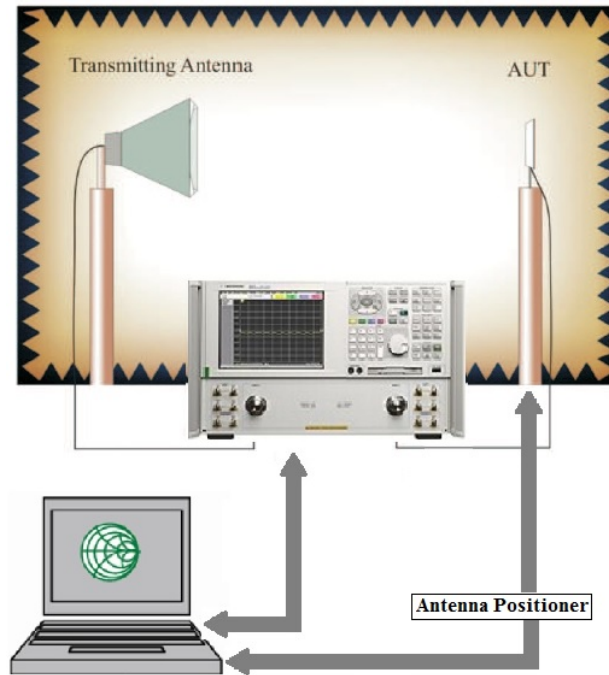
Figure 2.7: Experimental setup for antenna characterization

using the positioner. The positioner will stop at each step angle and take the S_{21} measurements till it reaches the stop angle. Measurements are repeated in the principal planes for both the co and cross-polar orientations of the test antenna and horn. From the stored data, different radiation characteristics like half power beam width, cross-polar level etc. in the respective planes are estimated.

Measurement of Envelope Correlation Coefficient

Envelope correlation coefficients are computed from the measured far-field radiation pattern data, obtained for the antenna elements. The measurements are similar to radiation pattern measurements and are performed using a network analyzer in an anechoic chamber. A procircle is fixed to the back side of the antenna on the mounting table to rotate the antenna along the phi axis. The antenna is rotated along the phi axis in measured steps, and for each angle, the positioner rotates along the theta plane recording the pattern data for various angles. Three dimensional far field distribution values are

obtained for varying phi and theta angles in steps of 30 degrees conformable to CTIA testing standards [154]. ECC is then computed with the measured results using the equation

$$\rho_{i,j} = \left[\frac{\oint (XPR \cdot E_{\theta i} E_{\theta j}^* P_\theta + E_{\phi i} E_{\phi j}^* P_\phi) d\Omega}{\sqrt{\oint (XPR \cdot E_{\theta i} E_{\theta i}^* P_\theta + E_{\phi i} E_{\phi i}^* P_\phi) d\Omega \oint (XPR \cdot E_{\theta j} E_{\theta j}^* P_\theta + E_{\phi j} E_{\phi j}^* P_\phi) d\Omega}} \right]^2$$

(2.17)

XPR is the cross polarization rate of the incident field and is defined as $XPR = P_V/P_H$ where P_V and P_H are the average power along the spherical coordinates θ and Φ. $E_\theta i$ and $E_\Phi i$ are the complex envelopes of θ and Φ components of far field radiated field, when only the ith port is excited and other ports are terminated with 50 Ω loads. P_θ and P_Φ are the probability distributions of the power incident on the antenna in the θ and Φ polarization's respectively. The angle Ω is defined by θ in elevation and Φ in azimuth. A standard isotropic channel environment is considered for all our measurements, where the powers of horizontal and vertically polarized incident waves are almost equal. Hence, the cross polarization discrimination $XPR = 1$ and probability distributions of the power incident on the antenna in the θ and Φ polarization's will be $P_\theta = P_\Phi = 1/4\pi$.

Measurement of Gain and Efficiency

The gain of the antenna under test is measured using the gain transfer method [155], [156], utilizing a reference antenna of known gain. The experimental setup for the measurement of gain is same as that used for radiation pattern measurement. A standard antenna with known gain Gs operating in the same frequency band as the test antenna is used as the reference antenna. S_{21} measurements are then carried out to determine the reference power with the wide band horn as the transmitter and the reference antenna as the receiver. A thru response calibration is performed for the frequency band of interest and saved in a new cal set. This is taken as the reference gain response (0 dB). The reference antenna is then replaced with the test antenna, retaining the earlier bore sight alignment. S_{21} is then measured with the new calibration on and power received in dB, Pr is recorded. The gain Gt of the test antenna

is calculated from the stored data based on Friss transmission formula as

$$Gt(dB) = Gs(dB) + Pr(dB). \tag{2.18}$$

The radiation efficiency is obtained using wheeler cap method which uses an oblate metallic chamber for measurements. Radiation efficiency can be defined as the ratio of the radiated power to the input power [157], where input power is the combination parameter of radiated power and loss power or reflection power. Thus the radiation efficiency, $'\eta'$, is given by

$$\eta = \frac{P_{rad}}{P_{in}} = \frac{P_{rad}}{P_{rad} + P_{loss}} \tag{2.19}$$

where P_{rad} is radiation power of antenna, P_{in} is input power, P_{loss} is loss power (reflection power). Assuming antenna has identical current distribution, the equation (2.19) will re-write to following equation.

$$\eta = \frac{I^2 R_{rad}}{I^2 R_{rad} + I^2 R_{loss}} = \frac{R_{rad}}{R_{rad} + R_{loss}} \tag{2.20}$$

where I is the input current, R_{rad} is radiation resistance of antenna, R_{loss} is loss resistance. Practically, the resistance of antenna cannot be easily obtained directly by any measurement equipment. This will require another simple and general parameter to solve the radiation efficiency during the measurement. Reflection coefficient is one of most important parameter during antenna measurement, and it shows on the VNA with another corresponding parameter which is called return loss (S_{11}). As we know, the reflection coefficient can also represent by the real part of impedance. So the relationship between resistance and reflection coefficient will be built using [158], [159], [160] for antenna efficiency measurement.

$$\eta = \frac{P_{rad}}{P_{rad} + P_{loss}} = 1 - \frac{(1 - \Gamma_1)(1 + \Gamma_2)}{(1 + \Gamma_1)(1 - \Gamma_2)} \tag{2.21}$$

$$\eta = \frac{R_{rad}}{R_{rad} + R_{loss}} = \frac{\Gamma_2^2 - \Gamma_1^2}{1 - \Gamma_1^2} \tag{2.22}$$

where Γ_1 is the reflection coefficient measurement without Wheeler cap (measured in free space) and Γ_2 is the reflection coefficient measurement with Wheeler cap.

2.6   Chapter Summary

This chapter has discussed the methodology to design MIMO antennas, to simulate, optimize and fabricate the various quad element antennas mentioned in the following chapters of the thesis. It has deduced the complete theory behind the MIMO antenna characterization, the isolation and diversity analysis of the MIMO antennas, along with their simulation and measurement techniques. The performance of the MIMO antennas are assessed not only in terms of the conventional antenna parameters like return loss, gain, efficiency and radiation pattern but also in terms of the MIMO quality measures like the mutual coupling, envelope correlation coefficient, diversity gain, mean effective gain and multiplexing efficiency. The ability of the antennas to effectively transmit-receive multiple waveform in a channel are also discussed and estimated in terms of the channel capacity, BLER and throughput.

<div align="right">Chapter 3</div>

Multimode MIMO Antennas Using Microstrip Patches

Contents

This chapter investigates the design and development of multimode MIMO antennas for application in 2.45 GHz wireless band. The chapter begins with a detailed literature review of available antennas belonging to this broad category followed by the sections detailing the evolution and performances of the multimode antenna designs. Here, multimode MIMO patch antennas are designed for compact wireless terminals incorporating the various forms of diversity like spatial, polarization and radiation pattern diversity.

Two different patch antenna elements, each exciting two complementary orthogonal modes are used, as a result, the space required to mount the MIMO antenna is very less. With overall dimensions, nearly half a guided wavelength, the patches excite multiple radiation modes in the same frequency band ensuring pattern diversity. The surface current and field distributions on the antenna together with their radiation patterns for the resonant modes are analyzed in detail. The results of the analysis along with the parametric studies have enabled us to deduce their design for the desired operating frequencies. The performance of the fabricated antennas is then experimentally verified and are found to be in reasonable agreement with the simulated results.

Mutual coupling between the closely spaced antenna elements is reduced by designing defected ground structures of various forms. The antenna design, simulation and measurement results are provided for each design. An investigation on the working principle of isolation enhancement structure is also provided. The MIMO performances of these antennas are explored in detail to understand how diversified the antenna elements are. The diversity performances of the MIMO antennas are evaluated by computing the envelope correlation coefficient between the antenna elements. The antennas prove to be suitable for MIMO application in terms of their isolation and diversity performances.

3.1 Multimode MIMO Antennas: Review

From the surplus of available literature of MIMO antenna designs, with the aim of showing typical examples of recent MIMO antenna systems, more focus is assigned particularly on planar MIMO antenna designs as they are more

conformable to the mounting host for wireless communication systems [161]. Antenna designs based on multiple resonant modes exploiting polarization and pattern diversity are considered particularly and their performances are analyzed. In all these cases, the types of printed antennas range from monopoles, dipoles, rings and slots to microstrip patches and subwavelength resonators depending on the type and shape of the terminal under consideration. Careful designing with minimal coupling and low correlation between elements is a challenge [162] for MIMO antennas. Making use of isolation enhancement techniques and diversity implemented in antennas ensuring low correlation is a necessity in these conditions [163–166].

Polarization diversity has been widely employed and has proved itself for its performance in MIMO antenna systems [44, 48, 167]. However, pattern diversity has not been much explored, particularly using dissimilar antenna designs. This can be attributed to antenna design constraints which require highly performing diverse antenna elements resonating at the same frequency and maintaining a low correlation between the various antenna shapes. There are two methods to achieve pattern diversity i.e. by positioning identical beams in different angular directions and secondly by creating diverse patterns by making use of different antenna designs or multiple modes of antennas ensuring diverse radiations. Experimental analysis of pattern diversity based multimode MIMO antenna designs has been studied for its channel capacity performances and MIMO diversity performances [168, 169].

The benefits of pattern diversity based multimode MIMO antenna systems using realistic channel models, adopted by the IEEE 802.11n standard body for wireless local area networks (WLANs) is described in [168]. The performance studies of collocated multimode antennas using two element circular microstrip antennas employing pattern diversity technique, yields improved performance, when compared to space diversity based half wave length separated uniform linear arrays. An indoor field analysis on the performance achievable with pattern and polarization diversity based multi-element reconfigurable antennas is performed using circular patch antennas [169]. The benefits offered by excited radiation pattern and polarization of the antennas are investigated in both line-of-sight (LOS) and non-line-of-sight (NLOS) scenarios. It was proved that polarization diversity exhibits consistent behavior in

both LOS and NLOS scenarios. The diversity based antenna system achieved an average capacity improvement of 17.5% when employed only at the receiver in a narrowband channel, relative to the 9% improvement achievable in a broadband channel.

A multimode quasi-analytical model is derived to analyze and provides guidelines to design reconfigurable multimode MIMO microstrip antennas [170]. Several multimode antennas appear in literature which adopts various structures like biconical antenna [171], spiral antenna [172], a simple metallic ring with different phase configurations [173] and patch antenna [174]. Short circuited ring patch antennas exciting multiple radiation modes have proved to obtain high spectrum efficiency by combining spatial and radiation pattern diversity [175]. Frequency mode convergence concept is used to obtain multimode antennas using square patch [176]. Few other multimode antennas are also reported using structures other than patch, however, the size is conventionally larger, making use of higher order modes to achieve pattern diversity [177,178].

Few other reported designs employing dissimilar antennas placed in a collocated fashion to achieve pattern diversity is analyzed in this section. One such design makes use of a pair of printed F antennas on the top metal layer and the back metal layer contains a pair of quarter-wave slot antennas [167]. An isolation of 10 dB between the elements was obtained for this compact quad element configuration with an overall area of $0.33\lambda_0 \times 0.33\lambda_0$. The quarter-wave length slot etched on the ground plane serves as a radiator, and meanwhile, helps in suppressing mutual coupling of the other antenna pair in a compact area. The capacity at 20 dB SNR is 19.7 b/s/Hz per receiver branch, making it suitable for MIMO wireless communications.

Two different types of antenna are used to get diverse patterns with reduced coupling and enhanced isolation in a compact four port MIMO antenna with an overall size of $82 \times 62 \times 2.6 mm^3$ for WLAN application [179]. To enhance isolation between adjacent square rings and slot antennas, a set of ground plane slits is employed between them. They act as a band stop filter and reduce the coupling currents on the ground plane, the isolation performances were better than 25 dB. Envelope correlation was less than 0.022 in the

operating band with a maximum measured gain of 2.8 dBi for slot antennas and 2.3 dBi for square ring antennas.

An important objective in designing collocated antennas is to design orthogonally polarized antenna elements with low cross polarization levels. This is taken advantage in the design of compact planar collocated MIMO antenna with high port isolation [180]. The proposed collocated antenna consists of a proximity-coupled fed square-ring patch antenna, and a coaxial fed PIFA, located inside the square ring patch. The inside PIFA takes no extra space for the multi-antenna system. A two port MIMO antenna with resonator separation of 0.029λ uses both polarization and pattern diversity. This has radiating structures etched on both sides of the substrate with reasonably good isolation [181].

Instead of two different antenna elements, there can be only one top radiating element with two isolated feeding ports which can save space and cost. This is adopted in the design of dual-feed planar inverted-F antenna (PIFA) suitable for wireless applications such as WLAN and LTE as a diversity MIMO antenna [182]. The two feed plates are placed perpendicular to each other to exploit both the polarization diversity and pattern diversity. The isolation between the two antenna ports is achieved by modifying the ground plane under the top radiating element.

A two-port pattern diversity antenna is presented using a combination of a low-profile monocone antenna and a broadband microstrip antenna [183]. The broadband microstrip antenna provides an impedance bandwidth of 44% from 1.89 to 2.9 GHz, covering UMTS/LTE2300/2500 bands. The isolation between the two antennas is greater than 15 dB in the entire band. The low-profile monocone antenna has a monopole type radiation pattern, and the broadband microstrip antenna has a microstrip antenna-type radiation pattern, providing pattern diversity characteristics.

A number of collocated multi-antenna structures for MIMO applications have been proposed in the last few years [133, 184, 185]. These multiple antenna systems make maximum usage of the available space and exhibit a low correlation between elements, since the antenna elements are not placed alongside as in the typical spatial diversity based antenna system. However, most of the collocated antenna systems are three-dimensional and are not perfect

for compact wireless terminals. Traditional diversity techniques such as spatial diversity by means of a linear antenna array or polarization diversity by means of a cross-polarized antenna array may prove to be unsuitable in the case of severe restrictions on antenna size and spacing.

A complete MIMO communication system with orthogonal frequency-division multiplexing (OFDM) based on multiple excitation modes for a single circular microstrip antenna is studied in [186]. A microstrip antenna employing multiple modes is found to be comparable to traditional antenna arrays in an urban micro-cell setting at a much lower cost in terms of size and spacing. The throughput performance and signal detection of multimode antennas in flat and frequency-selective fading environments prove the feasibility of the multiple mode diversity antenna.

It is clear from the literature review that often the quad element MIMO antenna systems designed by researchers are of big sizes for a compact handheld device. The high isolation (greater than 20 dB), and low envelope correlation has been achieved either through using 2-elements MIMO antenna systems or relatively big MIMO antenna systems. Therefore, it is required to reduce the size of the MIMO antenna by miniaturizing the resonator elements.

Generally, it has been noticed that the correlation between the envelopes of signals received by two antenna elements is decreased if the patterns of each antenna are different from each other. This is due to the fact that the relative amplitudes and phases or the weights of the incident multipath signals are distinct at each antenna, even if the antennas are collocated. This concept is used in the design of quad element MIMO antennas where pattern diversity of multiple radiation modes creates multiple beams in different directions, to access the uncorrelated signals. Pattern diversity using different patches, in fact, has an inherent space diversity due to antenna separation necessary to create those beams.

In addition to pattern diversity introduced by multiple modes, the proposed designs also introduce polarization diversity in such a way that each adjacent antenna has a different polarization. For a single polarized system, one polarization is extracted from each antenna. In the case of a dual polarized system, which is employed here, two orthogonal polarizations are extracted simultaneously. Collocating multiple antenna elements is highly desired, where

there is no physical separation between antenna elements and can further shrink the size of the multiple antennas in a MIMO system. In addition, two dissimilar antennas are also suitable to be collocated together and resonance can be achieved at the same frequency. However, in such scenarios, it is difficult to add any decoupling structures in the MIMO antenna system, hence, orthogonal polarization turn out to be the best decoupling method.

Based on this study, the evolution of three collocated MIMO antenna designs is presented. The antennas designed are simple in structure based on microstrip patch antenna design equations. We begin by investigating a microstrip square patch and square ring patch antenna to study the impact of antenna geometry and positioning for obtaining identical frequencies of resonance and diverse radiation patterns. Further, we modify the antenna design to optimize their performance for 2.45 GHz band applications. Dual polarization and multiple radiation modes are used to achieve minimal correlation and coupling. The antennas are coaxially fed for easy fabrication and better integration.

3.2   Microstrip square and ring patch MIMO Antenna with ring DGS

The multimode collocated microstrip patch antenna was designed considering the basic patch antenna shapes [187]. The multi-element antenna was intended to realize polarization and pattern diversity for use in multiple-input-multiple-output (MIMO) terminals. In order to achieve pattern diversity, two different antenna elements were considered. Further, improvement in angular diversity can be achieved by keeping the radiating modes diverse, i.e. by making use of fundamental and higher order modes. The design was initiated with a two element dual polarized square patch antenna. To achieve compactness of the overall quad element antenna, a simple square ring patch antenna was chosen which accommodates the square patch within its ring slot. The quad element antenna was designed for 2.45 GHz band. To improve isolation between the patch antenna elements, a square ring defected ground structure (DGS) is designed. Square ring slot etched on the ground plane between the

patches, improves isolation along both E and H planes for its ring structure. It reduces surface waves confined within the dielectric that causes coupling between closely spaced antenna elements.

3.2.1   MIMO Antenna Geometry and its Design

A microstrip antenna in its simplest form comprises of a radiating patch on the top side of a dielectric substrate and a ground plane on the bottom side. The patch is usually prepared using conducting material and can designed for any possible shape, but standard shapes are used to simplify the analysis and performance prediction. The fringing fields between the periphery of the patch and the ground plane cause radiation from a microstrip patch antenna. Microstrip patch antennas can be fed by means of various methods like microstrip line feed, coaxial feed, aperture coupled feed and proximity coupled feed. The proposed antenna system uses coaxially fed planar microstrip patch antennas for designing a quad element MIMO antenna.

The geometry and parameters of quad element antenna system are shown in Figure 3.1. The dimension of the antenna is given in Table 3.1. An FR4 substrate with relative permittivity $\varepsilon_r = 4.4$, loss tangent $tan\delta = 0.02$ and thickness of 1.6 mm is used. The antenna has a two port square patch which is orthogonally polarized to produce 0^0 and 90^0 polarized waves. A basic square patch antenna of length L, width W, on a substrate of thickness h with permittivity or dielectric constant ε_r resonates for a frequency given by [188]

$$f_r = \frac{c}{2L\sqrt{\varepsilon_r}} \tag{3.1}$$

The equation (3.1) says that the microstrip patch antenna should have a length equal to one half of a wavelength within the dielectric medium for operating in its fundamental mode. Here the electric field is zero at the center of the patch, maximum positive on one side, and minimum negative on the opposite side. These minima and maxima constantly change sides like the phase of the sine wave. Hence, for a square patch antenna for which length and width are equal, by choosing two feed ports P_1 and P_2 along the principal Y and X planes, TM_{01} and TM_{10} modes of the antenna are excited. TM stands for
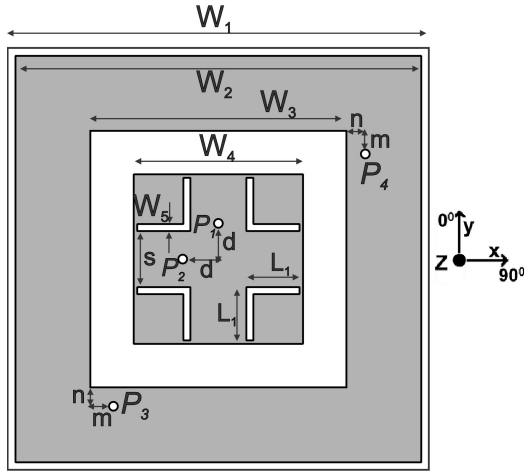
Parameter	Value (mm)	Parameter	Value (mm)
W_1	60.2	d	5.1
W_2	58	s	8
W_3	36.6	m	3.3
W_4	24.2	n	2.7
W_5	1	p	4
L_1	7.6	q	2

Figure 3.1: Geometry of the four port MIMO antenna system

Table 3.1: Antenna Dimensions of square and ring patch MIMO antenna

transverse magnetic, the magnetic field distribution between patch and the ground, this field is transverse to the z-axis of the patch antenna.

The simulated current distributions of the elements of the antenna are shown in Figure 3.2 from which the modes of operation can be identified. Elements P_1 and P_2 have a half wavelength current distributions along the Y axis and the X axis, exciting fundamental orthogonal modes TM_{01} and TM_{10}; i.e. one has a null in the direction in which other has a maximum. Square patch antenna has four L-shaped slots which reduces the dimensions of the antenna, making it resonate at 0.4λ, where λ is the wavelength at the resonant frequency. This makes the antenna more compact than conventional $\lambda/2$ patch antenna [189]. The impact of the L-shaped slots on the resonant behavior of the square patch antenna is investigated in Figure 3.3. It can be observed that the length of the slot significantly influences the resonant frequency of the square patch antenna, by increasing the electrical length of the fundamental resonant modes.

Square ring patch shape is chosen as the second patch antenna, which encircles around the square patch leaving a ring slot in between the two patches. In other words, it can be said that the ring slot structure on the upper side of the substrate, isolates feed ports P_3 and P_4 from inner square patch feed
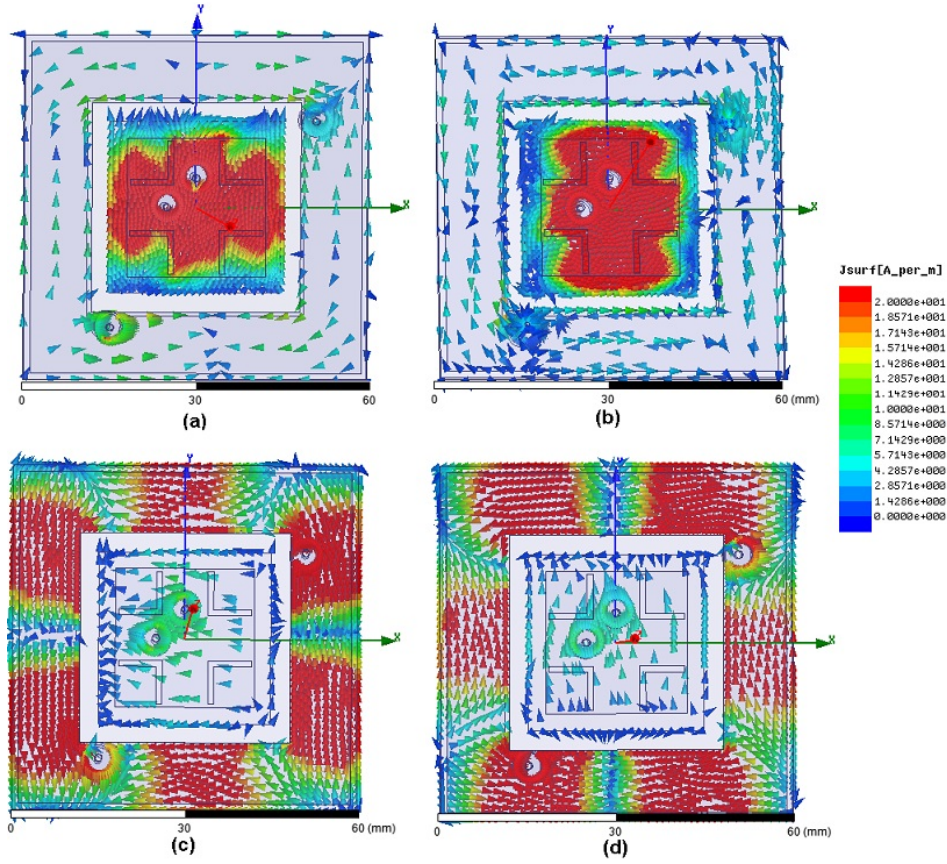
Figure 3.2: Vector current distribution with (a) P_1, (b) P_2, (c) P_3 and (d) P_4 excited at 2.45 GHz

points, making them resonate based on the principle of the square ring patch antenna. This results in diverse radiation patterns for square patch and ring patch antennas. Feed ports P_3 and P_4 are positioned on the outer ring antenna to excite higher order orthogonal modes of the square ring patch antenna. For a ring patch antenna, the resonant frequency is determined by both the inner and outer dimensions of the square ring. The fundamental resonant mode of a microstrip square ring patch antenna has a width W corresponding to 0.3λ. The width W is the average of outer and inner widths given by $W = \frac{W_2 + W_3}{2}$, where W_2 and W_3 are outer and inner dimensions of the ring as shown in Figure 3.1. In this case, higher order modes of square ring antenna are excited, which corresponding to a width W of 0.8λ for obtaining resonance at a

frequency of 2.45 GHz.
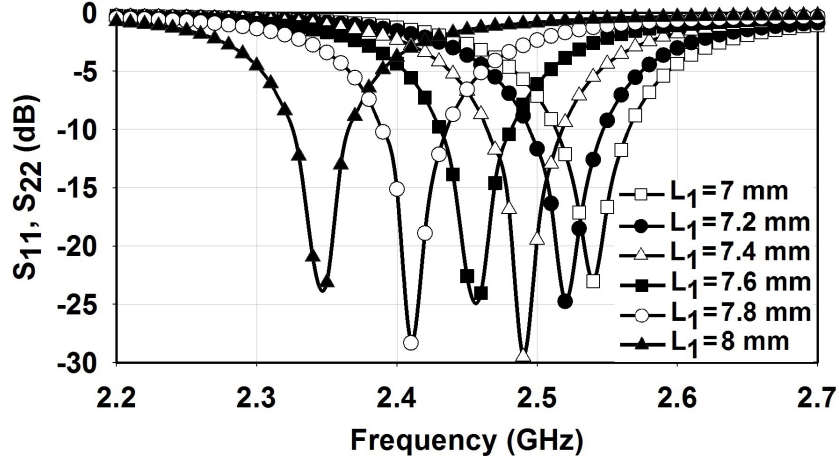
(a)
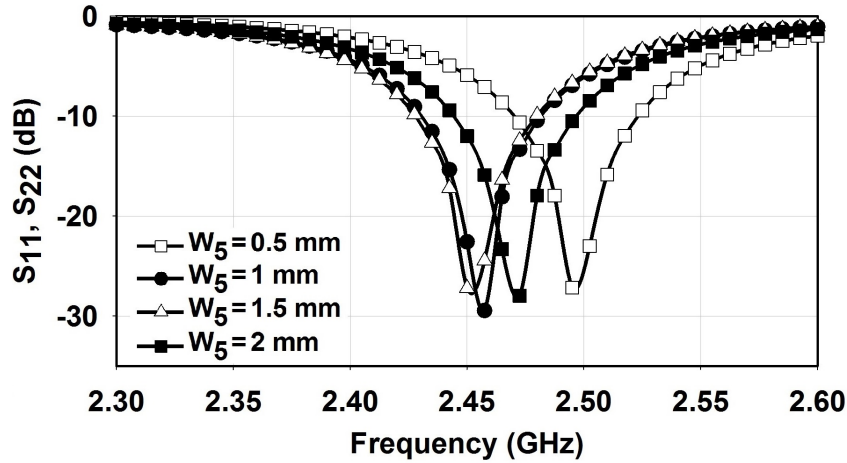
(b)

Figure 3.3: Effect of L slot length and width on reflection characteristics

For P_3, the current distribution in Figure 3.2 has one half wavelength distribution along the X direction with a current maximum and two minima's in the corners, whereas along the Y axis there is one full wavelength distribution with two maxima's. Therefore, it can be interpreted that P_3 resonates in TM_{12} mode. For P_4, current distribution has one half wavelength variation along the Y direction and a full wavelength variation with two maxima's along

the X plane, identified as TM_{21} mode.

The parametric study of the width of the outer ring antenna in determining the resonant frequency is shown in Figure 3.4. The outer width of the ring patch antenna W_2 is kept constant and the inner patch width W_3 is varied. An increase in W_3 results in lowering the average width W given by $W = \frac{W2+W3}{2}$, which in turn increases the ring resonant frequencies (S_{33} and S_{44}). By properly choosing the width to be nearly $0.8\lambda_g$, the second order modes of the square ring patch antenna are excited and resonance is achieved in the desired frequency similar to that of the square patch antenna. Higher order orthogonal modes created by the square ring patch antenna have a dissimilar radiation pattern than lower order modes of the square patch, thus guaranteeing pattern diversity in the multiple antenna system.
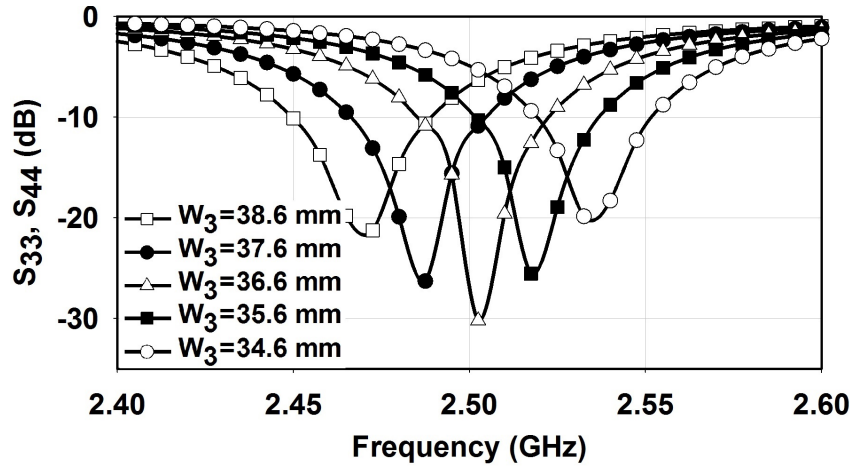
Figure 3.4: Effect of outer ring width on S_{33} / S_{44} characteristics

Simulations are done with the aid of CST Microwave Studio software. The simulated S parameters of the quad element MIMO antenna are shown in Figure 3.5. The ring shaped slot on the top of the substrate separating square patch and ring patch antenna physically isolates the two patch elements. This is reason why low coupling is achieved between P_1 & P_3 and P_2 & P_4. However, coupling between P_2 & P_3 and between P_1 & P_4 is still higher than -20 dB because of the identical orientation of surface currents for these elements.
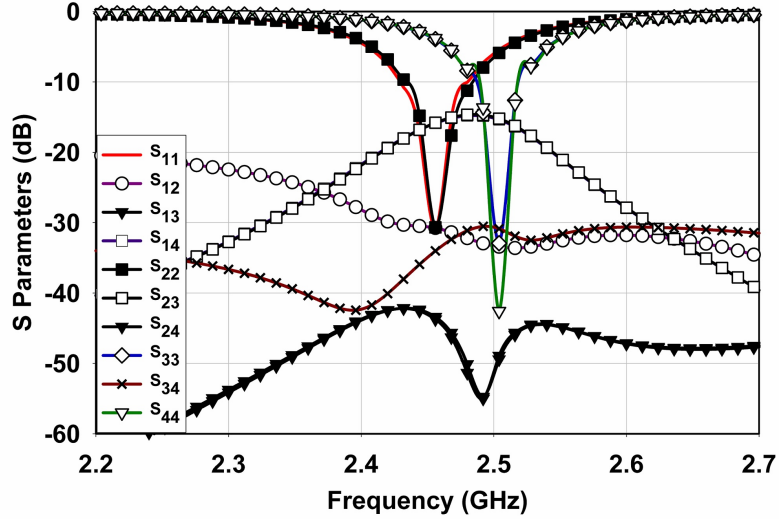
Figure 3.5: Simulated S Parameters

3.2.2   Study of square ring DGS for isolation enhancement

A square ring shaped defected ground structure is engraved between the patch antennas to provide high isolation between elements of the two patch antennas. The geometry of the DGS on the antenna ground plane is shown in Figure 3.6. Mutual coupling between closely spaced antenna elements is generally due to the far field coupling and surface wave coupling. Defected ground structures can effectively suppress both these types of coupling currents. By etching structures on the ground, common ground sharing currents can be blocked to reduce far-field coupling. Surface waves travel within the dielectric substrate and are guided by the substrate and the finite ground plane. These waves have the lowest propagation mode TM_0 having a cutoff frequency of zero [190], which acts as the most dominant reason for coupling in this case.

The square ring shaped DGS is designed to act as a slot antenna resonator at the operating frequency, so that it radiates coupling waves between the antenna elements into space [191]. This inhibits surface waves within the dielectric from reaching other ports in their traveling path and cause coupling. In this system, square and ring patch antennas have feed positions along both
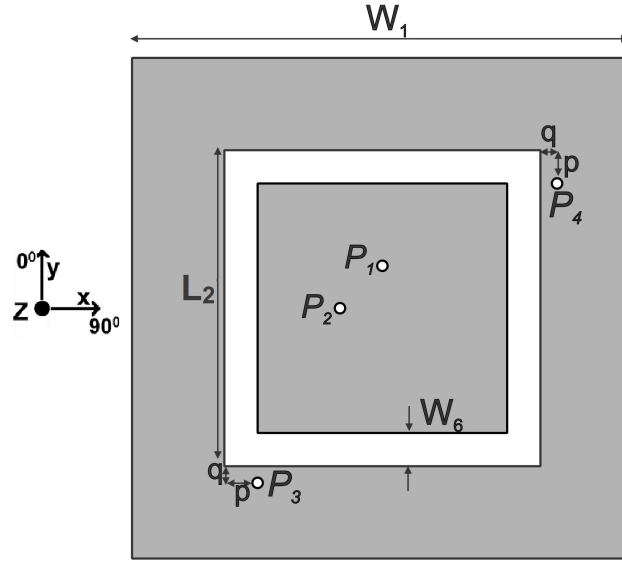
Figure 3.6: Geometry of ground plane of the antenna with ring DGS; $L_2 = 38mm$, $W_6 = 4mm$

E and H plane, so it is necessary to realize isolation in both these planes. By selecting DGS to be a ring shaped structure, this can be accomplished, with enhanced isolation for both combinations of the antenna elements i.e. P_1 & P_4 and P_2 & P_3.

To further comprehend the mechanism of the isolation enhancement, probes are placed within dielectric using CST Microwave Studio to measure E fields. It was observed that in both the high coupling areas, an addition of isolation structure has reduced E_Z field inside dielectric for the operating band. E_Z was measured in a direction normal to the ground layer. Figure 3.7 shows E_Z field measured nearby feed location P_4, when P_1 is excited. A similar decline in the field was perceived for P_2 and P_3 combination too with DGS. A decrease in the field indicates that more confined waves are coupled into space by the square ring DGS. It was also observed that the field E_Z decreases with a decrease in substrate thickness, which is true for the behavior of surface waves. A small increase in back radiation is observed, which again validates that the coupling waves are radiated by DGS due to its resonant behavior.

The square ring DGS having a width which is nearly a $\lambda/2$, act as a slot
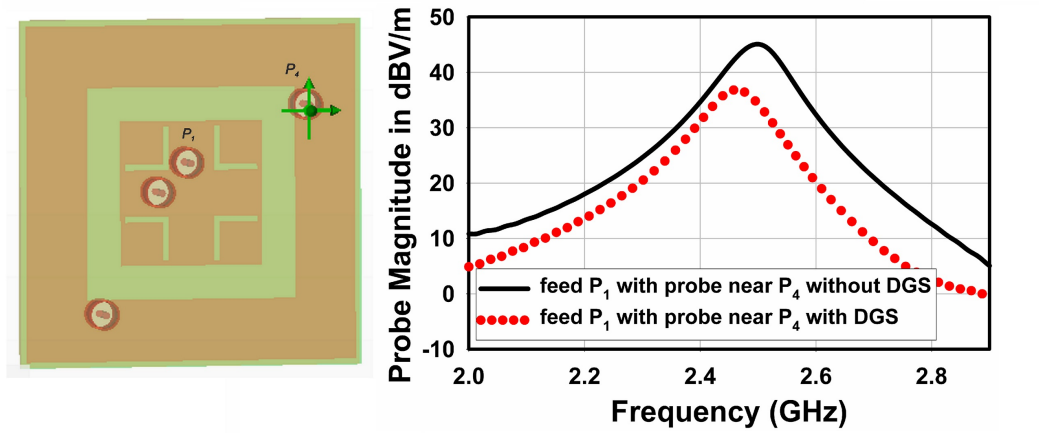
Figure 3.7: E Field measured within dielectric from simulation using probe

resonator at the operating frequency of the main antenna. For a ring slot, λ depends on the width of the ring, which takes into consideration both the inner and outer dimensions of the ring. Parametric study of the square ring DGS is performed to study the impact of length L_2 and width W_6 towards the mutual coupling and antenna resonances. Parametric study of the width W_6 of the ring slot in Figure 3.8(a) with L_2 fixed at 38 mm, shows that the resonance of inner patch antenna varies with W_6. A width of 4 mm provides good isolation and impedance matching at 2.45 GHz for square patch feed ports. The length of the ring slot affects the resonant frequency of the square ring antenna. Parametric simulation of S_{33} and S_{44} with the variations in the length of the ring slot is shown in Figure 3.8(b). The curves indicate that the resonant frequency of the square ring antenna decreases as the length of the DGS is increased. The length of the ring arm is chosen to be 38 mm for resonance at a frequency of 2.45 GHz. Parametric studies of S_{41} and S_{32} with variation in length and width of ring DGS are shown in Figure 3.8(c) and Figure 3.8(d) respectively. It can be inferred that an increase in the length and width of the ring slot improves isolation, however, it changes the impedance matching of the patch and ring antennas and shifts the resonant frequencies. Hence, this alters the individual resonant frequencies of the antenna elements.
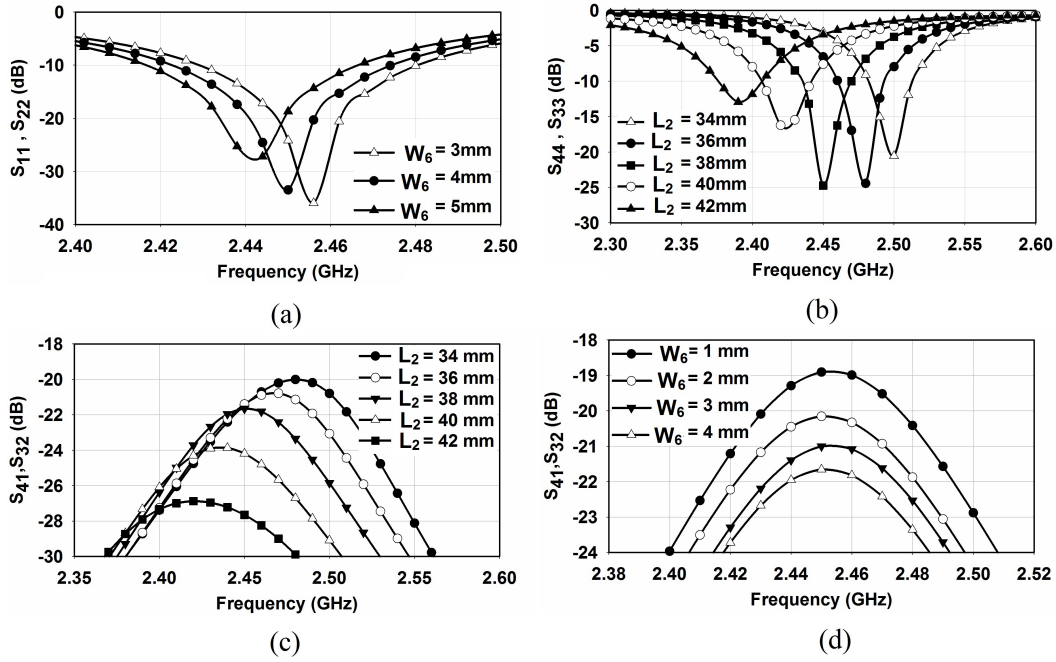
Figure 3.8: Parametric studies of length and width of ring DGS

(a) effect of the width of ring DGS on square patch antenna resonance

(b) effect of length of ring DGS on square ring patch antenna resonance

(c) effect on ring DGS length on S_{41} / S_{32}

(d) effect of ring DGS width on S_{41} / S_{32}

3.2.3 Simulations and Measurements

From the isolation studies, it can be observed that a ring shaped inductive slot etched on the ground plane of the multi-element antenna, improves isolation from -15 dB to -22 dB between highly coupled square and ring patch antenna elements. Ring DGS introduces some meandering on the current path of the outer ring patch antenna, thereby increasing its effective electrical length. In doing so, the resonant frequencies of the ring antenna decrease without an actual increase in antenna dimensions. Hence, by introducing the isolation structure, apart from improving isolation between the antenna elements, ring antenna elements are made to resonate at the same frequency of about 2.45 GHz as that of the square patch antenna. The simulated S parameters of the

quad element MIMO antenna with the ring DGS are shown in Figure 3.9. The
-10 dB impedance bandwidth is about 2 % for square patch ports P_1 and P_2,
and 1.5 % for ring ports P_3 and P_4. Simulated 3D radiation patterns obtained
for the four antenna elements are shown in Figure 3.10. Pattern shapes of
square patch antenna exciting fundamental orthogonal modes are similar to
each other, and differ from the patterns of the ring patch antenna exciting
higher order orthogonal modes.
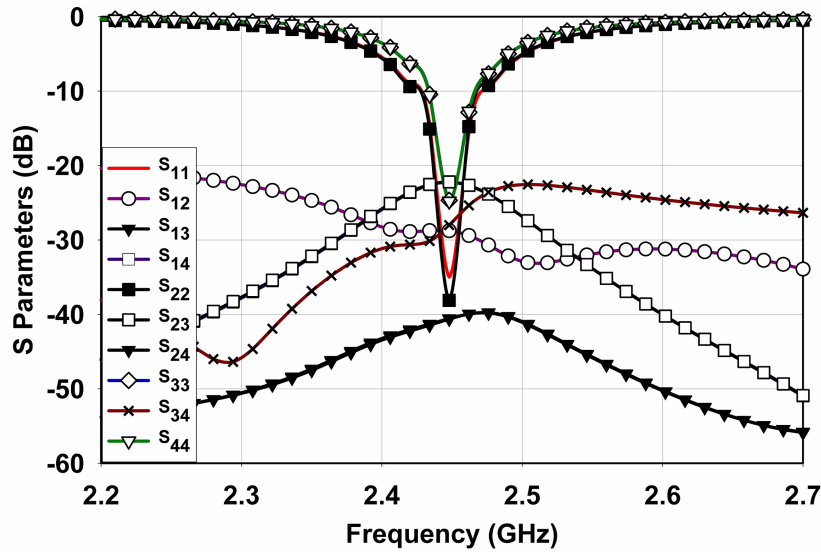
Figure 3.9: Simulated S parameters with ring DGS

The prototype of the quad element collocated multimode microstrip patch
antenna is fabricated on an FR4 substrate as shown in Figure 3.11. Measured
S parameter results using a Vector Network Analyzer is shown in Figure 3.12.
It can be observed that all the four elements resonate at the same frequency
of 2.45 GHz, similar to that of the simulation curves. The results achieved
guarantees good MIMO performance with mutual coupling between any pair
of ports well below -20dB. Minimum isolation between the inner and outer
microstrip patch antenna modes are about 25dB in the operating band. The
antenna elements have a measured peak gain of 4.4 dBi for square patch an-
tenna modes and 2.3 dBi for ring antenna modes. The efficiency measured are
86 % for square patch antenna elements and 71 % for ring antenna elements.
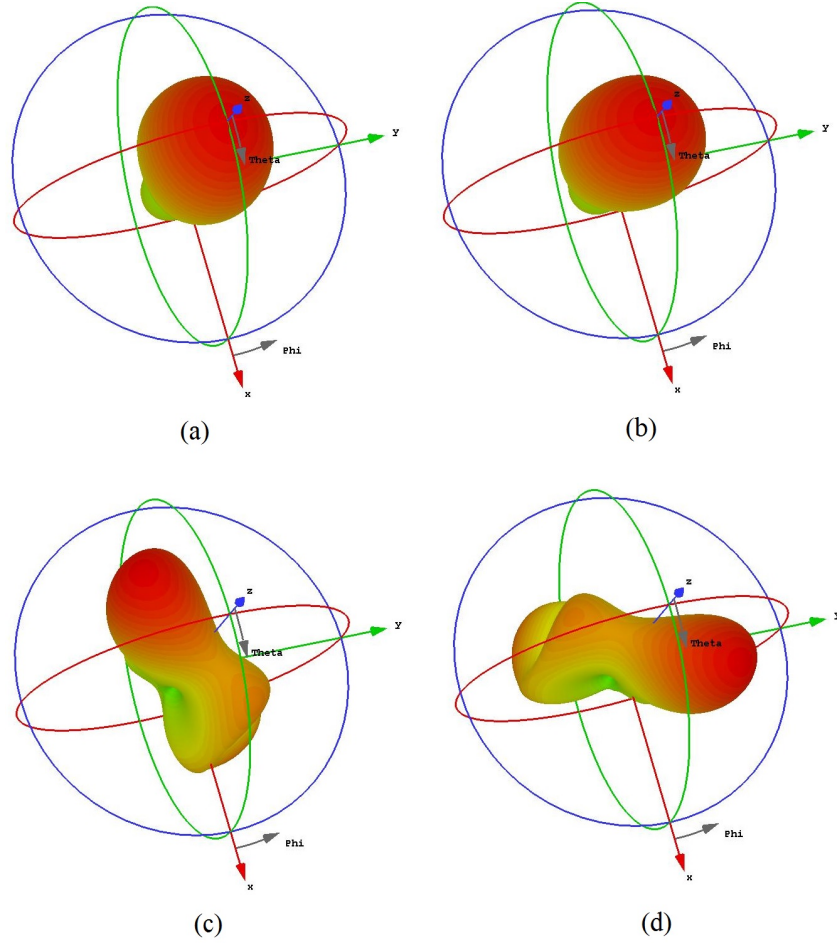
Figure 3.10: Simulated 3D radiation pattern of the MIMO antenna (a) P_1 excited (b) P_2 excited (c) P_3 excited (d) P_4 excited

Normalized far-field radiation patterns measured for all four antenna elements in the 0^0 plane and 90^0 planes of the antenna is as shown in Figure 3.13. It can be observed that the square patch elements P_1 and P_2 have polarization planes orthogonal to each other which by itself can ensure the least coupling between the ports. A similar polarization diversity can be observed between the radiation patterns of outer ring antenna elements. The asymmetric ring antenna elements P_3 and P_4 excites higher order modes and measures a little higher cross polar levels in the radiation pattern. The shape of the pattern is not the same for square and ring antenna elements. Hence, they radiate
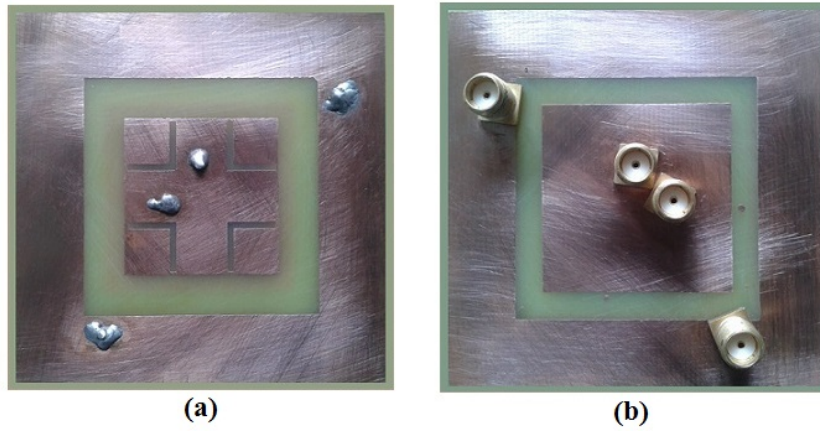
Figure 3.11: Fabricated prototype of the antenna (a) top view (b) bottom view
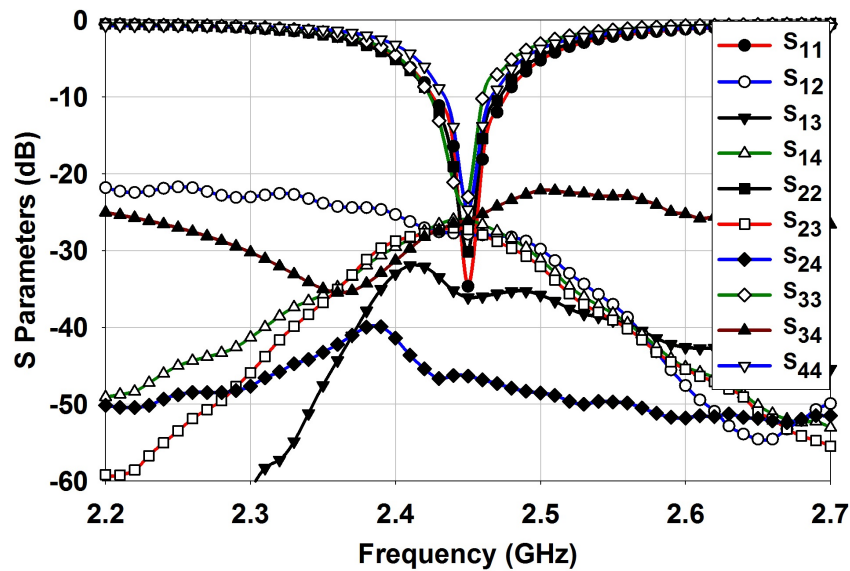
Figure 3.12: Measured reflection and transmission characteristics

distinctively which guarantees pattern diversity.

Diversity performance is analyzed to characterize the MIMO antenna system. In a wireless communication system, reflected signals in a channel environment cause multipath propagation. These multiple signals arrive at the receiver with a small time difference and can cause interference with one another. To study the diversity performance, a channel needs to be modeled as a statistical power distribution function. For example, an outdoor urban envi-
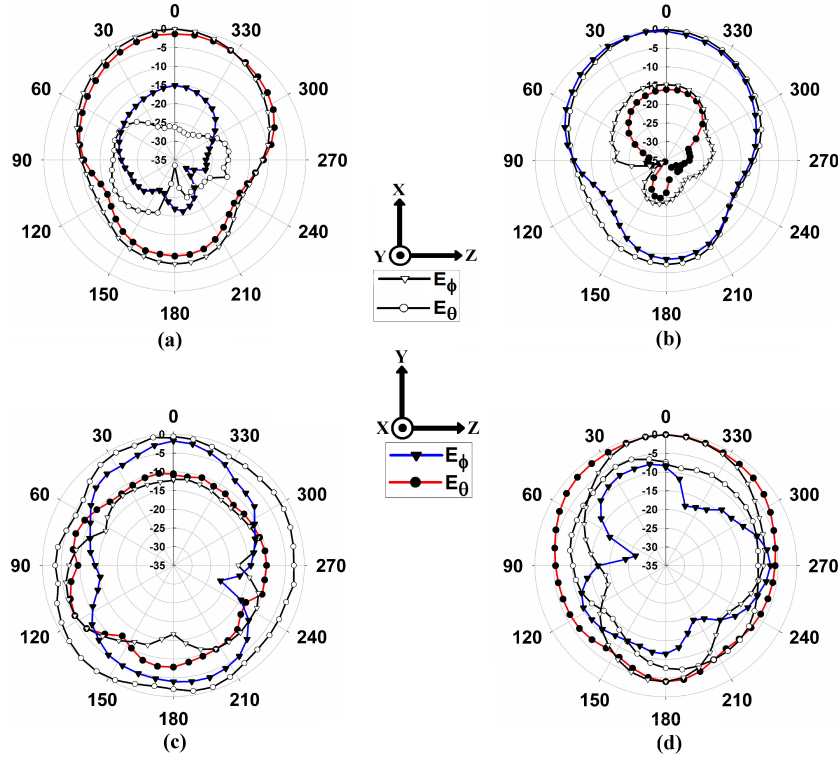
Figure 3.13: Measure radiation patterns of the antenna (a) P_1 excited (b) P_2 excited (c) P_3 excited (d) P_4 excited

ronment can be typically characterized by a Gaussian distribution in elevation and uniform along azimuth [142]. Scattering matrix and far field radiation patterns are used to evaluate the MIMO performance of the proposed antenna system. Envelope correlation ρ_{ij} gives a measure of antenna radiation pattern diversity. A relation between correlation factor ρ_{ij} and scattered parameters for N port antenna is derived in [192] and is given as

$$\rho_{i,j} = \frac{|\Sigma_{n=1}^{N} S_{ni}^* S_{nj}|}{\sqrt{(1 - \Sigma_{n=1}^{N}|S_{ni}|^2)(1 - \Sigma_{n=1}^{N}|S_{nj}|^2)}} \qquad (3.2)$$

Computation of correlation coefficients from S parameter gives very low values, less than 0.05. Because the S parameter approach is not so accurate, it is preferable to measure envelope correlation from far field radiation patterns [133] as given in equation (3.3). Here, XPR is the cross polarization ratio of the incident field and is defined as $XPR = P_V/P_H$ where P_V and P_H are the

average power along the spherical coordinates θ and Φ. $E_\theta i$ and $E_\Phi i$ are the complex envelopes of θ and Φ components of far field radiated field, when only the ith port is excited and other ports are terminated with 50 Ω loads. P_θ and P_Φ are the probability distributions of the power incident on the antenna in the θ and Φ polarization's respectively. The angle Ω is defined by θ in elevation and Φ in azimuth. An isotropic channel environment is considered where the powers of horizontal and vertically polarized incident waves are almost equal. For an isotropic environment, the cross polarization discrimination $XPR = 1$ and probability distributions of the power incident on the antenna in the θ and Φ polarization's is $P_\theta = P_\Phi = 1/4\pi$.

$$\rho_{i,j} = \left[\frac{\oint (XPR \cdot E_{\theta i}E_{\theta j}^* P_\theta + E_{\phi i}E_{\phi j}^* P_\phi)d\Omega}{\sqrt{\oint (XPR \cdot E_{\theta i}E_{\theta i}^* P_\theta + E_{\phi i}E_{\phi i}^* P_\phi)d\Omega \oint (XPR \cdot E_{\theta j}E_{\theta j}^* P_\theta + E_{\phi j}E_{\phi j}^* P_\phi)d\Omega}} \right]^2$$
(3.3)

Envelope correlation coefficients obtained are satisfactory with very low correlation values across the impedance bandwidth. The envelope correlation coefficients ρ_{ij} between any combination of elements of the fabricated prototype is below 0.3, across the operating frequency range as shown in Figure 3.14. It shows that the elements of the multiple antenna system radiate uncorrelated waveforms indicating very good MIMO performance. Polarization diversity and diverse patterns obtained from different radiating modes help in maintaining a low correlation between patch antenna elements.
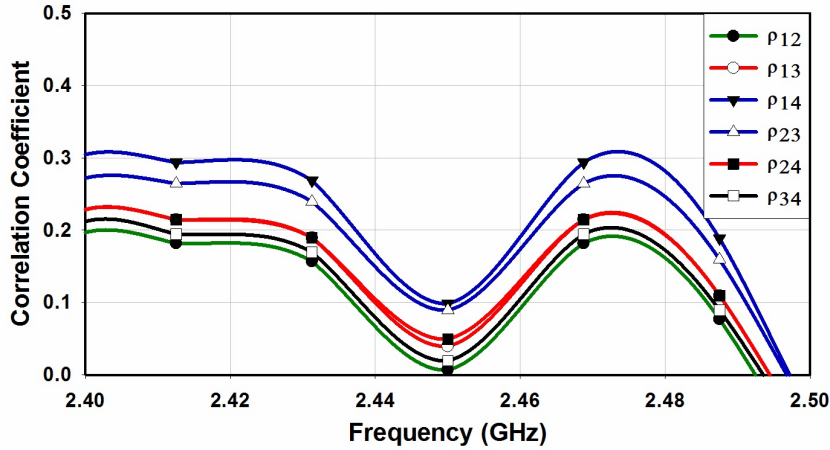
Figure 3.14: Envelope correlation coefficient between waveforms

3.3   Concentric square ring patch MIMO Antenna loaded with CSRR

In this section, a quad element multiple-input-multiple-output (MIMO) antenna system is designed and analyzed using concentric square ring patch antennas. Unlike the conventional $\lambda/2$ microstrip patch antennas, ring antennas are much more compact. The multiple resonant modes of square ring antennas are made to resonate at 2.45 GHz band with an overall system dimension of $0.48\lambda_0 \times 0.48\lambda_0$. Both polarization and angle diversity techniques are employed to create decoupled square ring patch antennas in forming a quad element MIMO. Coupling between elements, in the collocated concentric rings having E- fields in the same direction, are higher. Isolation is achieved here, by etching a pair of subwavelength resonant structure like complementary split ring resonator (CSRR) at the strong coupling areas. CSRRs are loaded in a non periodical fashion between the two ring antennas at the ring corners for enhancing isolation between patch antenna elements. The efficacy of concentric rings in the MIMO antenna design, along with proposed isolation improvement technique, is investigated and validated using measurements.

3.3.1   MIMO Antenna Geometry and its Design

The design uses concentric ring patches resonating in different transverse magnetic modes. The geometry of the antenna is shown in Figure 3.15 and its dimensions are shown in Table 3.2. This design was initialized with a single ring patch antenna made to resonate in the two fundamental orthogonal modes TM_{10} and TM_{01}. The square ring metal strip is supported by an $FR4$ dielectric substrate of relative permittivity $\varepsilon_r = 4.4$, loss tangent $tan\delta = 0.02$ and thickness 1.6 mm. The ring antenna have outer and inner dimensions as W_4 and W_5 to resonate in 2.45 GHz band.

Apart from being compact, the microstrip square ring antenna has a slightly enhanced bandwidth than square patch due to the low amount of energy stored under the metallic regions. A ring antenna is realized by removing the central conducting portion, thereby reducing the metallic portions which
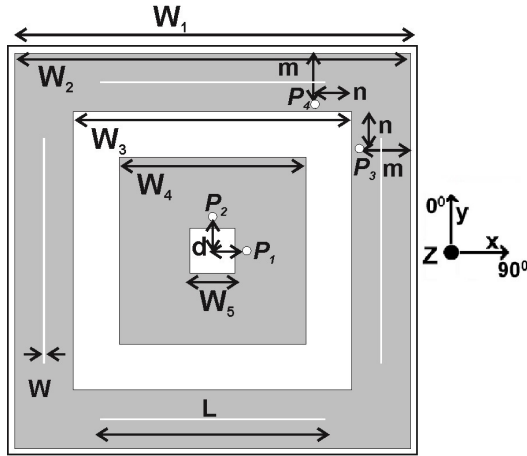
Figure 3.15: Geometry of the MIMO antenna using concentric rings

Parameter	Value (mm)	Parameter	Value (mm)
W_1	60	n	5.4
W_2	58	d	5
W_3	40.8	L	33
W_4	27.4	W	0.2
W_5	6.6	m	7.5

Table 3.2: Antenna Dimensions of concentric ring MIMO antenna

can reflect and confine energy within the dielectric. A 2:1 VSWR bandwidth of 75 MHz (about 40 % improvement), was achieved for the ring antenna, with W_5 increased to 6.6 mm as shown in Figure 3.16. Transmission curve S_{12} shifts to a lower frequency with an increase in W_5, however, coupling levels remain unaltered. The feeding structure is simple and impedance matching can be done easily by varying the feed position along the two principal X and Y axis.

The second square ring encloses the inner ring, thus making the structure compact than placing elements with half wave length spatial separation. Feed positions are chosen so as to excite higher order orthogonal modes TM_{21} and TM_{12} with high isolation between them. The two ports of the outer ring have low VSWR bandwidth which may restrict its practical applications. The small bandwidth of these ports is due to the feed positions chosen so as to excite orthogonal higher order modes with minimum coupling. For higher order modes where the substrate thickness is not negligible, the effects of surface wave propagation will be high.

To improve bandwidth, reactive loading of the antennas is done by etching slots on each ring arm. These half wave length slots have a resonant frequency near to the operating frequency of the main antenna. Thus the operating bandwidth is enhanced by 60 % from 50 MHz to 80 MHz as shown in
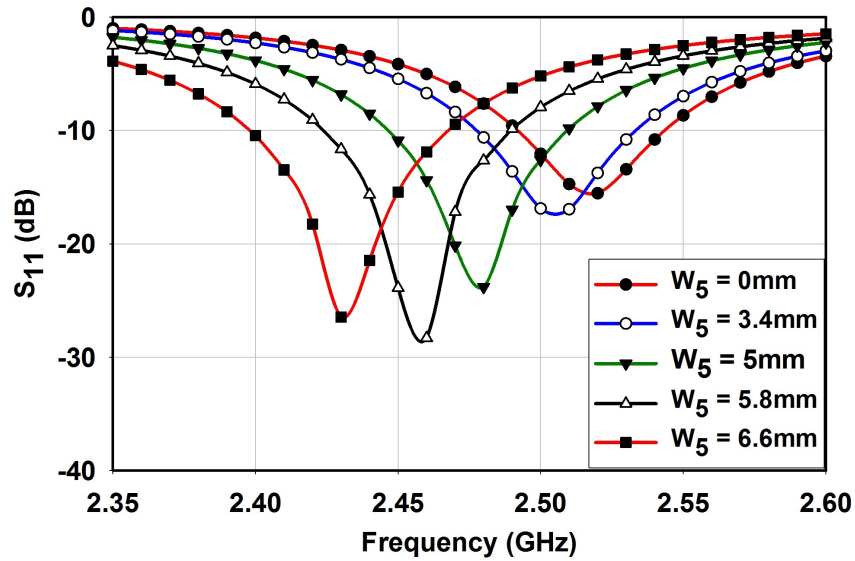
Figure 3.16: Effect of inner ring patch width on inner ring reflection characteristics

Figure 3.17. Slit loading also reduces the coupling between orthogonal higher order ring modes. Ports P_1 and P_4 being linearly polarized along the X axis have high coupling between them, similar is the case between Y polarized elements P_2 and P_3. The simulated S parameters of the MIMO antenna using microstrip concentric square ring patches are shown in Figure 3.18.
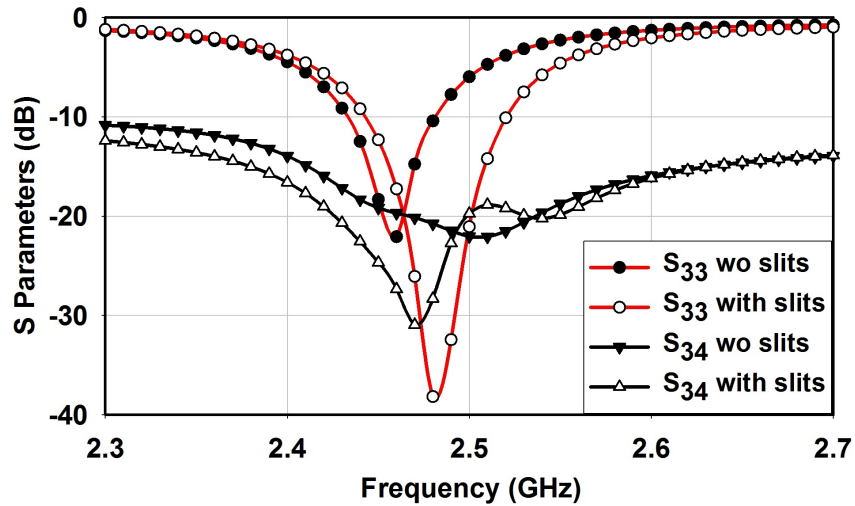
Figure 3.17: Effect of slits on outer ring patch antenna bandwidth
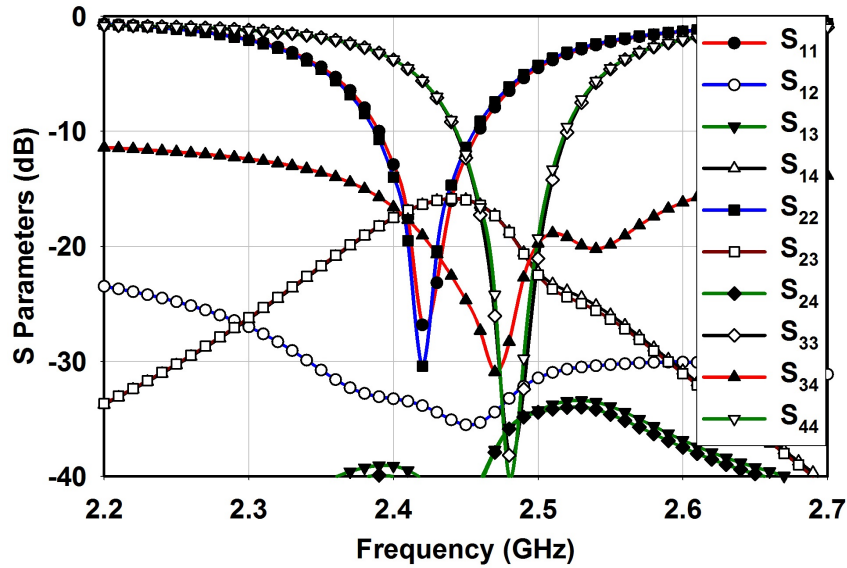
Figure 3.18: Simulated reflection and transmission characteristics

3.3.2   Study of CSRR for isolation enhancement

There are mainly two sources of mutual coupling, the surface wave coupling between antenna elements printed on the same substrate and the current flowing on the shared ground. In order to reduce coupling currents, complementary split ring resonators (CSRR's) are etched on the ground plane between the square rings using the design formula in [193]. The proposed structure consists of a pair of CSRR etched in the corners of the antenna in between the two concentric square rings with a tilt angle of 45^0. The ground plane of the concentric ring MIMO antenna with CSRRs etched on the ground is shown in Figure 3.19. These are points where coupling currents are stronger. CSRR exhibits a resonant property in the presence of vertically polarized electric fields. The presence of CSRR on the ground alters standing wave distribution within the antenna.

When an electromagnetic wave is incident on the antenna, the magnetic field along Z direction interacts with the CSRR etched on the ground of antenna as shown in Figure 3.20(a). This creates an electromotive force inside the antenna and disturbs the induced currents inside the ground plane. As a result, the ground currents on the adjacent ring changes its polarity by nearly
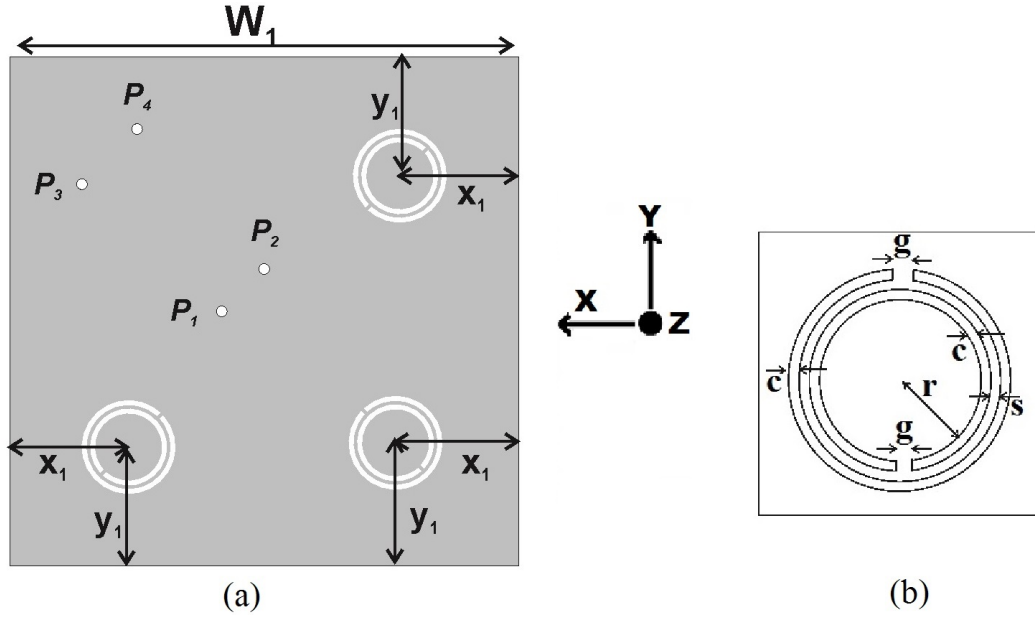
Figure 3.19: Geometry of ground plane of the antenna with CSRR (a) back view (b) CSRR enlarged view; $x_1 = 16.4mm$, $y_1 = 16.4mm$, $c = 0.5mm$, $s = 0.5mm$, $g = 0.5mm$, $r = 0.4mm$

180^0 which can be observed from ground current distribution in Figure 3.20(b). Thus, vertically polarized space waves of P_1 and P_4 are out of phase now, which ensures least coupling between them.

Ground coupling currents are diminished significantly, resulting in an isolation enhancement of 6.5 dB as shown in Figure 3.21. The disturbance can change the characteristics such as equivalent inductance and capacitance, thus obtaining the band stop at the frequency of interest. Further studies on the current distributions show an improved isolation between the two ring patches with the CSRR on the ground. Current distributions on the ground plane for four antenna elements at the resonant frequency 2.45 GHz is simulated and displayed in Figure 3.22.
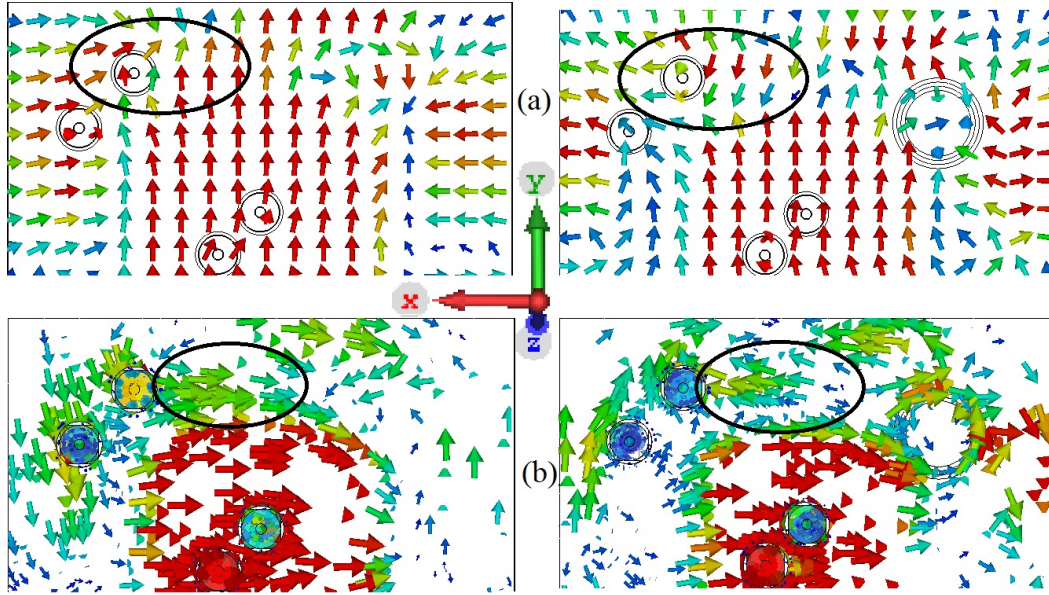
Figure 3.20: Polarity reversal on adjacent ring with P_1 excited at 0^0 phase with and without CSRR (a) H field (b) surface currents
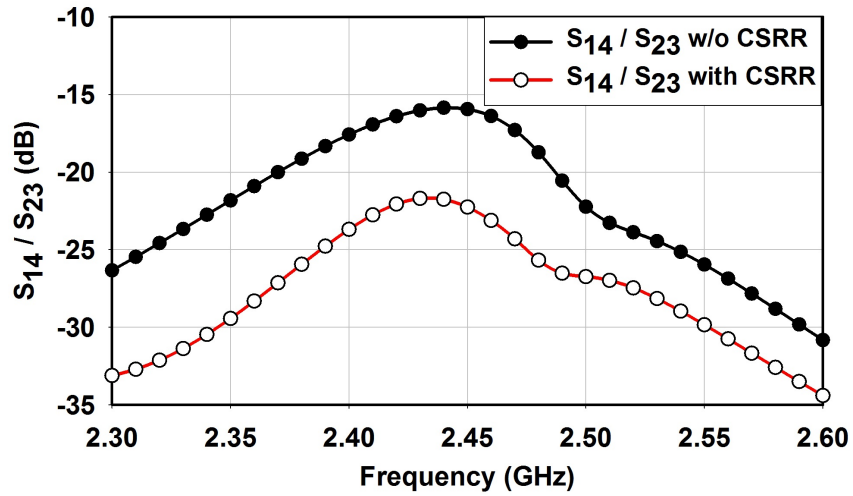
Figure 3.21: Isolation characteristics without and with CSRR

3.3.3   Simulation and Measurements

The simulated results of the concentric ring MIMO antenna with the CSRR isolation structure are shown in Figure 3.23. Simulated 3D radiation patterns
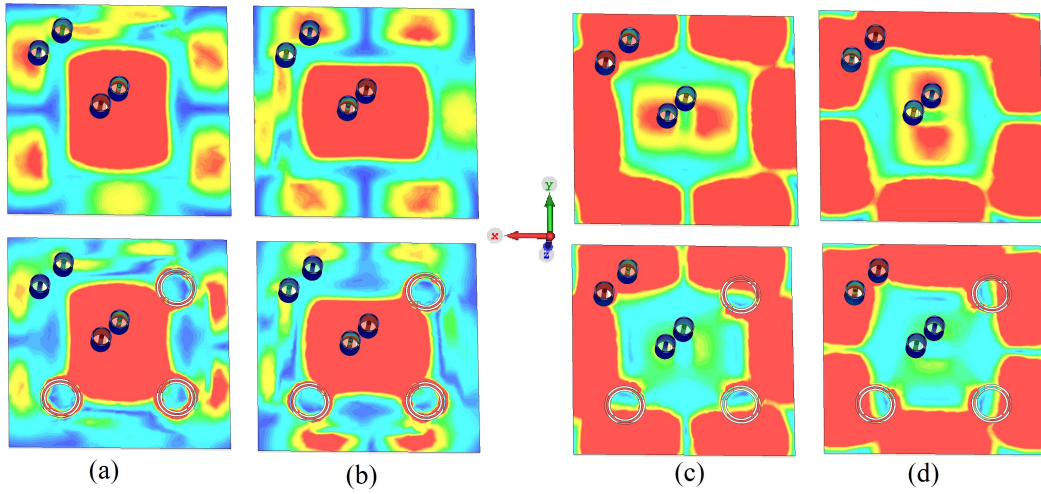
Figure 3.22: Surface current on ground without and with CSRR for (a) P_1 (b) P_2 (c) P_3 (d) P_4
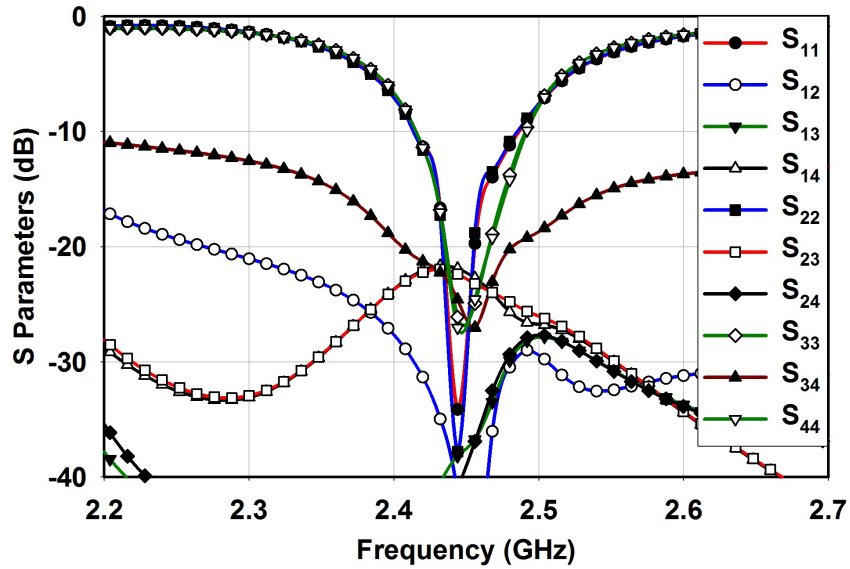
Figure 3.23: Simulated reflection and transmission characteristics with CSRR on ground

obtained for the four antenna elements are shown in Figure 3.24. Fabricated prototype antenna and its S parameters measured using a Vector Network Analyzer, are shown in Figure 3.25 and Figure 3.26 respectively. Reasonably

good agreement between the simulated and measured results are achieved. Measured peak gain values of inner ring modes and outer ring modes are 4 dBi and 3.4 dBi respectively. Peak efficiency obtained for inner ring ports is 84.6 %, and outer ring ports are about 72.5 % in the 2.4 GHz ISM band.

(a)   (b)

(c)   (d)
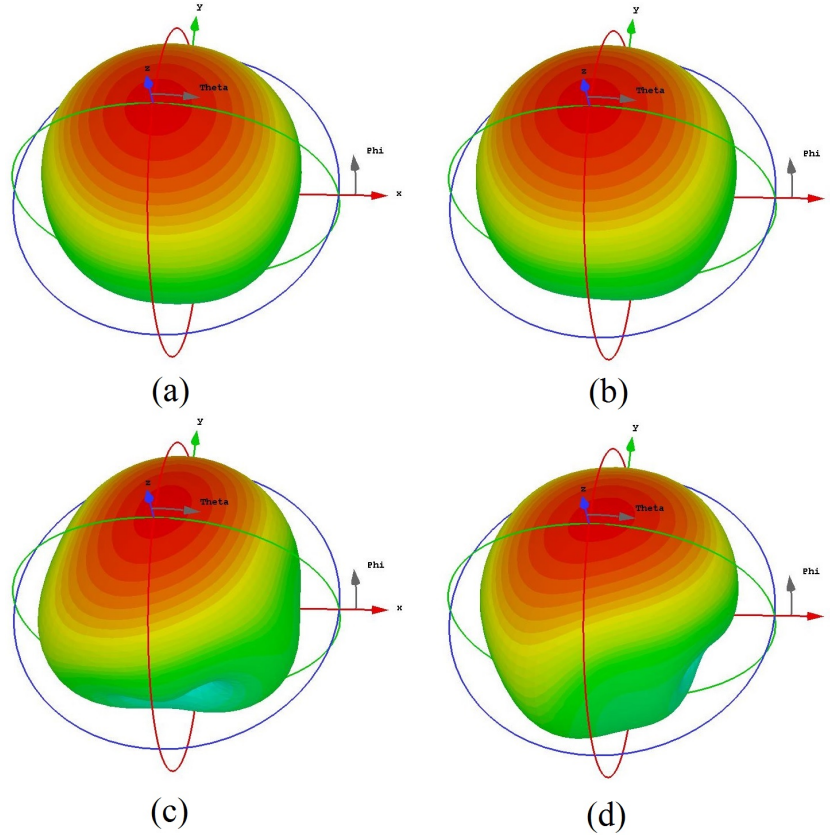
Figure 3.24: Simulated 3D radiation pattern of the MIMO antenna (a) P_1 excited (b) P_2 excited (c) P_3 excited (d) P_4 excited

Far-field radiation pattern measurements, obtained by exciting individual ports and terminating other ports with matching load, are shown in Figure 3.27. Normalized far-field radiation pattern measured for all the four ports in 0^0 plane and 90^0 planes of antenna shows that feed ports P_1 and P_2 have polarization planes perpendicular to each other, which ensures least coupling between ports. A similar polarization diversity can also be perceived between outer ring antenna elements P_3 and P_4. The shape of the pattern is different
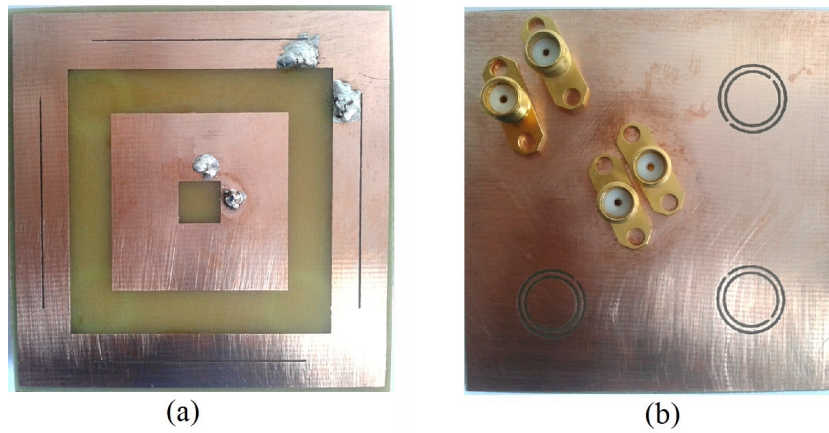
Figure 3.25: Fabricated prototype of the antenna (a) top view (b) bottom view
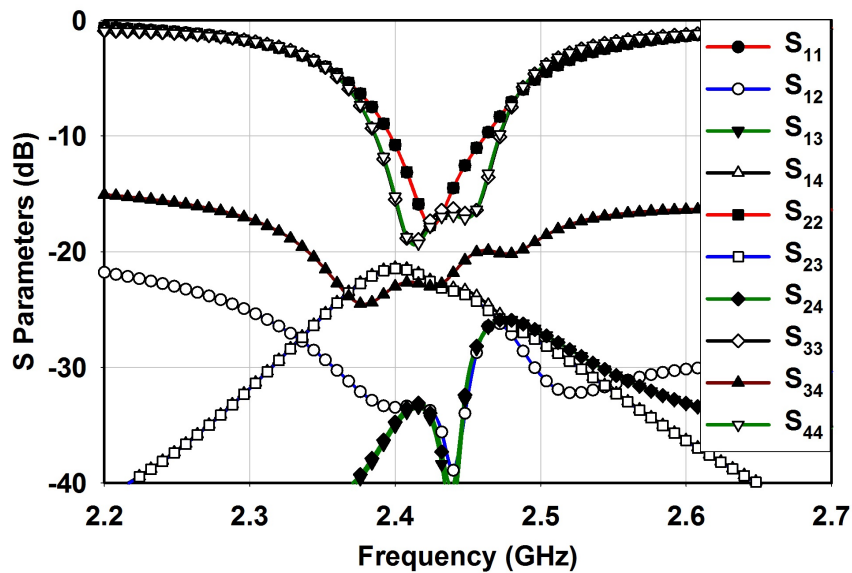
Figure 3.26: Measured S parameters of the MIMO antenna

for fundamental and higher order modes, so that they radiate differently and it ensures angle diversity.

The diversity performances of MIMO system are evaluated by computing envelope correlation coefficients. It provides correlation among the amplitudes of individual elements of the antenna. The computed values of envelope correlation coefficients using equation (3.3) are plotted in Figure 3.28. It is
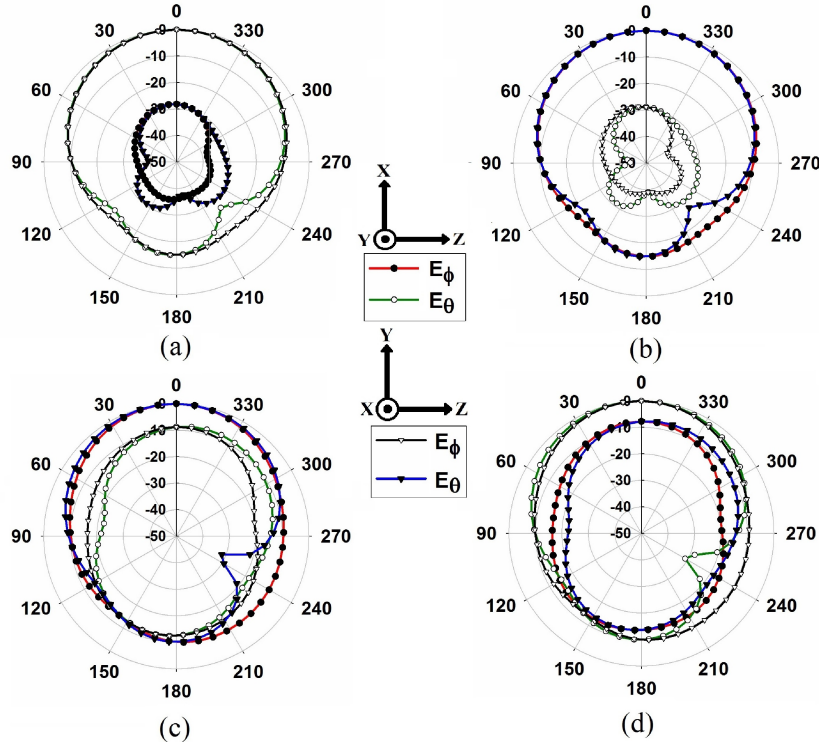
Figure 3.27: Measured radiation patterns of the antenna (a) P_1 (b) P_2 (c) P_3 (d) P_4 excited

observed that, within the operating band, correlation coefficients are below 0.4 which ensures good MIMO performance.

3.4   Microstrip cross and ring patch MIMO Antenna with interdigital structure

Another design of a quad element MIMO antenna system, employing polarization and pattern diversity technique, uses a microstrip cross patch embedded within a square ring patch antenna. The antenna system, resonating at 2.45 GHz band, uses a dual polarized two port cross patch antenna and an orthogonally polarized two port square ring patch antenna. The cross patch antenna has the benefit of lower cross polarization levels, which reduces the
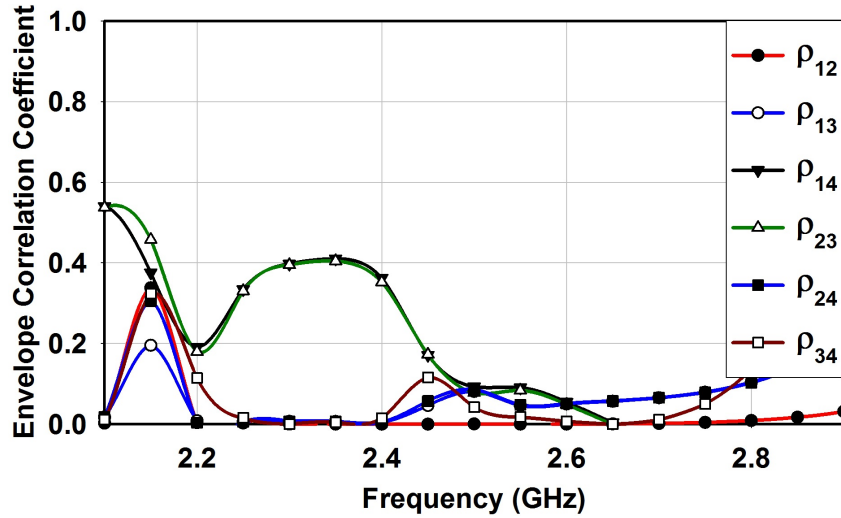
Figure 3.28: Envelope correlation coefficient between waveforms

coupling between its orthogonal elements. The narrow bandwidth of the outer
ring modes of the square ring antenna is doubled by etching half wavelength
slits along the four arms. High mutual coupling between elements of the cross
and ring patch, with identical field orientation, is lowered by incorporating
an interdigital structure on the ground plane. Interdigital ground structure
between cross and ring antenna elements is simple to fabricate and easy to
tune to a desired frequency range, which makes it a good candidate for fu-
ture miniature designs. The overall dimension of the four port multi-element
antenna is about $0.5\lambda_0 \times 0.5\lambda_0$, which makes it fairly compact. The antenna
achieves better performance by making use of a cross patch and ring patch
combination for the MIMO antenna design, along with the use of an interdig-
ital ground structure for obtaining high isolation between its elements.

3.4.1   MIMO Antenna Geometry and its Design

Based on the diversity techniques, a compact four port MIMO antenna is de-
signed. The geometry of the antenna is shown in Figure 3.29 and its dimen-
sions are shown in Table 3.3. An orthogonally polarized two port cross patch
antenna is designed initially with a larger dimension of 31 mm $(L_4 + W_1 + W_1)$
and a smaller dimension of 18.6 mm (L_4), resonating at a frequency of 2.45
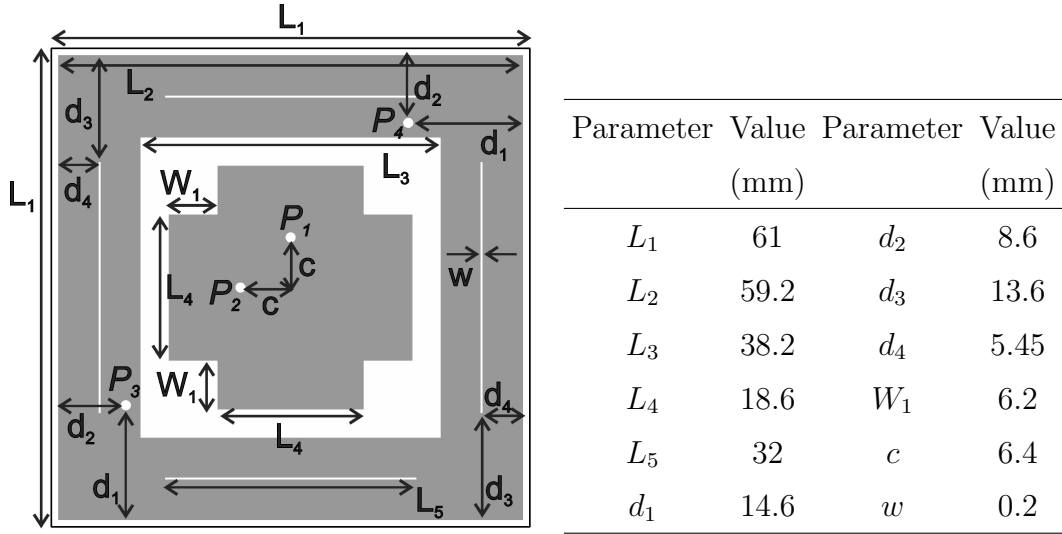
Figure 3.29: Geometry of the four port MIMO antenna system

Parameter	Value (mm)	Parameter	Value (mm)
L_1	61	d_2	8.6
L_2	59.2	d_3	13.6
L_3	38.2	d_4	5.45
L_4	18.6	W_1	6.2
L_5	32	c	6.4
d_1	14.6	w	0.2

Table 3.3: Antenna Dimensions of cross and ring patch MIMO antenna

GHz as shown in Figure 3.30 (a). Feed points are chosen along the principal X and Y planes, exciting two fundamental orthogonal modes TM_{10} and TM_{01}.

For cross patch antennas, L_4 can be reduced so that the pattern becomes more confined. The back lobe is reduced by 2-4 dB, with L_4 changing from 31 mm to 18.6 mm. An extended range of frequency ratio can be achieved by tuning L_4. Apart from a shift in the resonant frequency, there is no change in coupling levels between cross patch modes with varying L_4. In this case, about 41.6% enhancement in 2:1 VSWR bandwidth is obtained, by reducing the value of L_4 as shown in Figure 3.30 (b). The two port antenna has a VSWR bandwidth of 85 MHz, which covers the ISM band. Furthermore, the crosspatch geometry has a slightly improved performance in terms of reduced cross-polar and increased co-polar currents, making it a good candidate for polarization diversity based MIMO designs.

The outer antenna which encompasses the cross patch antenna within its structure is chosen to have a ring shape as in the previous designs. The spacing between antenna elements is much smaller, about $0.03\lambda_0$. Diverse radiation patterns of cross patch and the ring patch provides a low correlation between the waveforms. Feed positions for the ring antenna are chosen so as to excite
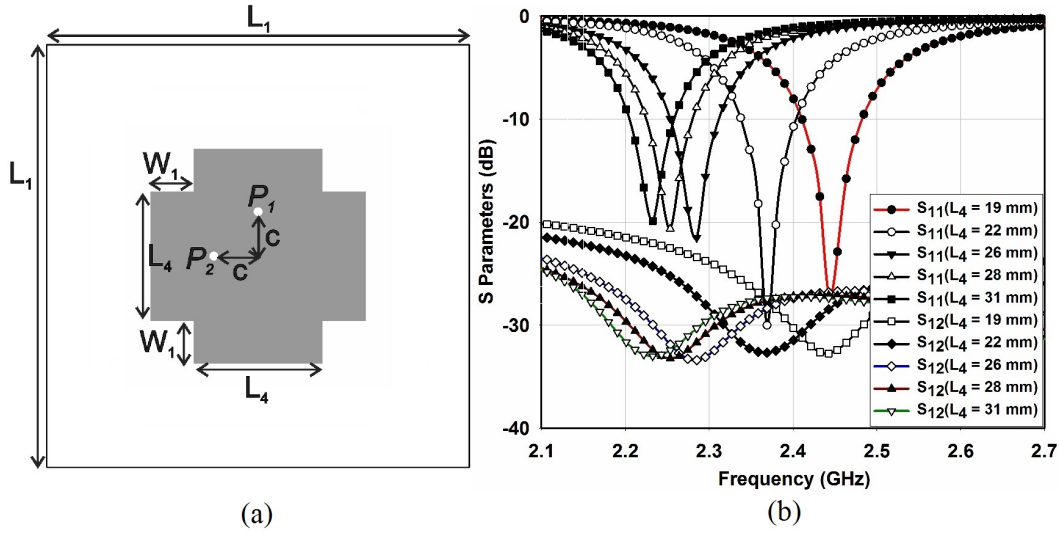
Figure 3.30: Two port cross patch antenna

(a) Geometry

(b) Effect of cross patch length on reflection and transmission characteristics of two
port antenna

two orthogonally polarized modes resonating at the same frequency as that
of the cross patch. The square ring dimensions are adjusted for transverse
magnetic modes TM_{21} and TM_{12} to resonate at 2.45 GHz, which corresponds
to a width of about $0.8\lambda_g$. These higher order orthogonal modes of the ring
antenna have a low bandwidth of about 35 MHz, which is not sufficient to cover
the 2.4 GHz ISM band. Therefore a method of reactive loading is employed
as discussed in section 3.3.1. The loading is achieved in the current design
by etching slots on the ring arm, which increases the bandwidth by 143 %,
without having any adverse effect on the mutual coupling between orthogonal
ports.

Effect of Slits on the Ring Patch

The microstrip square ring antenna is loaded inductively by etching slots on
each of its ring arms. The frequency ratio can be adjusted by changing the
length and width of these slots. Since the slots are closer to the radiating
edges, the fundamental modes of the ring will not be modified by its inclusion.
For TM_{21} and TM_{12} modes, currents are stronger in those areas where slots are

placed, and hence a strong influence on ring resonant frequency is observed. These half wavelength slots resonate near the operating frequency of the main antenna. Thus, slot resonance merges with the operating band of the square ring antenna to enhance the bandwidth from 35 MHz to 85 MHz as shown in Figure 3.31.
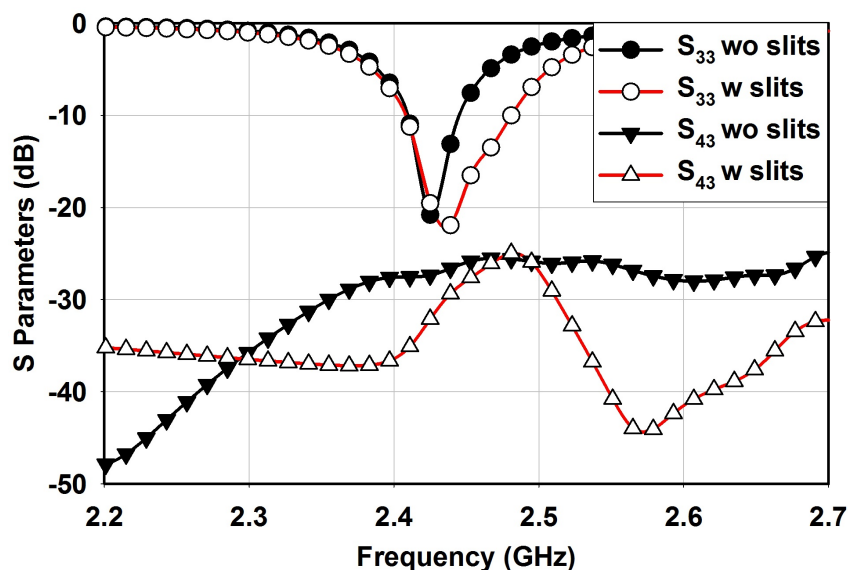
Figure 3.31: Bandwidth enhancement with slit dimensions

The parametric variation of slot length L_5 is shown in Figure 3.32(a), indicating that the slot resonance is adjacent to ring antenna resonance. The slot resonant frequency decreases with increase in length L_5. As the width w of the slot increases, current distribution along the ring arm with one half wave distribution is significantly altered. This causes an increase in cross polar currents which in turn results in increased coupling (S_{43}) between orthogonal ring ports as shown in Figure 3.32(b). The slot width is chosen so as to maintain minimum coupling between P_3 and P_4.

The proposed quad element MIMO antenna is simulated using CST microwave studio software. Reflection and transmission coefficients of antenna elements are analyzed and are shown in Figure 3.33. Orthogonal polarization between elements 1 and 2 guarantees high isolation, with low values of S_{21}. The same holds true for S_{34}, between orthogonal ring antenna ports P_3 and P_4.
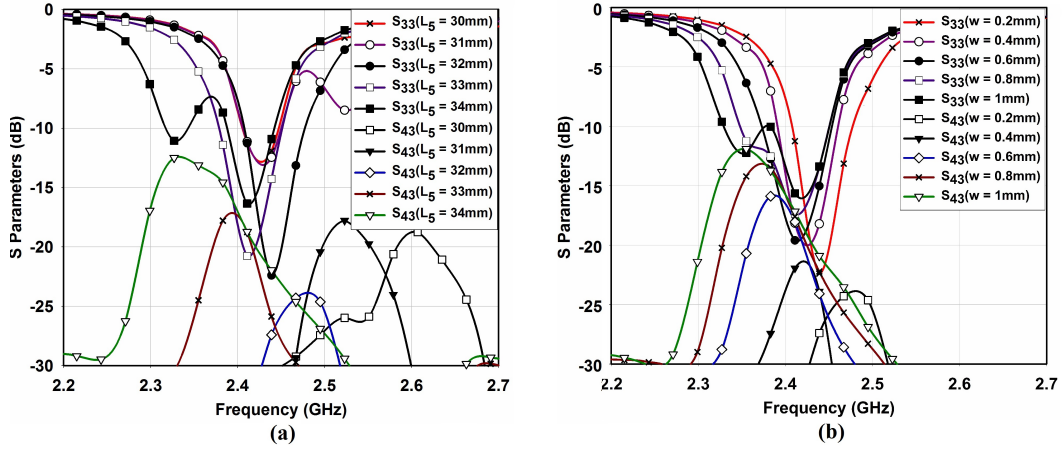
Figure 3.32: Effect of slit dimensions on ring antenna modes

(a) S_{33} / S_{43} with varying slit lengths

(b)S_{33} / S_{43} with varying slit widths

From the feed port orientation and current distribution, it can be interpreted that P_1 and P_3 are polarized along the X axis and P_2 and P_4 are polarized along the Y axis. Coupling between elements having identical E field orientation is significantly higher. This explains the reason why S_{13} & S_{24} are being high and S_{14} & S_{23} are being low. In the next section, the inclusion of interdigital structure in the ground of the MIMO antenna and the reduction in mutual coupling is investigated.

3.4.2 Study of Inter-digital structure to reduce mutual coupling

In order to reduce the TM_0 surface wave, an interdigital structure is etched on the ground between the cross and ring patches. This structure can suppress surface waves over a limited frequency range and can be easily accommodated between elements which have very little spacing between them. The designed isolation structure acts as a stop band filter which operates in the resonant band of the main antenna system. The inclusion of the structure in the ground, neither changes the resonant frequency nor the bandwidth of
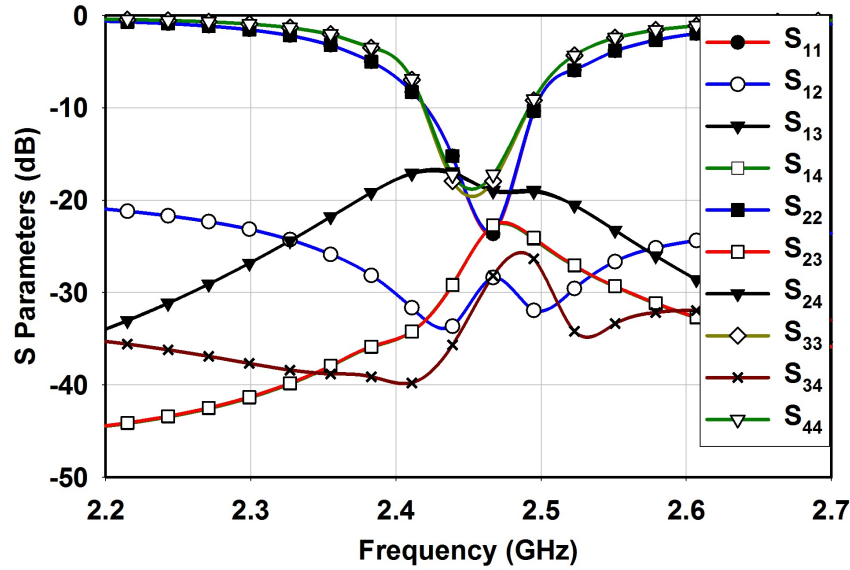
Figure 3.33: Simulated reflection and transmission characteristics of the antenna

the main antenna. In this design, one single strip of an interdigital structure is etched along both E and H planes between cross and ring antennas, as shown in Figure 3.34. This efficiently reduces coupling by 12.5 dB between elements having E-field vector orientation along the same direction. The coupling characteristics between cross and ring patch modes are shown in Figure 3.35. Isolation between other combinations of elements of cross and ring patch, i.e. between P_1 & P_4 and between P_2 & P_3 are also improved by 6 dB with the inclusion of interdigital structure. Isolation between orthogonally polarized fundamental modes of cross patch antenna (S_{12}) is improved by about 7 dB with its inclusion. Overall, the interdigital structure on the ground can efficiently suppress mutual coupling between all the feed elements rather than only enhancing isolation between highly coupled elements.

Isolation enhancement with the interdigital structure on the ground can be validated from the current distribution shown in Figure 3.36. The current distribution of an element of cross patch antenna (feed port P_1) and for an element of the square ring patch antenna (feed port P_3) on the ground plane is shown. It can be observed that with the interdigital structure, the two antenna elements are clearly isolated from each other with ground currents

(a)   (b)
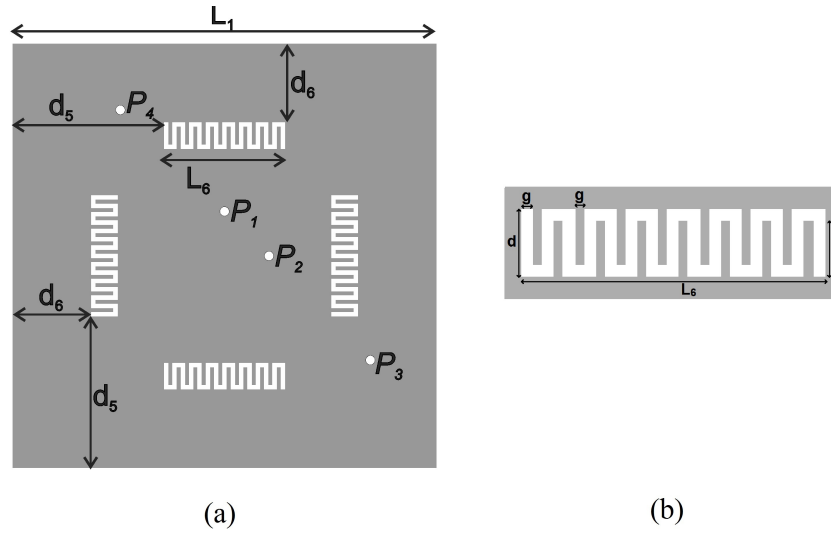
Figure 3.34: Geometry of ground plane of the antenna with ID-DGS (a) back view
of antenna (b) ID-DGS enlarged view; $d_5 = 20.9mm$, $d_6 = 10.4mm$, $L_6 = 17.4mm$,
$g = 0.6mm$, $l = 3.2mm$, $d = 3.8mm$
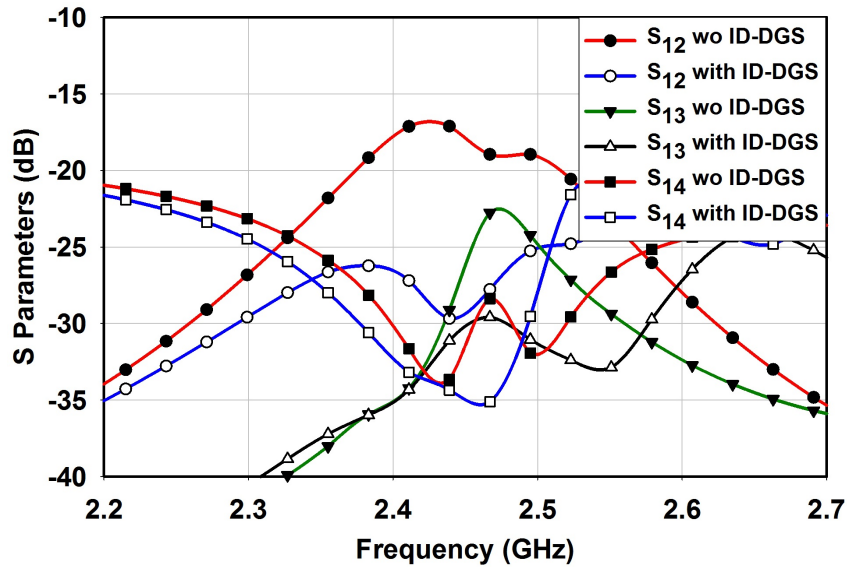
Figure 3.35: Isolation characteristics with ID-DGS

concentrated on its respective areas. All these current distributions are ob-
served at the resonant frequency of 2.45 GHz. Only distributions for P_1 and

P_3 are shown here. The other set of ports P_2 and P_4 have the same magnitude of current as that of P_1 and P_3 respectively, since the quad element antenna system is symmetric in nature. However, polarization of P_2 will differ from P_1 (similarly P_3 differs from P_4) depending on the modes excited by them.
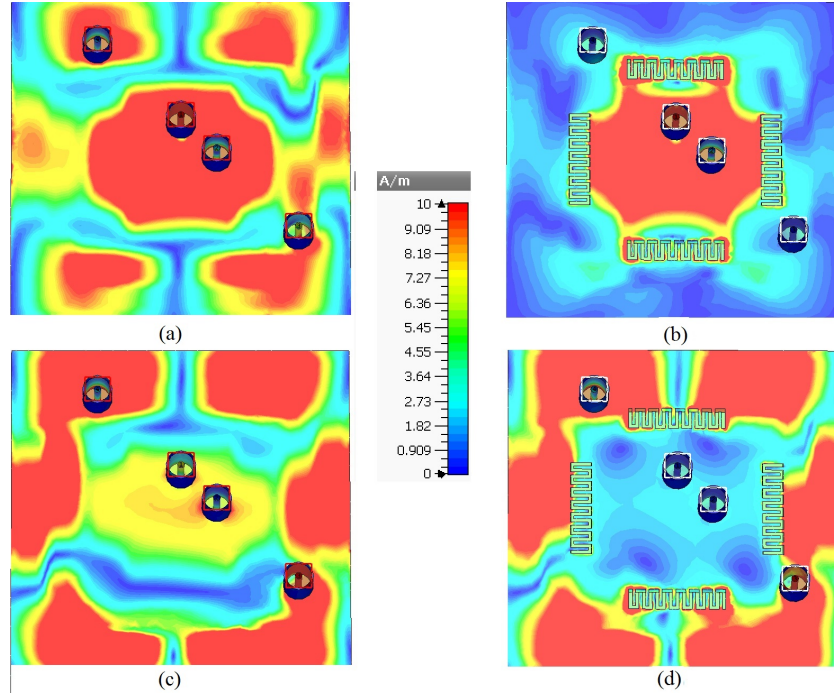
Figure 3.36: Ground surface current distribution (a) P_1 excited without DGS, (b) P_1 excited with DGS, (c) P_3 excited without DGS (d) P_3 excited with DGS

Further studies of the isolation enhancement structure, to evaluate the electromagnetic fields within the dielectric, is performed by E-field probing in the CST microwave studio as shown in Figure 3.37. The probes are placed near the feed positions, and the impact on E -fields with excitation of each feed is observed. Fields are measured along the Z axis at a height of about 0.8 mm in a 1.6 mm thick substrate. It was observed that, with interdigital structure, the E -field has gone down significantly along the Z axis for all combinations of feed elements. Two such combinations are shown in Figure 3.37, where probes are placed one on each cross and ring patch and E fields are measured for a worst case coupling scenario. The inclusion of the structure on the ground

reduced the field strength by about 13 dB. Displacement currents within the dielectric, which cause coupling between the feeds in their traveling path, are decreased significantly.
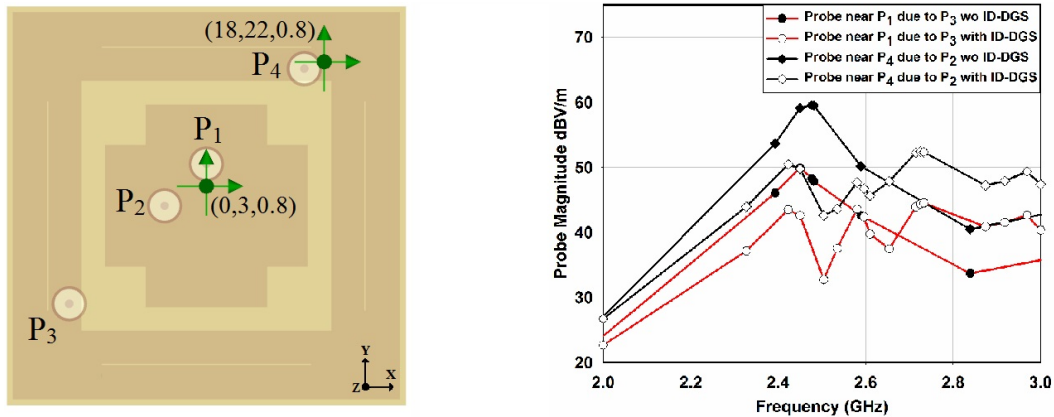
Figure 3.37: E field probe measurement without and with ID-DGS

Surface waves are examined by positioning two monopole probes near the surface at a distance of nearly 1 mm, as shown in Figure 3.38 and measuring the transmission between them. Measurements from a plane metallic ground and from a textured ground with the DGS, clearly indicates the frequency band with reduced surface waves. This method is adopted because a point source can launch all wave vectors and since surface waves cannot directly couple to external plane waves, it is measured using a very small probe. A small monopole probe antenna, when brought near the surface with which it is oriented normally, can couple to its surface wave modes [194]. The electric field of TM surface waves which extend vertically out of the surface, couples with a vertical electric field of the probe. A dielectric with similar dimensions as that of the proposed structure with a flat metallic ground plane and probes oriented vertically at the edges is used. Probe orientation, along both E and H plane edges, shows similar results, with a measured field near to -59 dB, which is very small owing to fading.

Now, with the same structure dimensions, having a flat metallic ground plane etched with interdigital structure, shows a notable decrease in measured E-field as shown in Figure 3.38. The reduction in the field shows a surface wave band gap in the frequency region, due to the inclusion of the structure on
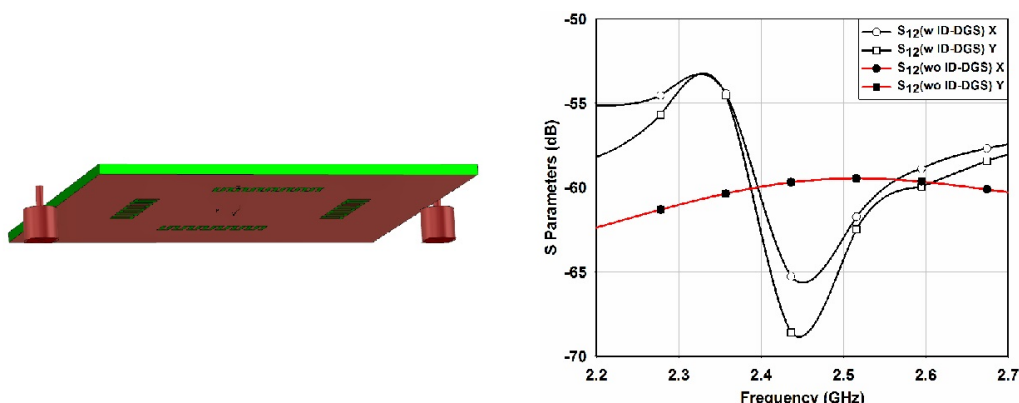
Figure 3.38: TM Surface wave measurement using probe antennas without and with ID-DGS on ground

the ground. This decrease in the field is more prominent in the E plane along the Y axis in spite of the symmetry of the textured surface on the ground. This is due to the fact that space wave coupling is stronger in the E plane of microstrip patch antennas. It is reported [195] that patch antennas launch a surface wave mode in the E-plane that decays as $\rho^{-1/2}$ while the lowest mode in H-plane decays as $\rho^{-3/2}$, where ρ is the distance between the two points or antennas between which coupling is considered. Therefore, higher surface coupling occurs in the E plane, compared to H plane orientation.

The interdigital structure etched on the ground has the capability to reduce cross polarization for the cross patch antenna. In this design, cross-polarization is reduced by about 4 dB and co-polarization is improved by 1.8 dB for P_1 as shown in Figure 3.39. The same scenario is observed for its orthogonal mode excited by P_2. For ring antenna modes no such improvement is observed. Therefore, this defected ground structure could be employed around any structures, to reduce the cross polarization of fundamental orthogonal modes. Due to this reduction in cross polar currents, S_{21} decreases by about 7 dB. It can also be explained as a decrease in the excited surface waves and an improvement in efficiency of cross patch elements. A slight increase in back radiation occurs due to the slots etched on the ground. However, this is comparatively less than other defected ground structures since interdigital structure requires a much smaller etching area.
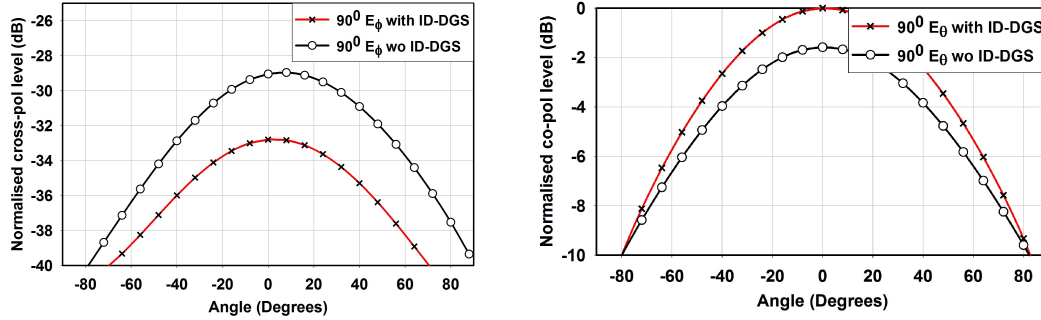
Figure 3.39: Cross and co-polarization levels without and with ID-DGS

Effect of Interdigital Structure Parameters on stop band frequency
One set of an interdigital structure is etched on each of the four arms between the cross patch and square ring patch, on the ground plane of the four port antenna system. By measuring transmission coefficients over the frequency range, the filtering nature of a DGS structure can be determined as shown in Figure 3.40. The interdigital structure can provide higher capacitive coupling to the patch than other commonly used defected ground structures. Apart from compactness, an advantage of this structure is that, its stop band frequency can be changed without changing the overall dimensions of the structure.

A transmission line method can be adopted to determine the stop band nature of the structure, which does not allow surface modes to propagate. A DGS is etched on the ground plane of a 50 ohm microstrip line fed at two ends. The substrate dimensions are chosen to be the same as the total dimension of the four port antenna. With the increase in length l of each element, capacitance increases and the stop band shift to a lower frequency. Alternatively, reducing the spacing between metal fingers also increases the capacitance, thereby shifting the stop band frequency to a lower range. The stopband can be tuned to the resonant frequency of the main antenna by varying the gap g and length l of the interdigital structure as shown in Figure 3.41(a) and Figure 3.41(b) respectively. The parameters are chosen such that the coupling is minimized between cross patch and ring patch modes.
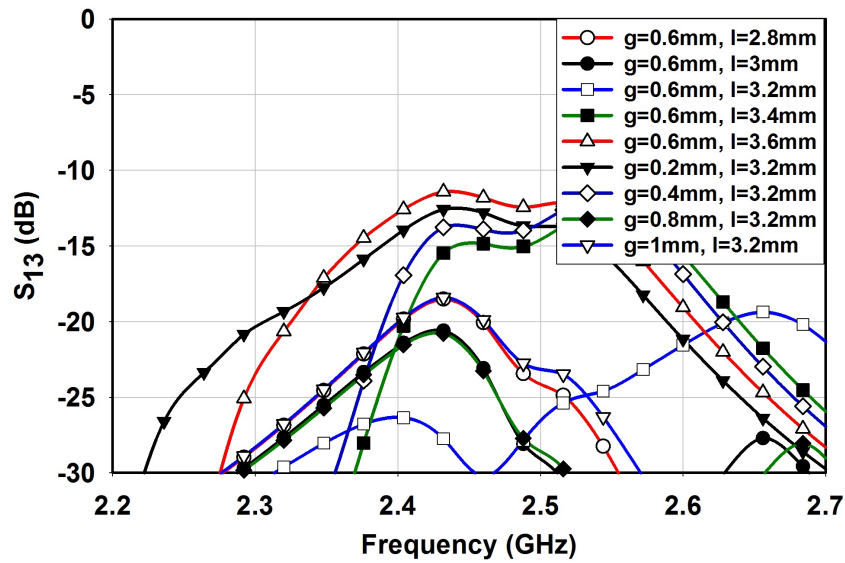
Figure 3.40: Effect of ID-DGS parameters (g, l) on isolation characteristics
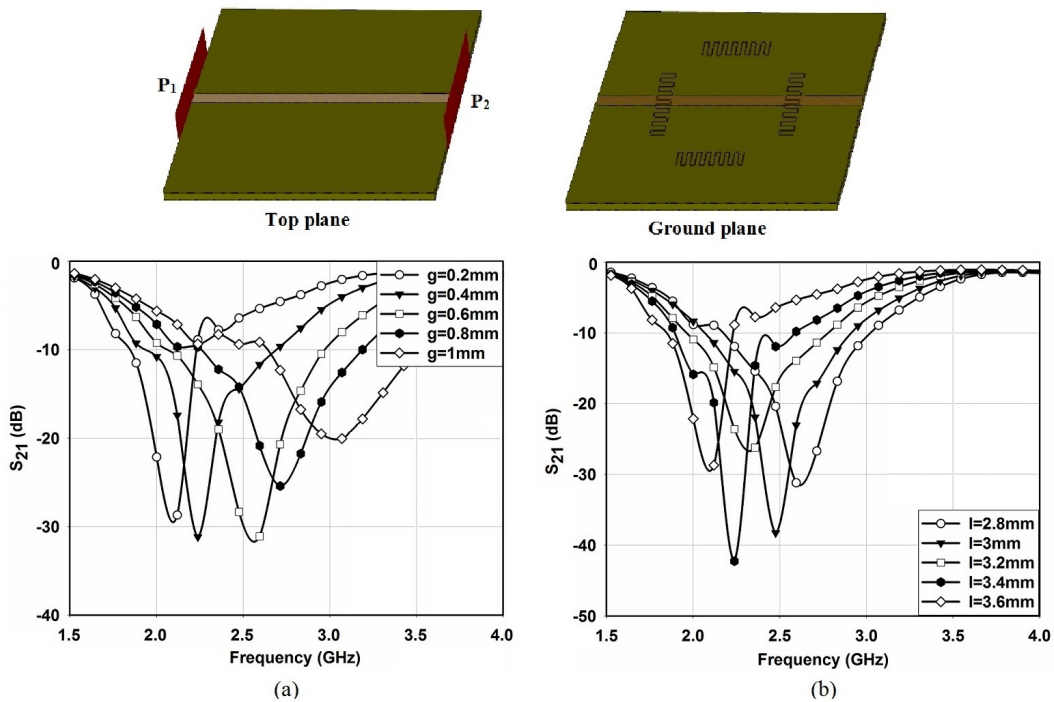
Figure 3.41: Stopband analysis with varying (a) gap and (b) length of ID-DGS

3.4.3 Simulation and Measurements

All the four elements of the designed microstrip printed MIMO patch antenna
resonate at a center frequency of 2.45 GHz with a 2:1 VSWR bandwidth of
about 85 MHz. The simulated results of the quad element MIMO antenna,
with the isolation enhancement structure, are shown in Figure 3.42. Simulated
3D radiation patterns obtained for the four antenna elements are shown in
Figure 3.43. The fabricated prototype of the proposed MIMO antenna system
is shown in Figure 3.44. An FR4 substrate with relative permittivity $\epsilon_r =$
4.4, loss tangent $tan\delta = 0.02$ and thickness of 1.6 mm is used. Measurement
results, using a Vector Network Analyzer in Figure 3.45, show that all antenna
elements resonate at 2.45 GHz, identical to the simulation curves. The results
obtained ensures good MIMO performance, as mutual coupling between all
ports is well below -28 dB.
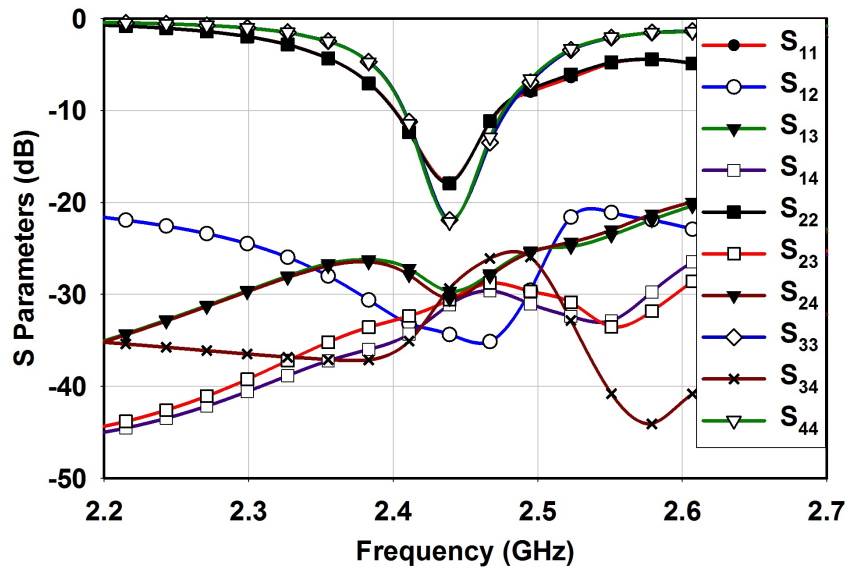
Figure 3.42: Simulated reflection and transmission characteristics of the antenna

Far-field radiation pattern measurements have been conducted inside an
anechoic chamber, by exciting individual ports, while terminating the other
ports with matching loads. Measured normalized far-field radiation patterns
for all four modes in the 0^0 and 90^0 planes of the antenna are as shown in
Figure 3.46. It is observed that the fundamental radiation modes of P_1 and
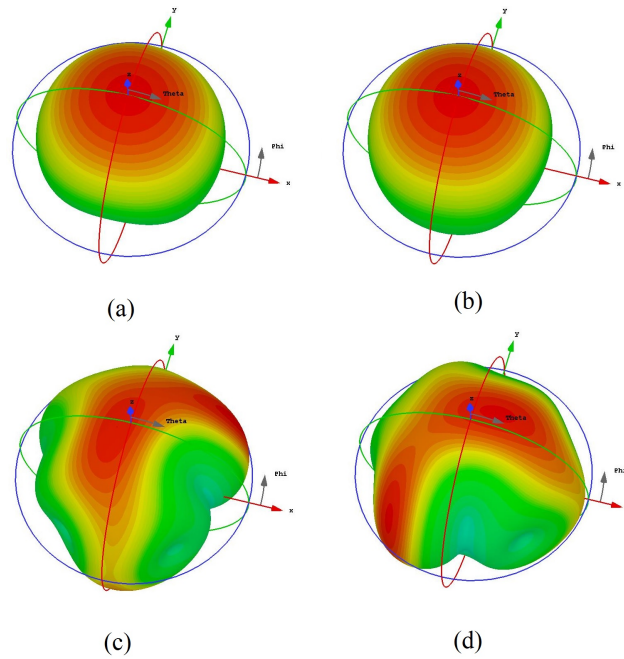
Figure 3.43: Simulated 3D radiation pattern of the MIMO antenna (a) P_1 excited (b) P_2 excited (c) P_3 excited (d) P_4 excited
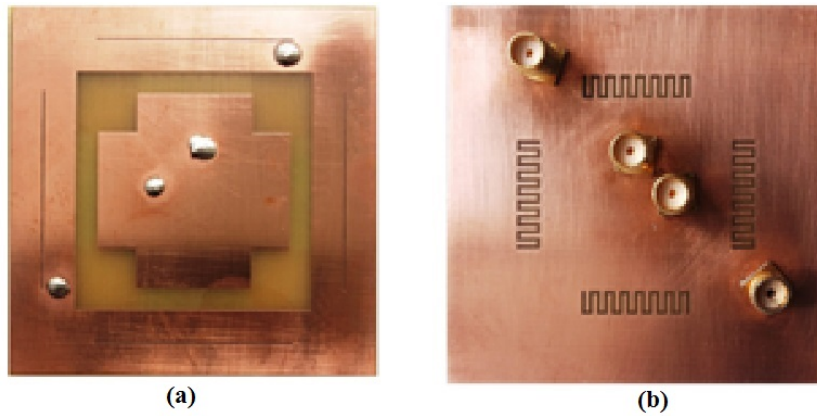
Figure 3.44: Fabricated prototype of the antenna (a) top view (b) bottom view

P_2 have polarization planes orthogonal to each other which guarantee low coupling between the ports. An identical polarization diversity can also be detected between the outer ring antenna ports P_3 and P_4. The shape of the radiation pattern is different for the cross patch and the square ring patch
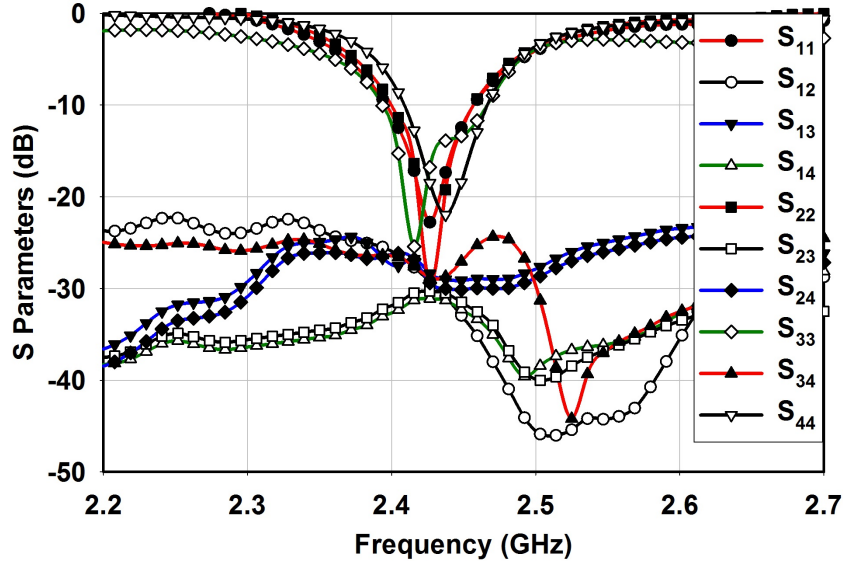
Figure 3.45: Measured S-parameters of the MIMO antenna

antenna, which ensures pattern diversity. Efficiency measurements using the wheeler cap method show a peak efficiency of 81 % for inner cross patch modes and 70.4 % for outer ring modes. Measured peak gain for cross patch modes and square ring patch modes are about 3.8 dBi and 2.9 dBi respectively.

Diversity performance is analyzed to characterize the MIMO antenna system. Apart from scattering matrix and far field radiation pattern measurements, envelope correlation coefficients are computed to evaluate the MIMO performance of the proposed antenna system. Envelope correlation coefficient ρ_{ij} gives a measure of antenna radiation pattern diversity. Computation of correlation coefficients from S parameter using equation (3.2) gives very low values, less than 0.02. Because the S parameter approach is not so accurate, envelope correlation coefficients are measured from far-field radiation patterns for an isotropic channel environment using equation (3.3). It is observed that within the operating band, envelope correlation coefficients are below 0.3, as shown in Figure 3.47, indicating a good MIMO performance.
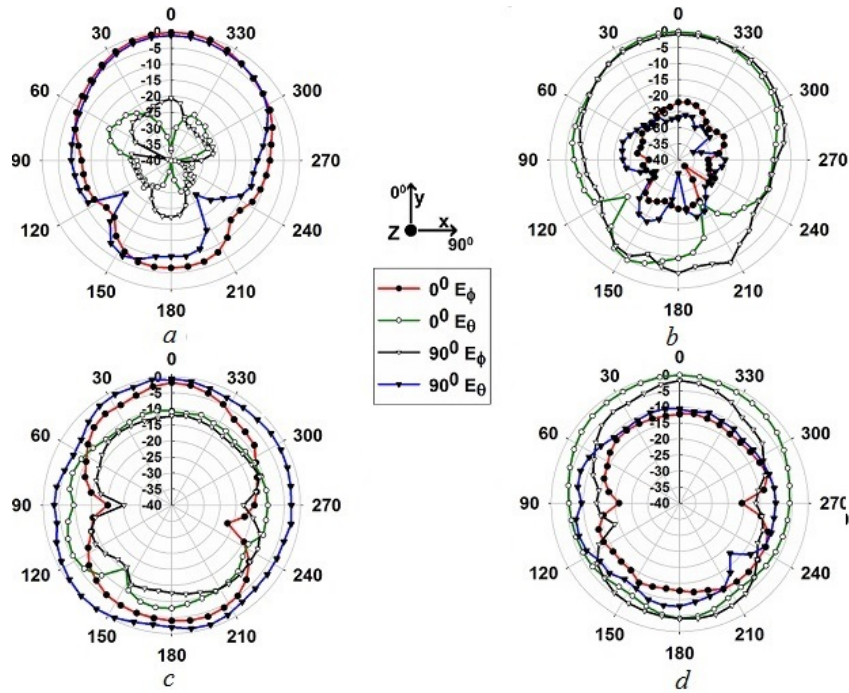
Figure 3.46: Measured radiation patterns of the antenna (a) P_1 excited (b) P_2 excited (c) P_3 excited (d) P_4 excited
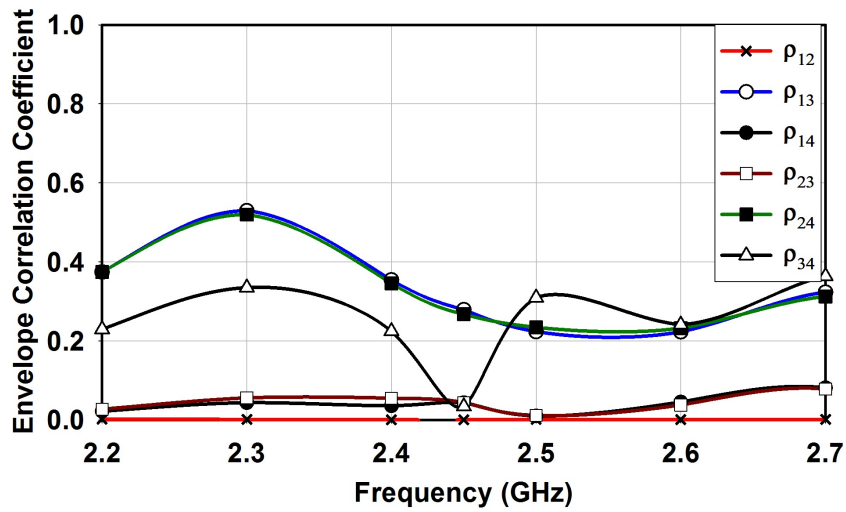
Figure 3.47: Envelope correlation coefficient between waveforms

3.5   Chapter Summary

Three types of quad element multiple-input-multiple-output antennas, (1) using a square and ring patch, (2) using two square ring patches and (3) using the cross and ring patch are presented in this chapter. The multiple modes of the two patches in each of these designs provide uncorrelated antenna elements in the MIMO design. The designed multimode antennas exhibit the various forms of spatial, polarization and pattern diversity. In all the designs, an outer ring patch antenna encompasses an inner patch antenna. In other words, the two patch antennas are collocated on the same ground plane with very little separation between them, compared to half wave length separated antennas.

The square patch antenna offers a standard design to start with, followed by a square ring as the inner patch antenna in the second design. Ring antenna is more compact compared to a square patch. This design also proposes a reactive loading method to improve the bandwidth of higher order orthogonal modes of ring antenna, without adversely affecting the isolation between the orthogonal resonating modes. In the third design, the ring patch is replaced with a cross patch. The cross patch antenna has the highest MIMO performance in terms of increased isolation between its orthogonal elements. The design of each patch shape for the various resonant modes is studied for its width expressed in terms of wavelength. Configurations that excite lower-order modes generally perform better than configurations with higher order modes. This is because they allow the receiver to collect more signal power due to their high radiation efficiency. However, there is a possibility to further increase the performance of the diversity antenna system by increasing the efficiency of the configurations that excite higher order modes.

The MIMO performances of each of these antenna designs are investigated, by taking the mutual coupling between the antenna elements as a major parameter. The design approach itself guarantees good isolation performances due to the arrangement of the antenna elements, using polarization and pattern diversity. However, for elements with identical field orientation, the coupling is comparatively higher. For reducing coupling between these elements three different types of isolation enhancement structures, (1) square

ring DGS, (2) complementary split ring resonator etched on the ground and (3) interdigital structure on the ground, are proposed. The ring DGS acts as a resonator which radiates coupling waves to space, thereby reducing surface wave coupling. CSRR on ground reverses the polarity of coupling waves, to improve isolation. The interdigital structure acts as a stop band filter which reduces coupling surface waves, thereby improving isolation between all combinations of antenna elements. Among the three designs, the cross patch and the square ring MIMO antenna with the interdigital structure on the ground, provides the highest isolation, with a minimum value of 28 dB between any pair of antenna elements. A comparison between the proposed antennas and few other diversity based single band MIMO antenna designs in terms of size, mutual coupling, and envelope correlation coefficient is shown in Table 3.4.

Ref	Minimum Isolation (dB)	Total Area of MIMO Antenna (λ_0^2)	No of Antenna Elements	Correlation Coefficient
[169]	9	-	2	0.39
[179]	25	0.307	4	0.22
[180]	25	-	2	0.32
[182]	17	-	2	-
[183]	15	-	2	0.25
[196]	17.5	0.167	4	-
[197]	16.6	1.435	4	-
[198]	15	0.589	4	0.21
[199]	10	0.100	4	0.26
section 3.2	25	0.236	4	0.3
section 3.3	22	0.200	4	0.37
section 3.4	28	0.248	4	0.35

Table 3.4: Comparison Table for Pattern & Polarization Diversity Based MIMO Antennas

The MIMO diversity performance can be analyzed from parameters like envelope correlation coefficient, mean effective gain, multiplexing efficiency and diversity gain. Among all the parameters the envelope correlation coefficient is the most significant parameters, for which a value lower than 0.5 ensures good MIMO performance. The ECC values have been computed for all the quad element MIMO antennas designs and it is observed to have low values, guaranteeing good MIMO performance.

Chapter 4

Compact Multi-band And Wide-band MIMO Antennas

Contents

This chapter discusses the investigations conducted in the design and performance evaluation of multiband and wideband MIMO antennas. We begin with an overview of the antennas belonging to this broad category, followed by a description of the evolution of the antenna designs. Experimental and

simulation studies, for explaining the MIMO performance like reflection characteristics, isolation characteristics and diversity performance, are described in detail in this chapter.

The antennas discussed in this chapter include a quad element antenna using meander line resonators loaded with quarter wave stubs. This antenna resonates in three bands, all of which are of great importance and practical significance, exhibiting very good bandwidth and performance. Isolation is enhanced for the meander line antenna elements by using an SRR based ring structure in between the antenna elements at the center of the antenna. Other work presented in this chapter is a wideband antenna which resonates with a bandwidth of 96.2 % covering the ISM, WLAN and WiMAX bands. The antenna design utilizes monopole, split ring resonator (SRR) and a modified ground plane, which helps in obtaining the wideband resonance. Both these antennas make use of polarization diversity for maintaining minimum coupling between the elements.

4.1 Multiband and Wideband MIMO Antenna: Review

The rapid development of antenna design engineering can be attributed to the fast growing wireless communications market. Often, the usage of new frequency bands for covering some communication systems having enhanced data rates and added services, demands fresh requirements for the terminals. For example, they need to operate in the new bands but also need to keep the operability in the existing ones. Owing to the advancement of the integrated technology, engineers are capable of combining several diversified applications functioning at dissimilar frequencies in a single wireless device. Accordingly, an increased demand for antenna technology, covering different wireless communication bands on the same boards, increased extremely. Earlier, antennas with wide bandwidth were generally employed for radar and tracking applications. However, the demand for high data rate and the advent of spread spectrum technology necessitated more research in wideband antennas.

Multiple antenna systems, realizing these functionalities can be broadly categorized into a wideband or a multiband MIMO antenna. Further, while deploying the wideband or multiband antenna in the terminal of a MIMO antenna system, multiple elements have to be designed and should be able to work in the desired frequencies. Here, the additional challenge of reducing mutual coupling between multiple elements of the various operating bands has to be addressed. The category of the antenna used in these terminals is very much identical to that of a single band antenna, i.e., patches, monopoles, slots, PIFAs etc.. They may take different alterations of shape or combinations to provide multiple band operation. Multiband operation has been reported, covering low frequency bands like LTE or GSM [200] as well as those resonating for lower and higher frequency bands [201].

The last few years reported a couple of multiband and wideband MIMO antennas for a wide range of applications [196–199, 202–209]. For multiband MIMO operation, it is essential to investigate all the design characteristics of the antenna such as size, resonant frequency, impedance matching, gain and radiation patterns of the various bands for the multiple elements. It is very challenging for a compact multi-band MIMO antenna to achieve desired results for all these requirements.

In general multiband antennas can be of either two types: (1) designing two or more radiating elements by using slits or slots (2) obtaining multiple operating bands using higher modes of the same radiating element. Both of these methods can cause undesired surface currents on radiating elements. For the former case, resonant frequencies can be easily tuned by adjusting the slots or the slits. However, it is difficult to obtain the desired impedance bandwidth in the desired frequency band. Each antenna performance can be optimized by the usage of several different radiating elements. In the latter case using multiple resonant modes of the same element, since the elements are not exactly independent from each other, the element resonating at one specific frequency may act as a parasitic load for other resonating elements. Also, fine-tuning of one element creates a noteworthy change on the other elements. Therefore, it is challenging for these techniques to avoid the undesired currents in each resonant frequency band. The may result in the degradation of antenna performances parameters like bandwidth, gain or radiation pattern.

Earlier designs of multiband antennas include simple creation of slots over a patch antenna [210], such as U-slot patch antenna [211–213], E-slot microstrip patch antenna [214], and C-slot. However, patch antennas are mostly limited by narrow bandwidth operation. In most cases, the bandwidth is lower than that required for latest MIMO wireless technologies like WLAN and LTE. Such antennas will therefore be capable of covering only a few numbers of application or frequency bands. Apart from this, they are mostly used as transmitter antennas and are coupled with an antenna tuning unit that can improve the efficiency of the narrow band operation [215].

Generally, matching networks are placed between the transmitter and the antenna input, in order to improve the efficiency of small multiband antennas. In addition to this, matching network components when introduced in the antenna structure at appropriate positions enhances the radiation and guarantees maximum radiation efficiency. However, such matching networks must be tuned for each of the transmitting frequency band. Also, tuning is difficult when the matching network is mounted on the antenna [215].

In the case of MIMO antennas which incorporates multiple elements in a single antenna, space constraints are very high, forget about the addition of tuning or matching networks. One of the most promising candidates, the planar monopole antenna is often adopted to realize multiband operation, with various structures such as meandered T shape [216], flared shape with V-sleeve [217], Yshape [218], and multifractal structure [219]. These antennas posses many beneficial characteristics including simple structure, low profile and weight, an adaptable structure for exciting wide impedance bandwidth, and generic omnidirectional radiation patterns. However, the large sizes of such antennas also limit their applications in modern compact portable wireless terminals.

Literature review studies show a few [196, 202–204] multiband MIMO antenna systems mostly covering ISM bands. Multiband antennas are significant for practical applications and its implementation is more troublesome in terms of compactness and decoupling of elements. Dual band MIMO antenna of size $50 \times 50 \ mm^2$ [196] has isolation of 13 dB and 16 dB in the two bands. A two port dual band MIMO antenna with an isolation of 20 dB is discussed [202], where the size of the two port PIFA is $100 \times 50 \ mm^2$. Another proposed two

port design [203] provides an isolation of 15 dB with dimension $100 \times 150 \ mm^2$. The quad band MIMO antenna in [204] covers the ISM and WiMAX bands with a minimum isolation of 14 dB.

The trend in modern wireless routers and adapters is miniaturization, making it difficult for the integration of multiple antennas. Closely spaced elements can suffer strong electromagnetic coupling and need smart designing to improve isolation between elements. Compact designs proposed for quad element MIMO antennas [220, 221] has sizes of $40 \times 40 \ mm^2$ and minimum isolation of 10 dB in the 2.4 GHz band. In addition to compactness, high isolation between elements is highly desired for multiband MIMO antennas. This can be achieved by making use of spatial, pattern and polarization diversity. Making slots over patch radiator is another common method for achieving isolation in multiband MIMO antenna design. Apart from achieving high isolation, compactness and coverage of multiple bands, the antenna system needs to be easily incorporated into a system for practical applications. A complete planar architecture is advantageous for an easier integration.

Although there is no specific definition of a wideband antenna, generally an antenna that has a fractional bandwidth of 50% or above is considered as a wideband antenna. A standard rule of thumb in antenna design is that an antenna can be made to have enhanced bandwidth by increasing the volume it occupies. For dipole antennas, the wideband operation can be achieved by increasing the radius of its arms. In the case of microstrip antennas, this is accomplished by choosing a substrate material with low permittivity and higher thickness. The use of proximity feeding technique in microstrip antenna enhances the bandwidth further [188, 222]. In proximity feeding method, the radiating patch is fed by a coupling strip. Wide bandwidth is achieved by the electromagnetic interaction between the radiation mode of the patch and the strip.

While the design of a wideband passive antenna is relatively easy, obtaining broader bandwidth for active antenna faces a greater challenge due to the introduction of active elements in the antenna structure [223, 224]. Typically, for active antennas, wide bandwidth of the entire structure is accomplished only if both the antenna as well as the active element, say for example an amplifier, individually exhibits wideband operation. In some antennas, the active

element works as a switch and hence the wideband characteristic thereof is not required as we find in [225,226], where active switches have been employed to achieve frequency-reconfigurability for the antenna.

The idea of a wideband radiator with a high Q can be realized with the help of the frequency-reconfigurable antenna. Achieving high efficiency for active integrated antennas is a popular area in antenna research [224,227,228]. For array antennas, achieving wideband operation is a challenge, due to the limitations offered by the sidelobe level and the array gain. The concept of the dual-wideband planar antenna has been put forward recently [229] in order to cope with the technological evolution in cellular communication.

In widely employed wireless applications that are based on IEEE 802.11n (WLAN) and 802.16e (WiMAX), two spatial streams ($M, N \leq 2$) are usually deployed, hence, wide-ranging studies have been performed on the two port MIMO antenna design. Elements with compact size and wideband characteristics belonging to this category have been proposed in [230–232]. However, with a growing demand for higher transmitting rates, new wireless standards appeared, such as 802.11ac (WLAN) [63] and 802.11m (WiMAX) [233] that support from four to eight spatial streams.

Therefore, multiple antenna systems with 4×4 up to 8×8 configurations have been deployed recently. Latest wireless devices such as portable wireless routers and adaptors, mandates wider bandwidth and size miniaturization in their built-in MIMO antenna system. This augments more challenges in MIMO antenna design, as the elements are closely spaced, and is limited by the trade-offs existing between the antenna size, bandwidth, and isolation between elements. In existing literature, sectorial antenna [234,235] is a good candidate, in that its patterns are directional and shaped, which can provide good pattern diversity for a MIMO antenna system. Nevertheless, these advantages are achieved by using large ground, director, or reflector, which is not applicable in size limited portable applications.

For multiband MIMO antennas, the radiation elements are mostly narrowband, and the designer may focus more on lowering the mutual coupling between closely spaced radiation elements. Representative designs include H-shaped elements with orthogonal arrangement [236], Planar Inverted F Antenna (PIFA)/slot elements with diagonal arrangement [221], patch/slot

elements with modified ground structure [86], Yagi- Uda elements with directional radiation patterns [237], among others. For wideband design, mostly reported structures include, cavity back tapered slot [128] and self-ground monopole [238] based MIMO antennas, which are nonplanar. They are difficult to be reproduced in mass production and the size is too large for compact applications.

For wideband planar design, such as the ultra-wideband (UWB) element [239] and the F-shaped slot element [240] based MIMO antenna, a similar problem exists in that the elements are independent, which cannot push the size into the limit. Wideband antennas arranged to form linear arrays is a good candidate [197, 205] in terms of isolation and diversity performances, though their applications are limited in compact portable devices. Quad element MIMO of size 120×140 mm^2 for LTE and WiFi application [198], uses a common radiating element with a slotted ground. Low profile two port planar inverted-L wideband antenna, resonates in 1.7-2.85 GHz with an isolation of 13 dB [206]. Nonplanar antennas for wideband MIMO application using self-grounded bowtie antenna [207], have an isolation of 10 dB in 1.5-3 GHz operating band.

Maintaining low correlation over wide frequency range is more difficult, compared to narrow-band elements. Hence, the design of MIMO antenna with small size and high isolation is crucial for the portable devices. Reported compact four port and tri-port MIMO antennas have element areas of $0.024\lambda^2$ (40×40 mm^2) and $0.029\lambda^2$, with an isolation of 10 dB in the 2.3-4.4 GHz and 2.3-3.9 GHz band [199], [241] respectively. Therefore, designing and developing planar multi-element antennas with compact size, wideband characteristic and high isolation between elements is still in demand for both the industrial and academic areas.

Multiband MIMO antenna has to overcome several design challenges; the first hurdle is the complexity and difficulty involved in adjusting the multi-resonating systems to match the desired frequency bands. The second problem is to achieve reduction in size with good isolation between elements, required by the limited size wireless devices against the antenna efficiency. These two problems are discussed here. Accordingly, innovative antenna designs are presented to lessen the degree of complexity and challenges in the design of

multiband and wideband MIMO antenna systems for compact wireless terminals. The design considerations and the simulated and measured results are also presented in the chapter.

4.2 Compact quad element Tri-band MIMO antenna

A compact multiband four port MIMO antenna is proposed in this section. The tri-band antenna resonates in three operating bands covering UMTS, LTE 2300, 2.4 GHz WLAN band, 3.5 GHz WiMAX band, and 5.2 GHz/5.8 GHz ISM bands. The proposed antenna includes a meander line loaded with two L-shaped stubs fed by a strip line [242]. The overall size of the compact multiport antenna system is $0.26\lambda_0 \times 0.26\lambda_0$. Mutual coupling between antenna elements is designed to be very low. Polarization diversity is employed to incorporate four antenna elements in a compact manner, maintaining high isolation between them. Employing multiple antennas in four corners of the antenna system maximizes the spatial separation between the elements. This along with the orientation of neighboring elements with an orthogonal shift, results in the isolation performance between diagonal meander line elements to be less when compared to that of elements lying along a plane, say along E-plane or H-plane. An isolation enhancement structure is provided for reducing coupling between diagonally placed meander line antenna elements. The MIMO antenna structure is fully planar and compact, and can be easily integrated with practical applications. Individual elements of the multiple antenna systems are performing equally well with high efficiency and gain. Diverse antenna patterns help to have a very low envelope correlation coefficient between the elements.

4.2.1 MIMO Antenna Geometry and its Design

The configuration of planar integrated quad element MIMO antenna is shown in Figure 4.1. The elements are placed in each quadrant of a square substrate with an orthogonal shift in polarization. The ground planes of each antenna

are of dimensions $L \times W mm^2$ and appears on the back side of the substrate, beneath the strip line feed. The antenna design can be explained in detail by considering the evolution of a tri-band antenna.
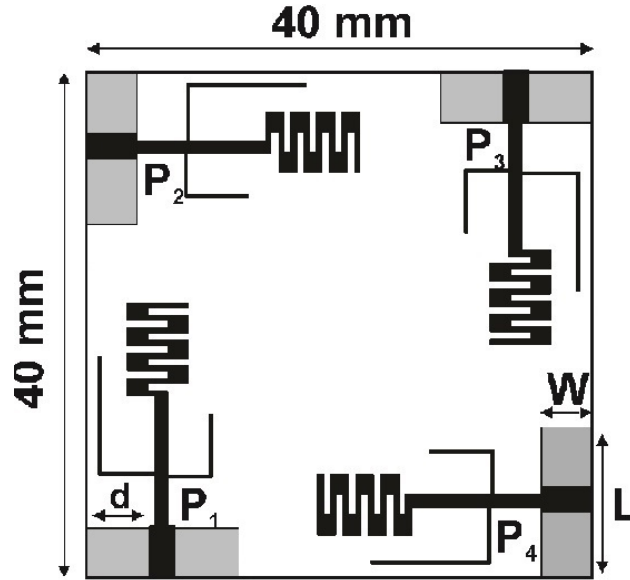
Figure 4.1: Geometry of quad element tri-band MIMO antenna; L = 12mm, W = 4mm, d = 5.5mm

4.2.1.1   Basic Meander Line Antenna Design

The basic element of the tri-band antenna is an electrically small planar meander line monopole antenna. A meander line antenna includes large number of folded elements which increases its electrical length, making the antenna resonate at a much lower frequency than a conventional antenna of same length. The meander line antenna size reduction factor β depends primarily on the number of meander elements per wavelength, and the spacing of the element widths of the rectangular loops, where $\beta = l/L$, L being the length of a conventional monopole, and l is the length of meander line antenna [243]. It is basically an LC resonant circuit, where the vertical element act as an inductor and horizontal elements act as a capacitor.

Here, a printed meander line monopole antenna is designed with dimensions as shown in Figure 4.2. The meander line dimension are chosen to have a horizontal length L_3 and vertical dimension W_2. The antenna feed is through a microstrip line of length L_1 and width W_1. It is connected to a meander line antenna through a transition of length L_2 for impedance matching. The quarter wavelength monopole antenna is designed to have a resonance in 2.4 GHz band. The vertical segments of meander line antenna shows in-phase current distribution and in successive horizontal segments currents are out of phase. A slightly higher thickness of this segment, compared to that of the horizontal segment, helps in enhancing the bandwidth to provide better coverage.
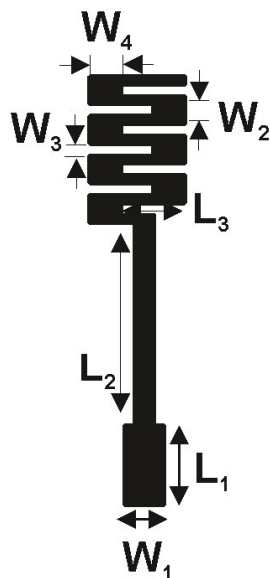
Figure 4.2: Geometry of the meander line antenna with dimensions $W_1 = 2mm$, $W_2 = 1mm$, $W_3 = 0.6mm$, $W_4 = 1.6mm$, $L_1 = 4mm$, $L_2 = 10.25mm$, $L_3 = 3.2mm$

4.2.1.2 Stub Loading on Meander Line Antenna

The objective of achieving additional resonances in desired band is accomplished with inductive loading. Adding stubs parallel to the meander line create inductive effects parallel to main resonance, at the frequency of interest. The meander line antenna is loaded with quarter wave stubs to realize

resonance at the next useful band, 3.5 GHz WiMAX band. The stub loading has no significant effect on the lower band. However, it creates resonance at the required band. Open and short circuited stubs may be used for the generation of inductive loadings.

In this design, the antenna is loaded inductively by adding open stubs to the strip line, connecting the meander line antenna, as shown in Figure 4.3. The resonant frequency is tuned by adjusting the length of the stub. The total length of the stub in this case is $W_5 + L_6$, which is nearly one fourth of guided wavelength λ_g. The third band is designed to cover the entire 5.2 GHz and 5.8 GHz ISM band. This is achieved by adding a second stub of length $W_6 + L_7$.
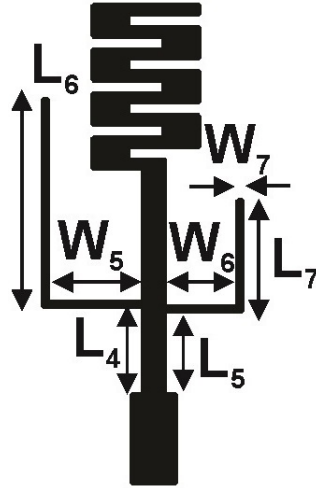
Figure 4.3: Geometry of the stub loaded meander line antenna with dimensions W_5 = 4.3mm, W_6 = 3.3mm, W_7 = 0.2mm, L_4 = 4mm, L_5 = 3.8mm, L_6 = 9.4mm, L_7 = 5mm

The reflection characteristics of the tri-band antenna at various stages is shown in Figure 4.4. The designed meander line antenna shows good impedance matching, with a -10 dB impedance bandwidth of 450 MHz from 2.15 GHz to 2.6 GHz as shown in case I. The higher mode of the meander line antenna, resonates at a frequency of 6.2 GHz. The longer stub resonates with a -10 dB impedance bandwidth of 480 MHz extending from 3.34 GHz to 3.82 GHz. The shorter stub resonance merges with the higher resonance of

the meander line antenna to generate broadband resonance with a fractional bandwidth of 24.2 %. This extends from 5 GHz to 6.55 GHz covering both 5.2 GHz and 5.8 GHz ISM bands. A small increase in bandwidth of the initial bands is observed, due to the effect of fringing fields when a radiating element is placed closer to each other. Fringing changes the electrical path length, resulting in a shift in the frequency. These can merge with nearby resonances, which can slightly improve their bandwidth performance.
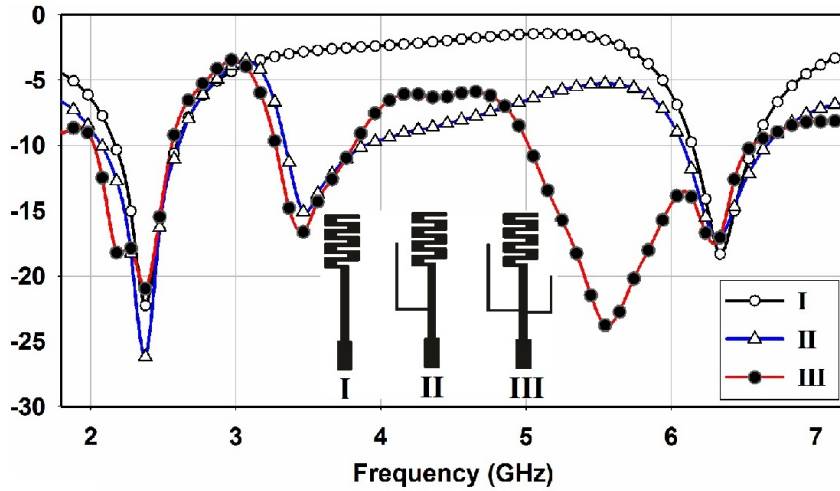
Figure 4.4: S_{11} characteristics at various stages of antenna evolution

Isolation studies using the transmission coefficients S_{ij} reveal that the coupling between diagonally placed meander line antenna elements (i.e. between P_1 & P_3, or between P_2 & P_4) is higher. This is mainly due to the identical orientation of the electric field, which increases the near field coupling. The inductively loaded quarter wave stubs are positioned on opposite sides of the central connecting strip line to increase the isolation between conducting elements. L shaped stubs can limit the space requirements for obtaining a resonance at a lower band of interest. Also, the cross polarization can be reduced, which would otherwise be higher, if the stubs are loaded in shunt to the strip line [244].

4.2.2   Study of SRR ring for Isolation Enhancement

Isolation enhancement structures are designed to reduce mutual coupling between diagonally placed meander line antenna elements. The design of an isolation structure was done, based on the SRR unit cell dimensions and negative group delay calculation using simulation software. The group delay is the negative derivative of the phase response, as a function of frequency $(\tau_g = -d\Phi/d\omega)$. Owing to limited space, long rectangular SRRs having widths and gaps of 0.2 mm are placed between the meander line antennas. The quad element MIMO antenna with the SRR ring isolation enhancement structure is shown in Figure 4.5. The unwrapped phase response between highly coupled diagonal antenna elements is shown in Figure 4.6. The combination of the SRRs arranged in the form of a shorted ring has an overturn in the phase response, at the meander antenna resonance. This is an indication that a negative group delay is occurring at this frequency, which acts like a stopband filter between highly coupled elements [245]. The SRR ring induced negative
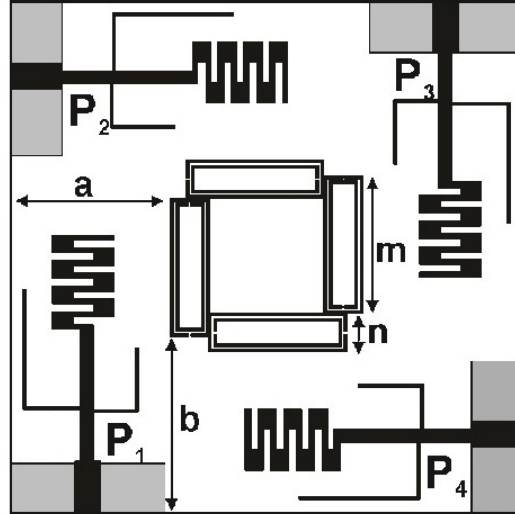
Figure 4.5: SRR ring for isolation enhancement with dimensions a = 12.5mm, b = 13.75mm, m = 10.75mm, n = 3mm

group delay results in the cancellation of coupling waves to the diagonal element. As the power dissipation in the nearby radiator is reduced, radiation
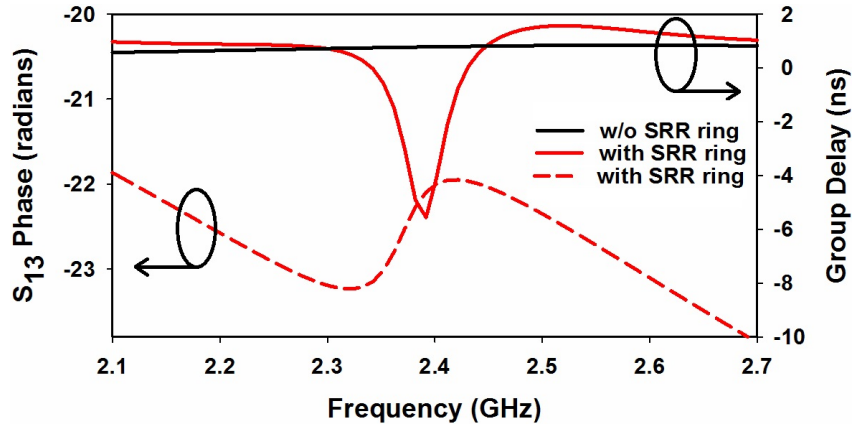
Figure 4.6: Unwrapped phase and group delay between P_1 and P_3

efficiency is enhanced by 5.7 %. Isolation enhancement with SRR ring can be validated from the surface current distribution in Figure 4.7 at the meander line resonant frequency. The increase in isolation with the inclusion of ring shaped SRR is shown in Figure 4.8. Isolation between diagonal elements is improved by 17 dB, with S_{13} (or S_{24}) being reduced from -17 dB to -34 dB in 2.4 GHz band with SRRs. Simulated reflection/transmission coefficients obtained for the four port MIMO antenna with isolation enhancement structure are shown in Figure 4.9.
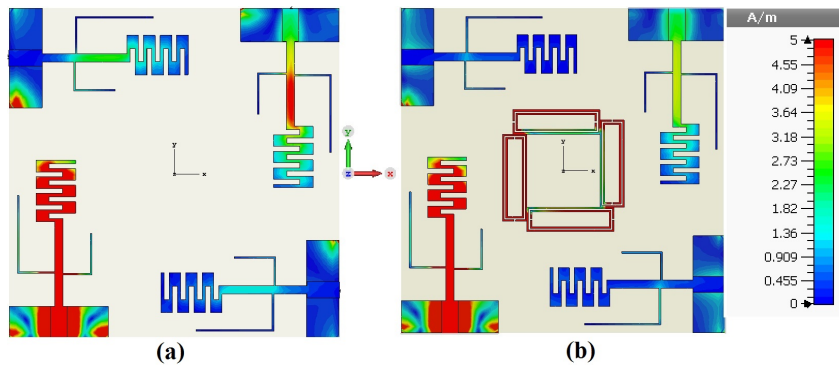
Figure 4.7: Surface current distribution of the four port MIMO antenna at 2.4 GHz (a) w/o SRR ring (b) with SRR ring
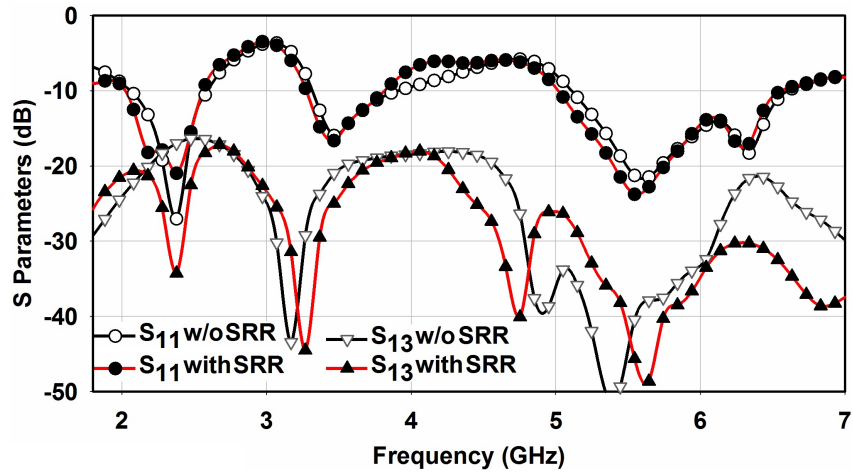
Figure 4.8: Reflection and transmission characteristics w/o and with SRR
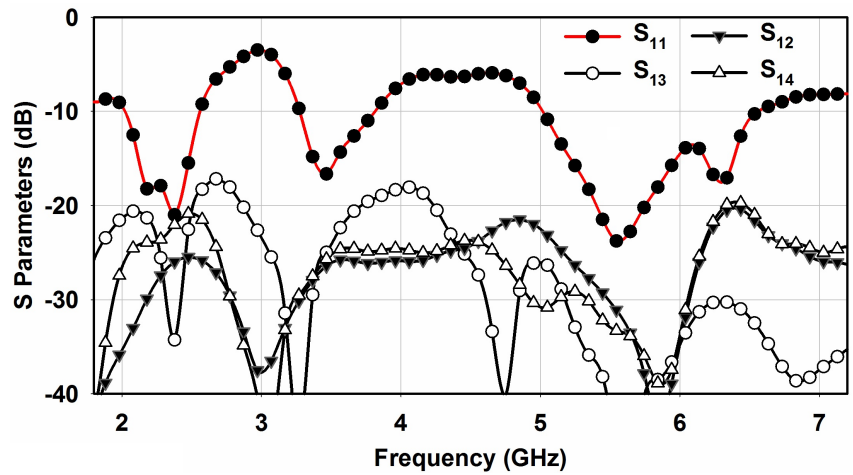
Figure 4.9: Simulated S parameters of the MIMO antenna

4.2.3   Measurements using prototype

The fabricated prototype of the four port tri-band MIMO antenna is shown in Figure 4.10. The proposed antenna is fabricated on a low cost FR4 substrate with relative permittivity of 4.4, thickness 1.6 mm and loss tangent $tan\delta = 0.02$. The measured S parameters using the prototype are shown in Figure 4.11 and are validated with the simulation results. All the four elements resonate in three operating bands with a fractional bandwidth of 24.7 %, 20 % and

28.6 % respectively.
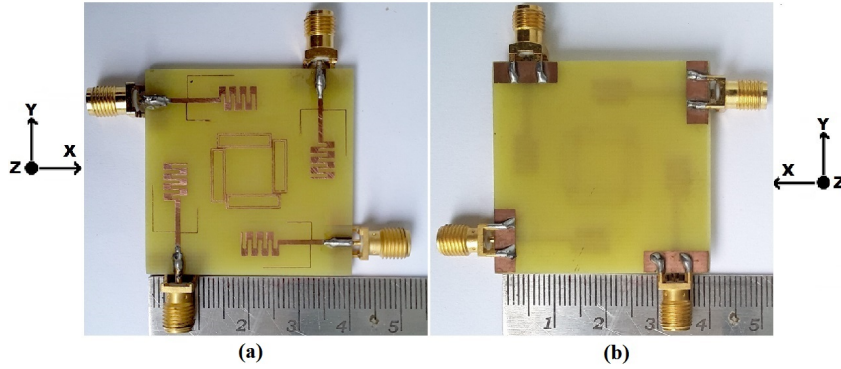
Figure 4.10: Fabricated prototype of the MIMO antenna (a)top view (b)bottom view
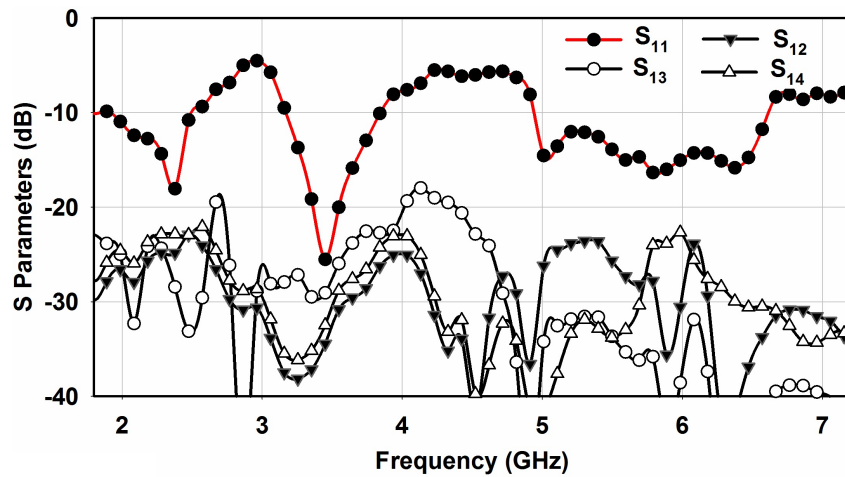
Figure 4.11: Measured S parameters of the MIMO antenna

The transmission coefficient curves show the isolation between elements in the operating bands. In the 2.4 GHz resonant band, the minimum isolation obtained is 24 dB in the entire band. The next higher resonant band at 3.6 GHz has good isolation performance, with a maximum coupling of -22 dB in the band. The stub, being along the outer edges of the antenna system, reduces the coupling between elements along E and H plane, thus keeping S_{12} and S_{14} low for the second resonant band. The third band offers a very low coupling in its entire operating band with a minimum isolation of 22.5 dB at

6 GHz. The second stub placed towards the center of the multiple antenna system causes the coupling between elements lying on the same plane, to be higher than coupling between diagonal elements. S_{13} goes to a very low value, below -50 dB, in this band.

The far field radiation patterns for element 1 are plotted in Figure 4.12. Radiation patterns are obtained in three resonant bands at 2.4 GHz, 3.5 GHz and 5.5 GHz. The patterns are plotted for XZ and YZ planes and includes both polarization components phi and theta. It is observed that all the four antennas have similar radiation properties, with an orthogonal shift in polarization. An orthogonal shift guarantees polarization diversity, and consequently the pattern correlation between individual elements is low for this antenna. Gain and efficiency measurements are plotted as shown in Fig-
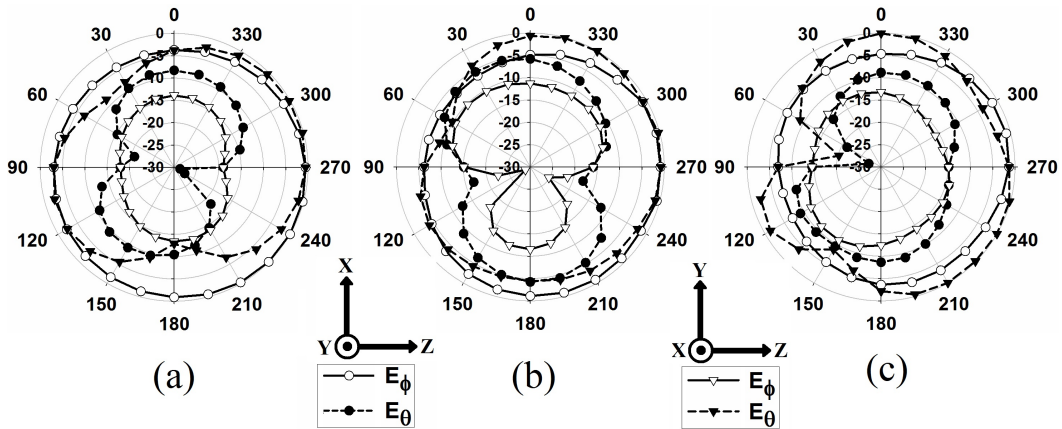
Figure 4.12: Measured radiation patterns of antenna element 1 at (a) 2.4 GHz, (b) 3.5 GHz and (c) 5.5 GHz

ure 4.13. Gain measurements show peak gains of 2.5 dBi, 3.7 dBi and 4.4 dBi at 2.5 GHz, 3.7 GHz and 6.3 GHz respectively in the three resonant bands. Efficiency measurements show peak efficiency of 83.4 %, 90.4 % and 92 % at 2.4 GHz, 3.76 GHz and 6.1 GHz respectively.

Diversity performance is analyzed by computing envelope correlation coefficient, to characterize the MIMO antenna system. Envelope correlation coefficient ρ_{ij} computed from the S parameter using equation (3.2) gives values as low as 0.05. Envelope correlation coefficients calculated from radiation
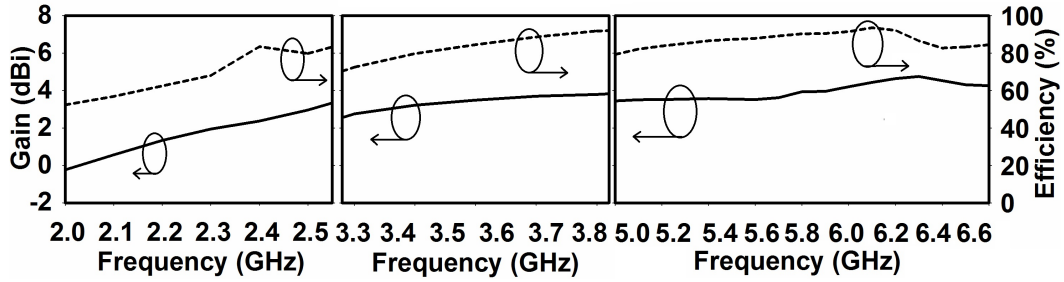
Figure 4.13: Measured gain and efficiency in the three operating bands

patterns using equation (3.3) for an isotropic channel environment, are plotted in Figure 4.14. It is observed that, within the operating bands, correlation coefficients are well below 0.3 which ensures good MIMO performance.
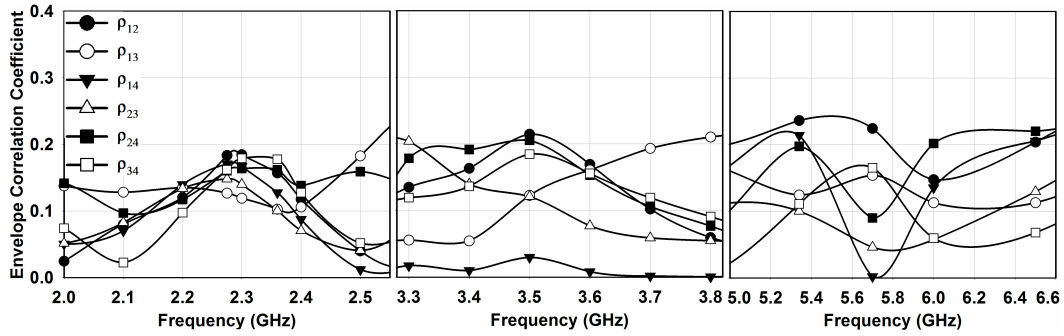
Figure 4.14: Correlation coefficients at three operating bands

4.3 Compact quad element Wide-band MIMO antenna

A compact planar quad element wideband antenna for MIMO system is proposed in this section. The technological developments in wireless communication often necessitate an increased allocation of spectrum. This has spurred the demand for MIMO antennas with wide efficiency bandwidth for use in multi-functional wireless communication systems. These multiple antenna

systems need to operate in wideband, and should be able to provide low mutual coupling between elements, across the broad band frequencies. The 2 GHz to 6 GHz band is extensively used for different applications like LTE, UMTS, WiMAX, WLAN, ZigBee and Bluetooth. Owing to the great demand of this band, a wideband antenna is designed to operate in this band. The wideband element consists of a partially grounded printed monopole antenna loaded with a split ring resonator (SRR) [246]. The compact planar printed wideband MIMO antenna, having an overall dimension of $0.33\lambda_0 \times 0.33\lambda_0$ has reasonably good isolation between elements over a broad range of frequencies.

4.3.1   MIMO Antenna Geometry and its Design

The geometry of the proposed quad element planar antenna is shown in Figure 4.15. In the multiple antenna system, each antenna element is polarized orthogonally to the neighboring ones, reducing the size of the antenna system. The antenna is designed to fabricate on an FR4 substrate with relative permittivity of 4.4 and thickness 1.6 mm. The characteristics of the antenna can be explored in detail by studying the wideband antenna. Various stages involved in the evolution of the element to have a wide resonant bandwidth is discussed in the following sections.
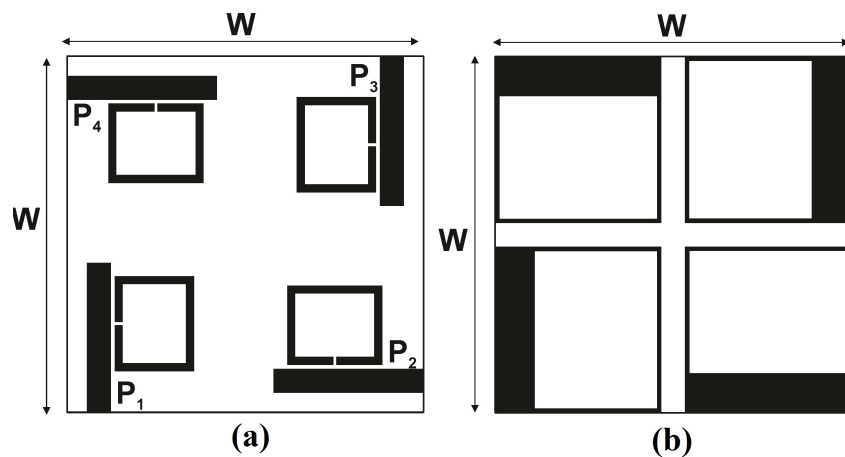
Figure 4.15: Geometry of quad element wideband MIMO antenna with W = 45mm (a)top side (b)bottom side

4.3.1.1 Basic Printed Monopole Antenna Design

The basic structure used in the antenna design is a simple printed monopole antenna. The geometry of a monopole antenna is shown in Figure 4.16 along with the antenna dimensions. The ground of the quarter wavelength monopole resonator is in the shape of a rectangle with dimensions $L_2 \times W_2$ mm^2 and appears on the lower side of the substrate. The unsymmetrical feeding position W_3 changes the effective current path of the antenna. This can create slight modifications in the resonant frequency of the monopole antenna and will be estimated based on the longest effective current path. In doing so, the resonant frequency is reduced slightly to have a resonance at 3.85 GHz, with a bandwidth of 1.3 GHz. Reflection characteristics of the antenna are shown in Figure 4.17.
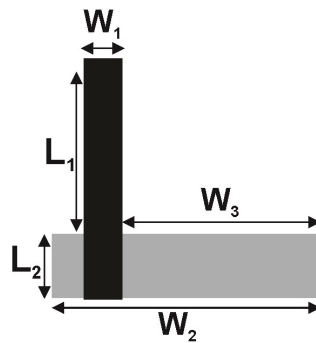
Figure 4.16: Printed monopole antenna with dimensions W_1 = 3mm, W_2 = 21mm, W_3 = 15.5mm, L_1 = 14mm, L_2 = 5mm; black: metal on top side; Grey: metal on back side

4.3.1.2 Design of Wideband Antenna

To accomplish a broadband resonance, the rectangular ground is extended in the shape of a ring, leaving the monopole and its sides. The printed monopole with the modified ground is shown in Figure 4.18. The slotted ground on either side of the monopole resonator increases the effective electrical length of the antenna. Thus, with the inclusion of the ground ring, the resonator becomes more compact, reducing the size by 25 %. The full wavelength resonance of
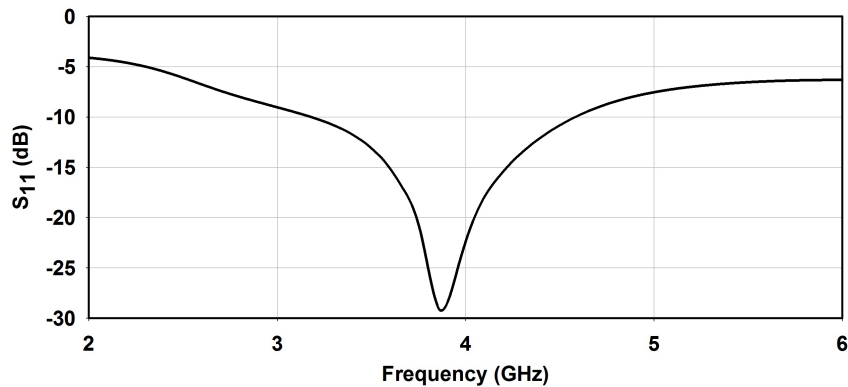
Figure 4.17: Return loss characteristics of the monopole antenna

the ring shaped ground merges with the monopole resonance to create a broad operating band ranging from 2.4 GHz to 4.2 GHz, with a -10 dB fractional bandwidth enhancement from 33.8 % to 54.5 % as shown in Figure 4.19.
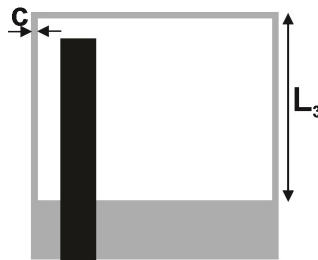
Figure 4.18: Slotted ground monopole antenna with dimensions c = 0.5mm, L_3 = 16mm

In order to further enhance impedance matching to cover the 2-6 GHz band, a subwavelength miniature resonant structure, a split ring resonator (SRR), is positioned close to monopole radiator as shown in Figure 4.20. SRR is electromagnetically coupled to the printed monopole, and can be easily housed in the limited space. Being a subwavelength resonator, it helps in achieving resonance at a frequency much lower than conventional resonator. The SRR dimensions are evaluated from standard design procedures [247] for a resonant frequency of 2 GHz. SRR has a narrow resonant bandwidth, however, with the introduction of ring shaped ground, the impedance matching range is extended, covering the frequencies between the resonances.
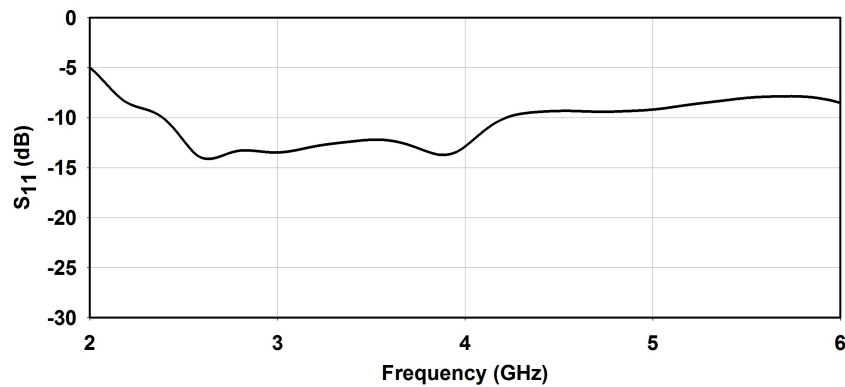
Figure 4.19: Reflection characteristics of slotted ground monopole antenna
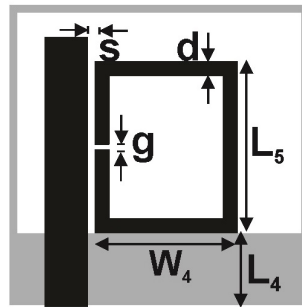
Figure 4.20: Slotted ground monopole antenna loaded with SRR having dimensions s = 0.5mm, d = 1mm, g = 0.4mm, W_4 = 10mm, L_4 = 5.2mm, L_5 = 12mm

The slotted ground on the monopole fed antenna can itself guarantee a wideband antenna. The current distribution of the wideband element with and without ring shaped ground at 2.2 GHz is shown in Figure 4.21. The high current intensity on the ground ring indicates that it becomes a part of radiator enhancing the impedance matching and extending the bandwidth coverage. Overall, the proper combination of the printed monopole and the SRR along with the slotted ground significantly increases the impedance matching. A wide bandwidth extending from 2 GHz to 6.15 GHz is achieved using this combination, with a fractional bandwidth of 98.2 % as shown in Figure 4.22.

Isolation performance of the quad element system shows how efficient the multiple antenna system can function as a MIMO antenna. Mutual coupling for various stages of evolution is analyzed for the elements lying along a plane,
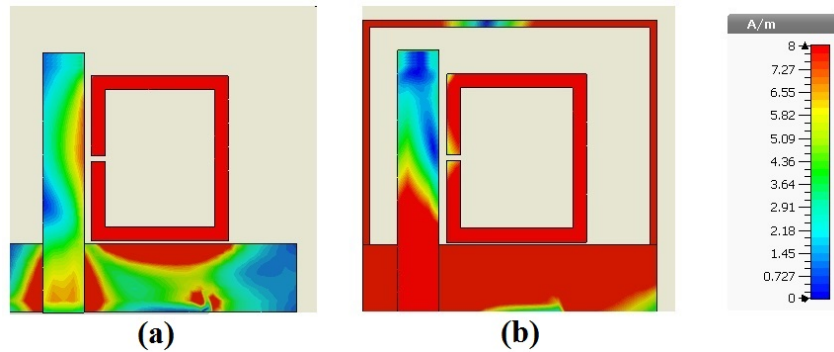
Figure 4.21: Current distribution (a) without (b) with ring shaped ground at 2.2 GHz
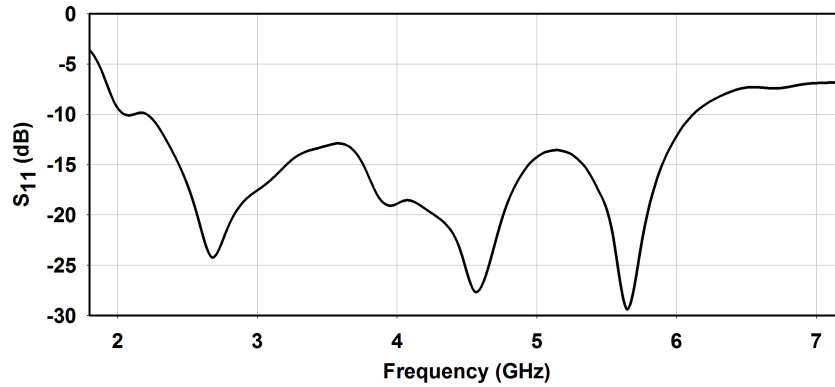
Figure 4.22: Reflection characteristics of wideband antenna

and is shown in Figure 4.23. Coupling analysis between the diagonally oriented elements is shown in Figure 4.24. The ring shaped ground plane functions as a reflector, decreasing the spatial coupling currents, thereby enhancing isolation by 3 to 11 dB in its resonant band extending from 2.5 to 4.5 GHz. This can be observed from the second curve in Figure 4.23 & Figure 4.24. Below the resonant band, the spurious emissions between the closed spaced adjacent ground ring elements causes an increase in the near field coupling for elements lying along a plane.

The addition of SRR does not alter the isolation curves considerably in the lower resonant frequency band. For higher frequencies, the polarization purity is comparatively lesser, resulting in increased cross polar levels. This, along

with the near field coupling caused by the orientation of SRR elements relative to each other, is the reason for reduced isolation in the higher frequency band around 5 GHz - 6 GHz. Overall, the MIMO antenna exhibits good isolation, with a minimum value of about 14 dB, over the entire wideband. The slotted ring shaped ground enhances the impedance matching and also contributes to suppress the wave propagation in space between the individual elements. Orthogonal arrangement of elements in the system also ensures high isolation between the adjacent elements.
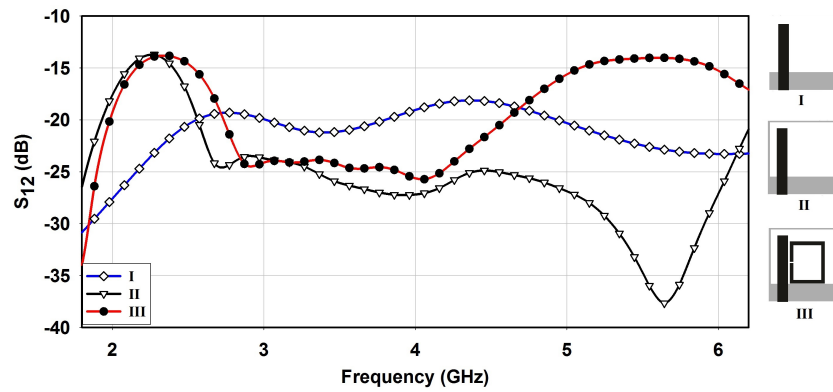
Figure 4.23: Transmission coefficients S12/S14 at various stages of antenna evolution
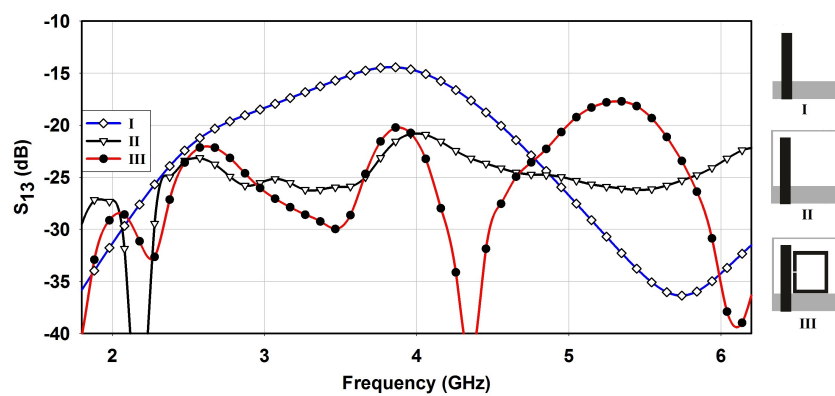
Figure 4.24: Transmission coefficients S13 at various stages of antenna evolution

4.3.2   Simulations and Measurements

The simulated S parameter results of the compact four port wideband MIMO antenna are shown in Figure 4.25. Commercial 3-D electromagnetic simulator CST Microwave Studio with time domain solver was used for performing simulations. The current distributions obtained at various frequency points like 2.5 GHz, 3.5 GHz and 5.5 GHz are shown in Figure 4.26. The high current densities of the wideband antenna elements at various frequency points indicate that the wideband characteristic is realized by properly combining the monopole resonator with slotted ground ring and the SRR.
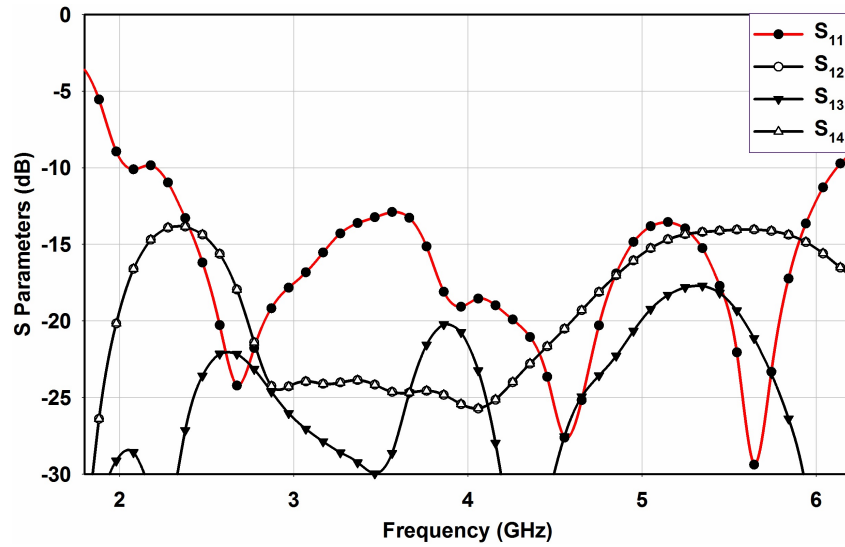
Figure 4.25: Simulated S parameters of the quad element antenna

Amongst different parameters of monopole, SRR and ground ring, the slotted ground ring dimensions have a considerable impact on the wideband resonant behavior. The width c of the ring shaped ground significantly affects the impedance matching in the band. An increase in ground ring width reduces the impedance matching of the entire operating band as shown in Figure 4.27. An increase in ground ring length L_5, increases the electrical length. This causes the resonance to shift to a lower frequency as observed in Figure 4.28. The lower limit of the wideband resonator can be tuned to a certain extend by adjusting the SRR dimensions. However, the initial dent
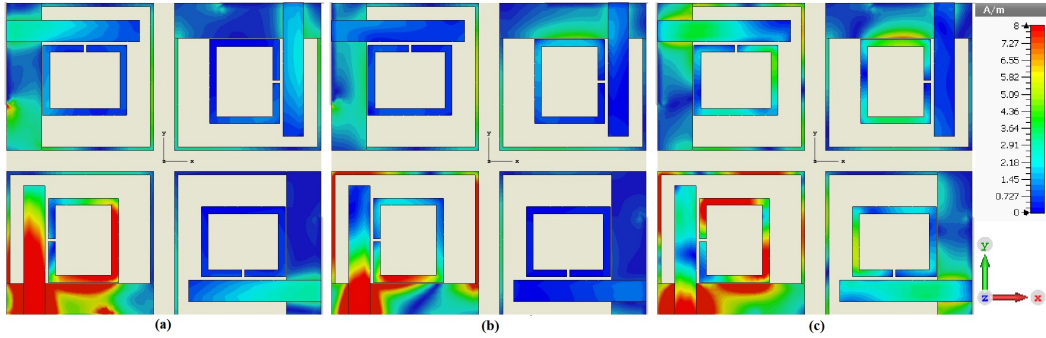
Figure 4.26: Surface current distributions of the four port MIMO antenna with P_1 excited at (a) 2.5 GHz (b) 3.5 GHz (c) 5.5 GHz

in the reflection characteristics is a combined resonance of the fundamental SRR mode and the ground ring resonance, as observed from the current distribution. In conclusion, both the monopole and SRR resonant frequencies are affected by the changes in the ground ring dimensions, and a fine-tuning of individual resonators enables to adjust to the desired frequency band.
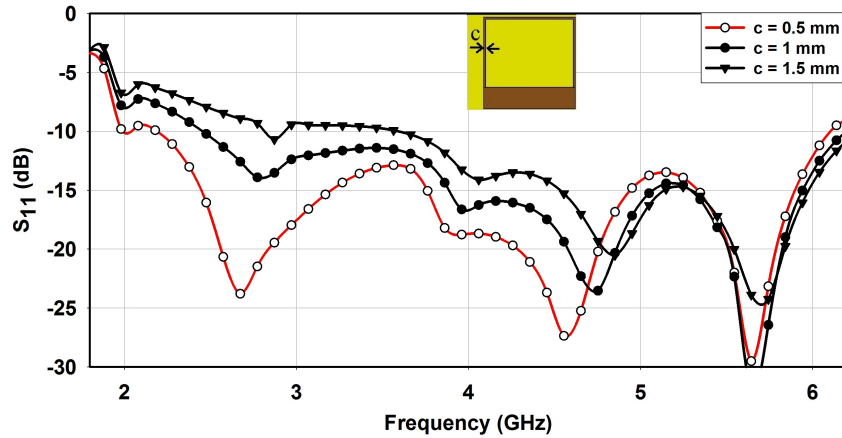
Figure 4.27: Effect of ground ring width on return loss characteristics

The prototype of the antenna is fabricated on an FR4 substrate having a loss tangent $tan\delta = 0.02$ and is shown in Figure 4.29. S parameter measurements of the MIMO antenna obtained from a network analyzer are shown in Figure 4.30. The measured results correlate well with the simulation curves, though minor differences in the frequency band are observed which can be
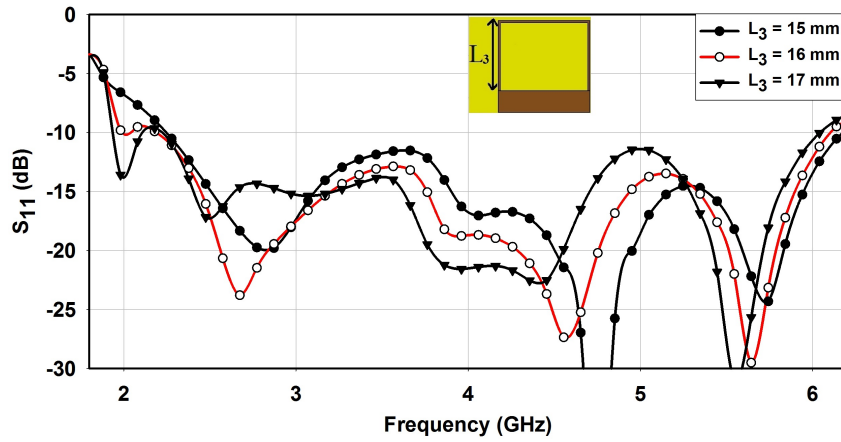
Figure 4.28: Effect of ground ring length on return loss characteristics

attributed to fabrication tolerances. Measured -10 dB impedance bandwidth is from 2.2-6.28 GHz with a fractional bandwidth of 96.2 %. From transmission curves, it can be observed that the antenna system exhibit good isolation between its elements throughout the operating band. Measured results show a minimum isolation of 14 dB and a maximum of 48 dB, in the operating range.

(a)   (b)
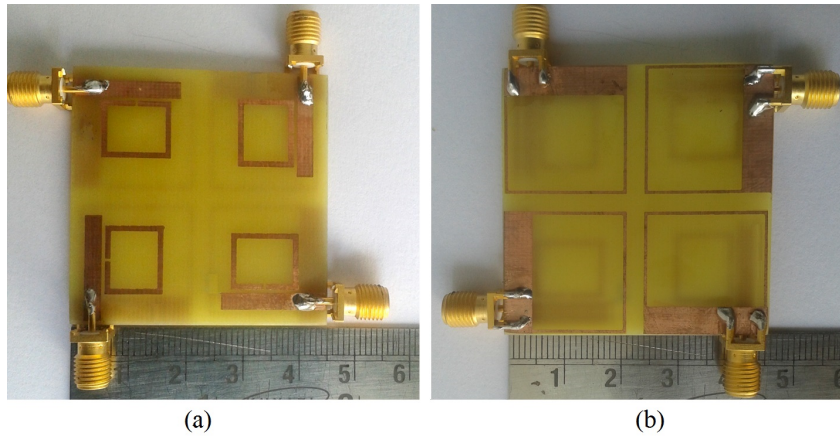
Figure 4.29: Prototype of fabricated antenna (a) Top view (b) Bottom view

Far field radiation pattern measurements are obtained inside an anechoic chamber for each element, while the other elements are terminated with matched loads. Measured radiation patterns for the two principal E and H
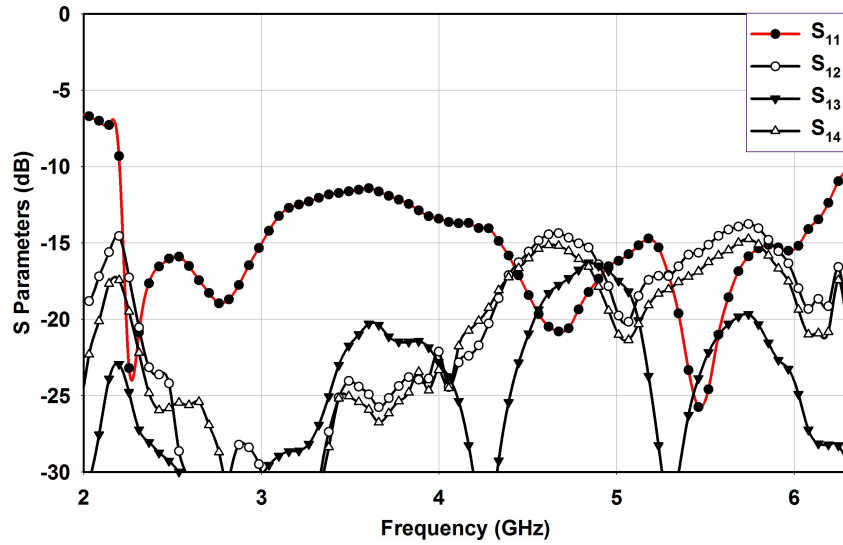
Figure 4.30: Measured S parameters of the quad element antenna

planes at three frequencies, 2.5, 3.5 and 5.5 GHz are shown in Figure 4.31. The pattern of only element 1 is shown as the antenna elements are symmetrical with complementary polarizations for adjacent elements. It was observed that the antenna elements have directional radiation patterns, which are mostly stable in the band. The patterns in Figure 4.31(b) show that the antenna elements exhibit a weak overlap in the azimuthal plane, ensuring uncorrelated channels.

Gain and efficiency of the antenna are also measured and are plotted in Figure 4.32. Gain measurements show an average gain of 2.75 dBi with a peak gain of 4 dBi at 3.3 GHz and a peak efficiency of 91 % is obtained at 3.2 GHz. The MIMO diversity performance of the quad element antenna is evaluated by computing the envelope correlation coefficient between the branch signals received by different elements. A lower value of the envelope correlation coefficient signifies higher pattern diversity. The widely adopted criteria for a MIMO antenna for ECC is to have values < 0.5, and is calculated using equation (3.3) with the far field results. ECC plotted for an isotropic environment in Figure 4.33 shows that across the operating bandwidth, correlation coefficients are well below 0.25 which ensures good MIMO performance.
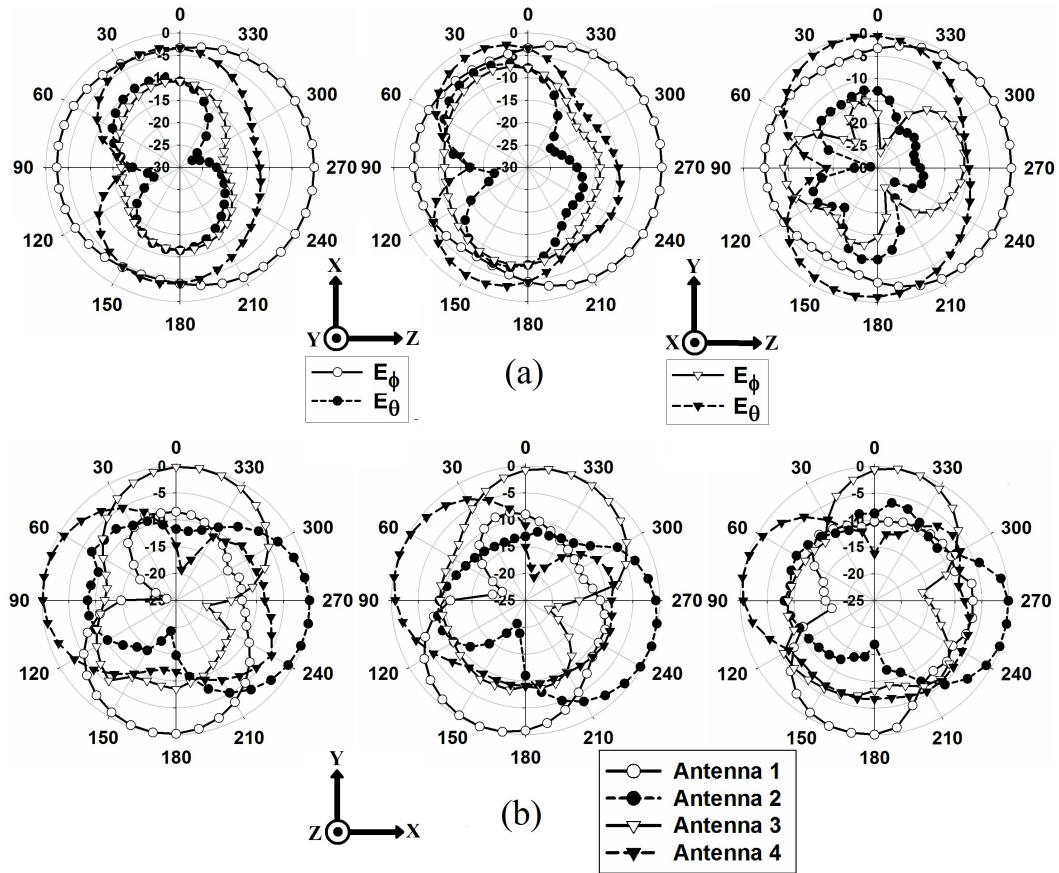
Figure 4.31: Measured radiation patterns (a) at 2.5 GHz, 3.5 GHz and 5.5 GHz for XZ and YZ planes for element 1 (b) in XY plane for four antenna elements

4.4   Chapter Summary

The proliferation of wireless communication services spurs the need for compact and efficient antennas capable of providing good performance while operating at a wide frequency range. It would be highly beneficial to cover all emergent standards using a single antenna. The research focused on design of multiband and wideband MIMO antennas which cover multiple desired frequencies, while retaining good radiation characteristics and reducing the space requirement of the antenna. The first design is a quad element tri-band MIMO antenna resonating in three highly desired bands like 2.4 GHz, 3.5
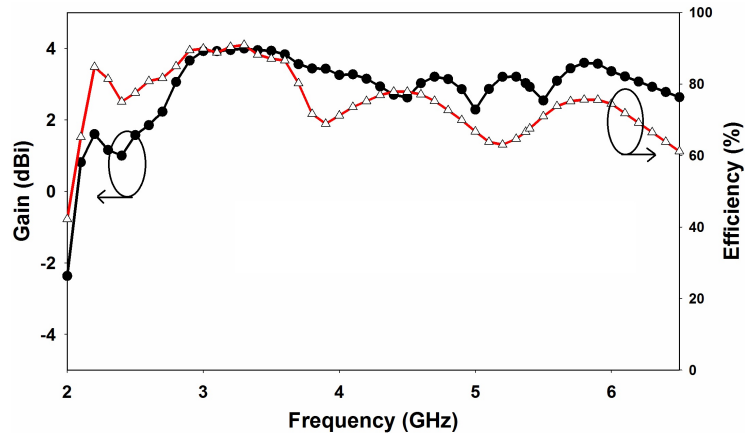
Figure 4.32: Gain and efficiency of the four port MIMO antenna
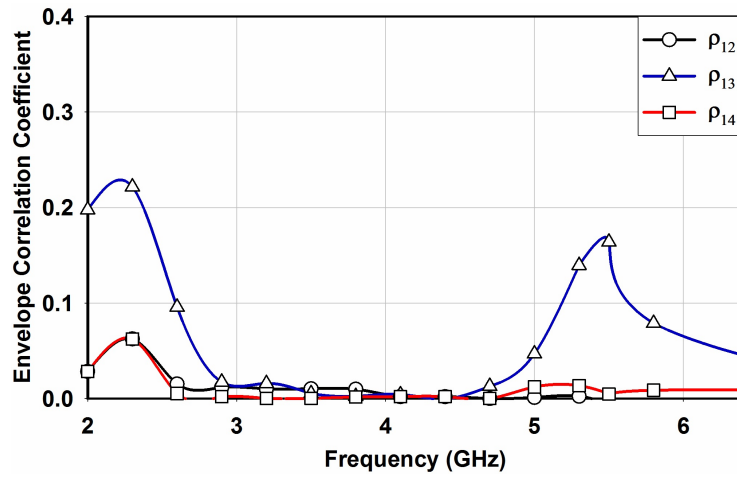
Figure 4.33: Envelope correlation coefficients between antenna elements

GHz and 5-6 GHz band, which covers a wide range of wireless applications. The design of the tri-band antenna is explained in stages which provide the flexibility to tune the antenna to any desired frequency of interest. The orientation of elements forming the tri-band antenna is chosen so as to maintain compact nature with less spurious effect between the individual bands. The MIMO antenna configuration guarantees good isolation performance with the orthogonal orientation of neighboring elements. Further, isolation between diagonal elements is improved by 17 dB by designing the SRR ring. MIMO diversity performance is also observed to be good for the quad element con-

figuration.

Ref	Minimum Isolation (dB)	Total Area of MIMO Antenna (λ_0^2)	No of Operating Bands	-10 dB Bandwidth (%)
[161]	10	0.247	1	3.8
[164]	15	0.605	wideband	46.8
[196]	13, 16	0.167	2	3.2,18.18
[204]	14	0.274	4	15.38, 8.57, 4.4, 1.7
[197]	16.6	0.500	wideband	82
[199]	10	0.096	wideband	60.6
[209]	10	0.600	Wideband	28.5
[221]	10	0.109	1	5.25
section 4.2	24, 22, 22.5	0.068	3	24.7, 20, 28.6
section 4.3	14	0.109	wideband	96.2

Table 4.1: Comparison Table for Multiband and Wideband Quad Element MIMO Antennas

The last section investigates the design and performance of quad element wideband MIMO antenna. All the four wideband antennas resonate in the 2-6 GHz band and support various wireless applications in the band. The printed monopole loaded with an SRR, has its ground plane modified to obtain wideband resonance. The tuning of the wideband resonance by adjusting the antenna dimensions, is investigated. The MIMO antenna provides a compact configuration with good isolation characteristics without using any additional decoupling structures. The slotted ground ring along with the orthogonal orientation of elements, guarantees good isolation and diversity performance as required for the MIMO antenna. A comparison between the proposed antennas and few other multiband and wideband MIMO antenna designs in terms of size, mutual coupling, and bandwidth is shown in Table 4.1. To

ascertain the over the air performance of the designed quad element MIMO antennas, the multi-antenna systems needs to be analyzed in a channel. This aspect of the antenna is studied in detail in Chapter 6.

<div align="right">

Chapter 5

</div>

Channel Performances Of The MIMO Antennas

Contents

The Multiple-Input-Multiple-Output (MIMO) antenna technique has proved to meet the growing demand for higher data-rate applications in communication standards like 3G, WLAN and WiMAX. Spatial correlation and antenna efficiency can partly describe the performance of MIMO systems [248]. To realize an effective MIMO system, it is essential to have an adequate number of uncorrelated and highly efficient antennas at each end of the link. Scattering parameters can give a fairly good idea on the performance of the MIMO antenna system, but a MIMO over the air (OTA) test is needed to understand the end to end performance of the system in a particular environment. Different approaches to this task are being discussed in European Cooperation in Science and Technology (COST) 2100, 3rd Generation Partnership Project

(3GPP) RAN WG4 and the Cellular Telecommunications Industry Association (CTIA). Currently, several major test methodologies exist to address MIMO OTA test. They include:

- Reverberation chamber method: A reverberation chamber generates echoes to mimic multipath propagation [249].

- Emulator and anechoic chamber method: Several wireless channel emulators in an anechoic chamber provide a realistic propagation environment [250, 251].

- Two-stage method: MIMO antenna radiation patterns are obtained from 3D simulation software or are measured within the anechoic chamber and are combined with the multipath fading emulation. This data is then used to perform the OTA performance test [252].

5.1 MIMO OTA Performance Analysis using Two Stage Method

Two-stage method of OTA testing is used to analyze the channel performances of the developed MIMO antennas. Agilent SystemVue software provides a powerful system architecture for verifying the antenna performances in a wireless channel environment. The MIMO Channel Builder in the software simulates the multi-channel fading, which incorporates realistic antenna patterns. As an alternative to the physical OTA test, it is based on a two-stage method that is both economic and repeatable and is shown in Figure 5.1. The steps involved in this MIMO antenna testing method include:

- Obtain radiation patterns of the individual elements of a MIMO antenna system either in a traditional anechoic chamber or simulated using 3D simulation software CST Microwave studio.

- Load these antenna patterns into SystemVue MIMO channel models and emulate the MIMO channel model with incorporated patterns.

Two different approaches exist in the SystemVue Channel Model Builder to integrate the antenna patterns to the MIMO channel model. One method is to use a correlation-based channel model. The other method is to use the WIN-NER II (Wireless world initiative new radio) channel model. This two-stage
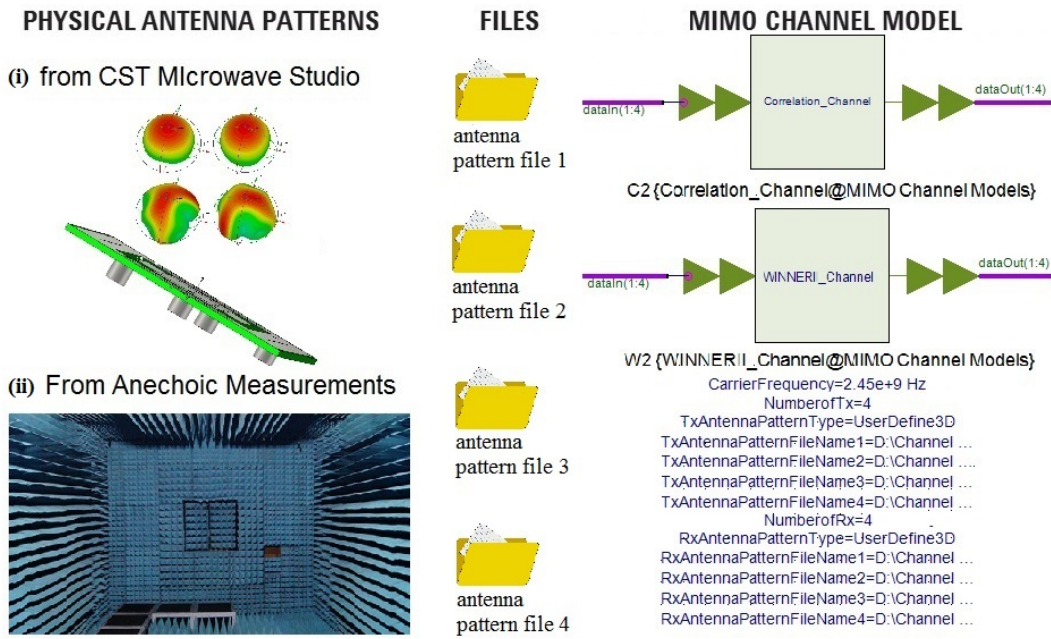
Figure 5.1: System for analysis using SystemVue

OTA testing method can be used to measure the following figures of merits of the multiple antenna systems like MIMO channel capacity, throughput and BLER [253]. In this chapter, we investigate and compare the channel performance of multiple antennas designs with the correlation-based model and the geometry based models implemented in the software [254]. In MIMO systems, both the radio channel propagation conditions and antenna characteristics influence the end user's quality-of-service (QoS). These MIMO channel models has the ability to simulate the multipath fading that incorporates the antenna patterns. The antenna effects and the channel characteristics are also coupled into these channel models.

5.2 Channel Model Approach

The evaluation of the developed MIMO antennas is performed using two channel approaches, namely correlation based channels and WINNER II channels.

5.2.0.1 Correlation Channel

The correlation based MIMO channel is flexible for customization by the user. Here, a correlation matrix is formed which attempts to model the correlation between paths in a given channel. This model is a good fit for the two-stage OTA method which combines the spatial properties of the multipath with the spatial properties of the transmitter and receiver antenna arrays. The spatial correlation matrix for the antenna radiation patterns can be given as [248]

$$\rho_{Tx,mn} = \frac{\int_{-\pi}^{\pi} e^{-j2\pi \frac{d_{mn}}{\lambda} sin(\theta)} PAS_{Tx}(\theta)\sqrt{G_{Tx,m}(\theta)G_{Tx,n}(\theta)}d\theta}{\sqrt{\int_{-\pi}^{\pi} PAS_{Tx}(\theta)G_{Tx,m}(\theta)d\theta}\sqrt{\int_{-\pi}^{\pi} PAS_{Tx}(\theta)G_{Tx,n}(\theta)d\theta}} \tag{5.1}$$

$$\rho_{Rx,mn} = \frac{\int_{-\pi}^{\pi} e^{-j2\pi \frac{d_{mn}}{\lambda} sin(\theta)} PAS_{Rx}(\theta)\sqrt{G_{Rx,m}(\theta)G_{Rx,n}(\theta)}d\theta}{\sqrt{\int_{-\pi}^{\pi} PAS_{Rx}(\theta)G_{Rx,m}(\theta)d\theta}\sqrt{\int_{-\pi}^{\pi} PAS_{Rx}(\theta)G_{Rx,n}(\theta)d\theta}} \tag{5.2}$$

where $PAS(\theta)$ is the power azimuth spectrum of the impinging signal, $G(\theta)$ is the power gain of the radiation pattern. The basic Kronecker model suggests that the transmitter and receiver side are uncorrelated. Considering this assumption the spatial correlation matrix, R_s, is calculated using the following equation

$$R_s = \frac{1}{tr R_{Rx}} R_{Tx} \bigotimes R_{Rx} \tag{5.3}$$

The combined correlation matrix R is given by [255]

$$R = R_s \bullet R_p \tag{5.4}$$

where R_s is the spatial correlation matrix and R_p is the polarization correlation matrix respectively. This basic kronecker model is further improved in

SystemVue software to include the antenna characteristics and channel characteristics. These characteristics are incorporated in forming the joint, spatial and polarization correlation matrices. The channel coefficients H_s is given by

$$H_s = \sqrt{R} H_u \tag{5.5}$$

where H_u is spatially uncorrelated Rayleigh fading sample and temporal correlated by the Doppler spectrum. The correlation model allows users to configure several parameters including power delay profile (PDP), the angle of arrival and departure, angular spread and power angular spectrum for evaluating the performance of the antennas under different conditions.

5.2.0.2   Winner II Channel

The WINNER II model is a geometry-based stochastic channel model approach for creating a radio channel model [256, 257]. The channel models are independent of the antenna, allowing the insertion of various antenna configurations and diverse element patterns. Winner II channel models are used to evaluate the link level and system level performances of various wireless communication systems. It is used to perform comparison studies between various algorithms and technologies. The model supports multiple antenna technologies, different polarizations and multi-user communications. The time variant impulse response matrix of the UxS MIMO channel is given by [257]. The channel impulse response from transmitter antenna element s to the receiver antenna u is given by

$$H(t;\tau) = \Sigma_{n=1}^{N} H_n(t;\tau) \tag{5.6}$$

where t is time, τ is delay, N is the number of paths, and n is path index. The impulse response matrix is composed of the antenna array response matrices F_{tx} and F_{rx} for the transmitter (TX) and the receiver (RX) respectively. The channel from the TX antenna element s to the RX element u, for cluster n, is expressed as

$$H_{u,s,n}(t;\tau) = \Sigma_{m=1}^{M} \begin{bmatrix} F_{rx,u,V} & (\Phi_{n,m}) \\ F_{rx,u,H} & (\Phi_{n,m}) \end{bmatrix}^T \begin{bmatrix} \alpha_{n,m,VV} & \alpha_{n,m,VH} \\ \alpha_{n,m,HV} & \alpha_{n,m,HH} \end{bmatrix} \begin{bmatrix} F_{tx,s,V} & (\Phi_{n,m}) \\ F_{tx,s,H} & (\Phi_{n,m}) \end{bmatrix} \times$$
$$exp(j2\pi\lambda_0^{-1}(\Psi_{n,m}r_{rx,u})) \times exp(j2\pi\lambda_0^{-1}(\Phi_{n,m}r_{tx,s})) \times exp(j2\pi\upsilon_{n,m}t)\delta(\tau - \tau_{n,m}) \tag{5.7}$$

where $F_{rx,u,V}$ and $F_{rx,u,H}$ are the antenna element u field patterns for vertical and horizontal polarizations, respectively, $\alpha_{n,m,VV}$ and $\alpha_{n,m,VH}$ are the complex gains of vertical-to-vertical and horizontal-to-vertical polarizations of ray n,m, respectively, λ_0 is the wavelength of the carrier frequency, $\phi_{n,m}$ is the AoD unit vector, $\varphi_{n,m}$ is the AoA unit vector, $r_{tx,s}$ and $r_{rx,u}$, are the location vectors of element s and u, respectively, and $V_{n,m}$ is the Doppler frequency component of ray n,m.

Environments used in WINNER II channel are called propagation scenarios. The covered propagation scenarios described for Winner channel include indoor, indoor to outdoor, urban micro-cell, outdoor-to-indoor, stationary feeder, suburban macro-cell, urban macro-cell, rural macro-cell, and rural moving networks. The WINNER model has been developed for 18 scenarios in SystemVUE which are divided into three major categories: local, metropolitan and wide areas [257].

5.3   Channel Capacity Measurements

The channel capacity of the developed quad element MIMO antennas is measured using both the Correlation and Winner II Channel models. The two channel models in the software are shown in Figure 5.2. The Correlation channel model computes the correlation matrix and channel coefficients to evaluate the channel capacity. It generates two files which have the real and imaginary parts of the channel correlation matrix R. R is the kronecker product of the transmit and receive correlation matrices with a matrix size of $K \times K$, where K is the *number of Tx antennas $\times$ number of Rx antennas*. The channel correlation matrix R combines all the paths together. The channel coefficients are then determined by the number of samples provided by the user. For example, for a 2×2 MIMO case, the combined channel coefficient is

$$\begin{bmatrix} Tx1Rx1 & Tx2Rx1 \\ Tx1Rx2 & Tx2Rx2 \end{bmatrix} \tag{5.8}$$

and the combined correlation matrix is

$$\begin{bmatrix} Tx1Rx1 \\ Tx1Rx2 \\ Tx2Rx1 \\ Tx2Rx2 \end{bmatrix} \times \begin{bmatrix} Tx1Rx1 & Tx1Rx2 & Tx2Rx1 & Tx2Rx2 \end{bmatrix}^* \qquad (5.9)$$

The 16 float elements of each file has both real and imaginary parts which forms the complex correlation matrix $Tx1Rx1 \times Tx1Rx1, Tx1Rx1 \times Tx1Rx2, \cdots \cdots, Tx1Rx1 \times Tx2Rx2, Tx1Rx2 \times Tx1Rx1, \cdots \cdots, Tx2Rx2 \times Tx2Rx2$. The channel capacity is then obtained using the equation [13]

$$C = log_2 det[1 + \frac{\rho}{N} HH^H] bits/sec/Hz \qquad (5.10)$$

where ρ is the Signal to noise ratio (SNR) in dB, N is the number of TX, H is the transfer matrix which is the cholesky decomposition of R multiply channel coefficients. For the performance analysis and comparative study of developed quad element MIMO antennas, the three-dimensional far field radiation patterns and obtained from CST Microwave Studio. These are then converted to a *.uan file format as specified by SystemVue software. The user defined pattern options in the software require distinct files for each antenna elements to be saved as separate files. Each file has a description or header section and a data section. The header section includes details such as maximum and minimum values of phi and theta angles, the step size with which pattern is obtained, the net input power and the antenna polarization's. The data section requires input parameters that include magnitude (dB) and phase (degrees) values of far field radiation patterns for different phi and theta angles.

The correlation based channel model unit is loaded with the radiation pattern data files and channel correlation matrix is computed. For comparison of the antenna performances, the channel capacities are obtained with an ideal half wavelength separated omnidirectional array source for a 4×4 MIMO, 3×3 MIMO and a 2×2 MIMO antenna systems. The omnidirectional source option has user input options like the position of the antennas, angular information and cross polarization ratio. The user can also assign no of paths, accordingly, the correlation matrix formed is a $K \times N$ array, where N is the

CorrChannel_Capacity

Calculate the Correlation Channel Capacity
Based on the Generated Correlation Matrix

C2 {Channel_Capacity@MIMO Channel Models}
NumberofTx=4 [NumberofTx]
NumberofRx=4 [NumberofRx]
NumSamples=30000
SNR=10 [SNR]
CorrMatrix_I_FileName=Ant_CorrChMatri...
CorrMatrix_Q_FileName=Ant_CorrChMatri...
Seed=1

S1 {Sink@Data Flow Models}
StartStopOption=Samples

(a)

WinnerIIChannel_Capacity

Calculate the WinnerII Channel Capacity
Based on the Generated Correlation Matrix

C4 {Channel_Capacity@MIMO Channel Models}
NumberofTx=4 [NumberofTx]
NumberofRx=4 [NumberofRx]
NumSamples=30000
SNR=10 [SNR]
CorrMatrix_I_FileName=Ant_WinnerIIChM...
CorrMatrix_Q_FileName=Ant_WinnerIIChM...
Seed=1

S1 {Sink@Data Flow Models}
StartStopOption=Samples

(b)

Figure 5.2: Channel capacity models (a) Correlation (b) WinnerII

Number of Tx × Number of Rx × Number of paths. The correlation matrix that is used to calculate the channel capacity is the compositive correlation matrix of all paths.

The channel capacities for the half-wave length separated orthogonal antenna array for 4×4, 3×3 and 2×2 MIMO are considered as ideal or reference values, to which channel capacities of the antennas under test (AUT) are compared. Channel capacities are obtained for different signal to noise ratio values, for all the designed antennas. The channel capacity calculation follows the method given in [258], which takes the antenna array performance and correlation into account. For user defined 3D patterns, the capacities are observed with both the transmitter antennas and the receiver end antennas

replaced with MIMO antenna under test.

The channel capacity performances of all the five proposed quad element MIMO antenna structures are measured from the far-field radiation patterns obtained in the 2.45 GHz band, as all these models which are defined in section 3.2, section 3.3, section 3.4, section 4.2, and section 4.3 resonate at 2.45 GHz band. Figure 5.3 shows the channel capacity with both the correlation and winner II channel models for the MIMO antenna configurations defined in section 3.2. The quad element multimode antenna consists of microstrip square patch and square ring patch antenna. The capacity measurements shown in Figure 5.3 has two subsections arranged side by side which corresponds to channel capacities obtained for the correlation and Winner II channel models. Channel capacity is measured for varying SNR values from 0 dB to 30 dB. It can be observed that the channel capacity increases from 3.9 bits/s/Hz to 34.9 bits/s/Hz with an increase in SNR for correlation based channel model.Capacity measurements using Winner II channel achieves a capacity of 23.5 bits/s/Hz at an SNR of 30 dB.
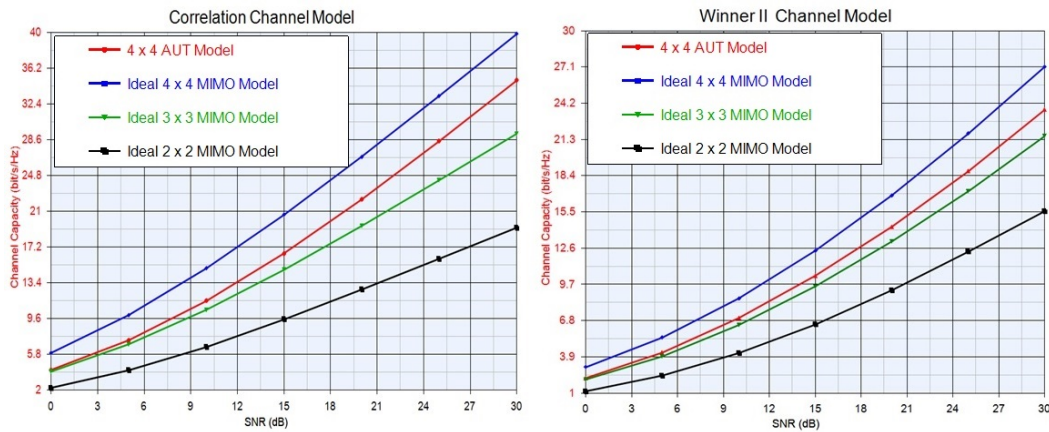
Figure 5.3: Channel capacity of square and ring patch MIMO antenna

The channel capacity of the four port MIMO antenna using concentric square ring microstrip patches, defined in section 3.3 is shown in Figure 5.4. It is observed that the antenna has a capacity of 4 bits/s/Hz at an SNR of 0dB, as the SNR increases the capacity increases. The antenna achieves a channel capacity value of 33.9 bits/s/Hz at an SNR of 30 dB when using a

correlation channel model. In a Winner II channel, the channel capacities are less compared to the correlation channel, with a value of 22.8 bits/s/Hz at an SNR of 30 dB. The radiation pattern of the multimode MIMO antenna using microstrip cross and ring patches when used with a correlation channel, has a capacity of 32.4 bits/s/Hz at an SNR of 30 dB. This can be observed from Figure 5.5 and the antenna is described in section 3.4. The same pattern values when loaded with Winner channel model has obtained a capacity of 25.2 bits/s/Hz at an SNR of 30 dB.
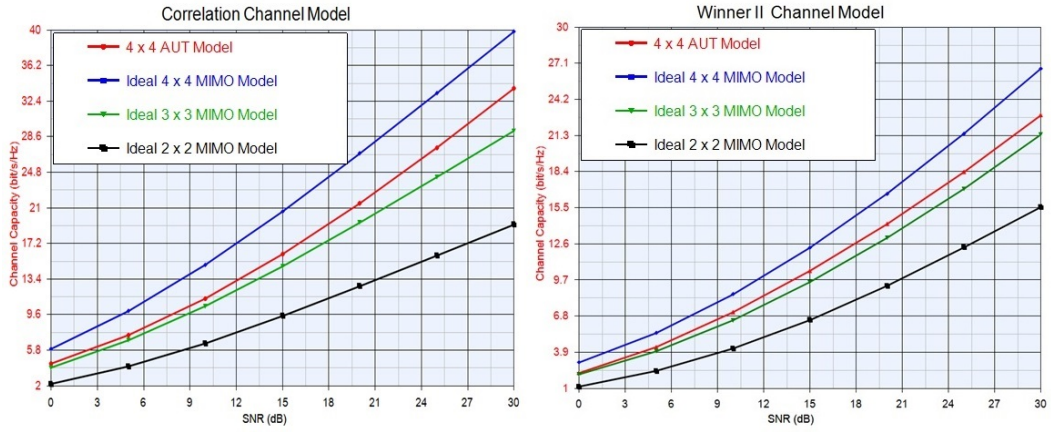
Figure 5.4: Channel capacity of concentric ring patch MIMO antenna
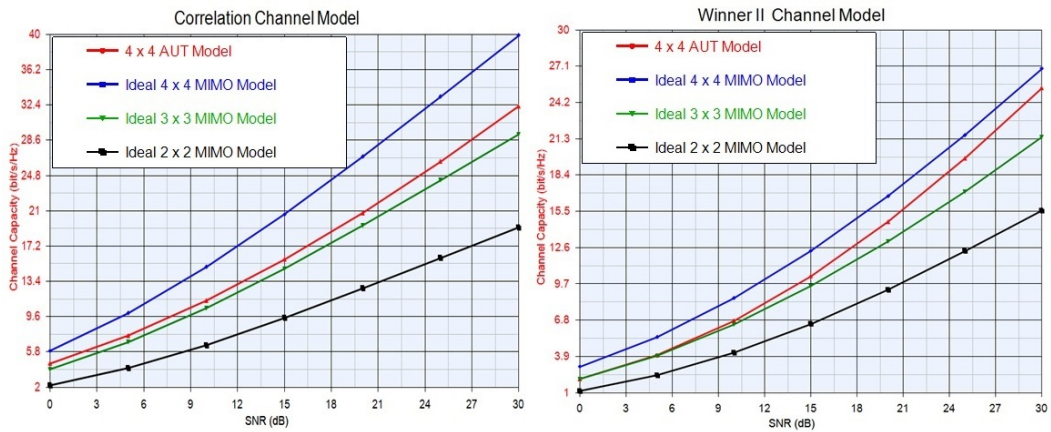
Figure 5.5: Channel capacity of cross and ring patch MIMO antenna

For the quad element tri-band MIMO antenna using meander line resonators loaded with stubs, radiation patterns are obtained for the first resonant band at a frequency of 2.45 GHz. The antenna is described in section 4.2 and the channel capacity analysis is shown in Figure 5.6. Channel capacity using correlation channel model with varying SNR values ranging from 0 dB to 30 dB shows a capacity improvement from 5.85 bits/s/Hz to 40 bits/s/Hz. Using a Winner II channel, channel capacities of the system range from 1.9 bits/s/Hz to 26.1 bits/s/Hz for SNR values from 0 dB to 30 dB. The channel capacity analysis for the wideband MIMO using monopole antenna with a modified ground plane discussed in section 4.3 is shown in Figure 5.7. Channel capacity values of the antenna ranges from 5.3 bits/s/Hz to 38.2 bits/s/Hz for SNRs ranging from 0 dB to 30 dB, when a correlation based channel is used. For a Winner II channel, the antenna achieves a capacity of 24.2 bits/s/Hz at an SNR of 30 dB.
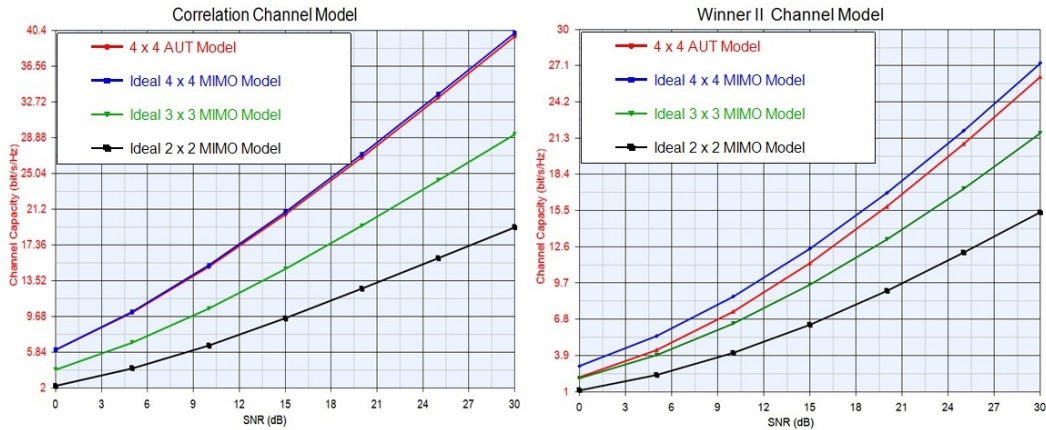
Figure 5.6: Channel capacity of triband MIMO antenna at 2.45 GHz

From the channel capacity performance analysis, it can be observed that with the correlation based channel model, better capacities are obtained. In the WINNER II channel model, an urban macro cell environment is modeled which is more closer to a practical environment and hence capacities obtained are lesser compared to correlation model. A larger enhancement of channel capacity is observed for MIMO antennas with all four elements having identical antennas exhibiting similar performance, exploiting polarization diversity.
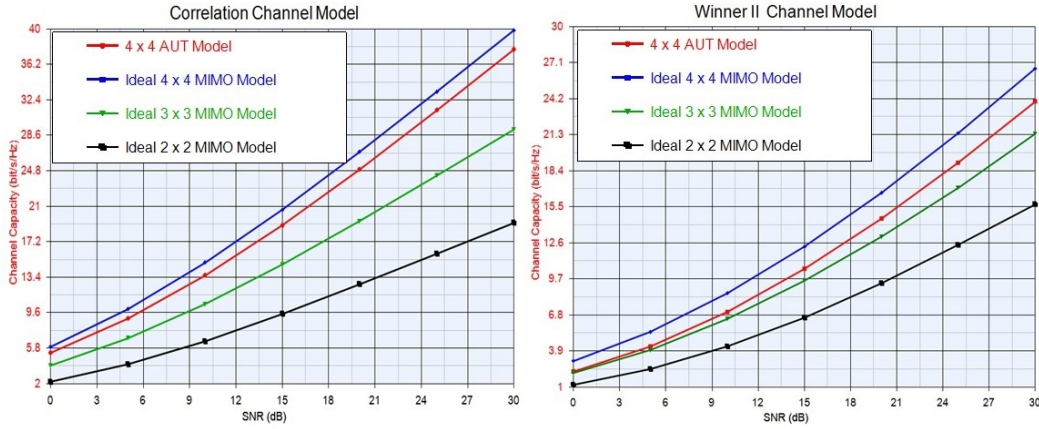
Figure 5.7: Channel capacity of wideband MIMO antenna at 2.45 GHz

An averaged improvement of around 5 bps/Hz is observed for Figure 5.6 and Figure 5.7 as compared to capacities in Figure 5.3, Figure 5.4 and Figure 5.5. The channel capacity obtained for the antenna defined in section 4.2 is the highest and is closer to 4×4 omnidirectional array.

For multimode antennas defined in section 3.2, section 3.3, section 3.4, employing both polarization and pattern diversity, the pattern correlation was observed to be very less. This may be due to the maximum exploitation of diversity in these designs, compared to antennas defined in section 4.2 and section 4.3 which are mainly polarization diverse. However, the capacities obtained for these antennas which employ both polarization and pattern diversity is less compared to the MIMO antenna which uses identical elements placed orthogonally. The individual antenna performance differed in the pattern diverse models due to the deployment of two different antenna structures. The efficiency of higher order modes of the outer ring antenna was comparatively less than the fundamental radiating modes of the inner patch antenna. For the multiband and wideband MIMO antennas defined in section 4.2 and section 4.3, all the four elements are equally efficient with good branch performance in the MIMO system and hence contributes towards higher channel capacity.

5.4   Channel Throughput and Block Error Rate Measurements

According to COST Action 2100, throughput is suggested to be an important system level figure of merit [259] for MIMO antenna. However, assessing the throughput of a MIMO, in a given multipath environment, is always challenging because it depends not only on the MIMO antenna array itself, but also on spatial and temporal characteristics of the radio channel as well as the space-time data processing algorithm. In this study, the two-stage method is adopted, which calculates the throughput using the passive antenna far-field pattern measurements and a MIMO channel model with appropriate parameters.

Throughput measurements are performed using the correlation and WINNER II channel model in Agilent's W1715 MIMO Channel Builder of SystemVue. Simulation is performed using Swept Throughput vs. RxPhiRotation measurement example in the software, using far field antenna patterns, for LTE downlink. The configuration is modified for a four port MIMO and is tested for 4×4 MIMO Spatial Multiplexing. The antenna patterns are configured to be omnidirectional or UserDefined 3D. The channel parameters for individual snapshots are based on the statistical distributions extracted from the channel measurement. The throughput fraction of the system designed in presence of rich scattering is investigated.

A correlation channel with finite discrete multipath components which are considered to be uniformly distributed about the transmitter and receiver is used. Each multipath component is considered uncorrelated and is characterized by the angle of arrival, angular spread and path gain. The WINNER II model is stochastic and geometry-based. The Winner II channel scenario C1 (Urban Micro-cell) is used in the throughput comparison of the 16 antenna pairs. Other parameters are set to be the default values in the model. The downlink transmitter and receiving end is configured to use a four-element linear array with omnidirectional elements and half-wavelength spacing for obtaining reference throughput fraction values for 4×4 MIMO using both correlation and Winner II channel. The antenna pairs under investigation are

placed horizontally at the receiver, facing the transmitter array. For Antenna under Test(AUT), user defined 3D pattern option is selected. The patterns of the antennas are imported from CST microwave studio farfield results corresponding to a frequency of 2.45 GHz.

The work space shown in Figure 5.8 provides the fully coded transmitter and receiver chain along with added noise to perform the test for a 4×4 multiple antenna system. The BLER and throughput measurements are the most important measurements for characterizing the receiver performance. Measurements are performed for the five quad element MIMO antenna models using the radiation pattern data obtained for each antenna element of the multi-element antenna. Performance curves for throughput vs signal to noise ratio and block error rate vs signal to noise ratios are provided. The fractional data throughput's, which are normalized with respect to their corresponding maximum achievable values, are superposed for various sweep values of AWGN.

The throughput performances of multimode MIMO antenna using microstrip square and ring patches defined in section 3.2 is shown in Figure 5.9. The reference curves obtained for an ideal omnidirectional 4×4 MIMO array with both the correlation and Winner II channel models are compared with the results obtained for the antennas under test. The figure has two subsections arranged side by side which corresponds to block error rate and throughput fraction measurements. The Figure 5.9 reveals that in a noisy channel for SNR values below 3 dB, throughput fraction is significantly low below 50 % for a correlation channel. For an urban Winner II channel, throughput fraction reduced below 50 % for an SNR of 6 dB.

BLER and throughput performances of quad element MIMO antenna using concentric square ring microstrip patches explained in section 3.3 are shown in Figure 5.10. It is observed that for an SNR value of 5 dB, a throughput fraction of 97 % and BLER of 0.03 is achieved using correlation channel model. Using Winner II channel channel throughput fraction is 44 % and BLER is 0.56 when the signal to noise ratio is set to 5 dB. Multimode MIMO antenna using microstrip cross and ring patches with high isolation described in section 3.4 achieves a throughput fraction of 100 % at an SNR of 6 dB and
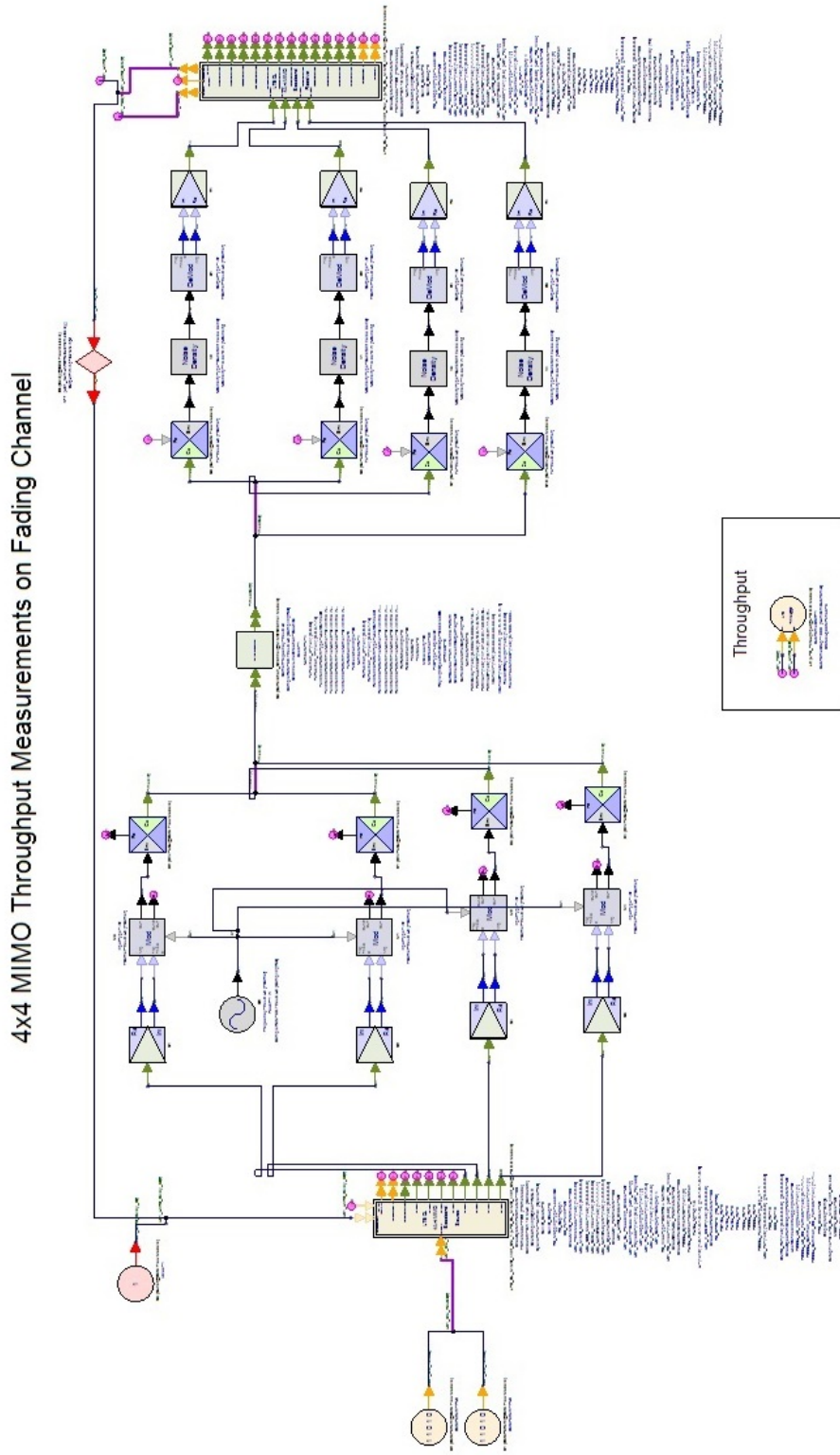
Figure 5.8: Throughput measurement model
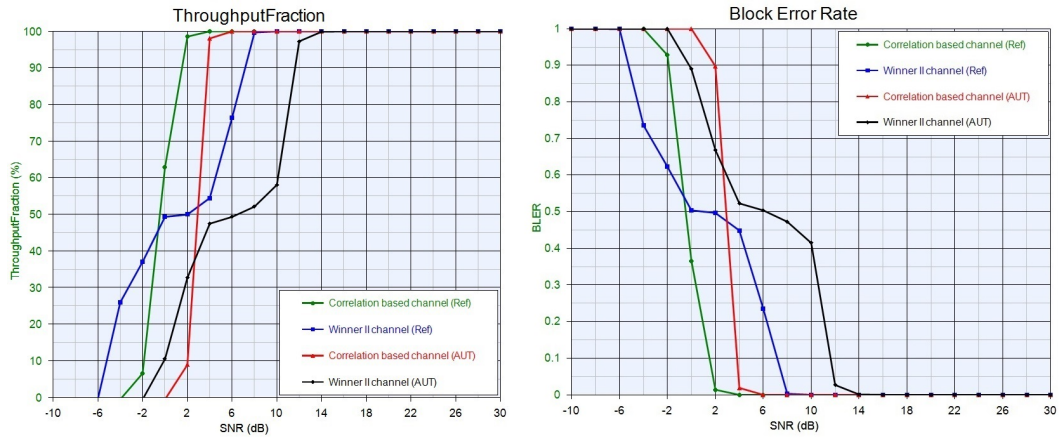
Figure 5.9: Throughput fraction and BLER of square and ring patch MIMO antenna

16 dB using correlation and Winner II channel models respectively. This is shown in Figure 5.11.
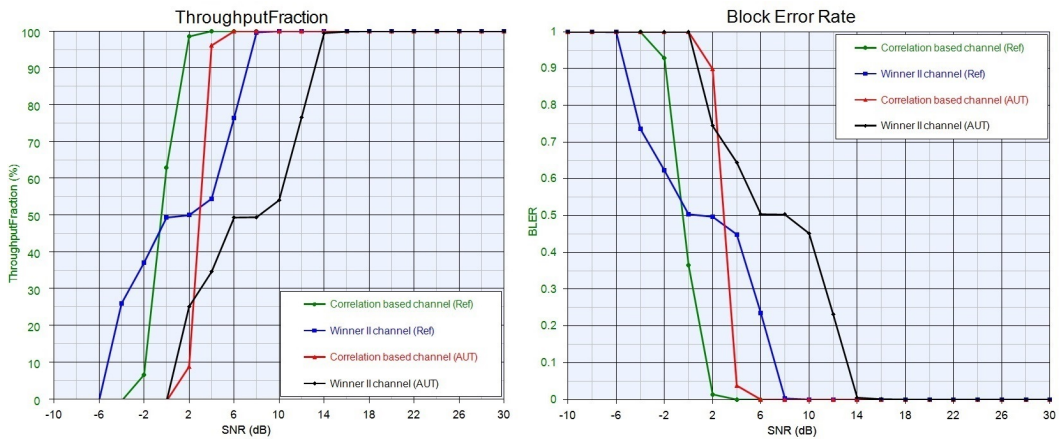
Figure 5.10: Throughput fraction and BLER of concentric ring patch MIMO antenna

For triband MIMO antenna using meander line loaded with stubs defined in section 4.2, 3D radiation pattern values obtained at 2.45 GHz are used for throughput performance analysis and is shown in Figure 5.12. For an SNR value of 5dB, a channel throughput fraction of 98 % and BLER of 0.02 is obtained with correlation channel model. For Winner II channel a throughput
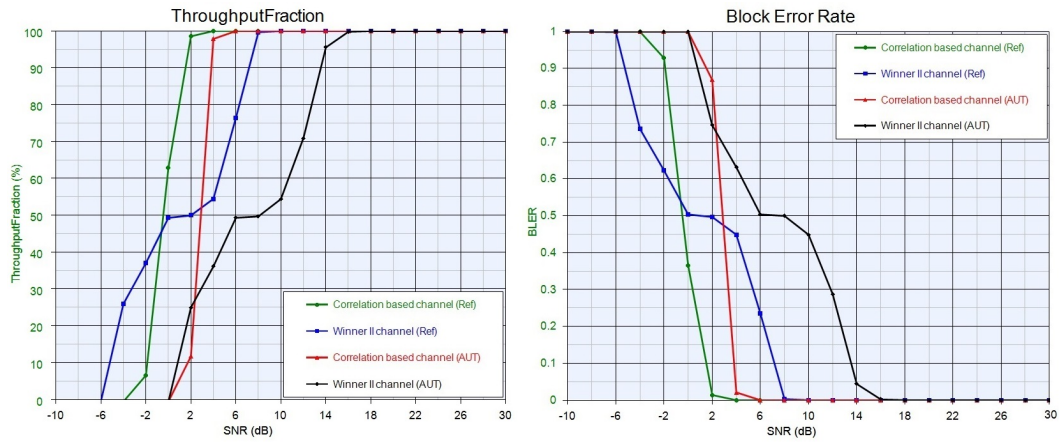
Figure 5.11: Throughput fraction and BLER of cross and ring patch MIMO antenna

fraction of 100 % is achieved at an SNR value of 14 dB. Throughput analysis of the quad element wideband MIMO antenna using monopole antenna loaded with a modified ground plane discussed in section 4.3, is shown in Figure 5.13 for a frequency of 2.45 GHz. It can be observed that a fractional throughput of 100 % is achieved at an SNR value of 5 dB for correlation channel and at an SNR of 16 dB for Winner II channel model.
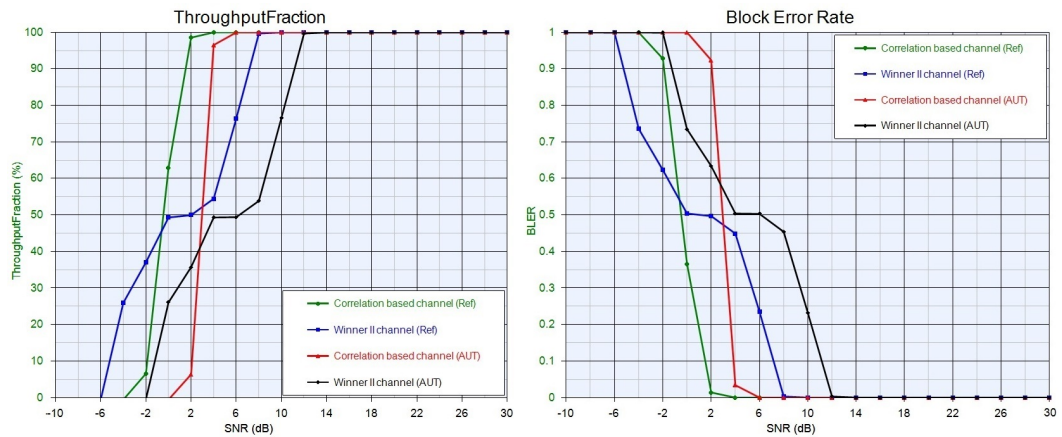
Figure 5.12: Throughput fraction and BLER of triband MIMO antenna at 2.45 GHz
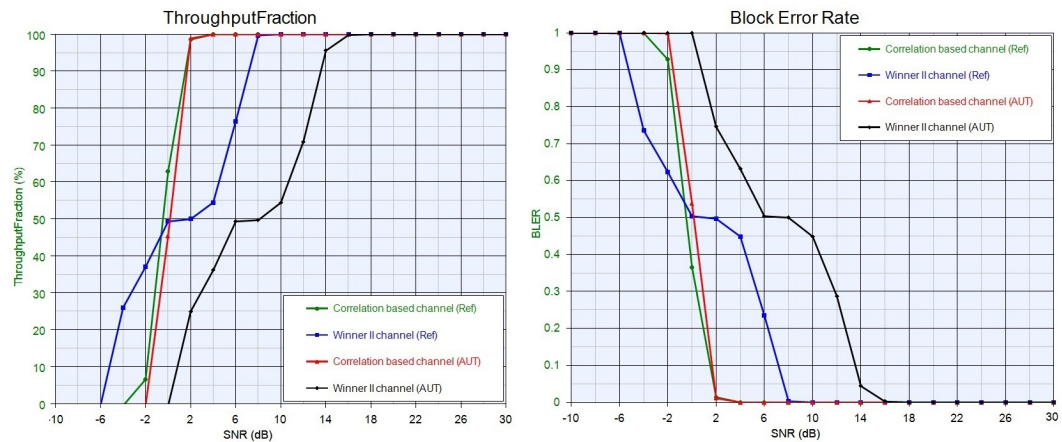
Figure 5.13: Throughput fraction and BLER of wideband MIMO antenna at 2.45 GHz

5.5 Chapter Summary

From the above performance evaluations and comparisons, it can be concluded that the decoupled MIMO antennas using various design techniques and decoupling methods exhibit satisfactory channel performances and behave considerably different with the two channel models. There are significant variations in the channel capacity and throughput values obtained with the various developed quad element MIMO antennas just as the antennas have dissimilar isolation performance, efficiency and ECC values. However, apart from all the performance variations, all the developed multi-antenna designs support multiple antenna communication and performs better than the SISO, 2 X 2 and 3 x 3 omnidirectional arrays. Moreover, the polarization diversity based wideband and triband quad element MIMO antennas have very good channel performance, the compact triband MIMO giving the best performance among all the quad element antennas under investigation. Therefore, it is worthwhile to design a compact MIMO antenna with a reasonably good isolation level, for wireless routers and adapter terminals in a realistic environment.

Chapter 6

Conclusion And Future Perspective

Contents

This chapter summarizes the results and highlights the conclusions drawn from the research work on MIMO antennas. This is followed by a few recommendations for future work. The studies and the results presented in the thesis have been published by the author in various international journals and conferences.

6.1 Conclusions

The aim of the thesis was to investigate the design considerations and radiation characteristics of multiple element antennas for MIMO applications. The background and theory of MIMO communication and multiple antenna systems were shortly discussed. The methodology for designing MIMO antennas is explained in brief. The performance measures or figure of merits for multiple antenna systems to exhibit good MIMO performance is discussed in the thesis. These include parameters like mutual coupling between antenna elements, envelope correlation coefficient, diversity gain, mean effective gain and multiplexing efficiency.

The evolution of antenna designs are investigated in detail to have an insight on the radiation characteristics at each stage. A method of using

multiple modes of microstrip patches as diversity branches in a MIMO antenna is introduced. Analysis using different patch antenna shapes shows that a quad element MIMO antenna can be designed using two different collocated patch antennas, exciting their fundamental and higher order radiation modes. Three multimode four port MIMO antenna designs are discussed in the thesis using the basic forms of microstrip patches such as square patch, ring patch and cross patch antenna. The various forms of diversity techniques like spatial, polarization and pattern diversity are combined to provide the best diversity performance for the MIMO antenna.

The thesis also explains the design and evolution of compact quad element antennas with multiband and wideband resonant characteristics. These antennas are of great significance for practical applications because of the design flexibility for various wireless applications. Polarization diversity is used to arrange the elements in the multi-element antenna. To achieve compactness, sub-wavelength miniature structures like monopole, stubs and split ring resonators are used in the antenna design. Two such quad element multiple antenna design one having triband resonance and other, with a wide bandwidth is investigated.

From the studies, it can be explained that the key to having a good MIMO performance is to have low mutual coupling between the elements in the multiple antenna systems. The high coupling can deteriorate the antenna performances like bandwidth, efficiency and wireless channel capacity. To alleviate the mutual coupling, several isolation enhancement structures are designed for use in MIMO antennas. These include defected ground structures, which are etched on the ground plane between microstrip patches in the multimode MIMO antennas. DGS has several functionalities; it acts as a resonator which radiates the coupling waves, it can reverse the polarity of coupling currents, as well as can function as a stop band filter for coupling waves. Apart from DGS, split ring resonators are also used to reduce coupling, SRRs are designed in the resonant frequency of the main antenna to improve isolation between elements with identical field orientation.

In addition to high isolation between elements, the MIMO diversity performances are analyzed for the various multi-element designs. Though there are various performance parameters like DG, MEG and multiplexing efficiency,

an improvement in wireless communication quality can be guaranteed when the MIMO antennas have simultaneously good isolation characteristics and low ECC values among its antenna elements [260]. Hence, both these values are measured for all the designed quad element antennas. The MIMO channel performances of the antennas are evaluated from the far-field radiation patterns to obtain channel capacity, throughput and BLER values with varying signal to noise ratios. The results show that polarization diversity based designs with highly efficient antenna elements, have improved channel performance in comparison to multimode antennas using both polarization and pattern diversity.

6.2   Thesis Summary

The key contributions and findings in the research work detailed in this thesis are summarized in the following sections.

1. Multimode MIMO Antenna using Microstrip Square and Ring Patches with Ring DGS

A four port multimode MIMO antenna using microstrip square and ring patch is investigated in section 3.2 of chapter 3. The antenna uses the two fundamental orthogonal resonant modes of the square patch and two orthogonal higher order modes of the ring patch antenna to achieve the multimode behavior. By this way, it makes use of polarization diversity offered by orthogonal resonant modes and antenna pattern diversity from two different patch shapes. The ring patch encompasses the square patch within its gap at the center to have an overall area of $0.236\lambda_0^2$. The elements are fed coaxially for resonance at a frequency of 2.45 GHz. These results are published in Paper no.1 in the list of publications.

Surface waves propagating within the dielectric increases coupling between closely spaced antenna elements for which fields are orientated in the same direction. In order to improve isolation in these areas, a ring-shaped DGS is etched between the square and the ring patch antenna. The arms of the ring

are of half wavelength at the operating frequency. Since the ring shape extends over both planes, isolation can be achieved along both E and H planes. An isolation improvement of 7 dB is obtained in simulation, and the MIMO antennas measure a minimum isolation of 25 dB between any pair of elements. The DGS effectively suppresses surface waves and reduces cross polar levels for the multiple radiation modes at 2.45 GHz. The study of ring DGS is published in Paper no.2 provided in the list of publications. Diverse radiation patterns of the square patch and the ring patch antenna ensures low correlation between the waveforms. The antenna measures a maximum envelope correlation coefficient of 0.3 between its elements which guarantees good diversity performance.

2. Multimode MIMO Antenna using Concentric Microstrip Square Ring Patches Loaded with CSRR

The multimode four port MIMO antenna uses two microstrip square ring patch antennas, one embedded within the other. The evolution of the antenna design and the radiation characteristics are discussed in section 3.3 of chapter 3. Coaxially fed four ports of the antenna excites fundamental and higher order orthogonal modes to resonate at 2.45 GHz. The overall dimension of the antenna is $60 \times 60 \times 1.6 \ mm^3$. The microstrip ring patch is a more compact antenna compared to the conventional $\lambda/2$ patch antenna. It also exhibits slightly improved bandwidth in comparison to a square patch antenna. To enhance the bandwidth of the higher order orthogonal modes of the outer ring antenna, half wavelength slits are added on each ring arms. The resonance of these slits merges with the ring antenna resonance which results in an enhancement of bandwidth. A bandwidth enhancement of 60% is achieved using slits on ring arms. Slit loading also improves isolation between higher order orthogonal ports of outer ring antenna at the resonant frequency.

Isolation studies reveal that isolation between orthogonal modes of patches is high ($> 20dB$). However, mutual coupling between inner and outer ring modes having fields oriented along the same direction are slightly higher. In order to improve isolation between aforesaid elements, sub-wavelength resonant structures called as complementary split ring resonator is etched on the ground plane between the two rings. CSRRs are placed on the high coupling

areas with a 45^0 tilt angle. Loading of CSRR alters the standing wave distribution, reversing the polarity of coupling waves. This improves isolation between highly coupled elements by 6.5 dB and measures a minimum isolation of 22 dB between any combination of elements. An ECC of 0.37 is measured between the diversity branches of the MIMO antenna. These findings are published in Paper no.3 in the list of publications.

3. Multimode MIMO Antenna using Microstrip Cross and Ring Patches with Interdigital Structure

A four port MIMO antenna using microstrip cross patch and square ring patch is designed and analyzed. The antenna is investigated in section 3.4 of chapter 3. Two fundamental orthogonal modes of the cross patch are excited, where as higher order orthogonal ports are excited for the outer ring antenna, which incorporates the cross patch within its ring gap at the center. The antenna resonates in 2.45 GHz ISM band with a bandwidth of 85 MHz. The cross patch antenna has low cross polarization levels when compared to that of square patch antenna. Bandwidth tuning is possible to some extend. An improvement of about 41.6 % is achieved by varying the length of the cross patch antenna. This reduces the coupling between its orthogonal radiation modes. The spacing between antenna elements is very less, about $0.03\lambda_0$. The overall area of the quad element antenna is $0.248\lambda_0^2$.

The narrow bandwidth of the higher order modes of the square ring antenna is enhanced by more than two times, by adding half wavelength slits along its arms. Isolation between highly coupled elements in the multiple antenna systems is enhanced by including an interdigital structure on the ground plane, between the cross and the ring patch. A strip of the interdigital structure is added on four arms of the antenna, which acts as a stop band filter along both the planes. The interdigital structure reduces coupling surface currents significantly, thereby improving isolation between all elements in the MIMO antenna. This ensures a high isolation of about 28 dB between any set of elements in the antenna system. Diverse antenna elements measure an ECC of 0.35 from far-field radiation patterns, which guarantees good MIMO diversity performance. These results are published in Paper no.4 provided in

the list of publications.

4. Compact Tri-Band MIMO antenna using Stub Loaded Meander Line Resonators with SRR Ring

A quad element compact tri-band MIMO antenna arranged using polarization diversity technique is discussed in section 4.2 of chapter 4. The multiple elements of the antenna resonate in three operating bands; first band from 1.95 GHz to 2.5 GHz, the second band from 3.15 GHz to 3.85 GHZ and third band ranging from 4.95 GHz to 6.6 GHz. All these bands are of great practical significance covering UMTS, LTE 2300, WLAN, WiMAX and ISM bands. Resonance is achieved using meander line resonators loaded with two quarter wave stubs. The design provides the flexibility to tune the elements for any desired resonant frequency. The overall size of the planar antenna is $40 \times 40 \times 1.6 \ mm^3$ which can be easily accommodated in a compact wireless terminal.

The isolation performances between the antenna elements are better than 20 dB for all bands except for the first resonant band. Coupling was observed to be slightly higher for diagonally placed meander line elements resonating in 2.4 GHz band. This is improved by including split ring resonators arranged in the form of a ring at the antenna center. SRRs are designed for the main antenna resonant frequency, and it creates a phase overturn acting as a stop band filter. This enhances isolation by 17dB at 2.4 GHz, the minimum isolation in three bands are 24 dB, 22 dB and 22.5 dB respectively. The antenna elements show good efficiency and gain characteristics in all the three bands. The MIMO diversity performances of the antenna are also verified from ECC values which are below 0.3 for all the bands. These results are published in Paper no.5 provided in the list of publications.

5. Compact Wideband MIMO antenna using Slotted Ground Plane

The evolution of a four port wideband MIMO antenna is investigated in section 4.3 of chapter 4. The wideband element consists of a quarter wavelength monopole resonator loaded with split ring resonator structure and a slotted

ground plane. The antenna bandwidth extends from 2.2 GHz to 6.28 GHz covering LTE, Bluetooth, WLAN, WiMAX and ISM bands which are of practical significance. Polarization diversity is used to arrange the four elements in a square substrate with 90^0 shift in orientation. The overall dimension of the multi-element antenna is $0.33\lambda_0 \times 0.33\lambda_0 \times 0.01\lambda_0$.

The monopole resonance is combined with the SRR resonance, which is electromagnetically coupled to the monopole antenna. The slotted ground plane under the monopole, is in the form of a ring, with a rectangular slot at the center. This improves the impedance matching of the antenna extending the bandwidth to form a wideband resonance. The ground ring also reduces the size of the monopole antenna, making the antenna compact. The wideband MIMO antenna exhibits a minimum isolation of 14 dB between its elements without using any isolation enhancement structures. The antenna shows a peak gain of 4 dBi and a peak efficiency of 91 % in its operating band. A fractional bandwidth of 96.2 % is achieved with ECC values less than 0.25 between its diversity branches. These findings are published in Paper no.6 in the list of publications.

6. MIMO Performance Analysis

The MIMO channel performance of the designed antennas are analyzed from the far-field radiation patterns using two-stage OTA method discussed in chapter 5. Correlation and Winner II channel models of Agilent SystemvUE software is used for this study. The far-field radiation patterns of the multiple elements of the MIMO antennas are loaded into the built-in models of the software for analyzing channel capacity, throughput and BLER performances. The results are obtained for varying SNR values to validate and compare the performances of the quad element antennas.

Multimode MIMO antenna using square and ring patches defined in section 3.2 show channel capacities of 34.9 bits/s/Hz and 23.5 bits/s/Hz using correlation based channel and Winner II channel models respectively for an SNR of 30 dB. Throughput fraction obtained shows values of 98.5 % and 48.5 % for correlation and Winner II channel models at an SNR of 5 dB. Quad element MIMO antenna using concentric square ring patches, discussed

in section 3.3, shows a channel capacity of 33.9 bits/s/Hz with correlation channel and 22.8 bits/s/Hz with Winner II channel models for 30 dB SNR. The throughput fraction obtained for an SNR of 5dB is 97 % and 44 % for correlation and Winner II channels. Channel capacity obtained for multi-mode MIMO antenna using microstrip cross and ring patches explained in section 3.4 are 32.4 bits/s/Hz and 24.4 bits/s/Hz for correlation and Winner II channel models respectively. The antenna shows a channel throughput fraction of 99 % and 45 % for correlation and Winner II channels.

Polarization diversity based compact quad element tri-band MIMO antenna investigated in section 4.2 shows a capacity of 40 bits/s/Hz for correlation channel and 26.1 bits/s/Hz for Winner channel at 2.4 GHz. Throughput fraction measurements at 2.4 GHz for an SNR of 5 dB using correlation and Winner II channel shows 98 % and 49 % respectively. Four port Wideband MIMO antenna using monopole with modified ground plane studied in section 4.3 achieves a channel capacity of 38.2 bits/s/Hz and 24.2 bits/s/Hz for correlation and Winner II channel at 30 dB SNR. Throughput studies at 2.4 GHz show a throughput fraction of 100% and 45 % using correlation and Winner channel for an SNR of 5 dB.

The channel studies of the proposed quad element MIMO antennas shows that there are differences in channel capacity and throughput obtained with the various antennas. Correlation channel model has better capacity and throughput when compared to Winner II channel model, as Winner II channel uses a more realistic channel for an urban environment. The polarization diversity based wideband and triband quad element MIMO antennas have better channel performance than multimode antennas. This can be attributed to the deterioration in efficiency of higher order modes of the multimode MIMO antennas. The channel performances are compared with omnidirectional MIMO array sources as references. It is observed that, despite the performance variations, all the developed multiple antenna designs support MIMO communication and outperform the SISO, 2 X 2 and 3 x 3 MIMO arrays.

6.3   Suggestions for Future Work

The future challenges for antenna engineers will be to design antenna geometries which can be accommodated in the upcoming wireless terminals. This is of great interest because of the tradeoffs that exist in the design requirements like compactness, bandwidth, high efficiency, high isolation and low correlation for the elements. In the emerging technologies like IEEE 802.11ac, up to 8 element MIMO is possible. This poses significant design constraints in terms of limited space and high diversity performance required for the terminals.

Active integrated MIMO antennas have been investigated recently as MIMO terminal antennas. These have proved highly advantageous in terms of antenna gain and MIMO performance. An active component like a power amplifier [261] which can enhance the gain by several times is highly beneficial for practical applications. Low noise amplifiers (LNA) have been proved to be very effective in receiver modes [262]. This technology can enhance the diversity performance and increase wireless throughput for future MIMO systems.

A detailed channel study will be highly advantageous to the design of MIMO antennas. This helps to design antennas which can prevail over the adverse effects of channel, improving the reliability and spectrum efficiency. Hence, considering particular channel, like urban or noisy environments, in the design stage will help to have more realistic antenna solutions. MIMO antennas in smart antenna arrays also have ample possibilities in future antenna market, leaving a heap of research opportunities.

MIMO antennas can be used in RFID technology to enhance the reliability of wireless communications. In RFID, near field measurements have to be examined thoroughly for best performance. This is a challenge for future antenna designers, as generally, MIMO antenna studies the far field characteristics of the multiple antenna elements.

Future wireless communication is expected to heavily depend on 5G standards for the wide bandwidth available. This requires antennas to be developed for millimeter wave frequencies and needs special attention for short distance communication due to the wide bandwidth. Millimeter wave communication provides new challenges for antenna design, as very high channel capacity is desired in such systems.

References

[1] T. Rappaport, R. Heath, R. Daniels, and J. Murdock, *Millimeter Wave Wireless Communications*, ser. Prentice Hall Communications Engineering and Emerging Technologies Series from Ted Rappaport. Pearson Education, 2014.

[2] A. F. Molisch, *Wireless communications.* John Wiley Sons, 2007.

[3] W. C. Jakes and D. C. Cox, Eds., *Microwave Mobile Communications.* Wiley-IEEE Press, 1994.

[4] Y. Okumura, E. Ohmori, T. Kawano, and K. Fukuda, "Field strength and its variability in vhf and uhf land-mobile radio service," *Rev. Elec. Commun. Lab*, vol. 16, no. 9, pp. 825–73, 1968.

[5] M. Hata and T. Nagatsu, "Mobile location using signal strength measurements in a cellular system," *IEEE Transactions on Vehicular Technology*, vol. 29, no. 2, pp. 245–252, 1980.

[6] V. Erceg, L. J. Greenstein, S. Y. Tjandra, S. R. Parkoff, A. Gupta, B. Kulic, A. A. Julius, and R. Bianchi, "An empirically based path loss model for wireless channels in suburban environments," *IEEE Journal on Selected Areas in Communications*, vol. 17, no. 7, pp. 1205–1211, 1999.

[7] P. F. Driessen and G. J. Foschini, "On the capacity formula for multiple input-multiple output wireless channels: A geometric interpretation," *IEEE Transactions on Communications*, vol. 47, no. 2, pp. 173–176, 1999.

[8] C. E. Shannon, "A mathematical theory of communication," *The Bell System Technical Journal*, vol. 27, no. July 1928, pp. 379–423, 1948.

[9] T. S. Rappaort, "Wireless communications: principles and practice," 2002.

[10] H. Bolcskei, "Multiple-input multiple-output (mimo) wireless systems," *The Communications Handbook*, pp. 90–1, 2002.

[11] A. Paulraj, R. Nabar, and D. Gore, *Introduction to space-time wireless communications.* Cambridge university press, 2003.

[12] J. H. Winters, "On the capacity of radio communication systems with diversity in a rayleigh fading environment," *IEEE Journal on Selected Areas in Communications*, vol. 5, no. 5, pp. 871–878, 1987.

[13] G. J. Foschini and M. J. Gans, "On limits of wireless communications in a fading environment when using multiple antennas," *Wireless personal communications*, vol. 6, no. 3, pp. 311–335, 1998.

[14] E. Telatar, "Capacity of multi-antenna gaussian channels," *European transactions on telecommunications*, vol. 10, no. 6, pp. 585–595, 1999.

[15] K. I. Pedersen, J. B. Andersen, J. P. Kermoal, and P. Mogensen, "A stochastic multiple-input-multiple-output radio channel model for evaluation of space-time coding algorithms," in *Vehicular Technology Conference, 2000. IEEE-VTS Fall VTC 2000. 52nd*, vol. 2.   IEEE, 2000, pp. 893–897.

[16] S. V. Hanly and D. N. Tse, "Multiaccess fading channels. ii. delay-limited capacities," *IEEE Transactions on Information Theory*, vol. 44, no. 7, pp. 2816–2831, 1998.

[17] G. Caire, G. Taricco, and E. Biglieri, "Optimum power control over fading channels," *IEEE Transactions on Information Theory*, vol. 45, no. 5, pp. 1468–1489, 1999.

[18] M. Stege, M. Bronze, and F. Fettweis, "Mimo-capacities for cost 259 scenarios," in *Broadband Communications, Access, Transmission, Networking. 2002 International Zurich Seminar on.*   IEEE, 2002, pp. 29–1.

[19] G. Caire and S. Shamai, "On the capacity of some channels with channel state information," *IEEE Transactions on Information Theory*, vol. 45, no. 6, pp. 2007–2019, 1999.

[20] A. J. Goldsmith and P. P. Varaiya, "Capacity of fading channels with channel side information," *IEEE Transactions on Information Theory*, vol. 43, no. 6, pp. 1986–1992, 1997.

[21] S. M. Alamouti, "A simple transmit diversity technique for wireless communications," *IEEE Journal on Selected Areas in Communications*, vol. 16, no. 8, pp. 1451–1458, 1998.

[22] M. Schwartz, W. R. Bennett, and S. Stein, *Communication systems and techniques.*   John Wiley & Sons, 1995.

[23] H. Jafarkhani, *Space-time coding: theory and practice.*   Cambridge university press, 2005.

[24] A. Wittneben, "Basestation modulation diversity for digital simulcast," in *Vehicular Technology Conference, 1991. Gateway to the Future Technology in Motion., 41st IEEE.*   IEEE, 1991, pp. 848–853.

[25] N. Seshadri, C.-E. W. Sundberg, and V. Weerackody, "Advanced techniques for modulation, error correction, channel equalization, and diversity," *AT&T technical journal*, vol. 72, no. 4, pp. 48–63, 1993.

[26] J. Proakis, *Digital Communications*, ser. Communications and signal processing.   McGraw-Hill, 1995.

[27] G. L. Stüber, *Principles of mobile communication.*   Springer Science & Business Media, 2011.

[28] J. W. Wallace and M. A. Jensen, "Mutual coupling in mimo wireless systems: A rigorous network theory analysis," *IEEE Transactions on Wireless Communications*, vol. 3, no. 4, pp. 1317–1325, 2004.

[29] D. Chizhik, F. Rashid-Farrokhi, J. Ling, and A. Lozano, "Effect of antenna separation on the capacity of blast in correlated channels," *IEEE Communications Letters*, vol. 4, no. 11, pp. 337–339, 2000.

[30] E.-H. Shin and S. Safavi-Naeini, "A simple theoretical model for polarization diversity reception in wireless mobile environments," in *IEEE Antennas and Propagation Society International Symposium, 1999*, vol. 2.   IEEE, 1999, pp. 1332–1335.

[31] R. U. Nabar, H. Bölcskei, V. Erceg, D. Gesbert, and A. J. Paulraj, "Performance of multiantenna signaling techniques in the presence of polarization diversity," *IEEE Transactions on Signal processing*, vol. 50, no. 10, pp. 2553–2562, 2002.

[32] S. Nordebo, M. Gustafsson, and G. Kristensson, "On the capacity of the free space antenna channel," in *IEEE Antennas and Propagation Society International Symposium 2006,*.   IEEE Press, 2006, pp. 3105–3108.

[33] A. Paulraj, D. Gesbert, and C. Papadias, "Encyclopedia for electrical engineering," 2000.

[34] T. M. CoVer and J. A. ThoMas, "Elements of information theory. new york: J," *Wiley and Sons*, vol. 5, p. 5, 1991.

[35] C.-N. Chuah, J. M. Kahn, and D. Tse, "Capacity of multi-antenna array systems in indoor wireless environment," in *IEEE Global Telecommunications Conference, 1998. GLOBECOM 1998. The Bridge to Global Integration.*, vol. 4.   IEEE, 1998, pp. 1894–1899.

[36] C.-N. Chuah, D. N. Tse, J. M. Kahn, and R. A. Valenzuela, "Capacity scaling in mimo wireless systems under correlated fading," *IEEE Transactions on Information Theory*, vol. 48, no. 3, pp. 637–650, 2002.

[37] C. A. Balanis and P. I. Ioannides, "Introduction to smart antennas," *Synthesis Lectures on Antennas*, vol. 2, no. 1, pp. 1–175, 2007.

[38] J. Butler, "Beam-forming matrix simplifies design of electronically scanned antennas," *Electron. Des.*, vol. 9, no. 8, pp. 170–173, 1961.

[39] Y. Lo and S. Lee, "Antenna handbook, ch. 15," 1988.

[40] P. H. Lehne and M. Pettersen, "An overview of smart antenna technology for mobile communications systems," *IEEE communications surveys*, vol. 2, no. 4, pp. 2–13, 1999.

[41] A. R. Lopez, "Performance predictions for cellular switched-beam intelligent antenna systems," *IEEE Communications Magazine*, vol. 34, no. 10, pp. 152–154, 1996.

[42] W. C. Lee, "Effects on correlation between two mobile radio base-station antennas," *IEEE Transactions on Communications*, vol. 21, no. 11, pp. 1214–1224, 1973.

[43] A. Aragon-Zavala, *Antennas and propagation for wireless communication systems*. John Wiley & Sons, 2008.

[44] Z. Zhao, S. Stapleton, and J. K. Cavers, "Analysis of polarization diversity scheme with channel codes," in *Vehicular Technology Conference, 1999. VTC 1999-Fall. IEEE VTS 50th*, vol. 3. IEEE, 1999, pp. 1377–1381.

[45] R. G. Vaughan, "Pattern translation and rotation in uncorrelated source distributions for multiple beam antenna design," *IEEE Transactions on Antennas and Propagation*, vol. 46, no. 7, pp. 982–990, 1998.

[46] P. L. Perini and C. L. Holloway, "Angle and space diversity comparisons in different mobile radio environments," *IEEE Transactions on Antennas and Propagation*, vol. 46, no. 6, pp. 764–775, 1998.

[47] J. L. Glaser and L. P. Faber Jr, "Evaluation of polarization diversity performance," *Proceedings of the IRE*, vol. 41, no. 12, pp. 1774–1778, 1953.

[48] P. C. Eggers, J. Toftgård, and A. M. Oprea, "Antenna systems for base station diversity in urban small and micro cells," *IEEE Journal on Selected Areas in Communications*, vol. 11, no. 7, pp. 1046–1057, 1993.

[49] E. Bruce, "Developments in short-wave directive antennas," *Bell System Technical Journal*, vol. 10, no. 4, pp. 656–683, 1931.

[50] E. Bruce and A. Beck, "Experiments with directivity steering for fading reduction," *Radio Engineers, Proceedings of the Institute of*, vol. 23, no. 4, pp. 357–371, 1935.

[51] H. Friis, C. Feldman, and W. Sharpless, "The determination of the direction of arrival of short radio waves," *Radio Engineers, Proceedings of the Institute of*, vol. 22, no. 1, pp. 47–78, 1934.

[52] H. T. Friis and C. B. Feldman, "A multiple unit steerable antenna for short-wave reception," *Radio Engineers, Proceedings of the Institute of*, vol. 25, no. 7, pp. 841–917, 1937.

[53] J. Vogelman, J. Ryerson, and M. Bickelhaupt, "Tropospheric scatter system using angle diversity," *Proceedings of the IRE*, vol. 47, no. 5, pp. 688–696, 1959.

[54] I. I.-a. Evaluation, "OVERVIEW OF IEEE P802 . 16m TECHNOLOGY AND CANDIDATE RIT FOR IMT-ADVANCED," *Control*, no. January, pp. 1–87, 2010.

[55] "Ieee standard for information technology– local and metropolitan area networks– specific requirements– part 11," *IEEE Std 802.11n-2009 (Amendment to IEEE Std 802.11-2007 as amended by IEEE Std 802.11k-2008, IEEE Std 802.11r-2008, IEEE Std 802.11y-2008, and IEEE Std 802.11w-2009)*, pp. 1–565, Oct 2009.

[56] E. U. T. R. Access, "Lte physical layer," *General Description, 3GPP TS*, vol. 36, p. v10, 2010.

[57] E. U. T. R. Access, "Further advancements for e-utra physical layer aspects," *3GPP TR 36.814, Tech. Rep.*, 2010.

[58] D. W. Browne, M. Manteghi, M. P. Fitz, and Y. Rahmat Samii, "Experiments with compact antenna arrays for mimo radio communications," *IEEE Transactions on Antennas and Propagation*, vol. 54, no. 11, pp. 3239–3250, 2006.

[59] M. Stoytchev, H. Safar, A. L. Moustakas, and S. Simon, "Compact antenna arrays for mimo applications," in *IEEE Antennas and Propagation Society International Symposium, 2001.*, vol. 3. IEEE, 2001, pp. 708–711.

[60] E. Eraslan, C.-Y. Wang, and B. Daneshrad, "Practical energy-aware link adaptation for mimo-ofdm systems," *IEEE Transactions on Wireless Communications*, vol. 13, no. 1, pp. 246–258, 2014.

[61] X. Ge, X. Huang, Y. Wang, M. Chen, Q. Li, T. Han, and C.-X. Wang, "Energy-efficiency optimization for mimo-ofdm mobile multimedia communication systems with qos constraints," *IEEE Transactions on Vehicular Technology*, vol. 63, no. 5, pp. 2127–2138, 2014.

[62] V. Erceg, L. Schumacher, P. Kyritsi *et al.*, "Ieee 802.11 document 03/940r4 tgn channel models,," *Garden Grove, California*, 2004.

[63] O. Bejarano, E. W. Knightly, and M. Park, "Ieee 802.11 ac: from channelization to multi-user mimo." *IEEE Communications Magazine*, vol. 51, no. 10, pp. 84–90, 2013.

[64] Q. Li, X. Lin, J. Zhang, and W. Roh, "Advancement of mimo technology in wimax: from ieee 802.16 d/e/j to 802.16 m," *IEEE Communications Magazine*, vol. 47, no. 6, pp. 100–107, 2009.

[65] E. Dahlman, S. Parkvall, J. Skold, and P. Beming, *3G evolution: HSPA and LTE for mobile broadband.* Academic press, 2010.

[66] C. Yu, B.-Z. Wang, and S.-q. Xiao, "Optimum design for compact diversity wire antenna with two highly isolated ports," *Electronics Letters*, vol. 38, no. 4, p. 1, 2002.

[67] S. Ko and R. Murch, "A planar diversity antenna for wireless handsets," in *IEEE Antennas and Propagation Society International Symposium, 2000.*, vol. 2. IEEE, 2000, pp. 968–971.

[68] "Ieee standard test procedures for antennas," *ANSI/IEEE Std 149-1979*, pp. 0–1, 1979.

[69] L. J. Chu, "Physical limitations of omni-directional antennas," *Journal of applied physics*, vol. 19, no. 12, pp. 1163–1175, 1948.

[70] R. F. Harrington, "Effect of antenna size on gain, bandwidth, and efficiency," *J. Res. Nat. Bur. Stand*, vol. 64, no. 1, pp. 1–12, 1960.

[71] M.-S. Han and J. Choi, "Multiband mimo antenna with a band stop filter for high isolation characteristics," in *Antennas and Propagation Society International Symposium, 2009. APSURSI'09. IEEE.* IEEE, 2009, pp. 1–4.

[72] J. Xiong, M. Zhao, H. Li, Z. Ying, and B. Wang, "Collocated electric and magnetic dipoles with extremely low correlation as a reference antenna for polarization diversity mimo applications," *IEEE Antennas and Wireless Propagation Letters*, vol. 11, pp. 423–426, 2012.

[73] H. Li, J. Xiong, Z. Ying, and S. He, "Compact and low profile colocated mimo antenna structure with polarisation diversity and high port isolation," *Electronics letters*, vol. 46, no. 2, pp. 108–110, 2010.

[74] R. Hwang, "A broadband cpw-fed t-shaped antenna for wireless communications," in *Microwaves, Antennas and Propagation, IEE Proceedings*, vol. 151, no. 6. IET, 2004, pp. 537–543.

[75] J.-M. Laheurte, L. P. Katehi, and G. M. Rebeiz, "Cpw-fed slot antennas on multilayer dielectric substrates," *IEEE Transactions on Antennas and Propagation*, vol. 44, no. 8, pp. 1102–1111, 1996.

[76] K. Tilley, X.-D. Wu, and K. Chang, "Coplanar waveguide fed coplanar strip dipole antenna," *Electronics Letters*, vol. 30, no. 3, pp. 176–177, 1994.

[77] Y. Chen, Y. Jiao, F. Zhang, and H. Gao, "A novel small cpw-fed t-shaped antenna for mimo system applications," *Journal of Electromagnetic Waves and Applications*, vol. 20, no. 14, pp. 2027–2036, 2006.

[78] M. Darvish and H. R. Hassani, "Quad band cpw-fed monopole antenna for mimo applications," in *6th European Conference on Antennas and Propagation (EUCAP)*, March 2012, pp. 1–4.

[79] R. S. Fakhr, A. A. Lotfi-Neyestanak, and M. Naser-Moghadasi, "Compact size and dual band semicircle shaped antenna for mimo aplications," *Progress In Electromagnetics Research C*, vol. 11, pp. 147–154, 2009.

[80] M. Han and J. Choi, "Mimo antenna using a decoupling network for 4g usb dongle application," *Microwave and Optical Technology Letters*, vol. 52, no. 11, pp. 2551–2554, 2010.

[81] V. Ssorin, A. Artemenko, A. Sevastyanov, and R. Maslennikov, "Compact bandwidth-optimized two element mimo antenna system for 2.5–2.7 ghz band," in *Proceedings of the 5th European Conference on Antennas and Propagation (EUCAP)*. IEEE, 2011, pp. 319–323.

[82] Y. Sung, M. Kim, and Y.-S. Kim, "Harmonics reduction with defected ground structure for a microstrip patch antenna," *IEEE antennas and wireless propagation letters*, vol. 2, pp. 111–113, 2003.

[83] D. Guha, M. Biswas, and Y. M. Antar, "Microstrip patch antenna with defected ground structure for cross polarization suppression," *IEEE Antennas and Wireless Propagation Letters*, vol. 4, no. 1, pp. 455–458, 2005.

[84] R. Carothers, C. Breslin, J. Denomy, and M. Foad, "Promoting occupational safety and health for working children through microfinance programming," *International journal of occupational and environmental health*, vol. 16, no. 2, pp. 164–174, 2010.

[85] Y. Chung, S.-S. Jeon, D. Ahn, J.-I. Choi, and T. Itoh, "High isolation dual-polarized patch antenna using integrated defected ground structure," *Microwave and Wireless Components Letters, IEEE*, vol. 14, no. 1, pp. 4–6, 2004.

[86] H. Li, J. Xiong, and S. He, "A compact planar mimo antenna system of four elements with similar radiation characteristics and isolation structure," *IEEE Antennas and Wireless Propagation Letters*, vol. 8, pp. 1107–1110, 2009.

[87] H. Li, J. Xiong, Z. Ying, and S. He, "High isolation compact four-port mimo antenna systems with built-in filters as isolation structure," in *Proceedings of the Fourth European Conference on Antennas and Propagation (EuCAP)*. IEEE, 2010, pp. 1–4.

[88] C.-Y. Chiu, C.-H. Cheng, R. D. Murch, and C. R. Rowell, "Reduction of mutual coupling between closely-packed antenna elements," *IEEE Transactions on Antennas and Propagation*, vol. 55, no. 6, pp. 1732–1738, 2007.

[89] S. Y. Huang and Y. H. Lee, "A compact e-shaped patterned ground structure and its applications to tunable bandstop resonator," *IEEE Transactions on Microwave Theory and Techniques*, vol. 57, no. 3, pp. 657–666, 2009.

[90] T. Kokkinos, E. Liakou, and A. P. Feresidis, "Decoupling antenna elements of pifa arrays on handheld devices," *Electronics Letters*, vol. 44, no. 25, pp. 1442–1444, 2008.

[91] F. Zhu, J. Xu, and Q. Xu, "Reduction of mutual coupling between closely-packed antenna elements using defected ground structure," in *Microwave, Antenna, Propagation and EMC Technologies for Wireless Communications, 2009 3rd IEEE International Symposium on*. IEEE, 2009, pp. 1–4.

[92] H.-T. Chou, H.-C. Cheng, H.-T. Hsu, and L.-R. Kuo, "Investigations of isolation improvement techniques for multiple input multiple output (mimo) wlan portable terminal applications," *Progress In Electromagnetics Research*, vol. 85, pp. 349–366, 2008.

[93] D. Ahn, J.-S. Park, C.-S. Kim, J. Kim, Y. Qian, and T. Itoh, "A design of the low-pass filter using the novel microstrip defected ground

structure," *IEEE Transactions on Microwave Theory and Techniques*, vol. 49, no. 1, pp. 86–93, 2001.

[94] C.-S. Kim, J.-S. Lim, S. Nam, K.-Y. Kang, and D. Ahn, "Equivalent circuit modelling of spiral defected ground structure for microstrip line," *Electronics Letters*, vol. 38, no. 19, p. 1, 2002.

[95] J. Ouyang, F. Yang, and Z. Wang, "Reducing mutual coupling of closely spaced microstrip mimo antennas for wlan application," *IEEE Antennas and Wireless Propagation Letters*, vol. 10, pp. 310–313, 2011.

[96] M. S. Sharawi, A. B. Numan, and D. N. Aloi, "Isolation improvement in a dual-band dual-element mimo antenna system using capacitively loaded loops," *Progress In Electromagnetics Research*, vol. 134, pp. 247–266, 2013.

[97] Y. Lee, H. Chung, J. Ha, and J. Choi, "Design of a mimo antenna with improved isolation using meta-material," in *Antenna Technology (iWAT), 2011 International Workshop on.* IEEE, 2011, pp. 231–234.

[98] J. Itoh, N. Michishita, and H. Morishita, "A study on mutual coupling reduction between two inverted-f antennas using mushroom-type ebg structures," in *Antennas and Propagation Society International Symposium, 2008. AP-S 2008. IEEE.* IEEE, 2008, pp. 1–4.

[99] L. Inclan-Sanchez, J.-L. Vazquez-Roy, and E. Rajo-Iglesias, "High isolation proximity coupled multilayer patch antenna for dual-frequency operation," *IEEE Transactions on Antennas and Propagation*, vol. 56, no. 4, pp. 1180–1183, 2008.

[100] F. Yang and Y. Rahmat-Samii, "Microstrip antennas integrated with electromagnetic band-gap (ebg) structures: A low mutual coupling design for array applications," *IEEE Transactions on Antennas and Propagation*, vol. 51, no. 10, pp. 2936–2946, 2003.

[101] E. Rajo-Iglesias, O. Quevedo-Teruel, and L. Inclan-Sanchez, "Mutual coupling reduction in patch antenna arrays by using a planar ebg structure and a multilayer dielectric substrate," *IEEE Transactions on Antennas and Propagation*, vol. 56, no. 6, pp. 1648–1655, 2008.

[102] Z. D. Liu, P. S. Hall, and D. Wake, "Dual-frequency planar inverted-f antenna," *IEEE Transactions on Antennas and Propagation*, vol. 45, no. 10, pp. 1451–1458, 1997.

[103] Y. Gao, C. Chiau, X. Chen, and C. Parini, "Modified pifa and its array for mimo terminals," in *Microwaves, Antennas and Propagation, IEE Proceedings*, vol. 152, no. 4. IET, 2005, pp. 255–259.

[104] Y. Gao, X. Chen, Z. Ying, and C. Parini, "Design and performance investigation of a dual-element pifa array at 2.5 ghz for mimo terminal," *IEEE Transactions on Antennas and Propagation*, vol. 55, no. 12, pp. 3433–3441, 2007.

[105] H. Li, J. Xiong, and S. He, "Extremely compact dual-band pifas for mimo application," *Electronics letters*, vol. 45, no. 17, pp. 869–870, 2009.

[106] S. Dossche, S. Blanch, and J. Romeu, "Optimum antenna matching to minimise signal correlation on a two-port antenna diversity system," *Electronics Letters*, vol. 40, no. 19, p. 1, 2004.

[107] S. Dossche, S. Blanch, and J. Romeu, "Decorrelation of a closely spaced four element antenna array," in *Antennas and Propagation Society International Symposium, 2005 IEEE*, vol. 1. IEEE, 2005, pp. 803–806.

[108] J. Coetzee and Y. Yu, "Closed-form design equations for decoupling networks of small arrays," *Electronics Letters*, vol. 44, no. 25, pp. 1441–1442, 2008.

[109] S.-C. Chen, Y.-S. Wang, and S.-J. Chung, "A decoupling technique for increasing the port isolation between two strongly coupled antennas," *IEEE Transactions on Antennas and Propagation*, vol. 56, no. 12, pp. 3650–3658, 2008.

[110] J. Weber, C. Volmer, K. Blau, R. Stephan, and M. A. Hein, "Miniaturized antenna arrays using decoupling networks with realistic elements," *IEEE Transactions on Microwave Theory and Techniques*, vol. 54, no. 6, pp. 2733–2740, 2006.

[111] J. C. Coetzee and Y. Yu, "Port decoupling for small arrays by means of an eigenmode feed network," *IEEE Transactions on Antennas and Propagation*, vol. 56, no. 6, pp. 1587–1593, 2008.

[112] T.-I. Lee and Y. E. Wang, "Mode-based information channels in closely coupled dipole pairs," *IEEE Transactions on Antennas and Propagation*, vol. 56, no. 12, pp. 3804–3811, 2008.

[113] X. Q. Lin, H. Li, S. He, and Y. Fan, "A decoupling technique for increasing the port isolation between two closely packed antennas," in *Antennas and Propagation Society International Symposium (APSURSI), 2012 IEEE*.   IEEE, 2012, pp. 1–2.

[114] C. Volmer, J. Weber, R. Stephan, K. Blau, and M. A. Hein, "An eigenanalysis of compact antenna arrays and its application to port decoupling," *IEEE Transactions on Antennas and Propagation*, vol. 56, no. 2, pp. 360–370, 2008.

[115] A. Diallo, C. Luxey, P. Le Thuc, R. Staraj, and G. Kossiavas, "Enhanced two-antenna structures for universal mobile telecommunications system diversity terminals," *Microwaves, Antennas & Propagation, IET*, vol. 2, no. 1, pp. 93–101, 2008.

[116] A. Diallo, C. Luxey, P. Le Thuc, R. Staraj, and G. Kossiavas, "Study and reduction of the mutual coupling between two mobile phone pifas operating in the dcs1800 and umts bands," *IEEE Transactions on Antennas and Propagation*, vol. 54, no. 11, pp. 3063–3074, 2006.

[117] A. Chebihi, C. Luxey, A. Diallo, P. L. Thuc, and R. Staraj, "A novel isolation technique for closely spaced pifas for umts mobile phones," *IEEE Antennas and Wireless Propagation Letters*, vol. 7, pp. 665–668, 2008.

[118] B. Lau, *MIMO: From Theory to Implementation (Alain Sibille, and Claude Oestges, and Alberto Zanella).* Elsevier, 2011.

[119] S. Park and C. Jung, "Compact mimo antenna with high isolation performance," *Electronics letters*, vol. 46, no. 6, p. 1, 2010.

[120] B. K. Lau and J. B. Andersen, "Antenna system and method for operating an antenna system," Nov. 15 2011, uS Patent 8,059,058.

[121] B. K. Lau and J. B. Andersen, "Unleashing multiple antenna systems in compact terminal devices," pp. 1–4, 2009.

[122] K.-S. Min, D.-J. Kim, and Y.-M. Moon, "Improved mimo antenna by mutual coupling suppression between elements," in *The European Conference on Wireless Technology, 2005.*, 2005.

[123] A. C. Mak, C. R. Rowell, and R. D. Murch, "Isolation enhancement between two closely packed antennas," *IEEE Transactions on Antennas and Propagation*, vol. 56, no. 11, pp. 3411–3419, 2008.

[124] L. Minz and R. Garg, "Reduction of mutual coupling between closely spaced pifas," *Electronics letters*, vol. 46, no. 6, pp. 392–394, 2010.

[125] K. Q. Da Costa, V. Dmitriev, D. Nascimento, and J. C. S. Lacava, "Broadband l-probe fed patch antenna combined with passive loop elements," *IEEE Antennas and Wireless Propagation Letters*, vol. 6, pp. 100–102, 2007.

[126] S. Lim and H. Ling, "Design of electrically small, pattern reconfigurable yagi antenna," *Electronics Letters*, vol. 43, no. 24, p. 1, 2007.

[127] R. H. Clarke, "A statistical theory of mobile-radio reception," *Bell System Technical Journal*, vol. 47, no. 6, pp. 957–1000, 1968.

[128] J. R. Costa, E. B. Lima, C. R. Medeiros, and C. A. Fernandes, "Evaluation of a new wideband slot array for mimo performance enhancement in indoor wlans," *IEEE Transactions on Antennas and Propagation*, vol. 59, no. 4, pp. 1200–1206, 2011.

[129] S. Blanch, J. Romeu, and I. Corbella, "Exact representation of antenna system diversity performance from input parameter description," *Electronics letters*, vol. 39, no. 9, pp. 705–707, 2003.

[130] P. Hallbjörner, "The significance of radiation efficiencies when using s-parameters to calculate the received signal correlation from two antennas," *IEEE Antennas and Wireless Propagation Letters*, vol. 4, pp. 97–99, 2005.

[131] C. Di Nallo, "Estimation of multiple antennas correlation from s-parameters and efficiency measurements," in *COST*, vol. 273, pp. 19–21.

[132] R. G. Vaughan, "Signals in mobile communications: A review," *IEEE Transactions on Vehicular Technology*, vol. 35, no. 4, pp. 133–145, 1986.

[133] R. G. Vaughan and J. B. Andersen, "Antenna diversity in mobile communications," *IEEE Transactions on Vehicular Technology*, vol. 36, no. 4, pp. 149–172, 1987.

[134] M. A. Jensen and B. K. Lau, "Uncoupled matching for active and passive impedances of coupled arrays in mimo systems," *IEEE Transactions on Antennas and Propagation*, vol. 58, no. 10, pp. 3336–3343, 2010.

[135] B. K. Lau and J. B. Andersen, "Simple and efficient decoupling of compact arrays with parasitic scatterers," *IEEE Transactions on Antennas and Propagation*, vol. 60, no. 2, pp. 464–472, 2012.

[136] S. Zhang, A. A. Glazunov, Z. Ying, and S. He, "Reduction of the envelope correlation coefficient with improved total efficiency for mobile lte mimo antenna arrays: mutual scattering mode," *IEEE transactions on antennas and propagation*, vol. 61, no. 6, pp. 3280–3291, 2013.

[137] R. Vaughan and J. B. Andersen, *Channels, propagation and antennas for mobile communications*. Iet, 2003, vol. 50.

[138] V. Plicanic, *Characterization and Enhancement of Antenna System Performance in Compact MIMO Terminals*. Lund University, 2011.

[139] V. Plicanic, B. K. Lau, A. Derneryd, and Z. Ying, "Actual diversity performance of a multiband diversity antenna with hand and head effects," *IEEE Transactions on Antennas and Propagation*, vol. 57, no. 5, pp. 1547–1556, 2009.

[140] P.-S. Kildal, K. Rosengren, J. Byun, and J. Lee, "Definition of effective diversity gain and how to measure it in a reverberation chamber," *Microwave and Optical Technology Letters*, vol. 34, no. 1, pp. 56–59, 2002.

[141] K. Rosengren and P.-S. Kildal, "Radiation efficiency, correlation, diversity gain and capacity of a six-monopole antenna array for a mimo system: theory, simulation and measurement in reverberation chamber," in *IEE Proceedings Microwaves, Antennas and Propagation*, vol. 152, no. 1. IET, 2005, pp. 7–16.

[142] T. Taga, "Analysis for mean effective gain of mobile antennas in land mobile radio environments," *IEEE Transactions on Vehicular Technology*, vol. 39, no. 2, pp. 117–131, 1990.

[143] G. F. Pedersen and J. B. Andersen, "Handset antennas for mobile communications: integration, diversity and performance," *Review of Radio Science*, vol. 1999, pp. 119–138, 1996.

[144] M. B. Knudsen, *Antenna systems for handsets*. Department of Control Engineering, Aalborg University, 2001.

[145] R. Tian, B. K. Lau, and Z. Ying, "Multiplexing efficiency of mimo antennas," *IEEE Antennas and Wireless Propagation Letters*, vol. 10, pp. 183–186, 2011.

[146] R. Tian, B. K. Lau, and Z. Ying, "Multiplexing efficiency of mimo antennas in arbitrary propagation scenarios," *6th European Conference on Antennas and Propagation (EUCAP)*, pp. 373–377, 2012.

[147] "European Co-operation in the field of Scientific and Technical Research," http://www.cost2100.org, online; accessed on 21 March 2017.

[148] "Cellular Telecommunications Industry Association," http://www.ctia.org, online; accessed on 21 March 2017.

[149] "The 3rd Generation Partnership Project," http://www.3gpp.org, online; accessed on 21 March 2017.

[150] 3GPP, "Measurements of radiated performance for mimo and multi-antenna reception for hspa and lte terminals," in *Tech. Rep.*, vol. v11.0.0, 2012.

[151] P. S. Kildal, X. Chen, C. Orlenius, M. Franzen, and C. S. L. Patane, "Characterization of reverberation chambers for ota measurements of wireless devices: Physical formulations of channel matrix and new uncertainty formula," *IEEE Transactions on Antennas and Propagation*, vol. 60, no. 8, pp. 3875–3891, Aug 2012.

[152] Y. Jing, Z. Wen, H. Kong, S. Duffy, and M. Rumney, "Two-stage over the air (ota) test method for mimo device performance evaluation," in *2011 IEEE International Symposium on Antennas and Propagation (APSURSI)*, July 2011, pp. 71–74.

[153] E. Eda, "Cst Studio Suite 2015 : System Assembly and Modeling," 2015.

[154] G.-Y. Chen, K.-L. Wu, Y. Chen, and J.-S. Sun, "Small antenna chamber design and measurement," *Session 3P7*, p. 645.

[155] C. A. Balanis, *Antenna theory: analysis and design.* John Wiley & Sons, 2016.

[156] J. D. Kraus, "Antennas mcgraw-hill," *New York*, p. 166, 1950.

[157] *ANSI/IEEE Std 149-1979: IEEE Standard Test Procedures for Antennas.* IEEE, 1979. [Online]. Available: https://books.google.com/books?id=-gFhAQAACAAJ

[158] H. A. Wheeler, "The radiansphere around," 1959.

[159] R. Johnston, L. Ager, and J. McRory, "A new small antenna efficiency measurement method," in *Antennas and Propagation Society International Symposium, 1996. AP-S. Digest*, vol. 1. IEEE, 1996, pp. 176–179.

[160] D. Agahi and W. Domino, "Efficiency measurements of portable-handset antennas using the wheeler cap," *Applied Microwave and Wireless*, vol. 12, no. 6, pp. 34–43, 2000.

[161] S. Soltani and R. D. Murch, "A compact planar printed mimo antenna design," *IEEE Transactions on Antennas and Propagation*, vol. 63, no. 3, pp. 1140–1149, 2015.

[162] M. L. Pablo-González, M. Sánchez-Fernández, and E. Rajo-Iglesias, "Combination of the three types of diversity to design high-capacity compact mimo terminals," *IEEE Antennas and Wireless Propagation Letters*, vol. 13, pp. 1309–1312, 2014.

[163] H. Raza, A. Hussain, J. Yang, and P. S. Kildal, "Wideband compact 4-port dual polarized self-grounded bowtie antenna," *IEEE Transactions on Antennas and Propagation*, vol. 62, no. 9, pp. 4468–4473, Sept 2014.

[164] A. Moradikordalivand, T. A. Rahman, and M. Khalily, "Common elements wideband mimo antenna system for wifi/lte access-point applications," *IEEE Antennas and Wireless Propagation Letters*, vol. 13, pp. 1601–1604, 2014.

[165] R. Anitha, V. P. Sarin, P. Mohanan, and K. Vasudevan, "Enhanced isolation with defected ground structure in mimo antenna," *Electronics Letters*, vol. 50, no. 24, pp. 1784–1786, 2014.

[166] L. Zhao and K.-L. Wu, "A decoupling technique for four-element symmetric arrays with reactively loaded dummy elements," *IEEE Transactions on Antennas and Propagation*, vol. 62, no. 8, pp. 4416–4421, Aug 2014.

[167] C. Y. Chiu and R. D. Murch, "Compact four-port antenna suitable for portable MIMO devices," *IEEE Antennas and Wireless Propagation Letters*, vol. 7, pp. 142–144, 2008.

[168] A. Forenza, F. Sun, and R. W. Heath, "Pattern diversity with multi-mode circular patch antennas in clustered MIMO channels," *IEEE Antennas and Propagation Society, AP-S International Symposium (Digest)*, vol. 3 B, pp. 438–441, 2005.

[169] D. Piazza, P. Mookiah, M. D'Amico, and K. R. Dandekar, "Experimental analysis of pattern and polarization reconfigurable circular patch antennas for MIMO systems," *IEEE Transactions on Vehicular Technology*, vol. 59, no. 5, pp. 2352–2362, 2010.

[170] C. Redondo and L. de Haro, "On the analysis and design of reconfigurable multimode mimo microstrip antennas," *IEEE Transactions on Antennas and Propagation*, vol. 62, no. 1, pp. 119–129, 2014.

[171] F. Demmerle and W. Wiesbeck, "A biconical multibeam antenna for space-division multiple access," *IEEE Transactions on antennas and propagation*, vol. 46, no. 6, pp. 782–787, 1998.

[172] C. Waldschmidt and W. Wiesbeck, "Compact wide-band multimode antennas for mimo and diversity," *IEEE Transactions on Antennas and Propagation*, vol. 52, no. 8, pp. 1963–1969, 2004.

[173] E. Antonino-Daviu, M. Cabedo-Fabrés, M. Ferrando-Bataller, and M. Gallo, "Design of a multimode mimo antenna using the theory of characteristic modes," *Radioengineering*, vol. 18, no. 4 Part 1, pp. 425–430.

[174] R. Vaughan and J. B. Andersen, "A multiport patch antenna for mobile communications," in *Microwave Conference, 1984. 14th European*. IEEE, 1984, pp. 607–612.

[175] E. Rajo-Iglesias, O. Quevedo-Teruel, and M. Sánchez-Fernández, "Compact multimode patch antennas for mimo applications," *IEEE Antennas and Propagation Magazine*, vol. 50, no. 2, pp. 197–205, 2008.

[176] J. Sarrazin, Y. Mahe, S. Avrillon, and S. Toutain, "A new multimode antenna for MIMO systems using a mode frequency convergence concept," *IEEE Transactions on Antennas and Propagation*, vol. 59, no. 12, pp. 4481–4489, 2011.

[177] T. Svantesson, "Correlation and channel capacity of mimo systems employing multimode antennas," *IEEE Transactions on Vehicular Technology*, vol. 51, no. 6, pp. 1304–1312, 2002.

[178] R. G. Vaughan, "Two-port higher mode circular microstrip antennas," *IEEE Transactions on Antennas and Propagation*, vol. 36, no. 3, pp. 309–321, 1988.

[179] X. J. H. S. Li, Hui, "A Compact Planar MIMO Antenna System of Four Elements With Similar Radiation Characteristics and Isolation Structure," vol. 8, pp. 1107–1110, 2009.

[180] H. Li, J. Xiong, Z. Ying, and S. He, "Compact and low profile co-located MIMO antenna structure with polarisation diversity and high port isolation," *Electronics Letters*, vol. 46, no. 2, p. 108, 2010.

[181] J. Malik, A. Patnaik, and M. Kartikeyan, "Novel printed mimo antenna with pattern and polarization diversity," *IEEE antennas and wireless propagation letters*, vol. 14, pp. 739–742, 2015.

[182] H. T. Chattha, Y. Huang, S. Member, and S. J. Boyes, "Polarization and Pattern Diversity-Based Dual-Feed Planar Inverted-F Antenna," vol. 60, no. 3, pp. 1532–1539, 2012.

[183] L. Sun, W. Huang, B. Sun, Q. Sun, and J. Fan, "Two-Port Pattern Diversity Antenna for 3G and 4G MIMO Indoor Applications," vol. 13, pp. 1573–1576, 2014.

[184] C.-Y. Chiu, J.-B. Yan, and R. D. Murch, "Compact three-port orthogonally polarized mimo antennas," *IEEE Antennas and Wireless Propagation Letters*, vol. 6, pp. 619–622, 2007.

[185] A. S. Konanur, K. Gosalia, S. H. Krishnamurthy, B. Hughes, and G. Lazzi, "Increasing wireless channel capacity through mimo systems employing co-located antennas," *IEEE Transactions on Microwave Theory and Techniques*, vol. 53, no. 6, pp. 1837–1844, 2005.

[186] A. Mukherjee and H. M. Kwon, "Compact multi-user wideband MIMO system using multiple-mode microstrip antennas," *IEEE Vehicular Technology Conference*, no. May, pp. 584–588, 2007.

[187] R. Anitha, P. V. Vinesh, S. Mathew, P. Mohanan, and K. Vasudevan, "Collocated mimo antenna with reduced mutual coupling using square ring dgs," *Progress In Electromagnetics Research C*, vol. 53, pp. 119–125, 2014.

[188] R. Garg, *Microstrip antenna design handbook.*   Artech house, 2001.

[189] J.-S. Row, S.-H. Yeh, and K.-L. Wong, "Compact dual-polarized microstrip antennas," *Microwave and Optical Technology Letters*, vol. 27, no. 4, pp. 284–287, 2000.

[190] R. Waterhouse, *Microstrip patch antennas: a designers guide.* Springer Science & Business Media, 2013.

[191] R. Anitha, V. Sarin, P. Mohanan, and K. Vasudevan, "Enhanced isolation with defected ground structure in mimo antenna," *Electronics Letters*, vol. 50, no. 24, pp. 1784–1786, 2014.

[192] B. Rembold, "Relation between diagram correlation factors and s-parameters of multiport antenna with arbitrary feeding network," *Electronics letters*, vol. 44, no. 1, pp. 5–7, 2008.

[193] R. Marqués, F. Martín, and M. Sorolla, *Metamaterials with negative parameters: theory, design and microwave applications.*   John Wiley & Sons, 2011, vol. 183.

[194] D. M. Pozar, *Microwave Engineering 3e.*   Wiley India Pvt. Limited, 2009.

[195] P. Haddad and D. Pozar, "Anomalous mutual coupling between microstrip antennas," *IEEE Transactions on Antennas and Propagation*, vol. 42, no. 11, pp. 1545–1549, 1994.

[196] W.-J. Liao, C.-Y. Hsieh, B.-Y. Dai, and B.-R. Hsiao, "Inverted-F / Slot Integrated Dual-Band Four-Antenna," *IEEE Antennas and Wireless Propagation Letters*, vol. 14, pp. 847–850, 2015.

[197] M. Sonkki, D. Pfeil, V. Hovinen, K. R. Dandekar, and S. Member, "Wideband Planar Four-Element Linear Antenna Array," vol. 13, pp. 1663–1666, 2014.

[198] A. Moradikordalivand, T. A. Rahman, and M. Khalily, "Common Elements Wideband MIMO Antenna System for WiFi / LTE Access-Point Applications," vol. 13, pp. 1601–1604, 2014.

[199] H. Wang, L. Liu, Z. Zhang, Y. Li, and Z. Feng, "A Wideband Compact WLAN / WiMAX MIMO Antenna Based on Dipole With V-shaped Ground Branch," vol. 63, no. 5, pp. 2290–2295, 2015.

[200] K. Payandehjoo and R. Abhari, "Compact multi-band pifas on a semi-populated mobile handset with tunable isolation," *IEEE Transactions on Antennas and Propagation*, vol. 61, no. 9, pp. 4814–4819, 2013.

[201] A. Foudazi, H. R. Hassani, and S. A. Nezhad, "Small uwb planar monopole antenna with added gps/gsm/wlan bands," *IEEE Transactions on Antennas and Propagation*, vol. 60, no. 6, pp. 2987–2992, 2012.

[202] K. Haneda, A. Diallo, P. L. Thuc, C. Luxey, S. Member, R. Staraj, and P. Vainikainen, "Dual-Band WLAN Multiantenna System and Diversity / MIMO Performance Evaluation," vol. 62, no. 3, pp. 1409–1415, 2014.

[203] R. Addaci, A. Diallo, C. Luxey, P. Le Thuc, and R. Staraj, "Dual-band WLAN diversity antenna system with high port-to-port isolation," *IEEE Antennas and Wireless Propagation Letters*, vol. 11, pp. 244–247, 2012.

[204] R. Karimian, H. Oraizi, S. Fakhte, and M. Farahani, "Novel F-shaped quad-band printed slot antenna for WLAN and WiMAX MIMO systems," *IEEE Antennas and Wireless Propagation Letters*, vol. 12, pp. 405–408, 2013.

[205] J.-S. Row and Y. H. Chen, "Wideband Planar Array With Broad Beamwidth and Low Cross Polarization," vol. 63, no. 9, pp. 4161–4165, 2015.

[206] S. S. Aljarafreh, Y. Huang, L. Xing, Q. Xu, and X. Zhu, "A Low-Profile and Wideband PILA-Based Antenna for Handset Diversity Applications," *IEEE Antennas and Wireless Propagation Letters*, vol. 14, pp. 923–926, 2015.

[207] H. Raza, A. Hussain, J. Yang, and P.-S. Kildal, "Wideband Compact 4-Port Dual Polarized Self-Grounded Bowtie Antenna," vol. 62, no. 9, pp. 4468–4473, 2014.

[208] L. Liu, Z. Feng, H. Wang, and Z. Zhang, "Wideband tri-port MIMO antenna with compact size and directional radiation pattern," *Electronics Letters*, vol. 50, no. 18, pp. 1261–1262, 2014.

[209] Y. Luo, Q. X. Chu, J. F. Li, and Y. T. Wu, "A planar H-shaped directive antenna and its application in compact MIMO antenna," *IEEE Transactions on Antennas and Propagation*, vol. 61, no. 9, pp. 4810–4814, 2013.

[210] S. Maci, G. Biffi Gentili, P. Piazzesi, and C. Salvador, "Dual-band slot-loaded patch antenna," in *Microwaves, Antennas and Propagation, IEE Proceedings*, vol. 142, no. 3. IET, 1995, pp. 225–232.

[211] G. F. Khodae, J. Nourinia, and C. Ghobadi, "A practical miniaturized u-slot patch antenna with enhanced bandwidth," *Progress In Electromagnetics Research B*, vol. 3, pp. 47–62, 2008.

[212] S. Weigand, G. H. Huff, K. H. Pan, and J. T. Bernhard, "Analysis and design of broad-band single-layer rectangular u-slot microstrip patch

antennas," *IEEE Transactions on Antennas and Propagation*, vol. 51, no. 3, pp. 457–468, 2003.

[213] K.-F. Tong, K.-M. Luk, K.-F. Lee, and R. Q. Lee, "A broad-band u-slot rectangular patch antenna on a microwave substrate," *IEEE Transactions on Antennas and Propagation*, vol. 48, no. 6, pp. 954–960, 2000.

[214] B.-K. Ang and B.-K. Chung, "A wideband e-shaped microstrip patch antenna for 5-6 ghz wireless communications," *Progress In Electromagnetics Research*, vol. 75, pp. 397–407, 2007.

[215] T. J. Warnagiris and T. J. Minardo, "Performance of a meandered line as an electrically small transmitting antenna," *IEEE Transactions on Antennas and Propagation*, vol. 46, no. 12, pp. 1797–1801, 1998.

[216] N. Chang and J.-H. Jiang, "Meandered t-shaped monopole antenna," *IEEE Transactions on Antennas and Propagation*, vol. 57, no. 12, pp. 3976–3978, 2009.

[217] G. Augustin, P. Bybi, V. Sarin, P. Mohanan, C. Aanandan, and K. Vasudevan, "A compact dual-band planar antenna for dcs-1900/pcs/phs, wcdma/imt-2000, and wlan applications," *IEEE Antennas and Wireless Propagation Letters*, vol. 7, pp. 108–111, 2008.

[218] W.-C. Liu and C.-F. Hsu, "Dual-band cpw-fed y-shaped monopole antenna for pcs/wlan application," *Electronics Letters*, vol. 41, no. 7, pp. 390–391, 2005.

[219] B. Manimegalai, S. Raju, and V. Abhaikumar, "A multifractal cantor antenna for multiband wireless applications," *IEEE Antennas and Wireless Propagation Letters*, no. 8, pp. 359–362, 2009.

[220] H. Wang, L. Liu, Z. Zhang, Y. Li, and Z. Feng, "A wideband compact wlan/wimax mimo antenna based on dipole with v-shaped ground branch," *IEEE Transactions on Antennas and Propagation*, vol. 63, no. 5, pp. 2290–2295, 2015.

[221] C.-Y. Chiu and R. D. Murch, "Compact four-port antenna suitable for portable mimo devices," *IEEE Antennas and Wireless Propagation Letters*, vol. 7, pp. 142–144, 2008.

[222] R. T. Cock and C. Christodoulou, "Design of a two-layer, capacitively coupled, microstrip patch antenna element for broadband applications," in *Antennas and Propagation Society International Symposium, 1987*, vol. 25. IEEE, 1987, pp. 936–939.

[223] Y. Qin, S. Gao, and A. Sambell, "Broadband high-efficiency circularly polarized active antenna and array for rf front-end application," *IEEE Transactions on Microwave Theory and Techniques*, vol. 54, no. 7, pp. 2910–2916, 2006.

[224] K. Chang, R. A. York, P. S. Hall, and T. Itoh, "Active integrated antennas," *IEEE Transactions on Microwave Theory and Techniques*, vol. 50, no. 3, pp. 937–944, 2002.

[225] Y. E. Erdemli, R. A. Gilbert, and J. L. Volakis, "A reconfigurable slot aperture design over a broad-band substrate/feed structure," *IEEE Transactions on Antennas and Propagation*, vol. 52, no. 11, pp. 2860–2870, 2004.

[226] C. Y. Rhee, J. H. Kim, W. J. Jung, T. Park, B. Lee, and C. W. Jung, "Frequency-reconfigurable antenna for broadband airborne applications," *IEEE Antennas and Wireless Propagation Letters*, vol. 13, pp. 189–192, 2014.

[227] J. A. Navarro and K. Chang, *Integrated active antennas and spatial power combining*. Wiley, 1996.

[228] K. C. Gupta and P. S. Hall, *Analysis and design of integrated circuit-antenna modules*. Wiley Online Library, 2000.

[229] Y. Cui, R. Li, and P. Wang, "Novel dual-broadband planar antenna and its array for 2g/3g/lte base stations," *IEEE Transactions on Antennas and Propagation*, vol. 61, no. 3, pp. 1132–1139, 2013.

[230] J.-F. Li, Q.-X. Chu, and T.-G. Huang, "A compact wideband mimo antenna with two novel bent slits," *IEEE Transactions on Antennas and Propagation*, vol. 60, no. 2, pp. 482–489, 2012.

[231] L. Liu, S. Cheung, and T. Yuk, "Compact mimo antenna for portable devices in uwb applications," *IEEE Transactions on Antennas and Propagation*, vol. 61, no. 8, pp. 4257–4264, 2013.

[232] T. S. See and Z. N. Chen, "An ultrawideband diversity antenna," *IEEE Transactions on Antennas and Propagation*, vol. 57, no. 6, pp. 1597–1605, 2009.

[233] Q. Li, G. Li, W. Lee, M.-i. Lee, D. Mazzarese, B. Clerckx, and Z. Li, "Mimo techniques in wimax and lte: a feature overview," *IEEE Communications Magazine*, vol. 48, no. 5, pp. 86–92, 2010.

[234] M. S. Sharawi, F. Sultan, and D. N. Aloi, "An 8-element printed v-shaped circular antenna array for power-based vehicular localization," *IEEE Antennas and Wireless Propagation Letters*, vol. 11, pp. 1133–1136, 2012.

[235] N. Honma, T. Seki, and K. Nishikawa, "Compact planar four-sector antenna comprising microstrip yagi-uda arrays in a square configuration," *IEEE Antennas and Wireless Propagation Letters*, vol. 7, pp. 596–598, 2008.

[236] Y. Luo, Q. Chu, J. Li, and Y. Wu, "A planar h-shaped directive antenna and its application in compact mimo antenna," *IEEE Transactions on Antennas and Propagation*, vol. 61, no. 9, pp. 4810–4814, 2013.

[237] A.-D. Capobianco, F. M. Pigozzo, A. Assalini, M. Midrio, S. Boscolo, and F. Sacchetto, "A compact mimo array of planar end-fire antennas for wlan applications," *IEEE Transactions on Antennas and Propagation*, vol. 59, no. 9, pp. 3462–3465, 2011.

[238] A. Al-Rawi, A. Hussain, J. Yang, M. Franzén, C. Orlenius, and A. A. Kishk, "A new compact wideband mimo antennathe double-sided tapered self-grounded monopole array," *IEEE Transactions on Antennas and Propagation*, vol. 62, no. 6, pp. 3365–3369, 2014.

[239] S.-Y. Lin and H.-R. Huang, "Ultra-wideband mimo antenna with enhanced isolation," *Microwave and Optical Technology Letters*, vol. 51, no. 2, pp. 570–573, 2009.

[240] R. Karimian, H. Oraizi, S. Fakhte, and M. Farahani, "Novel f-shaped quad-band printed slot antenna for wlan and wimax mimo systems," *IEEE Antennas and Wireless Propagation Letters*, vol. 12, pp. 405–408, 2013.

[241] H. Wang, L. Liu, Z. Zhang, and Z. Feng, "Wideband tri-port mimo antenna with compact size and directional radiation pattern," *Electronics Letters*, vol. 50, no. 18, pp. 1261–1262, 2014.

[242] A. Ramachandran, S. Mathew, V. Rajan, and V. Kesavath, "A compact triband quad-element mimo antenna using srr ring for high isolation," *IEEE Antennas and Wireless Propagation Letters*, vol. 16, pp. 1409–1412, 2017.

[243] J. Rashed and C.-T. Tai, "A new class of resonant antennas," *IEEE Transactions on Antennas and Propagation*, vol. 39, no. 9, pp. 1428–1430, 1991.

[244] D. M. Pozar, "Microstrip antennas," *Proceedings of the IEEE*, vol. 80, no. 1, pp. 79–91, 1992.

[245] J.-Y. Chung, T. Yang, and J. Lee, "Low correlation mimo antennas with negative group delay," *Progress In Electromagnetics Research C*, vol. 22, pp. 151–163, 2011.

[246] R. Anitha, P. Vinesh, K. Prakash, P. Mohanan, and K. Vasudevan, "A compact quad element slotted ground wideband antenna for mimo applications," *IEEE Transactions on Antennas and Propagation*, vol. 64, no. 10, pp. 4550–4553, 2016.

[247] M. Kafesaki, T. Koschny, R. Penciu, T. Gundogdu, E. Economou, and C. M. Soukoulis, "Left-handed metamaterials: detailed numerical studies of the transmission properties," *Journal of Optics A: Pure and Applied Optics*, vol. 7, no. 2, p. S12, 2005.

[248] L. Schumacher and B. Raghothaman, "Closed-form expressions for the correlation coefficient of directive antennas impinged by a multimodal truncated laplacian pas," *IEEE transactions on wireless communications*, vol. 4, no. 4, pp. 1351–1359, 2005.

[249] Y. Okano, "Evaluation of ota performance for mobile terminal antennas reflecting practical usage and improvement of measurement efficiency, ntt docomo technical journal vol. 11, no.2, p.17-25," vol. 2009.

[250] Elektrobit, "3gpp r4-093959 verification of the anechoic chamber and fading emulator based mimo ota method," 2009.

[251] S. Communications, "3gpp r4-094673 evaluating channel models for mimo ota," November 2009.

[252] K. Technologies, "3gpp r4-093094 performance analysis of two-stage mimo ota method versus scm approximation method," 2009.

[253] "3gpp tr37.976 v01.03.0 measurement of radiated performance for mimo and multi-antenna reception for hspa and lte terminals," 2010.

[254] S. E. S. www.agilent.com/find/eesof systemvue.

[255] I. C802.16m-07/062, "Draft channel model for 802.16m - advanced air interface," 2007.

[256] A. A. Note, "Accounting for antenna and mimo channel effects using agilent systemvue," pp. 5990–6535, September 2010.

[257] I. winner I. I. Deliverable 1.1.2 v.1.2, "Winner ii channel models," *IST-WINNER*, vol. 2, 2008.

[258] J. X. Yun and R. G. Vaughan, "Multiple element antenna efficiency and its impact on diversity and capacity," *IEEE Transactions on Antennas and Propagation*, vol. 60, no. 2, pp. 529–539, 2012.

[259] R. Verdone and A. Zanella, *Pervasive Mobile and Ambient Wireless Communications: COST Action 2100.* Springer Science & Business Media, 2012.

[260] Z. Ying, C.-Y. Chiu, K. Zhao, S. Zhang, and S. He, "Antenna design for diversity and mimo application," in *Handbook of Antenna Technologies.* Springer, 2015.

[261] F. Y. Zulkifli, M. Fahmi, Basari, and E. T. Rahardjo, "Active integrated microstrip mimo antenna for gain enhancement," in *2013 IEEE International Conference on Communication, Networks and Satellite (COMNETSAT)*, Dec 2013, pp. 37–40.

[262] M. Sharawi and S. Dhar, "Multi-band active integrated mimo antennas," Jan. 7 2016, uS Patent App. 14/325,318.

[263] M. P. Karaboikis, V. C. Papamichael, G. F. Tsachtsiris, C. F. Soras, and V. T. Makios, "Integrating compact printed antennas onto small diversity/mimo terminals," *IEEE Transactions on Antennas and Propagation*, vol. 56, no. 7, pp. 2067–2078, 2008.

Appendix A

Diversity Based MIMO Antenna With Square Ring DGS

The thesis presented few quad element multimode MIMO designs using printed microstrip patch antennas. In this section, the study is extended to investigate the radiation characteristics with an arrangement of printed microstrip cross patch and ring patch antenna, along with a ring shaped DGS for isolation enhancement. The multiple modes of the antennas are excited by coaxial feed to achieve resonance at 2.45 GHz band for all the four elements. Here, the theory of mutual coupling reduction using ring shaped DGS is verified in a different antenna configuration and is compared to section 3.2. The antenna exhibits diverse radiation characteristics and achieves better isolation in the operating band. This proves that the DGS is an attractive choice for use in multiple antenna systems for reducing surface waves and enhancing isolation along both E and H planes.

A.0.1 MIMO Antenna Geometry and its Design

The geometry of the four port MIMO antenna is shown in Figure A.1 and the antenna dimensions are shown in table A.1. The overall size of the MIMO antenna is $60 \times 60 \times 1.6$ mm^3. The antenna consists of a two port orthogonally polarized cross patch antenna resonating in TM_{01} and TM_{10} modes. This, along with a two port orthogonally polarized square ring patch antenna resonating in TM_{12} and TM_{21}, constitutes a four port MIMO antenna.

The isolation enhancement between highly coupled antennas elements, for which fields are oriented in the same direction, is achieved by etching the
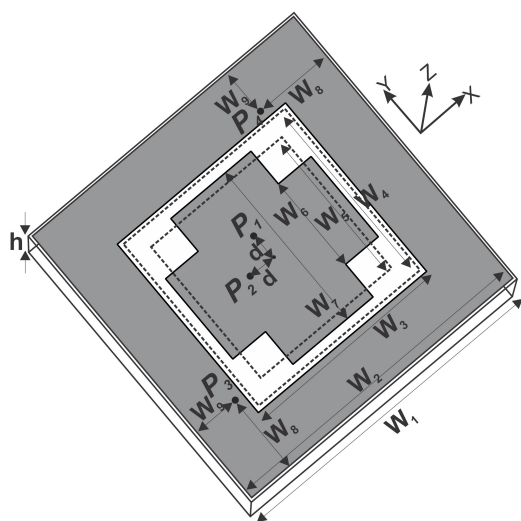
Figure A.1: Geometry of the four port MIMO antenna

Parameter	Value (mm)	Parameter	Value (mm)
W_1	60	W_7	33.6
W_2	59	W_8	14.5
W_3	38.6	W_9	8.5
W_4	37	d	5.2
W_5	30	h	1.6
W_6	18.4		

Table A.1: Antenna Dimensions

square ring defected ground structure. The proposed isolation structure reduces surface waves confined within the dielectric, that causes coupling between the antenna elements. It can effectively reduce coupling in both E and H planes because of its ring shaped structure. The design and working principle of the isolation enhancement structure is similar to what is explained in subsection 3.2.2. It was observed that the inclusion of DGS effectively decreases cross polar levels and also improves isolation between co-polar and cross polar currents. This ensures that the confined waves within dielectric which would otherwise be radiated sideways are reduced. All the four antenna elements are resonating in 2.45 GHz frequency band.

A.0.2 Simulations and Measurements

The antenna simulations are carried out using CST Microwave studio software. With the inclusion of ring shaped defected ground structure, low mutual coupling is ensured between the two patch antenna elements. The DGS acts as an inductive slot and improves the mutual coupling from -15.5 dB to -24 dB. By reducing coupling currents using a simple square ring DGS, about
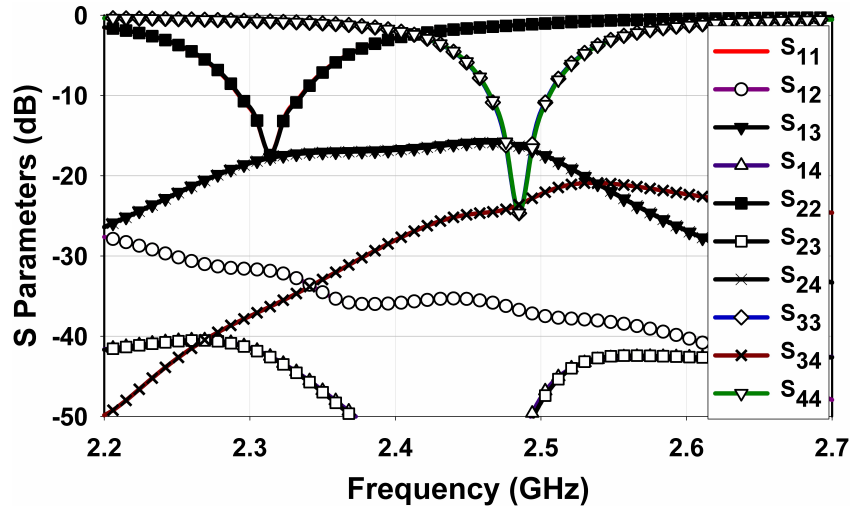
Figure A.2: Simulated S parameters of the four port MIMO antenna without DGS

8.5 dB improvement in isolation is achieved. Ground slot causes meandering of surface current path of the ring antenna, thereby decreasing resonant frequencies of the ring antenna without any increase in antenna dimensions. The ring shaped DGS etched around the cross patch antenna on the ground plane, reduces the electrical length of the antenna, thereby increasing the resonant frequency of cross patch modes. Simulated S parameters of four port antenna without DGS and with DGS are shown in Figure A.2 and Figure A.3 respectively.

Therefore by introducing the isolation structure, apart from improving isolation between the cross patch and the ring patch ports, all ports are made to resonate at the same frequency of about 2.45 GHz. The -10 dB impedance bandwidth is about 2.5% for P_1 and P_2, and 2% for ring ports P_3 and P_4. The cross polarization levels of the fundamental modes of the quad element MIMO antenna with and without isolation structure is shown in Figure A.4. From simulated radiation curves it is observed that in both 0^0 and 90^0 planes, the cross-polar radiation has been reduced by a maximum value of 15 dB in the presence of DGS for ports 1 and 2. The co-polar radiation patterns for the elements in corresponding planes are almost similar with the inclusion of isolation structure and therefore isolation between co-polar and cross-polar components are improved.
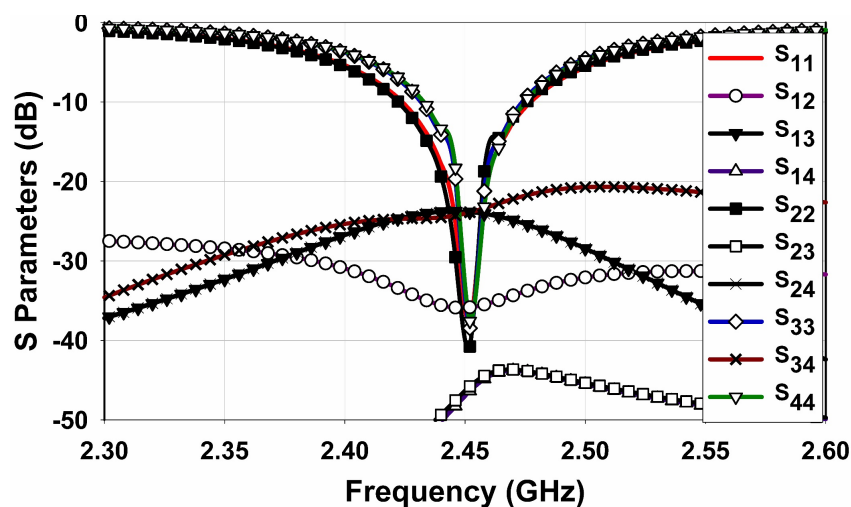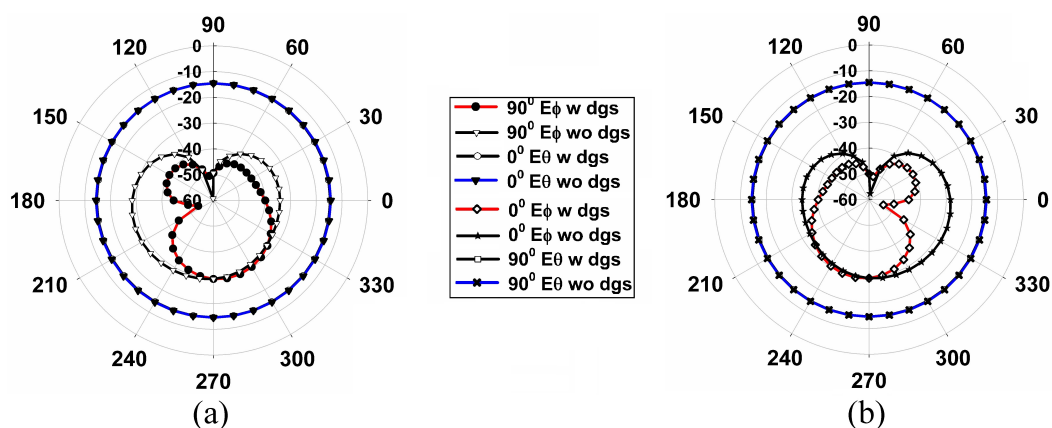
Figure A.3: Simulated S parameters with ring DGS

Figure A.4: Cross Polarization levels with and without isolation structure (a) P_1 excited (b) P_2 excited

The prototype of four port coaxially fed multimode microstrip patch antenna is fabricated as shown in Figure A.5 using an FR4 substrate with relative dielectric constant (ϵ_r) 4.4 and substrate thickness 1.6 mm. Measured S parameter results in Figure A.6 shows that all feed ports resonate at 2.45 GHz, identical to simulation curves, though a slight variation accounts for manufacturing tolerances. The results obtained ensure good MIMO performance as the mutual coupling between all ports is well below -20 dB. Isolation between

patch and ring modes are reduced below -24 dB with DGS. Far field radiation patterns are measured for all four ports in the 0^0 and 90^0 planes of antenna and is shown in Figure A.7.
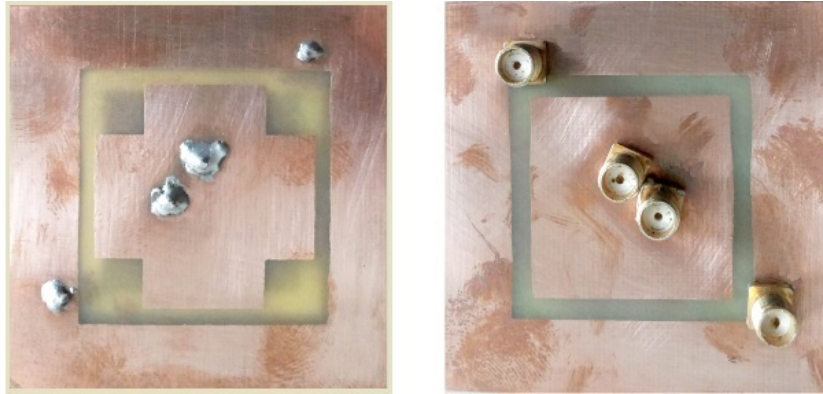

Figure A.5: Fabricated prototype of quad element antenna
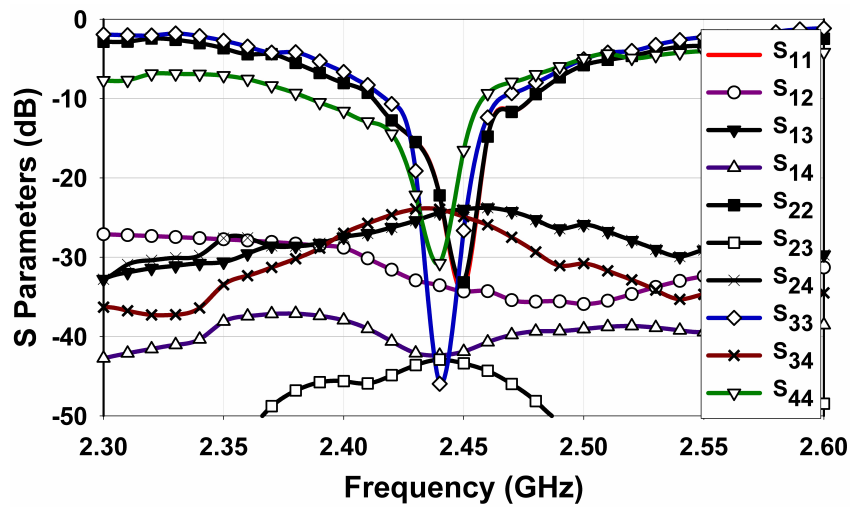

Figure A.6: Measured S parameters of the antenna

A.0.3   Summary

In order to validate the performance of diversity based multimode MIMO antenna system and the isolation enhancement structures proposed in the thesis,
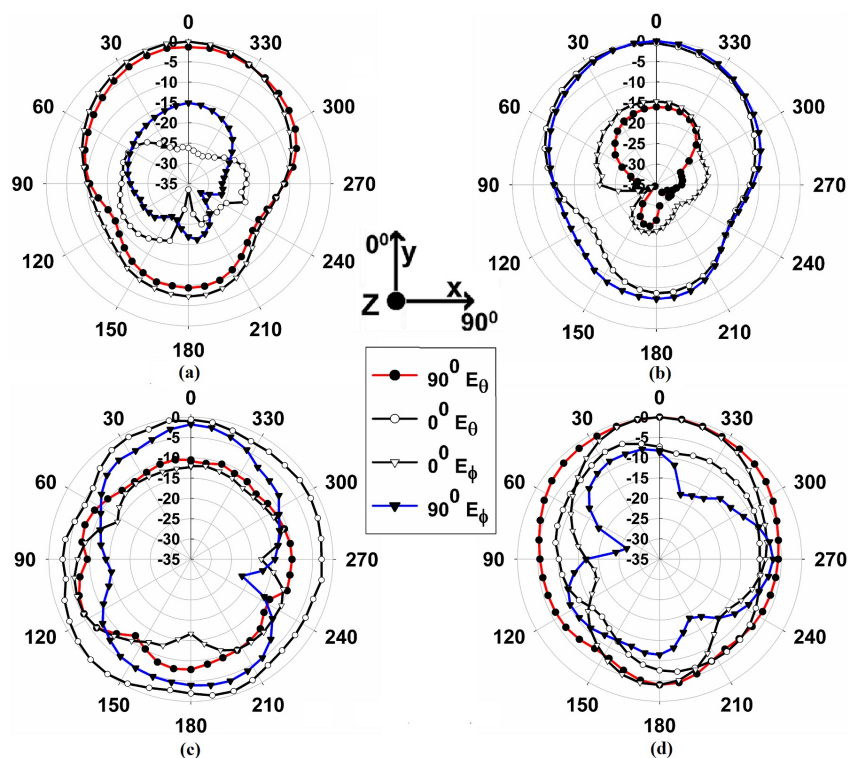
Figure A.7: Measured radiation patterns of the antenna (a) P_1 (b) P_2 (c) P_3 (d) P_4 excited

a new design is investigated with antennas and defected ground structures interchanged. The cross and ring patch antenna elements are chosen as the resonating elements with a ring shaped defected ground structure between them for enhancing isolation. The antennas and the isolation enhancement structure fits together and exhibit better isolation performance compared to the antenna described in section 3.2. An isolation enhancement of 8.5 dB is achieved using ring DGS in this antenna configuration compared to 7 dB improvement obtained for MIMO antenna defined in section 3.2. Therefore it can be validated that the designs are capable of replacing the other(s) without causing a need for significant alteration or adjustment to fulfill the requirement.

Appendix B

GUI For MIMO Antenna Diversity Measurements

A graphical user interface (GUI) is designed and developed as part of the research work for evaluating the MIMO diversity performances. The three dimensional far field radiation pattern data is used for the calculation of MIMO figure of merit parameters. Parameters like envelope correlation coefficient, mean effective gain, diversity gain and multiplexing efficiency of the multiple antenna configurations [263] can be calculated from the obtained far field data. The software was developed using National Instruments LabVIEW 2014 version. The LabVIEW GUI supports measurements for four channel MIMO by taking into consideration the far field responses of the four antenna elements separately.

The user controls on the front panel of the GUI is shown in Figure B.1. The path controls are pointed to choose four folders each containing several .txt files. Each of these files contains far field results obtained at specific frequency points for the four antenna elements. The gain and efficiency information of the four antenna elements are provided in a separate .txt file and the path needs to be given as an input to the GUI. The other user inputs are cross polarization ratio and power distribution function (PDF) $P(\phi), P(\theta)$ which by default considers an isotropic channel environment with a cross polarization ratio (XPR) of 1 and PDF $P(\phi) = P(\theta) = \frac{1}{4\pi}$.

The three dimensional far field gain distribution for the multiple antenna elements in a MIMO antenna can be either measured using Network Analyzer in an anechoic chamber or can be saved from CST microwave studio simulation environment. The data saved in the .txt file for a single frequency contains several columns which correspond to θ angles, Φ angles, the absolute value or magnitude of E_θ, the phase values of E_θ, the absolute value of E_ϕ, the phase
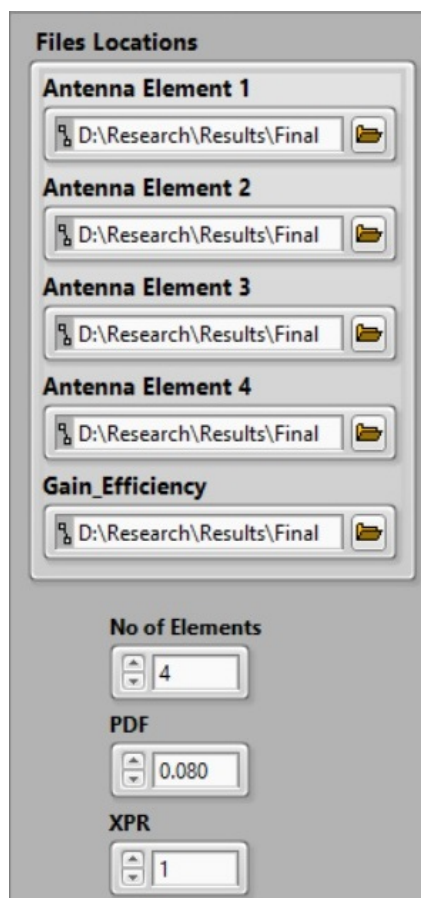
Figure B.1: Front panel controls of MIMO diversity measurements GUI

value of E_ϕ etc. The GUI reads these files from the folders corresponding to each antenna element and normalizes the data initially. These values are then used in the computation of MIMO diversity measurements.

The front panel of the LabVIEW GUI is shown in Figure B.2. Four plots showing envelope correlation coefficient vs. frequency, mean effective gain vs. frequency, diversity gain vs. frequency and multiplexing efficiency vs. frequency are plotted on the front panel of the GUI for user convenience in reading the results. These are shown in the Figure B.2, Figure B.3, Figure B.4, and Figure B.5 respectively. Envelope correlation coefficient between all possible combinations of antenna elements is calculated using equation (2.17) which gives a measure of how correlated the two different antenna radiation

patterns are. An ECC value less than 0.5 is considered to be pretty good for MIMO applications.
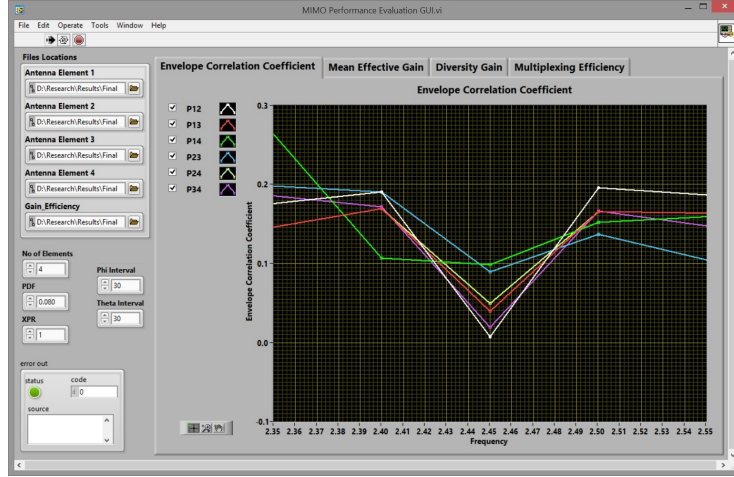
Figure B.2: Front panel of the GUI for measuring ECC

Mean effective gain is measured for various frequency points using equation (2.8) and is plotted. This provides the average gain of the antenna in a fading environment based on the channel under consideration. For good diversity performance, the MIMO antenna system has to satisfy balanced power requirement with the ratio $MEG_i/MEG_j \leq 3dB$.
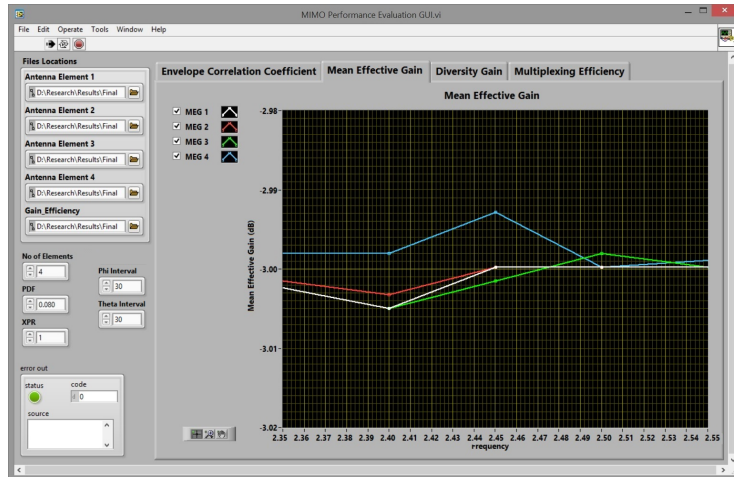

Figure B.3: Front panel of the GUI for measuring MEG
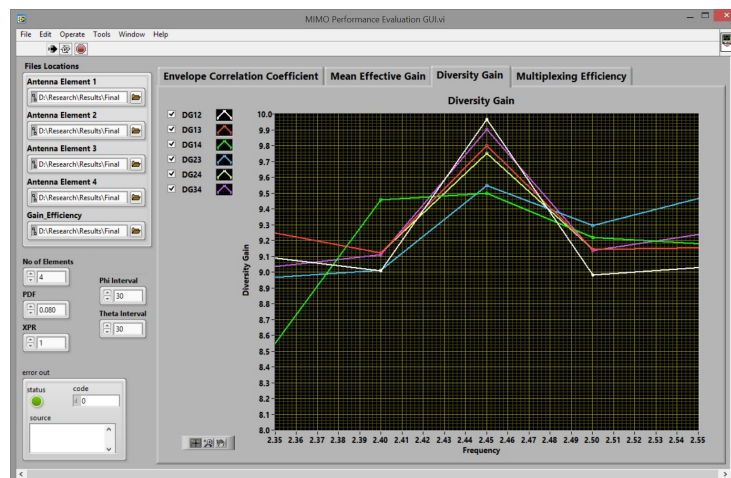
Figure B.4: Front panel of the GUI for measuring diversity gain

Another figure of merit of multiple antenna systems is diversity gain discussed in subsection 2.2.2. This is calculated using equation (2.6) which provides an improvement in reliability of the MIMO antenna system implemented using diversity techniques. Multiplexing efficiency is another metric which describes the performance of the multiple antenna systems in spatial multiplexing mode by taking into account the antenna efficiency and correlation. This metric is calculated using equation (2.15) and is plotted on the front panel of GUI.

Figure B.5: Front panel of the GUI for measuring multiplexing efficiency

List Of Publications

International Journals

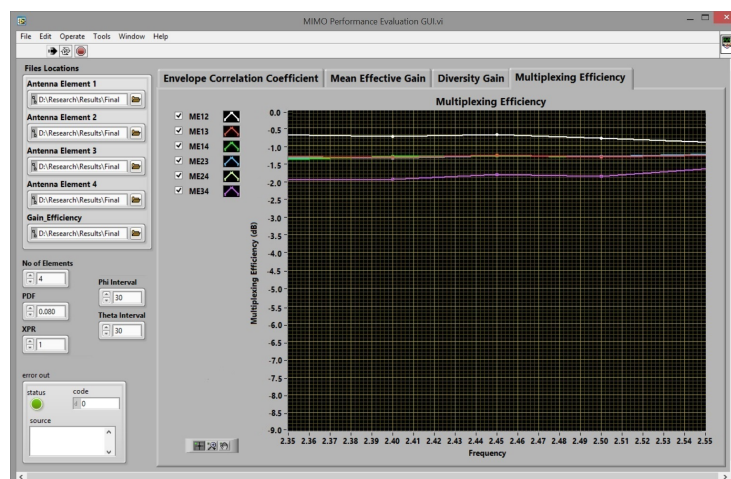1. **Anitha R.**, P. V. Vinesh, S. Mathew, P. Mohanan, and K. Vasudevan, "Collocated MIMO antenna with reduced mutual coupling using square ring dgs", Progress In Electromagnetics Research C, Vol. 53, pp. 119-125, 2014.

2. **Anitha R.**, V.P. Sarin, P. Mohanan and K. Vasudevan, "Enhanced isolation with defected ground structure in MIMO antenna", Electronics Letters, Vol. 50 No. 24 pp. 1784-1786, 2014.

3. **Anitha R.**, Sarin V. P., Mohanan Pezholil, and Vasudevan Kesavath, "A Four Port MIMO Antenna using Concentric Square Ring Patches Loaded with CSRR for High Isolation", IEEE Antennas Wireless Propagation Letters, vol. 15, pp. 1196-1199, 2016.

4. **Anitha R.**, V. P. Viswanathan, M. Pezholil, S. Mathew, and Vasudevan Kesavath, "Diversity-based four-port multiple input multiple output antenna loaded with interdigital structure for high isolation", IET Microwaves, Antennas & Propagation, vol 10, No.15, pp. 1633-1642, 2016.

5. **Anitha R.**, Sumitha Mathew, Vivek Rajan, and Kesavath Vasudevan, "A Compact Tri-Band Quad Element MIMO Antenna Using SRR Ring for High Isolation", IEEE Antennas and Wireless Propagation Letters, Vol 16, pp. 1409-1412, 2017.

6. **Anitha R.**, P. V. Vinesh, K. C. Prakash, P. Mohanan, and K. Vasudevan, "A Compact Quad Element Slotted Ground Wideband Antenna for MIMO Applications", IEEE Transactions on Antennas and Propagations, Vol 64, No.10, pp. 4550-4553, 2016.

7. Sumitha Mathew, **R. Anitha**, U. Deepak, C. K. Aanandan, P. Mohanan and K. Vasudevan, "A Compact Tri-Band Dual-Polarized Corner- Truncated Sectoral Patch Antenna", IEEE Trans. Antennas Propag., vol. 63, no. 12, 2015.

8. K. C. Prakash, Sumitha Mathew, **R. Anitha**, P. V. Vinesh, M. P. Jayakrishnan, Pezholil Mohanan, and Kesavath Vasudevan, "Circularly Polarized Dodecagonal Patch Antenna with Polygonal Slot for RFID Applications", Progress In Electromagnetics Research C, vol. 5, no. 2, 2016.

9. Sumitha Mathew, **R. Anitha**, T. K. Roshna, C. M. Nijas, C. K. Aanandan, P. Mohanan and K.Vasudevan, "A Fan-shaped circularly polarized patch antenna for UMTS band": Progress In Electromagnetics Research C, Vol. 52, pp. 101-107, 2014.

10. P. V. Vinesh, C. M. Nijas, **R. Anitha**, R. Vivek, C. K. Aanandan, P. Mohanan, and K. Vasudevan, "A Compact capacitive coupled dual-band planar inverted F antenna": Progress In Electromagnetics Research C, Vol. 52, pp. 93-99, 2014.

Conferences

1. **Anitha R.**, P. V. Vinesh, Sumitha Mathew and K. Vasudevan, "Compact 4 port MIMO Antenna using polarization and pattern diversity", IEEE Wireless and Microwave Technology Conference (WAMICON 2015) Florida, USA, April 13-15, 2015.

2. **Anitha R.**, C. K. Aanandan, P. Mohanan, K. Vasudevan, "Bandwidth and Isolation Enhancement in Compact MIMO Antenna using Ring Shaped Ground", International Symposium on Antennas and Propgation (APSYM 2016), Kochi, India, December 15-17, 2016.

3. Vinesh P. V., **Anitha R.**, Prakash K. C., Sumitha Mathew, Mohammad Ameen , Vivek R., Vasudevan K., "Compact Wide Band Planar Inverted F Antenna for LTE Applications", Twelfth International Conference on Microwaves, Antenna, Propagation & Remote Sensing ICMARS-2017, Jodhpur, India, Feb. 15-17, 2017.

4. Prakash K. C., Mohammad Ameen, Manoj M., Sumitha Mathew, **Anitha R.**, Vinesh P. V., Vivek R., Vasudevan K., "A Compact UWB Circularly Polarized Hexagonal Slot Antenna for Wireless Applications", International Symposium on Antennas and Propgation (APSYM 2016), Kochi, India, December 15-17, 2016.

5. Sumitha Mathew, **R. Anitha**, Vinesh P. V., Mohammed Ameen and K. Vasudevan, "Dual Band Corner Truncated Sectoral Patch antenna with dual slits for GPS and WLAN", International Symposium on Antennas and Propagation (APSYM 2016), Kochi, India, December 15-17, 2016.

6. Ameen, M., Mathew, S., **Anitha R.**, Mohanan, P., and Vasudevan, K., "A compact S-shaped 2x1 MIMO antenna for WLAN/WiMAX applications", Fifth International IEEE Applied Electromagnetics conference, IIT Guwahati, India, 18-21 December, 2015.

7. Prakash K.C, Vivek R. Kurup, Vinesh P.V, M. Ameen, Jayakrishnan M. P, **Anitha R.**, Sumitha Mathew and K. Vasudevan, "Dodecagonal Circularly Polarized Patch Antenna for RFID Applications" , Fifth International IEEE Applied Electromagnetics conference , IIT Guwahati, India, 18-21 December, 2015.

8. Vinesh P V, **Anitha R.**, Prakash K C, Sumitha Mathew, Mohanan P, Vasudevan K, "Compact L-Slot Loaded Planar Inverted F Antenna For GPS And WLAN Applications", Fifth International IEEE Applied Electromagnetics conference, IIT Guwahati, India, 18-21 December, 2015.

9. Sumitha Mathew, **R. Anitha**, P. V. Vinesh, K. Vasudevan, "Sector-shaped dual-polarized Patch Antenna forUMTS/WiMAX Applications", International Microwave and RF Conference (IMaRC 2014), Bangalore, India, December 15-17, 2014.

10. Sumitha Mathew, **R. Anitha** and K.Vasudevan, "Wideband circularly polarized patch antenna forWiMax applications", International Symposium on Antennas and Propagation (APSYM 2014), Kochi, India, December 17-19, 2014.

11. Sumitha Mathew, **R. Anitha**, P.V. Vinesh and K. Vasudevan ,"Circularly polarized sector- shaped patch antenna for WLAN applications", International Conference on Information and Communication Technologies (ICICT 2014), Kochi, India, Dec 2014.

12. Sumitha Mathew, **R. Anitha**, A.O.Lindo and K.Vasudevan, "A 2.4/5.1GHz Annular RingWideband Patch Antenna using Defected Ground Plane", International Conference on Information Sciences (ICIS14), College of Engineering, Cherthala, Kerala, 2014.

Resume

Areas of Interest

Multiple-Input Multiple-Output (MIMO) Antennas, Isolation enhancement techniques for antennas, Microstrip Antennas, Antenna Arrays, RF test and measurements.

Education

- June 2013 - Present
  Doctoral degree in Microwave Electronics, Department of Electronics, Cochin University of Science and Technology, Cochin, India.

- June 2003 - May 2005
  M. Sc. (Masters in Science) degree in Electronics, Department of Electronics, Cochin University of Science and Technology, Cochin, India.

- June 1999 - May 2002
  B. Sc. (Bachelors in Science) degree in Electronics, College of Applied Sciences, Calicut University, Kerala, India.

Awards and Fellowships Received

- Awarded Junior Research Fellowship (JRF) in 2013 and qualified National Eligibility Test (NET) for lectureship by University Grants Commission (UGC), Government of India.

- Second Rank holder for Common Admission Test (CAT) exam in 2003 conducted by Cochin University of Science and Technology, Cochin, India.

- University Second Rank holder for M.Sc. Electronics in 2005 from Cochin University of Science and Technology, Cochin, India.

- University Third Rank for B.Sc. Electronics in 2002 from Calicut University, Kerala, India.

Technical Skills

- Development Software: CST Studio Suite, Ansys HFSS, NI LabVIEW, MATLAB, NI Teststand, Agilent ADS, Embedded C, Visual Studio, C, Assembly language

- Hardware Expertise: Vector Network Analyzer, RF Spectrum Analyzer, RF Signal Generator, RF Swicthes, DAQs and Power Meters

- Operating System: Windows, Linux

- Documentation: LaTeX, Open Office

Experience

Research Experience

- June 2013 - Present. Ph.D., "Investigations on the Radiation Characteristics of Compact Multiple Antenna Systems for MIMO Applications", at Centre for Research in Electromagnetics and Antennas (CREMA), Cochin University of Science and Technology, India.
Designed and developed quad element MIMO antennas exploiting the various forms for diversity techniques. The main focus of the research is to provide compact, decoupled and efficient multiple antenna designs for the terminal devices. Microstrip patch antennas are configured to form multimode MIMO antenna for application in the 2.4 GHz band. Efficient multiband and wideband MIMO antenna with multiple standard

support are designed and developed for compact MIMO terminal applications. Various isolation enhancement techniques are designed and validated for its effectiveness in reducing mutual coupling between closely spaced antenna elements. Isolation performances, MIMO diversity performances and channel performances of the multiple antenna systems are verified through simulation and measurement results. Experience in software's like HFSS, CST MWS, Matlab, Agilent ADS, SystemVUE, antenna fabrication, antenna measurements using Network Analyzer, far-field measurements in anechoic chamber.

Industrial Experience

- Nov 2010 Sep 2011. ATE Test Engineer II, Powerwave Technologies Inc., Hyderabad, India.
  Understanding LTE BTS Compliance tests as per 3Gpp standard, documented and developed test cases in LabVIEW. Developed LabVIEW drivers for controlling RF Instruments using GPIB and LAN. Worked in developing automated DVT and Manufacturing Test solutions for testing RadioHeads. Designed and developed automated testing software and GUIs in LabVIEW and TestStand for testing various products. Developing LabVIEW based automated manufacturing and DVT test solution for testing LTE RadioHead's. Experience gained in using various RF Instruments and Agilent VSA 89600.

- March 2010 Oct 2010. Software Programmer, Mimowaves Technologies, Bangalore, India.
  Developed front end algorithms in C for ZigBee PHY layer processing and correction. Developed algorithms for ZigBee 868/915MHz, Test and Measurement APIs, and decoding of entire PHY payload. Developed C DLLs for ZigBee Measurements. Developed LabVIEW ZigBee Measurement APIs using C DLLs. Designed entire vector signal analyzer for decoding WLAN 802.11b signal. Developed all front end algorithms and PHY measurement APIs and bit decoding algorithms in C for WLAN 802.11b decoder. Developed LabVIEW measurement APIs for WLAN. LabVIEW GUI development for customer to test API functionalities.

- Feb 2007 June 2009. Senior Software Engineer, Seasolve Software Inc.,A div. of Cranes Software International Ltd., Bangalore, India.
  Developed Manufacturing and Compliance Test solutions for ZigBee (802.15.4) DUTs. Development of RF functional Test and Measurement APIs for Wireless LAN (802.11.a, 802.11b and 802.11g) and ZigBee in LabVIEW. Development of front-end signal processing algorithms for WPAN ZigBee, WLAN, WCDMA and WiMAX Physical layer in LabVIEW. Designed and developed an RF Mutisignal analyzer for testing multiple wireless standards. Performed simulation tests on WLAN Analyzer in Matlab and evaluated PER and BER for various SNR conditions and channel models. Development of GUIs in LabVIEW for ZigBee and WLAN Analyzers and Generators. Development of GUI in Matlab for WCDMA Generator and Analyzer. Designed and developed complex C DLL for entire ZigBee Vector Signal Analyzer, WLAN Analyzer, WLAN Generators and measurement APIs.

- Jan 2005 Feb 2007. R & D Engineer, Premier Evolvics Pvt Ltd., Coimbatore, India.
  Involved in development of automation software which monitors several machines simultaneously in Textile industry. Developed software for production monitoring of weaving machines using ATMEGA controllers and sensors. Designed and developed a system called capacitive sensor and Measuring Head Simulator using PSOC Designer, for Textile Industry which simulate different yarn faults in both static and dynamic conditions. Designed and developed Canteen Reader using Employee RFID tag. Experience gained in using LabVIEW, Microcontrollers, Analog Circuit design for Buffer amplifiers, Filters, ADC, and DAC. Communication protocols like RS 485, RS 232, I2C, SPI, JTAG and Ethernet were used extensively.